Karnatak University
Journal of Science

Vol. 52, September 2021

Chief Editor
Dr. Sanjeev R. Inamdar F.R.S.C. (UK)
Professor, Department of Physics
Karnatak University, Dharwad-580003

The journal is published annually in order to disseminate new knowledge and research findings of the faculty and students of Karnatak University and other academic institutions belonging to various disciplines in the area of Science. The journal also encourages interdisciplinary research.

Journal in exchange may be sent to:
Librarian
Professor S. S. Basavanal Library
Karnatak University, Dharwad
Pavate Nagar, Dharwad-580 003, INDIA

Research articles and books for review should be addressed to:
Director
Prasaranga
Karnatak University, Dharwad
Pavate Nagar, Dharwad-580 003, INDIA

FOREWORD

Karnatak University, as a habit, is producing quality research since the beginning, with science departments being always ahead. The University provides ample scope to researchers to pursue cutting edge research in frontline areas. In addition to National and International journals our researchers are also publishing their work in our own Journal "Karnatak University Journal of Science".

I am very happy to note that, this journal is expanding its horizon, by receiving quality research work from various Universities and premier research institutions including IIT Bombay, Mumbai, Delhi University, Allahabad University, MS Ramaiah University, Bangalore and other Universities in Karnataka. Certainly, the journal has gained high visibility; the journal in electronic version is available on the University Website.

The present 52nd volume of Karnatak University Journal of Science comprises Regular Research Papers and Review articles on current topics in frontier areas of Physics, Mathematics, Geography and Zoology. I am confident that the efforts of the Editorial Board will take our journal to greater academic standards. This volume has set the standards for future volumes to come. I congratulate the Chief Editor, Prof. Sanjeev R. Inamdar and the entire Editorial Board comprising National and International researchers of eminence for having accomplished a wonderful job to elevate the Status of the journal.

Prof. K. B. Gudasi
Vice Chancellor
Karnatak University, Dharwad

From Editor's Desk

While all areas of science are witnessing significant advances, I take a special note of the enormous prospects of advancement in the field of photonics that is playing key role in the fields like: optical data communications, imaging, lighting and displays, manufacturing sector, life sciences, health care, security, safety, etc. The impact of photonics in our daily lives offers new, unique solutions in terms of speed, capacity and accuracy.

Lasers have become a versatile tool and form heart and brain of photonics research resulting in numerous applications in all the fields of scientific research that are helpful for the societal needs. At Karnatak University, we have a Laser Spectroscopy programme (established by Prof. M.I. Savadatti in 1990 at the Department of Physics with funding from DRDO, New Delhi) which has been actively pursuing research in ultrafast spectroscopy of laser dyes, laser photobiology, biophysics, etc. Of late, the programme has significantly contributed to research on spectroscopy of nanomaterials which have emerged as powerful photoluminescent materials and become integral part of photonics. It is worth noting that several groups in the Department of Chemistry are involved in synthesis and characterizing novel materials for variety of applications as such as non-linear optics, organic light emitting diodes (OLEDs), metal ion complexes, optical sensors, etc. This has resulted in a faction of researchers from Physics, Chemistry and Zoology departments (laser photobiology using animal models and nanobiophotnics) working in the photonics related research areas. The quality research output from all these researchers, has resulted in successful scientific collaboration with premier research institutions in India and abroad. Certainly, photonics related research is leading the way at Karnatak University. I foresee greater chances of university-industry interaction/collaboration in these areas in the near future as envisaged in the NEP-2020.

I am grateful to all the esteemed members of the Editorial Board for their constructive efforts in bringing this 52nd volume of Karnatak University Journal of Science to the readers. All the publishing ethics on par with international publishers are followed. All the papers are strictly subjected to similarity check and peer reviewed before acceptance. Looking forward to your valuable feedback,

Dr. Sanjeev R. Inamdar F.R.S.C. (UK)
Chief Editor

CONTENTS

REVIEW ARTICLES

REGULAR ARTICLES

Extraction of Nanocellulose for Futuristic Materials

Onkarappa H S[1], Radha V[1], Nikhileshwar V[1], Virupaxappa S Betageri[1*], Nandeshwarappa B P[2], Latha M S[3], Shilpa V Allipur[1], Sushma Katti[4], G H Pujar[4*]

[1]Research Centre, Department of Chemistry, GM Institute of Technology, Davangere, Karnataka, India-577006
[2]Research Centre, Department of Chemistry, Davangere University, Davangere, Karnataka, India-577004
[3]R L Science Institute (Autonomous), Belagavi Karnakata, India
[4]Research Centre, Department of Physics, GM Institute of Technology, Davangere, Karnataka, India-577006
***Corresponding author:** puttpuja@gmail.com*

ARTICLE INFO

ABSTRACT

In frontier applications, there is a never-ending demand for nanocellulose due to its unique compatibility and ability to fit in. It has impressive characters like presence of rich hydroxyl group, physical and mechanical properties, high surface area and thermal stability. In this review, the background of nanocellulose originated from lignocellulosic biomass and the typical extraction methods like acid hydrolysis, TEMPO oxidation and Ionic liquid methods are summarized with a detailed procedure to obtain nano cellulose. It is expected to provide a complete guidance on the types of nanocellulose and detailed extraction methods.

1. Introduction

Over the years, natural bio-polymers like alginate, starch, collagen, elastin, chitosan and cellulose have played a vital role of promising starting materials over the conventional materials [1-4]. Cellulose when compared with other sources steals the spotlight because of its excellent physical and chemical properties. It is a linear, poly-carbohydrate, semi-crystalline biopolymer with outstanding inter and intra molecular hydrogen bonding between the hydroxyl groups and the molecules. The idiosyncratic nature of it is due to the existence of both amorphous and crystalline regions in an orderly fashion [5]. Because of its bio-degradability, bio-compatibility and availability in copious makes it an ideal starting

material and stimulates great interest in scientific attention [6].

The stiffness of the exterior parts in plants is credited to the existence of cellulose along with lignin and hemicellulose [7]. Thus, it is most commonly found organic compound with approx. 40% of the entire organic matter [8]. Cellulose is a linear, natural glucose polymer water insoluble polysaccharides linked with β-1,4 linked anhydro-D-glucose units (AGU). Its degree of polymerisation is 20000 units of glucose connecting via 1-4 linkage fashion. The carbon position C6 hydroxyl group is more reactive than the C2 and C3 [9]. The isolation of cellulose can be done from various plant source like bamboo hemp, flax, cotton, jute, kenaf, wheat, sisal, rime, coconut, hardwood, softwood, sugarcane, maize and rubber wood [10-17]. The existence of ordered

(crystalline) and disordered (amorphous) varies depending on the source of a plant [18]. The natural flexibility existing in cellulose gives it a fair run-in paper, veterinary foods, wood, beauty products, pharmaceuticals and apparels [19].
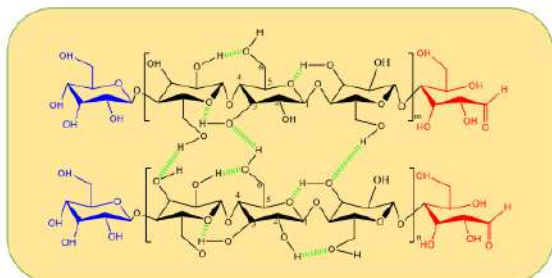
Figure 1. Hydrogen bonding in cellulose with AGU repeating units.

Nanocellulose (NC) is the newest form of the cellulose with more improved properties as a novel material. In a plant cell the primary wall consists the cellulose chain of <1 micrometer and the size is in the range of 1-500nm is termed as nanocellulose [20]. Thus, a greater consideration is given to the bio-materials like nanocellulose due to its sole ability to reduce the usage of water in water treatments. The other reasons being, unique morphology with the ability to alter it according to hydrophilic/hydrophobic application. NC benefit from other biomaterials with regard to, mechanical reinforcement, perfect architecture, rheological property, large specific-area to volume ratio, optical transparency, low thermal expansion, elasticity. It also behaves as a liquid crystalline [21]. The latter properties not only make it an ideal material to use over the conventional sources like glass and artificial polymer but also has the potential to replace it as a promising starting material [22-24].

Nanocellulose has marked its place in every possible application in the present day due to myriad of reasons. Due to its excellent physical and chemical properties it is seen in packaging and paints because of its water retaining capacity [25-27], composites for its natural strength [28], in biomedicine [18], in optical materials as the size of NC is less than that of the visible light wavelength [29].

Figure 2. Applications of nanocellulose.

In the present century a significant shift of the paradigm on the usage of NC can be seen in nanotechnology not seizing to limited ideas. A great deal of work has been done using NC thus, rounding up every versatile use of it in a single article would be only an inundation [18].

The present review article intends to give a detailed elucidation on different synthesis methods to obtain NC. It also enlightens on its mechanisms and characterization data of NC obtained from different extraction methods. This is a one stop solution for different extraction methods that can be employed to obtain NC.

Based on the extraction method used the NC obtained has significant characters differing from each other. Like cellulose, nanocellulose also varies in its crystalline and amorphous regions based on the plant extract which give raise to different types of NC [16]. To start with they can be classified as CNCs (Cellulose nano crystals), CNF (Cellulose nano fibers), CNWs (Cellulose nano whiskers) and BNC (Bacterial nano cellulose).

2. Extraction of Nanocellulose from cellulose

Lignocellulose biomass contains hemicellulose, α-cellulose and lignin on a broad scale and NC is obtained by using only α-cellulose. However, the pre-treatment of any lignocellulosic material is highly recommended to obtain a good NC. As prescribed by Onkarappa et. al. [16] hemicellulose and lignin can be removed by treating the lignocellulose mass by bleaching and alkali treatments. Agricultural residues not only contain

huge amount of cellulose but is also available in chief thus, it has the ability to lead the society sustainably as cellulose exits as a bio-polymer. It is seen that agricultural residues like, maize husk, sugar cane bagasse, rubber wood [15-17], empty fruit bunches [30], apple stem [31], bean and rice hulls [32], coir fibre [33], mulberry bark [34] are exploited to get nanocellulose. There exists diverse approaches in extraction methods to obtain NC under mechanical and chemical process. It is encouraged to use a mechanical process prior to any chemical process to obtain better results [15-17]. The mechanical process includes high intensity ultrasonication or HPH (high pressure homogenization) whereas chemical process popularly contains either one of acid hydrolysis, ionic liquid or TEMPO oxidation method [17,35-37].

2.1. Pre-treatment of lignocellulose materials

The desired raw material is to be washed, dried and sieved to smallest size before any pre-treatments. This is further purified to remove any non-cellulosic compositions and further isolation process is carried out.

2.1.1. Alkaline Pre-treatment

This is a chemical treatment involving an alkali. The immersion of the natural fibers is to be done at a specified temperature and time period with a defined concentration of aq. NaOH. Even today this remains a popular process to break down the natural fibers into finer ones. This process distresses the chemical structure of the fibre by getting rid of wax, hemicelluloses and pectins. Both at lower and higher concentrations the interaction of the matrix fibre is possible. The end result yields the small particles with a rougher topography with better aspect ratio enhancing the interaction between the fibers and the matrix [38].

Briefly, fine powder of desired raw material is dispersed in 5% NaOH for about 3 hours under constant stirring at 80-100°C. The resulting cellulose is washed until the effluent is clear and reaches a neutral pH. This facilitates the further exposure of fibre for the acid treatment and extraction procedures. The above procedure has been reproduced without any alterations as mentioned by Onkarappa et. al. [16].

2.1.2 Bleaching Treatment

This method is employed to remove any residual hemicellulose and lignin in phenolic compounds and chromophore groups. On bleaching the exclusion of lignin takes place without posing any threat to the crystallinity or the polymorphism of cellulose. After bleaching, a colourless cellulose with improved ageing resistance is obtained. Various bleaching agents like $NaClO_2$, O_3, O_2, and H_2O_2 are used in this process [39].

The general procedure involves the treatment of alkali treated material with a solution of 5% $NaClO_2$ (2-3 hrs, 80-100°C) under acidic pH. Any residual lignin is completely omitted in this process. The pulp obtained is washed and filtered until it reaches a neutral pH and is dried in an oven, stored for future use. The above procedure has been reproduced without any alterations as mentioned by Onkarappa et. al. [17]

2.2. Extraction of Nanocellulose

As mentioned earlier many mechanical and chemical treatments are present to prepare NC from lignocellulosic biomasses. Here the light is upon the chemical approach of the extraction methods. Popular chemical treatments that yield NC is acid hydrolysis (AH), TEMPO oxidation and ionic liquid (IL). Each of the methods gives rise to different types of NC with different set of morphologies and characters [40].

2.2.1 Acid hydrolysis

Several methods are in practise to prepare NC that are in the arrangement like in cellulose nanocrystals (CNCs). The acid hydrolysis cycle is highly encouraged to chemically transform cellulose. It is done under controlled conditions of time, cellulose to acid ratio with a determined temperature. Formic acid, H_2SO_4, nitric acid, maleic, HCl, nitric and hydrobromic acid is used for AH generally. Variety of organic acid are also being used for this purpose recently [41-48]. H_2SO_4, as a hydrolysing agent, reacts with nanocrystallite surface, -OH groups form the

sulfonic groups with negative charges. The AH of cellulose in amorphous domain engages a rapid protonation of glycosidic oxygen or cyclic oxygen (path 1& 2) followed by glycosidic bond breaking due to addition of water. Hydrolysis creates 2 shorter chain-fragments, thus maintaining the fundamental structure of the backbone. Here, there is a selective hydrolysis i.e., amorphous zone is selectively hydrolysed whereas crystalline zone is unhindered thus, increasing its crystallinity [49].
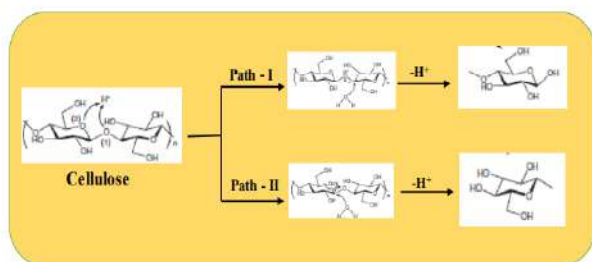
Figure 3. Acid hydrolysis mechanism.

Along with splitting of the chain, acid hydrolysis of cellulose also involves esterification of -OH groups partially. The surface of the NC obtained by H_2SO_4 gives it a negative charge due to the presence of the sulphate groups. This method also prevents the aggregation of CNC and increases the thermal stability by this method. In order to enhance its thermal stability, the introduction of NaOH is to be done to neutralize the sulphate groups [50].

CNCs obtained using HCl result in a low surface charge as it experiences electrostatic repulsion whereas when synthesized from H_2SO_4 gives a better colloidal suspension [51]. To obtain NC from cellulose, AH is more recommendable when the influencing factors like cost-effectiveness, availability and time factor is considered [52].

The general practice encompasses the dissolution of desired amount of cellulose in 50 mL of 60% wt./vol sulphuric acid (45°C, 1 hr, 500 rpm). The reaction is quenched by the addition of cold water. The resulting slurry is to be washed using NaOH and ultrasonicated for better results. The end product is stored at 4°C in a refrigerator [17].

Derived from the results of X-ray investigations, the CNCs crystallinity slightly increased in the acid concentration range of 50–

60wt percent. On the other hand, due to enhancement of solubility in conc. H_2SO_4, partial decrystallization of the nanoparticles occurred when concentration of H_2SO_4 is larger than 60wt percent. Output characterization showed that 60wt percent acid cellulose hydrolysis yielded 65–70wt percent CNC. The cellulose sample was completely dissolved when concentration of H_2SO_4 is larger than 65wt percent. The yield of cellulose-composed and regenerated particles from 65wt percent acid was low (around 20wt percent). These particles also showed a decreased crystallinity degree (around 30 percent) & DP (around 60).

Due to the cellulose's rapid acid depolymerisation with the 67wt % acid, the water-soluble oligomers are formed. SEM and TEM studies revealed that aggregates with 300 to 500nm in length & 40 to 60 nm in size were obtained after hydrolysis with 50 –55wt %. A rise in acid concentration to about 60wt percent has led to the development of nanoscale CNCs of 10–20 nm. Thus, decrement in concentration of acid (50–55wt percent) resulted an overly coarse aggregates, on the other hand, increment of acid concentrations (>60wt percent) resulted in a low yield of nanoparticles with re-crystallized structures. The concentration of H_2SO_4 utilized for cellulose hydrolysis has to be 60 wt. percent (approx.) in order to get highly crystalline NPs at optimum yield. Compared to SA hydrolysis, HA cellulose hydrolysis needs a high temperature (60 to 80°C) to obtain similar dimensions [53-55].

2.2.2 TEMPO Oxidation

TEMPO stands for 2, 2, 6, 6-tetramethyl-1-piperidinyloxy. It is a water-soluble stable radical. It is used to isolate nanocellulose fibrils (CNFs) with selective oxidation. To carboxyl in water at pH range 10-11. The use of mechanical treatment of oxidized cellulose will achieve a decrease in the results of the polymerisation degree and nano-scale particles. This approach of nanocellulose synthesis demonstrates that individual nanocellulose with 65-95 percent crystallinities can be obtained [56-58]. It is testified that there is significant decrease

Onkarappa H S. et al.,

in the usage of energy (early over 100) when NC is exposed to this method particularly [59].

De Nooy et.al., was the first one, who applied TEMPO-mediated oxidation to water soluble polysaccharides. The method calls for catalytic TEMPO & NaBr dissolved in solutions of polysaccharide at 10–11pH, and oxidation started by adding NaCl as primary oxidant [60,61]. Likewise, there are various such reactions examined for the region-selective conversion of p-hydroxyls to carboxylate groups [62,63].
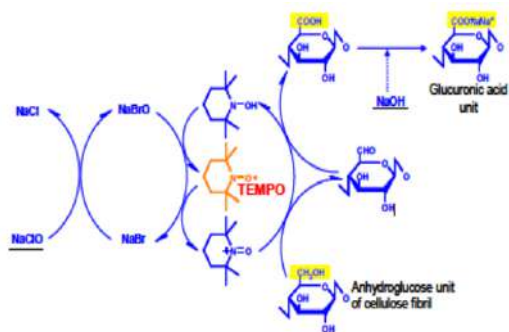
Figure 4. Mechanism of TEMPO Oxidation.

The C6 p-hydroxyl groups are either possibly oxidized by NaCl/TEMPO/NaBr dissolved in water which is maintained at the pH of 10-11. The monitoring of the oxidation is done by the external addition of the aqueous NaOH. There is an increasing need of NaOH consumption by the reaction to maintain the pH at 10-11. It is seen than that this reaction does not yield any water-soluble products [64].

In this method about 1g of cellulose is dispersed in 100 ml of water. 0.1 g NaBr and 0.06 g TEMPO taken with 50 ml of water is added separately to the dispersed cellulose by slowly combining together. The initiation of the oxidation is done by the addition of the 10% (w/v) NaClO. The pH of the reaction mixture is maintained around 10 by using NaOH. The solution is water and the suspension volume is made up to 200 ml which is followed by series of treatments like ultrasonication and homogenization. The end suspension is washed again is stored at 4°C. It is reported that the yield of this method is 95% [16].

2.2.3 Ionic Liquid

Ionic Liquids (IL) are the class of organic slats that exist in fluid state at 373K. They are couples with intriguing properties like chemical stability, thermal stability, extreme low pressure and non-flammability [65,66]. The dissolution of cellulose in IL permits the use of natural biopolymers in green-chemistry which not only results in bio-renewability but is also environment friendly and cost efficient. Hydrophilic ionic liquids like 1-butyl-3-methylimidazolium chloride and 1-allyl-3-methylimidazolium can readily dissolve cellulose at a specified temperature resulting in a transparent material.

The general mechanism is that the cations present in ILs are interacted by the oxygens present in the cellulose. The latter results in the breakage of heavy H-bonding and yields the desired product [67]. It is also reported that microwave heating can also fasten the process. By observing the above mechanism, it can be encouragingly said that IL can be considered as a method of extraction of NC from cellulose.
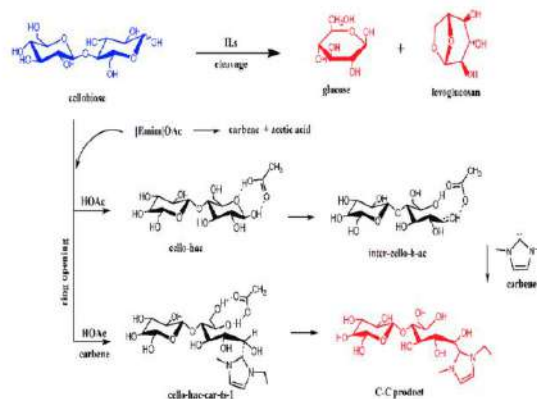
Figure 5. Mechanism of Ionic Liquid method.

Briefly, 1g of cellulose powder slowly introduced to the IL solution at high temperature under constant homogenization. The pale solution formation indicates the formation NC. The precipitated NC is to be filter washed and dried for future use. This method is comparatively easy to perform when compared to the other conventional methods [18].

3. Types of nanocellulose

When the length or the diameter of the cellulose is in the size of the nano, these cellulose derivatives are termed as Nanocellulose [68]. There exist different types of NC based on its extraction

methods. It is important to note that nanofibers contain both crystalline and amorphous regions. Bacterial Cellulose (BC), Cellulose nano crystals (CNC), and Electron spun nanofibers (ECNF) are the different class of nanocellulose and each of them depend on the extraction method employed. For instance, a top-down process results in CNC and NFC whereas BC and ECNF are obtained by bottom-up process where sugars with lower molecular formulas (Cellulose or BC) can be obtained into nanofibers [69]. The major concern in producing CNF in large scale is the geographical limit to find the bacteria in the respective area and also the yield obtained is comparatively less than that of the plant-based cellulose. All the cellulose derivatives are analogous in nature slightly differ in morphology, particle size, structure and crystallinity index based on its method of extraction and raw material [70-72]

3.1 Cellulose Nanocrystal (CNC)
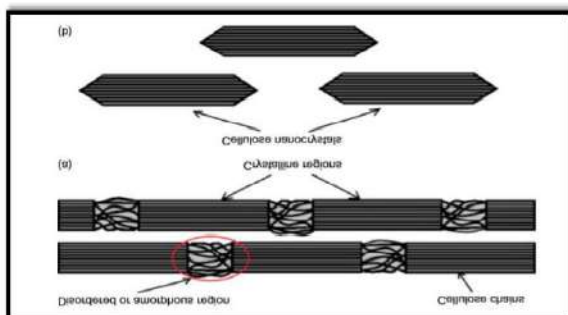
Figure 6. Selective degradation of Acid Hydrolysis leading to rod like structures of CNC.

These are "rod" like or "pointy" structures that are highly crystalline with length and breadth around <25nm and <750nm respectively. When cellulose under goes acid hydrolysis, they result in CNCs where the amorphous regions detain itself from the crystalline domain. The crystalline domains are not affected by hydrolysis but the amorphous regions are; because they are easily accessible by acid for its hydrolytic action caused due to steric hindrance and kinetic force. CNCs can be achieved through acid hydrolysis using two different acids namely HCl (Hydrochloric Acid) and H_2SO_4 (Sulphuric Acid). In Acid Hydrolysis, there is more scope for selective degradation. There is a significant difference between CNC's obtained from HCl to that of H_2SO_4. The end product obtained by H_2SO_4 hydrolysis yields in a

stable suspension as surface charge is present; on the other hand, HCl hydrolysis yields CNC that is having no surface charge resulting in less stable suspension [73]. The negative charge is due to the di-carboxylic acid formed by substituting ester for one acid group. This leads to repulsion of the particles which prevents from the aggregation of the particles in dispersion [74].

It is important to remember that the surface charge of the fibers is higher for the longer time of the reaction. It also effects on the length of the fibers of CNC's [75,76]. Because of its high crystallinity, it is less compatible when compared to CNF's [77]. They are also referred as nano-rods. The crystalline contact in the cellulose is broke by hydrolysis with concentrated acids. The formation of sulphate ester groups gives negative charge to this, thus improving the phase-stability of the particles in dispersion form. The estimated Young's Modulus of CNC's is 167.5 GPa which is larger than that of Young's modulus of steel [78]. BC have longer nano crystallites and higher crystallinity when compared to other source of cellulose. The CNC's obtained are longer than that of Wood sourced CNC's. CNC has "chiral nematic phases". When CNC's are dispersed in water beyond these critical concentrations, they show "chiral nematic liquid crystalline phase" [79,80].
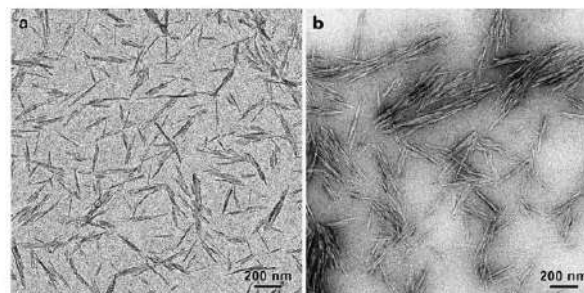
Figure 7. TEM images of cellulose nanocrystals

3.2 Cellulose Nanofibers (CNF)

In sense of literature terms, CNF and CMF are considered as synonyms of each other. CNF's are basically nanofibrils found in bundles with alternate amorphous and crystalline areas. The typical width and length of CNF can go up to 50nm and 2000nm respectively. The nanocellulose obtained from mechanical treatment is addressed by various terms like NFC (Nano fibrillated Cellulose), CNF (Cellulose Nano Fibers), and CF

Onkarappa H S. et al.,

(Cellulose Filaments). The mechanical treatment is mainly used to achieve the bands of cellulose microfibrils. As the name suggests the morphology of this is in terms of nanoscale. In 1983, with the aid of "Gaulin Laboratory homogenizer", NFC was first obtained [81]. The number of hydrogen bonds and surface area is increased during delamination process. Due to this, CNF's show high viscosity and ability to form gels. Since they form in gels, they have hydrophilicity and this restricts them back to form dispersion with hydrophobic polymers. The need of high energy for this process can be overcome by surface modifications and with selected pre-treatments. Inspite of the drawbacks of CNC's, it is highly entertained by researchers due to its applications in coatings, construction, personal care, composites, etc. [82].

There is no need for pre-treatment if the material subjecting to the mechanical pre-treatment is soft wood. Thus, soft wood is highly recommended to quarantine CNF. CNF's so obtained tend to form in suspension with strong surface area. The large consumption of energy in producing CNF's has always remained challenge but treatments like oxidation using TEMPO, mild acid treatment, HPH (High Pressure Homogenization), carboxylation, enzymatic treatment of cellulose reduce the energy consumption significantly.

Figure 8. Cellulose nano fibers and TEM image of CNF

Studies show that the raw material used to produce CNF's through mechanical degradation influence the energy consumed majorly. CNF's cannot be used in paper manufacturing since they contain a greater number of hydrophilic hydroxyl groups which decrease CNF strengthening with polymers [83]. The nanocellulose obtained from mechanical treatment is addressed by various terms like NFC (Nano fibrillated Cellulose), CNF

(Cellulose Nano Fibers), and CF (Cellulose Filaments). The mechanical treatment is mainly used to achieve the bands of cellulose-microfibrils. As the name suggests, the morphology of this is in terms of nanoscale

3.3 Cellulose Nanowhiskers (CNW)

Nanowhisker class of filament has diameter in the range 1-100 nm & length/diameter ratio greater than 100 nm. CNW is rod-like crystalline particles (relative crystallinity-index above 75%) with rectangular cross-section. The acid hydrolysis of natural cellulose fibres usually requires hydrochloric or sulfuric acid to form these. The cellulosic extraction in the form of CNW's can also synthesised by acid hydrolysis method. Whiskers are nearly several hundred times stronger compared to normal crystals & can show great durability, resistance to corrosion. Micro-scale whiskers were widely employed as reinforcing fibres to yield composites with improved mechanical properties. But however, spontaneous whisker configuration at metal surfaces such as zinc or tin, for example, can lead to short circuits and electrical equipment malfunction [84-88].

Figure 9. TEM images of Cellulose nano whiskers (CNW)

The goals to achieve green chemistry, eco-efficiency and sustainability are greatly motivated by researching the production of new materials and green processes. Eco concerns have attained substantial interest to date and could not be disregarded. Hence, it is becoming increasingly necessary to create recycle-based and sustainable communities. A strong driving force is introduced into the synthetic production of environmentally friendly and biocompatible goods towards the exploitation of nanocellulose as promising green, safe and biodegradable material.

4. Future aspect and applications

Onkarappa H S. et al.,

To this date, nanocellulose is having numerous applications in different fields like in bio-medicine, composites, paper industry, aerospace construction, bioelectronic sensors, automobiles, etc. NC can be used in the preparation of films formed from nanocomposites with the aid of VIT research pouches that are bio-based flexible nano-paper transistor which is transparent. With NFC and alginate, one can produce the stream of human-ear. Because of its high-water holding capacity, high strength, good aspect ratio which makes it more applicable in the composite production field [89-94].

It is versatile in nature as it has good water-retaining capacity. They are used in making products used in personal care and also in paints. It is used in ultra-filter papers, transparent solar cells, sensors, and electronics due to its striking optical properties. It plays an imperative role in the pharmaceutical sector, such as in the production of human artificial body parts, biomedicine, tissue engineering and drug packaging [95]. It also acts as a strengthened so it is used in crack reduction, lightweight appliances, concrete and foamed structures [96].

NC can be used in construction and construction materials as it enhances the strength of the building materials like biodegradable and renewable matrix polymers [97]. NFC acts as a dimensional strengthened and is also transparent in nature. This can be applied in building huge flexible screens, compatible computers and also solar panels [98,99]. It is also used as a storage device as it is flexible in nature and has high thermal capacity. Apart from these, Packaging, Composites, Coatings and Paints, Biomedicine, Optical Materials are the major sectors which use NC as one of their major source/raw material.

5. Conclusion

Nanocellulose built materials is significant in major applications. To find any compatible material, it is vital to do the necessary literature survey regarding the extraction methods. The present article gives a proper insight on the various extraction methods that can be employed to obtain NC. The focus entitles to give the thorough procedures in one single articles with a comparative data to select the relevant extraction method depending on the raw material.

References

[1] Dang, J.M. and Leong, K.W., 2006. Natural polymers for gene delivery and tissue engineering. Advanced drug delivery reviews, 58(4), pp.487-499.

[2] Pillai, O. and Panchagnula, R., 2001. Polymers in drug delivery. Current opinion in chemical biology, 5(4), pp.447-451.

[3] Pushpamalar, J., Veeramachineni, A.K., Owh, C. and Loh, X.J., 2016. Biodegradable polysaccharides for controlled drug delivery. ChemPlusChem, 81(6), p.504.

[4] Trache, D., 2018. Nanocellulose as a promising sustainable material for biomedical applications. AIMS Mater Sci 5: 201–205.

[5] Xu, Y. X., Dzenis, Y., & Hanna, M. A. (2005). Water solubility, thermal characteristics and biodegradability of extruded starch acetate foams. Industrial Crops and Products, 21(3), 361-368.

[6] Deepa, B., Abraham, E., Cordeiro, N., Mozetic, M., Mathew, A.P., Oksman, K., Faria, M., Thomas, S. and Pothan, L.A., 2015. Utilization of various lignocellulosic biomass for the production of nanocellulose: a comparative study. Cellulose, 22(2), pp.1075-1090.

[7] Lennholm, H., & Henriksson, G. (2007). Cellulose and Carbohydrate chemistry. Ljungberg Textbook Book, 1.

[8] Du, H., Liu, W., Zhang, M., Si, C., Zhang, X. and Li, B., 2019. Cellulose nanocrystals and cellulose nanofibrils based hydrogels for biomedical applications. Carbohydrate polymers, 209, pp.130-144.

[9] Kondo, T., 1997. The assignment of IR absorption bands due to free hydroxyl groups in cellulose. Cellulose, 4(4), pp.281-292.

[10] Bhimte, N.A. and Tayade, P.T., 2007. Evaluation of microcrystalline cellulose prepared from sisal fibers as a tablet excipient: a technical note. Aaps Pharmscitech, 8(1), pp.E56-E62.

[11] Jahan, M.S., Saeed, A., He, Z. and Ni, Y., 2011. Jute as raw material for the preparation of microcrystalline cellulose. Cellulose, 18(2), pp.451-459.

Onkarappa H S. et al.,

[12] Liu, R., Yu, H. and Huang, Y., 2005. Structure and morphology of cellulose in wheat straw. Cellulose, 12(1), pp.25-34.

[13] Rosa, M.F., Medeiros, E.S., Malmonge, J.A., Gregorski, K.S., Wood, D.F., Mattoso, L.H.C., Glenn, G., Orts, W.J. and Imam, S.H., 2010. Cellulose nanowhiskers from coconut husk fibers: Effect of preparation conditions on their thermal and morphological behavior. Carbohydrate polymers, 81(1), pp.83-92.

[14] Zhang, J., Song, H., Lin, L., Zhuang, J., Pang, C. and Liu, S., 2012. Microfibrillated cellulose from bamboo pulp and its properties. Biomass and Bioenergy, 39, pp.78-83.

[15] Onkarappa, H.S., Prakash, G.K., Pujar, G.H., Kumar, C.R., Latha, M.S. and Betageri, V.S., 2020. Synthesis and characterization of nanocellulose using renewable resources through Ionic liquid medium. Advances in Natural Sciences: Nanoscience and Nanotechnology, 11(3), p.035001.

[16] Onkarappa, H.S., Prakash, G.K., Pujar, G.H., Kumar, C.R., Latha, M.S. and Betageri, V.S., 2020. Hevea brasiliensis mediated synthesis of nanocellulose: Effect of preparation methods on morphology and properties. International Journal of Biological Macromolecules, 160, pp.1021-1028.

[17] Onkarappa, H.S., Prakash, G.K., Pujar, G.H., Rajith Kumar, C.R. and Betageri, V.S., 2020. Facile synthesis and characterization of nanocellulose from Zea mays husk. Polymer Composites, 41(8), pp.3153-3159.

[18] Raghav, N., Sharma, M.R. and Kennedy, J.F., 2021. Nanocellulose: A mini-review on types and use in drug delivery systems. Carbohydrate Polymer Technologies and Applications, 2, p.100031.

[19] Pathania, D., Gupta, D., Kothiyal, N.C., Eldesoky, G.E. and Naushad, M., 2016. Preparation of a novel chitosan-g-poly (acrylamide)/Zn nanocomposite hydrogel and its applications for controlled drug delivery of ofloxacin. International journal of biological macromolecules, 84, pp.340-348.

[20] Kimura, S., & Itoh, T. (1996). New cellulose synthesizing complexes (terminal complexes) involved in animal cellulose biosynthesis in the tunicateMetandrocarpa uedai. Protoplasma, 194(3-4), 151-163.

[21] Sjostrom, E. (1993). Wood chemistry: fundamentals and applications. Gulf professional publishing.

[22] Nechyporchuk, O., Belgacem, M. N., & Bras, J. (2016). Production of cellulose nanofibrils: A review of recent advances. Industrial Crops and Products, 93, 2-25.

[23] Lin, N., & Dufresne, A. (2014). Nanocellulose in biomedicine: Current status and future prospect. European Polymer Journal, 59, 302-325.

[24] Neto, W. P. F., Silvério, H. A., Dantas, N. O., & Pasquini, D. (2013). Extraction and characterization of cellulose nanocrystals from agro-industrial residue–Soy hulls. Industrial Crops and Products, 42, 480-488.

[25] Okubo, K., Fujii, T., & Yamashita, N. (2005). Improvement of interfacial adhesion in bamboo polymer composite enhanced with micro-fibrillated cellulose. JSME International Journal Series A Solid Mechanics and Material Engineering, 48(4), 199- 204.

[26] Hentze, H. P. (2010). From nanocellulose science towards applications. Developments in advanced biocomposites, 71.

[27] Saini, S., Sillard, C., Belgacem, M. N., & Bras, J. (2016). Nisin anchored cellulose nanofibers for long term antimicrobial active food packaging. RSC advances, 6(15), 12422-12430.

[28] Johansson, C., Bras, J., Mondragon, I., Nechita, P., Plackett, D., Simon, P., . & Aucejo, S. (2012). Renewable fibers and bio-based materials for packaging applications–a review of recent developments. BioResources, 7(2), 2506-2552.

[29] Jackson, J. K., Letchford, K., Wasserman, B. Z., Ye, L., Hamad, W. Y., & Burt, H. M. (2011). The use of nanocrystalline cellulose for the binding and controlled release of drugs. International journal of nanomedicine, 6, 321.

[30] M.K.M. Haafiz, A. Hassan, Z. Zakaria, I.M. Inuwa, Isolation and characterization of cellulose nanowhiskers from oil palm biomass microcrystalline cellulose, Carbohydr. Polym. 103 (2014) 119–125.

[31] M.K.M. Haafiz, S.J. Eichhorn, A. Hassan, M. Jawaid, Isolation and characterization of microcrystalline cellulose from oil palm biomass residue, Carbohydr. Polym. 93 (2013) 628–634.

Onkarappa H S. et al.,

[32] A.M. Adel, Z.H.A. El-Wahab, A.A. Ibrahim, M.T. Al-Shemy, Characterization of microcrystalline cellulose prepared from lignocellulosic materials. Part I. acid catalyzed hydrolysis, Bioresour. Technol. 101 (2010) 4446–4455.

[33] E. Abraham, B. Deepa, L.A. Pothen, J. Cintil, S. Thomas, M.J. John, R. Anandjiwala, S.S. Narine, Environmental friendly method for the extraction of coir fibre and isolation of nanofibre, Carbohydr. Polym. 92 (2013) 1477– 1483.

[34] R. Li, J. Fei, Y. Cai, Y. Li, J. Feng, J. Yao, Cellulose whiskers extracted from mulberry: a novel biomass production, Carbohydr. Polym. 76 (2009) 94–99.

[35] Jagadesh, P., Ramachandramurthy, A. and Murugesan, R., 2018. Evaluation of mechanical properties of Sugar Cane Bagasse Ash concrete. Construction and Building Materials, 176, pp.608-617.

[36] Lin, N. and Dufresne, A., 2014. Nanocellulose in biomedicine: Current status and future prospect. European Polymer Journal, 59, pp.302-325.

[37] Liu, S., Cheng, G., Xiong, Y., Ding, Y. and Luo, X., 2020. Adsorption of low concentrations of bromide ions from water by cellulose-based beads modified with TEMPO-mediated oxidation and Fe (III) complexation. Journal of hazardous materials, 384, p.121195.

[38] Naveen, J., Jawaid, M., Amuthakkannan, P., & Chandrasekar, M. (2019). Mechanical and physical properties of sisal and hybrid sisal fiber-reinforced polymer composites. In Mechanical and physical testing of biocomposites, fibre-reinforced composites and hybrid composites (pp. 427-440). Woodhead Publishing.

[39] Yuan, Z., Ni, Y., and Van Heiningen, A. (1997) Kinetics of peracetic acid decomposition: part I: spontaneous decomposition at typical pulp bleaching conditions. Can. J. Chem. Eng., 75 (1), 37–41.

[40] Jagadesh, P., Ramachandramurthy, A., & Murugesan, R. (2018). Evaluation of mechanical properties of Sugar Cane Bagasse Ash concrete. Construction and Building Materials, 176, 608-617.

[41] Lin, N., & Dufresne, A. (2014). Nanocellulose in biomedicine: Current status and future prospect. European Polymer Journal, 59, 302-325.

[42] Araki, J., Wada, M., Kuga, S., & Okano, T. (1998). Flow properties of microcrystalline cellulose suspension prepared by acid treatment of native cellulose. Colloids and Surfaces A: Physicochemical and Engineering Aspects, 142(1), 75-82.

[43] Yu, H., Qin, Z., Liang, B., Liu, N., Zhou, Z., & Chen, L. (2013). Facile extraction of thermally stable cellulose nanocrystals with a high yield of 93% through hydrochloric acid hydrolysis under hydrothermal conditions. Journal of Materials Chemistry A, 1(12), 3938-3944.

[44] Camarero Espinosa, S., Kuhnt, T., Foster, E. J., & Weder, C. (2013). Isolation of thermally stable cellulose nanocrystals by phosphoric acid hydrolysis. Biomacromolecules, 14(4), 1223-1230.

[45] Koshizawa, T. (1960) Degradation of wood cellulose and cotton linters in phosphoric acid. Jpn. Tappi J., 14 (7), 455–458, 475.

[46] Um, B.H., Karim, M.N., and Henk, L.L. (2003) Effect of sulfuric and phosphoric acid pretreatments on enzymatic hydrolysis of corn stover. Appl.Biochem. Biotechnol., 105 (1–3), 115–125.

[47] Filson, P.B. and Dawson-Andoh, B.E. (2009) Sono-chemical preparation of cellulose nanocrystals from lignocellulose derived materials. Bioresour.Technol., 100 (7), 2259–2264.

[48] Liu, D., Zhong, T., Chang, P.R., Li, K., and Wu, Q. (2010) Starch composites reinforced by bamboo cellulosic crystals. Bioresour. Technol., 101, 2529–2536.

[49] Bai, W., Holbery, J., and Li, K.C. (2009) A technique for production of nanocrystalline cellulose with a narrow size distribution. Cellulose, 16 (3), 455–465.

[50] De Souza Lima, M.M. and Borsali, R. (2002) Static and dynamic light scattering from polyelectrolyte microcrystal cellulose. Langmuir, 18 (4), 992–996.

[51] M. A. Hubbe, O. J. Rojas, L. A. Lucia, M. Sain, Bioresources 2008, 3(3), 929

[52] F. Deng, M.-C. Li, X. Ge, Y. Zhang, U. R. Cho, Polym. Compos. 2015, 38, E137.

Onkarappa H S. et al.,

[53] Ioelovich, M. (2012) Optimal conditions for isolation of nano-crystalline cellulose particles. Nanosci. Nanotechnol., 2 (2), 9–13.

[54] Ioelovich, M. and Leykin, A. (2006) Formation of nanostructure of microcrystalline cellulose. Cellul. Chem. Technol., 40 (5), 313–317.

[55] Li, Y. and Ragauskas, A.J. (2011) Cellulose nano whiskers as a reinforcing filler in polyurethanes. Algae, 75 (80), 10–15.

[56] Saito, T., & Isogai, A. (2004). TEMPO-mediated oxidation of native cellulose. The effect of oxidation conditions on chemical and crystal structures of the water-insoluble fractions. Biomacromolecules, 5(5), 1983-1989.

[57] Saito, T., Kimura, S., Nishiyama, Y., & Isogai, A. (2007). Cellulose nanofibers prepared by TEMPO-mediated oxidation of native cellulose. Biomacromolecules, 8(8), 2485- 2491.

[58] Isogai, A., Saito, T., & Fukuzumi, H. (2011). TEMPO-oxidized cellulose nanofibers. nanoscale, 3(1), 71-85.

[59] Bragd, P. L., Van Bekkum, H., & Besemer, A. C. (2004). TEMPO-mediated oxidation of polysaccharides: survey of methods and applications. Topics in Catalysis, 27(1-4), 49- 66.

[60] De Nooy, A. E., Besemer, A. C., & van Bekkum, H. (1996). On the use of stable organic nitroxyl radicals for the oxidation of primary and secondary alcohols. Synthesis, 1996(10), 1153-1176.

[61] De Nooy, A. E., Besemer, A. C., & van Bekkum, H. (1995). Highly selective nitroxyl radical-mediated oxidation of primary alcohol groups in water-soluble glucans. Carbohydrate research, 269(1), 89-98.

[62] Bailey, W. F., Bobbitt, J. M., & Wiberg, K. B. (2007). Mechanism of the oxidation of alcohols by oxoammonium cations. The Journal of organic chemistry, 72(12), 4504- 4509.

[63] de Nooy, A. E., Besemer, A. C., & van Bekkum, H. (1995). Selective oxidation of primary alcohols mediated by nitroxyl radical in aqueous solution. Kinetics and mechanism. Tetrahedron, 51(29), 8023-8032.

[64] Bragd, P. L., Van Bekkum, H., & Besemer, A. C. (2004). TEMPO-mediated oxidation of polysaccharides: survey of methods and applications. Topics in Catalysis, 27(1-4), 49- 66.

[65] Liu Q, Janssen M H, van Rantwijk F and Sheldon R A 2005 Green Chemistry 7 39–42

[66] Xie H, Li S and Zhang S 2005 Green Chemistry 7 606–8.

[67] Feng L and Chen Z L 2008 Journal of Molecular Liquids 142 1–5.

[68] Moon, R.J., Martini, A., Nairn, J., Simonsen, J. and Youngblood, J., 2011. Cellulose nanomaterials review: structure, properties and nanocomposites. Chemical Society Reviews, 40(7), pp.3941-3994.

[69] Bhushan, B. (2017). Introduction to nanotechnology. In Springer handbook of nanotechnology (pp. 1-19). Springer, Berlin, Heidelberg.

[70] Borrega, M. and Orelma, H., 2019. Cellulose Nanofibril (CNF) Films and xylan from hot water extracted birch kraft pulps. Applied Sciences, 9(16), p.3436.

[71] Lavoine, N., Desloges, I., Dufresne, A. and Bras, J., 2012. Microfibrillated cellulose–Its barrier properties and applications in cellulosic materials: A review. Carbohydrate polymers, 90(2), pp.735-764.

[72] Phanthong, P., Reubroycharoen, P., Hao, X., Xu, G., Abudula, A. and Guan, G., 2018. Nanocellulose: Extraction and application. Carbon Resources Conversion, 1(1), pp.32-43.

[73] Favier, V., Canova, G. R., Cavaillé, J. Y., Chanzy, H., Dufresne, A., & Gauthier, C. (1995). Nanocomposite materials from latex and cellulose whiskers. Polymers for Advanced Technologies, 6(5), 351-355.

[74] Lu, A., Hemraz, U., Khalili, Z., & Boluk, Y. (2014). Unique viscoelastic behaviors of colloidal nanocrystalline cellulose aqueous suspensions. Cellulose, 21(3), 1239-1250.

[75] Klemm, D., Heublein, B., Fink, H. P., & Bohn, A. (2005). Cellulose: fascinating biopolymer and sustainable raw material. Angewandte chemie international edition, 44(22), 3358-3393.

[76] Börjesson, M., & Westman, G. (2015). Crystalline nanocellulose—preparation, modification, and properties. Cellulose-fundamental aspects and current trends, 159-191.

[77] Dong, X. M., Revol, J. F., & Gray, D. G. (1998). Effect of microcrystallite preparation

Onkarappa H S. et al.,

conditions on the formation of colloid crystals of cellulose. Cellulose, 5(1), 19-32

[78] Dugan, J. M., Gough, J. E., & Eichhorn, S. J. (2013). Bacterial cellulose scaffolds and cellulose nanowhiskers for tissue engineering. Nanomedicine, 8(2), 287-298.

[79] Revol, J. F., Bradford, H., Giasson, J., Marchessault, R. H., & Gray, D. G. (1992). Helicoidal self-ordering of cellulose microfibrils in aqueous suspension. International journal of biological macromolecules, 14(3), 170-172

[80] Tashiro, K., & Kobayashi, M. (1991). Theoretical evaluation of three-dimensional elastic constants of native and regenerated celluloses: role of hydrogen bonds. Polymer, 32(8), 1516-1526.

[80] Tashiro, K., & Kobayashi, M. (1991). Theoretical evaluation of three-dimensional elastic constants of native and regenerated celluloses: role of hydrogen bonds. Polymer, 32(8), 1516-1526.

[81] Peng, B. L., Dhar, N., Liu, H. L., & Tam, K. C. (2011). Chemistry and applications of nanocrystalline cellulose and its derivatives: a nanotechnology perspective. The Canadian Journal of Chemical Engineering, 89(5), 1191-1206.

[82] Moon, R. J., Martini, A., Nairn, J., Simonsen, J., & Youngblood, J. (2011). Cellulose nanomaterials review: structure, properties and nanocomposites. Chemical Society Reviews, 40(7), 3941-3994.

[83] Jonoobi, M., Oladi, R., Davoudpour, Y., Oksman, K., Dufresne, A., Hamzeh, Y., & Davoodi, R. (2015). Different preparation methods and properties of nanostructured cellulose from various natural resources and residues: a review. Cellulose, 22(2), 935- 969.

[84] Ciolacu, D., Ciolacu, F., & Popa, V. I. (2011). Amorphous cellulose—structure and characterization. Cellulose chemistry and technology, 45(1), 13.

[85] Missoum, K., Belgacem, M. N., & Bras, J. (2013). Nanofibrillated cellulose surface modification: a review. Materials, 6(5), 1745-1766.

[86] Lia, X. F., Dinga, E. Y., & Li, G. K. (2001). A method of preparing spherical nanocrystal cellulose with mixed crystalline forms of cellulose. 19(3), 291-296.

[87] Heath, L., & Thielemans, W. (2010). Cellulose nanowhisker aerogels. Green Chemistry, 12(8), 1448-1453.

[88] Fang, F., & Markwitz, A. (2009). Controlled fabrication of Si nanostructures by high vacuum electron beam annealing. Physica E: Low-dimensional Systems and Nanostructures, 41(10), 1853-185

[89] Liu S, Liu YJ, Deng F, Ma M-G, Bian J.(2015). Comparision of the effects of microcrystalline cellulose and nanocrystalline cellulose on Fe3O4/C nanocomposites.RSC Adv 5:7419874205.

[90] Khalil, H. A., Davoudpour, Y., Islam, M. N., Mustapha, A., Sudesh, K., Dungani, R., & Jawaid, M. (2014). Production and modification of nanofibrillated cellulose using various mechanical processes: a review. Carbohydrate polymers, 99, 649-665.

[91] Österberg, M., & Cranston, E. D. (2014). Special issue on nanocellulose. Nordic Pulp & Paper Research Journal, 29(1), 4-5.

[92] Xiaoyun, Q., & Shuwen, H. (2013). 'Smart. materials based on cellulose: a review of the preparations, properties, and applications. Materials, 6, 738-781.

[93] Kim, J. H., Shim, B. S., Kim, H. S., Lee, Y. J., Min, S. K., Jang, D., ... & Kim, J. (2015). Review of nanocellulose for sustainable future materials. International Journal of Precision Engineering and Manufacturing-Green Technology, 2(2), 197-213.

[94] Krupa, A., Descamps, M., Willart, J. F., Strach, B., Wyska, E., Jachowicz, R., & Danede, F. (2016). High-energy ball milling as green process to vitrify tadalafil and improve bioavailability. Molecular pharmaceutics, 13(11), 3891-3902.

[95] Rajinipriya, M., Nagalakshmaiah, M., Robert, M., & Elkoun, S. (2018). Importance of agricultural and industrial waste in the field of nanocellulose and recent industrial developments of wood based nanocellulose: a review. ACS Sustainable Chemistry & Engineering, 6(3), 2807-2828

[96] Su, Y., Yang, B., Liu, J., Sun, B., Cao, C., Zou, X.... & He, Z. (2018). Prospects for replacement of some plastics in packaging with lignocellulose materials: A brief review. BioResources, 13(2), 4550-4576.

Onkarappa H S. et al.,

[97] Zhu, H., Hu, L., Cumings, J., Huang, J., Chen, Y., Preston, C., & Rohrbach, K. (2013). Highly transparent and flexible nanopaper transistor. ACS Nano, 7(3), 2106-2113.

[98] Markstedt, K., Mantas, A., Tournier, I., Martínez Ávila, H., Hagg, D., & Gatenholm, P. (2015). 3D bioprinting human chondrocytes with nanocellulose–alginate bioink for cartilage tissue engineering applications. Biomacromolecules, 16(5), 1489-1496.

[99] Hentze, H. P. (2010). From nanocellulose science towards applications. Developments in advanced biocomposites, 71.

Karnatak University Journal of Science

Rotational Diffusion Dynamics: A Tool for Exploring Solute–Solvent Interactions

Prajakta S. Kadolkar, Sanjeev R. Inamdar*

Laser Spectroscopy (DRDO/KU) Programme, Department of Physics, Karnatak University, Dharwad-580 003, India.
Corresponding author: *him_lax3@yahoo.com*

ARTICLE INFO	ABSTRACT
	Understanding solute-solvent interactions has been of great importance in physical-chemistry to determine properties of liquids and solutions. This mini review describes the effect of solute-solvent interactions on rotational relaxation of molecules in solvents. To understand experimental results different theories such as hydrodynamic friction, dielectric friction and specific solute-solvent interactions, particularly hydrogen bonding which affects the molecular rotation is discussed for both polar and nonpolar probes. Effect of bivaluedness of viscosity of binary solvent mixtures at different compositions is discussed separately. Finally the rotational dynamics of three polar dyes were investigated in Binary solvent mixtures of aqueous Dimethyl Sulfoxide and aqueous 2-Propanol.

1. Introduction:

The liquid phase is bordered by solid phase on one side, in which spatial relationship between the molecules is fixed on time scale which can be accessed using structural measurements such as X-ray diffraction and multidimensional NMR spectrometry, and molecules of gas phase on the other side, which can be understood by simple statistical description of collisional interactions between gas molecules. Molecules in liquid phase interact with each other as they possess both the mobility and proximity. These intermolecular interactions in liquid phase are more complex because of their characteristic strength and have a strong bearing on many physicochemical properties of liquids and solutions. Hence, the study of intermolecular interactions between solvent-solvent and solute-solvent forms one of the central topics on

research in physical chemistry. Regardless of continuous investigation, the details of solute-solvent interactions, particularly for polar probe in polar solvent, is yet to be understood systematically. To tackle this problem different approaches (experimental, theoretical and computational) are being adopted [1-3].

Rotational reorientation of molecules in solution is an important concept in experimental and theoretical studies of investigating intermolecular interactions. This has proven to be the most useful due to the generality of the effect and the well-developed theoretical composition for the interpretation of experimental results [4-9]. In molecular reorientation or rotational diffusion experiments, the excitation of isotropically distributed molecules with linearly polarized light produces anisotropy in the orientational

Prajakta S. Kadolkar and Sanjeev R. Inamdar

distribution of molecules which then decays in time (the reorientational relaxation time, τ_r). Thus, this randomized rotational motions of the molecules leads to depolarization of the emitted radiation [10]. The effect of solute-solvent interactions on the rotational motion of probe molecule is generally described as a friction to probe's rotational motion and can be classified in three types. The first class includes short-range repulsive forces which influence intermolecular dynamics of molecular collisions. These interactions, which are present in all liquids, lead to viscous dissipation and is well described by hydrodynamic theories [11]. The second class includes long range electrostatic interactions between a polar probe and polar solvent molecules. A rotating solute induces solvent polarization, that lags behind rotation of solute creating a torque and reducing the rate of rotational diffusion. This effect is termed as dielectric friction[12-14]. The third type includes specific solute-solvent interactions. The most encountered example of this is hydrogen bonding. Strong hydrogen bonds will lead to the solute-solvent complexes of well-defined stoichiometry. These larger species can last for fairly long time and will rotate slowly then bare solute. Formation and breakage of weak hydrogen bonds occurring on time scales faster than probe rotation will dissipate the rotational energy of solute, giving rise to additional friction.

Experimental Methods

The experimental techniques used to determine the rotational reorientation times mainly consist of steady state spectrofluorometer and time resolved fluorescence spectrometer employing time correlated single photon counting (TCSPC).

The steady state fluorescence anisotropy for vertical excitation can be expressed as [15,16]

$$\langle r \rangle = \frac{I_\parallel - GI_\perp}{I_\parallel + 2GI_\perp} \qquad (1)$$

Where $I_\parallel$ and $I_\perp$ are the fluorescence intensities parallel and perpendicular polarized components with respect to the polarization of the exciting beam. G=1.14 is an instrumental factor that corrects the polarization bias in the detection system [25] and is given by

$$G = \frac{I_{HV}}{I_{HH}} \qquad (2)$$

Where I_{HV} is the fluorescence intensity when the excitation polarizer is horizontal and emission polarizer is vertical. I_{HH} is the fluorescence intensity when both the polarizers kept constant.

The fluorescence lifetimes (τ_f) of probes is determined using time resolved fluorescence techniques such as time correlated single photon counting (TCSPC). If the decay of fluorescence and of anisotropy$\langle r \rangle$ is presented by single exponential, then the reorientation time (τ_r) is given by the Perrin equation [10].

$$\tau_r = \frac{\tau_f}{\frac{r_0}{\langle r \rangle} - 1} \qquad (3)$$

Where r_0 is the limiting anisotropy. It is determined by freezing all the rotational motions of the molecule.

Understanding rotational diffusion

The rotational diffusion model by Debye [4] is most commonly used among many other proposed models for the study of rotational motion. In this model the reorientation of molecule is assumed to occur in small angular steps. Due to high frequency collisions, a molecule can rotate through a very small angle before undergoing another collision. The rotational diffusion equation solved to obtain the rotational reorientation time τ_r of the density function $\rho(\theta, \varphi)$ is given by [10]

$$\frac{\partial \rho}{\partial t} = D \frac{1}{sin\theta} \frac{\partial}{\partial \theta} \left[\frac{1}{sin\theta} \frac{\partial \rho}{\partial \theta} + \frac{1}{sin^2\theta} \frac{\partial^2 \rho}{\partial \varphi^2} \right] \qquad (4)$$

Where D is the rotational diffusion coefficient. By Stokes-Einstein model the rotational diffusion of a solute is

$$D = \frac{kT}{\zeta} \qquad (5)$$

Where ζ is the friction coefficient and kT is the thermal energy. This friction is of great importance in theoretical as well as experimental studies. A molecule rotating in liquid experiences friction, as a result of its continuous

Prajakta S. Kadolkar and Sanjeev R. Inamdar

interaction with its neighbours. To understand these interactions is the motivating force to study rotational diffusion of liquids.

Hydrodynamic description:

In hydrodynamic theory, mechanical friction on a rotating solute in solvent is computed by treating the solute as a smooth sphere rotating in a continuum fluid, which is characterized by shear viscosity. If η is the viscosity of the liquid and a is the radius of the solute molecule, then according to Stokes law [17]

$$\zeta = 8\pi a^3 \eta \qquad (6)$$

Equation (5) reduces to

$$D = \frac{kT}{8\pi\eta a^3} \qquad (7)$$

The rotational reorientation time τ_r is given by

$$\tau_r = \frac{1}{6D} = \frac{\zeta}{6kT} \qquad (8)$$

Substituting equation (6) in (8) gives

$$\tau_r = \frac{\eta V}{kT} \qquad (9)$$

Where V is the molecular volume of solute. The most widely used Stokes-Einstein-Debye (SED) hydrodynamic equation for spherical molecule is given by

$$\tau_r = \frac{\eta V}{kT} + \tau_0 \qquad (10)$$

where τ_0 is the rotational reorientation time when there is no viscosity. A considerable degree of success in understanding the rotational dynamics of medium sized molecules (few hundred cu.A^0 volumes) has been possible with the Stokes-Einstein-Debye (SED) equation [18-20]

In reality, the exact shape of most solute molecules will be non-spherical and therefore it is necessary to include a parameter which should describe the exact shape of solute molecules. Hence equation of non-spherical molecule proposed by Perrin [5] is given as follows

$$\tau_r = \frac{\eta V}{kT}(fC) \qquad (11)$$

Where f is shape factor and is well specified. For spherical molecules $f=1$. For non-spherical molecules $f>1$ and the magnitude of deviation of f from unity describes the non-spherical nature of the solute molecule. The boundary condition

parameter C, signifies the extent of coupling between solute and the solvent [13]. In the two limiting cases of hydrodynamic boundary condition namely stick and slip for non-spherical solute molecule, the value of C follows inequality, $0<C\geq1$ and the axial ratio of the probe gives the exact value of C. There are experimental evidences of the observed rotational reorientation times being either much longer than stick prediction (called *superstick*) [21,22] or much shorter than slip estimation (called *subslip*) [23-25], both signifying deviation from hydrodynamic boundary condition. A faster rotation than predicted by C_{slip} is not within the framework of hydrodynamics and it becomes necessary to invoke the molecularity of the system.

N. Ohtori et al. suggest that the SED equation depends on shape rather than the size on probe. This is in contrast with the SED relation where size play important role. This suggests overall reconsideration of the relation on a molecular scale. The results from this computational study directly produce a molecular basis SED relation [26], the validity of which is need to be confirmed by undertaking studies of different probes.

Theoretical basis for this approach is provided by the theory of Gierer and Wirtz (GW) [27] which takes into account the relative sizes the solute and solvent molecules whereby a modified value for C can be calculated. A slight variant of the GW model, referred to as "free space model", has been suggested by Dote, Kivelson and Schwartz (DKS) [28], that incorporates the effects of free space in the liquid as well as the relative sizes of solute and solvent. The results for a molecule of size $6.0A^0$ and 6.27Å(largest reported so far), show a significant deviation from the expectations of the existing hydrodynamic theory but is successfully explained using quasihydrodynamic theories [25, 29].

Dielectric friction:

For polar and charged solutes, simple hydrodynamic description arising due to viscosity of solvent becomes inadequate. A

polar molecule rotating in polar solvent experiences additional friction known as dielectric friction along with mechanical friction. These mechanical and dielectric friction are not separable as they are linked due to electro-hydrodynamic coupling [30-35]. Despite this, for practical purpose the sum of the two frictions is used as follows.

$$\zeta_{Total} = \zeta_M + \zeta_{DF} \qquad (12)$$

Different dielectric friction theories such as Nee-Zwanzig theory [36], van der Zwan and Hynes theory [38] and Alavi-Waldeck theory [39] have included the electro-hydrodynamic treatment which explicitly considers the coupling between the hydrodynamic and dielectric friction components.

The Nee-Zwanzig (NZ) theory:

The most influential early treatment of rotational dielectric friction was made by Nee and Zwanzig [36]. The authors presented a theory of dielectric relaxation in polar liquids by generalizing Onsager's well known theory of the static dielectric constant. His static model is turned into a dynamical model by analyzing the dynamical effects of long range dipolar interactions. The expression for dielectric friction coefficient is given as

$$\zeta_D(\omega) = \frac{2kT}{i\omega} \frac{(\varepsilon_0 - \varepsilon_\infty)[\varepsilon(\omega) - \varepsilon_0]}{\varepsilon_0[2\varepsilon(\omega) + \varepsilon_\infty]} \qquad (13)$$

Where ε_0 and ε_∞ are zero frequency dielectric constant and high frequency dielectric constant of the solvent. $\varepsilon(\omega)$ is the complex dielectric constant which is function of frequency ω.

Nee and Zwanzig considered the case of a pure polar fluid and eliminated the cavity radius a and the molecular dipole moment μ. For experimental applications where the solute molecule is different from the solvent molecules Hubbard and Wolynes [37] have rewritten the equation (13) as follows.

$$\tau_{DF}^{NZ} = \frac{\mu^2}{9a^3kT} \frac{(\varepsilon_\infty + 2)^2(\varepsilon_0 - \varepsilon_\infty)}{(2\varepsilon_0 + \varepsilon_\infty)^2} \tau_D \quad (14)$$

$$\tau_{DF}^{NZ} = \frac{\mu^2}{a^3kT} \frac{(\varepsilon_0 - 1)}{(2\varepsilon_0 + 1)^2} \tau_D \qquad (15)$$

$$when\ \varepsilon_\infty = 1$$

where τ_D is debye relaxation time of the solvent. If mechanical and dielectric friction is assumed to be separable, then the observed rotational reorientation time (τ_r^{Obs}) is given as the sum of reorientation time calculated using hydrodynamic theory and dielectric friction theory.

$$\tau_r^{Obs} = \tau_{SED} + \tau_{DF} \qquad (16)$$

Therefore,

$$\tau_r^{obs} = \frac{\eta VfC}{kT} + \frac{\mu^2}{9a^3kT} \frac{(\varepsilon_\infty + 2)^2(\varepsilon_0 - \varepsilon_\infty)}{(2\varepsilon_0 + \varepsilon_\infty)^2} \tau_D$$

$$(17)$$

It is evident from the above equation that dielectric friction contribution is most significant for small molecules with large dipole moments in solvents of low ε and large τ_D values.

The van der Zwan- Hynes (vdZH) theory:

van der Zwan and Hynes (vdZH) [38] proposed a semiempirical method for finding dielectric friction which relates the dielectric friction experienced by solute in a solvent, to stoke's shift (Δv) and solvation time, τ_s as

$$\tau_{DF} = \frac{\mu^2}{(\Delta\mu)^2} \frac{S\tau_s}{6kT} \qquad (18)$$

Where μ is the excited state dipole moment of solute, $\Delta\mu$ is the difference between the ground and excited state dipole moment of the solute and

$$S = h\nu_a - h\nu_f \qquad (19)$$

Where $h\nu_a$ and $h\nu_f$ are the energies of the 0-0 transition for absorption and fluorescence, respectively. The solvation time is approximately equal to solvent longitudinal relaxation time, $\tau_L = \tau_D(\varepsilon_\infty/\varepsilon_0)$ and relatively independent of the solute properties. The observed rotational reorientation time (τ_r^{Obs}) is given by

$$\tau_r^{obs} = \frac{\eta VfC}{kT} + \frac{\mu^2}{(\Delta\mu)^2} \frac{hc\Delta v}{6kT} \qquad (20)$$

The Alavi-Waldeck theory

This theory strongly recommended that the charge distribution, and not the dipole moment, of the solute should be used to calculate the dielectric friction experienced by solute molecule [39]. Not only the dipole moment but also higher order moments of solute, contribute

significantly to dielectric friction and molecules with zero net dipole moment can also experience dielectric friction. Thus, the expression for the dielectric friction is given as

$$\tau_{DF} = P \frac{(\varepsilon_0 - 1)}{(2\varepsilon_0 + 1)^2} \tau_D \qquad (21)$$

where

$$P = \frac{4}{3akT} \sum_{j=1}^{N} \sum_{i=1}^{N} \sum_{L=1}^{L_{max}} \sum_{M=1}^{L} \left(\frac{2L+1}{L+1}\right) \frac{(L-M)!}{(L+M)!} \times$$

$$M^2 q_i q_j \left(\frac{r_i}{a}\right)^L \left(\frac{r_j}{a}\right)^L P_L^M(cos\theta_i) P_L^M(cos\theta_j) cosM\phi_{ij} \qquad (22)$$

Where $P_L^M(x)$ are the associated Legendre polynomials, a is cavity radius, N is the number of partial charges, q_i is the partial charge on atom$i$, whose position is given by $(r_i, \theta_i, \varphi_i)$, and $\varphi_{ji} = \varphi_j - \varphi_i$.

Thus, the magnitude of dielectric friction contribution to the rotational reorientation time τ_r, crucially depends on the dipole moment of the solute (dye) molecule in the first excited electronic state S₁ in Nee-Zwanzig theory, and in van der Z wan and Hynes theory, it depends on the cavity radius a₀, dielectric constant ε and the Debye relaxation time τ_D of the solvent.

Hence, alongside rotational dynamics, the ground and excited state dipole moments of the probe need to be determined in neat/ binary solvent mixtures using steady state spectral data. Excited state dipole moment is another important parameter in dielectric friction theories to be determined. Solvatochromic method is most widely used for determination of dipole moments as the experiments are simple and the data analysis is easy compared to other methods. The procedures were evolved by Lippert [40] and Mataga [41] and in their method, the shift of absorption and fluorescence band maxima is followed using the solvent polarity.

The following equations by Bilot and Kawski [42,43] are based on the quantum mechanical perturbation theory of the absorption and fluorescence band shifts (in wavenumbers) in different solvents of varying dielectric constant (ε) and refractive index (n). Here ground state

(μg) and excited state (μe) dipole moment are assumed to be parallel and α/a₃ = 1/2 (α is the polarizability and 'a' is the Onsager interaction radius of the solute).

$$v_a - v_f = m_1 f(\varepsilon, n) + const \qquad (23)$$

$$v_a - v_f = -m_2 \phi(\varepsilon, n) + const \qquad (24)$$

Where

$$f(\varepsilon, n) = \frac{(2n^2 + 1)}{(n^2 + 2)} \left[\frac{(\varepsilon - 1)}{(\varepsilon + 2)} - \frac{(n^2 - 1)}{(n^2 + 2)}\right] \qquad (25)$$

is the solvent polarity parameter and

$$\phi(\varepsilon, n) = f(\varepsilon, n) + 2g(n) \qquad (26)$$

Where

$$g(n) = \frac{3}{2} \left[\frac{(n^4 - 1)}{(n^2 + 2)^2}\right] \qquad (27)$$

With

$$m_1 = \frac{2(\mu_e - \mu_g)^2}{(hca_0^3)} \qquad (28)$$

And

$$m_2 = \frac{2(\mu_e^2 - \mu_g^2)}{(hca_0^3)} \qquad (29)$$

v_a and v_f are the absorption and emission maxima in wavenumbers. The difference $v_a - v_f$ and the sum $v_a + v_f$ of the wave numbers are linear functions of the solvent polarity parameters $f(\varepsilon, n)$ and $\phi(\varepsilon, n)$, respectively. m₁ and m₂ in Eqs. (23) and (24) are the slopes of these straight lines. In Eqs. (28) and (29) μg and μe represent the dipole moments in the ground and excited state, respectively, h is the Planck's constant, c the velocity of light in vacuum and a₀ the cavity radius of the solute molecule.

The values of μg and μe from (28) and (29)

$$\mu_g = \frac{|m_2 - m_1|}{2} \left[\frac{(hca_0^3)}{2m_1}\right]^{(1/2)} \qquad (30)$$

$$\mu_e = \frac{|m_2 + m_1|}{2} \left[\frac{(hca_0^3)}{2m_1}\right]^{(1/2)} \qquad (31)$$

Thus, the ground and excited state dipole moments can simultaneously be determined by the spectroscopic methods for a given Onsager cavity radius.

Another method proposed by Reichardt [44, 45] gives correlation between spectral shift and

Prajakta S. Kadolkar and Sanjeev R. Inamdar

empirical microscopic solvent polarity parameter (E_T^N) by

$$\nu_a - \nu_f = 11307.6 \left[\left(\frac{\Delta\mu}{\Delta\mu_B} \right)^2 \left(\frac{a_B}{a} \right)^3 \right] E_T^N + const. \tag{32}$$

where $\Delta\mu_B = 9D$ is the change in dipole moment upon excitation and $a_B = 6.2$ Å is Onsager cavity radius for betaine dye. E_T^N is defined using water and tetramethylsilane (TMS) as extreme reference solvent with the equation.

$$E_T^N = \frac{E_T(Solvent) - E_T(TMS)}{E_T(Water) - E_T(TMS)}$$
$$= \frac{E_T(Solvent) - 30.7}{32.4} \tag{33}$$

$$\Delta\mu = \mu_e - \mu_g = \sqrt{\frac{m \times 81}{\left(\frac{6.2}{a} \right)^3 \times 11307.6}} \tag{34}$$

where m is the slope of linear plot of E_T^N vs. Stokes shift.

Dipole moment can also be computed using Gaussian09/16 software [46] and can be compared to experimentally determined value. Gaussian-09/16 is a general purpose electronic structure package for use in computational chemistry. It can predict various properties of molecules and reactions using different theoretical models such as semi empirical model, density functional theory (DFT) and many more. Dipole moment of a molecule is generally obtained by optimizing ground and excited state structure using one of the theories and appropriate basis set. Most commonly used theory for this purpose is Density functional theory (DFT) and Time-dependent density functional theory (TD-DFT) to optimize ground state and excited state structures respectively [47-49].

Polar Probes in Binary Solvent:

In binary mixtures of polar solvents changing the composition of one of the solvent can lead to a change in solubility, polarizability, viscosity and many other static and dynamic properties. In hydrogen bonding systems such as alcohol-water mixtures, intermolecular correlations are strong, and the dielectric properties of the mixture and of individual components do not correspond linearly. Binary mixtures such as DMSO-water show bivalued profile of viscosity for the composition range. These properties are different for what one would have expected from ideal mixing. The properties of some binary solutions were studied using theoretical calculations and molecular dynamics (MD) simulations [50-55]. It is seen that the dynamical features of binary solutions are fairly dissimilar from those of neat solutions, and the properties of the solute can strongly affect these dynamic features of binary mixtures. Therefore, these non-ideal properties of binary solvent mixtures provide a good medium to study rotational diffusion.

Beddard et al. first reported the hook type profile of τ_r vs. η for cresyl violet in ethanol-water mixtures [56]. The observed re-entrance type behavior of the orientational relaxation time plotted against viscosity could not be explained only in terms of non-ideality in viscosity exhibited in a binary mixture. Beddard et al. also reported that the re-entrance behavior is strongly dependent on the specific interaction of the solute with the solvents. This is because interaction of solute with two different species of binary mixture is different. Therefore its rotational relaxation time will depend more on the composition than on the viscosity of the binary mixture. In our studies too orientational relaxation times of the probe vs. solvent viscosity, indeed showed re-entrance or hook type profile [57], thus confirms the fact that the rotational relaxation of solute molecule in binary solvent mixtures, strongly depends on the interactions of solute with two different species in mixed solvents.

The molecular structures of three dyes used for the rotational diffusion study viz. Alexa fluor 350 (neutral molecule) alexa fluor 430 (monoanionic) and alexa fluor 488 (dianionic) are given in figure 1.
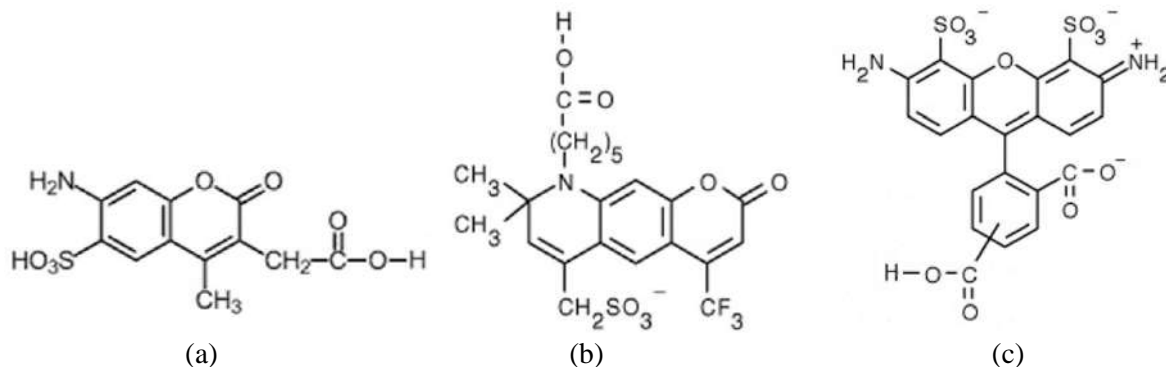
Fig. 1 Molecular structures of a) Alexa fluor-350, b) Alexa fluor-430 and c) Alexa flour-488

The viscosity profile of DMSO-water binary mixtures is given in figure 2a). At 37.18% of DMSO in water, viscosity reaches to its peak value of 3.291mPa and then decreases gradually. The dielectric constant value decreases with increase in DMSO percentage. τ_D profile is similar as viscosity profile. The viscosity of the mixture at 40% DMSO composition is four times that of the water alone. Due to the bivalued profile there are isoviscous points at different DMSO compositions. Rotational reorientation times are also expected to be same at those isoviscous points of different mole fractions of DMSO in water. Hence one should obtain linear plot for η vs$\tau_r$as predicted by hydrodynamic friction theories. But from the plots of η vs τ_r, all the three probes show hook type curve. All the

after highest viscosity is reached. We have calculated dielectric friction from two dielectric friction theories (NZ and ZH) to check the dielectric friction contribution to the total friction experienced by the probes.

Figure 3 (a) shows the viscosity profile of 2-propanol-water mixtures. At around 26.11% of 2-propanol in water composition, viscosity reaches its peak value of 2.70 mPa and decreases gradually. The dielectric constant value decreases exponentially and τ_D value increases rapidly from 8.7 to 245 ps with increase in 2-propanol in water. Rotational reorientation times (τ_r) due to dielectric friction is roughly proportional to τ_D/ε. Therefore dielectric friction in 2-propanol rich zone is expected to be very high than in water rich zone.
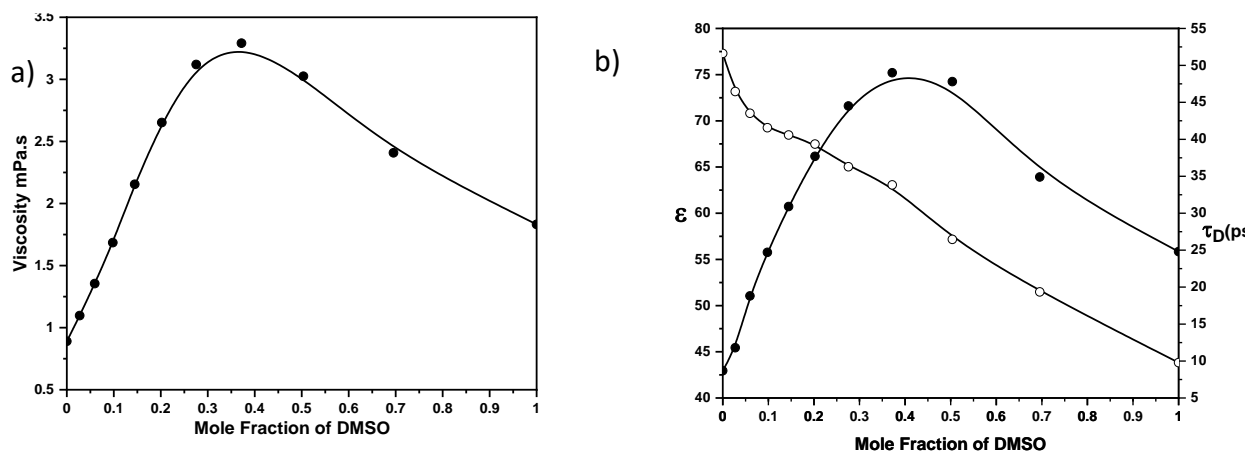
Fig. 2 a) Plot of viscosity vs. mole fraction of DMSO (●), b) Plot of dielectric constant vs. mole fraction of DMSO (○) and Debye relaxation time (τ_D) vs. mole fraction of DMSO (●).

Prajakta S. Kadolkar and Sanjeev R. Inamdar
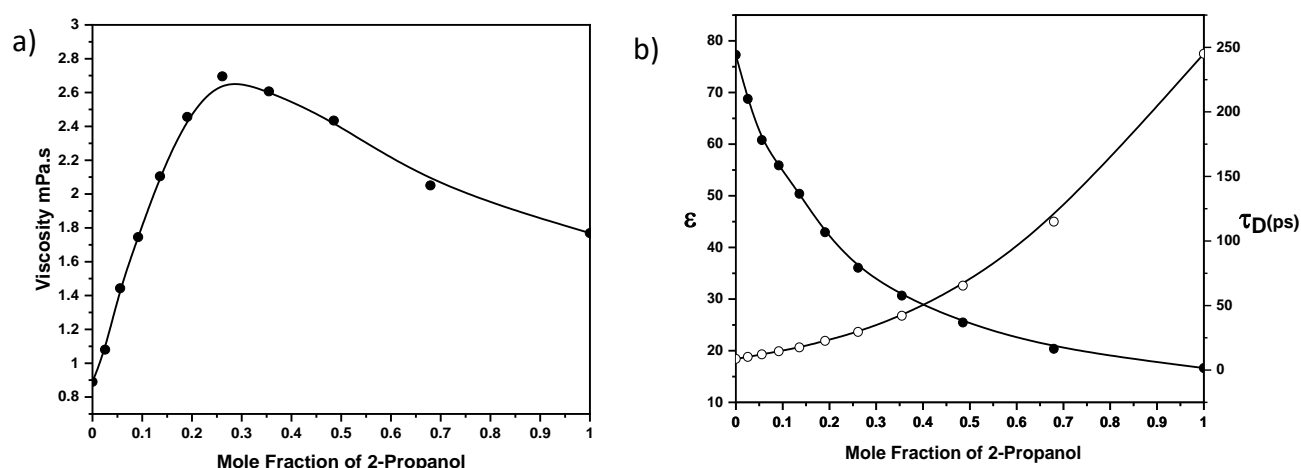
Fig. 3 a) Plot of viscosity vs. mole fraction of 2-Propanol (●), b) Plot of dielectric constant vs. mole fraction of 2-Propanol (●) and Debye relaxation time (τ_D) vs. mole fraction of 2-Propanol (○).

Table 1. Experimentally determined values of viscosity (η), Dielectric constant (ε), Debye relaxation time (τ_D) of solutions of indicated mole fraction of DMSO in water along with experimentally determined anisotropy (r) and fluorescence lifetime (τ_f) and rotational reorientation time τ_r^{Obs} of the Alexa flour dyes at different mole fractions of DMSO in water

| MF of DMSO in water	Viscosity (η) (mPa.s)	ε	τ_D (ps)	Alexa flour-350			Alexa flour-430			Alexa flour-488		
				r	τ_f (ns)	τ_r^{Obs} (ps)	r	τ_f (ns)	τ_r^{Obs} (ps)	r	τ_f (ns)	τ_r^{Obs} (ps)
0	0.89	77.29	8.68	0.00751	4.26	97.30	0.01360	2.82	131.93	0.01199	3.91	171.00
0.0274	1.097	73.17	11.8	0.00896	4.04	110.50	0.01741	2.83	171.82	0.01590	3.53	207.70
0.0596	1.355	70.82	18.8	0.01106	3.99	135.43	0.01861	2.93	190.64	0.01706	3.47	220.05
0.0980	1.685	69.25	24.7	0.01402	3.79	164.79	0.02158	3.07	234.46	0.02227	3.24	272.87
0.1446	2.155	68.46	30.9	0.01810	3.72	211.41	0.02590	3.83	356.32	0.02977	3.14	363.96
0.2023	2.652	67.48	37.7	0.02184	3.53	245.17	0.02980	3.98	431.91	0.03744	3.27	492.49
0.2756	3.119	65.03	44.5	0.03492	3.18	367.69	0.04045	3.83	587.12	0.05479	2.99	708.56
0.3718	3.291	63.06	49.0	0.03711	3.06	378.80	0.03869	4.29	624.38	0.06466	2.90	846.55
0.5036	3.025	57.17	47.8	0.03780	3.06	387.55	0.03767	3.94	556.93	0.06889	3.01	953.89
0.6954	2.408	51.48	34.9	0.03494	3.25	375.83	0.02586	3.99	370.21	0.07287	2.81	960.35
1	1.832	43.83	24.8	0.02734	3.33	294.29	0.02039	4.00	287.15	0.05298	2.79	633.82

The rotational reorientation time of three probes were determined experimentally in series of two different aqueous mixtures. Theoretical rotational reorientation times were calculated using hydrodynamic SED theory and two dielectric friction theories to understand the slow rotation of probes in organic solvent rich zone. From hydrodynamic (SED) theory one would have expected a straight line i.e., similar τ_r values at isoviscous points but experimentally τ_r values are higher in organic solvent rich zone for the same viscosity in water rich zone. Clearly τ_r

values are influenced by local molecular structure of binary mixtures. SED theory is inadequate to explain this and dielectric friction theories were used to explain this observed data. Where ever dielectric friction is not adequate to explain the slow rotation in organic solvent rich zone it can be attributed to specific solute solvent interaction like hydrogen bonding. In water however there is little interaction with solutes as compared to organic solvent. This may be because of strong water-water interactions. At low concentrations of organic

Prajakta S. Kadolkar and Sanjeev R. Inamdar

solvent in water, water surrounds the organic solvent molecules preventing interaction of organic solvent with solute[4, 38]. For Alexa fluor 350 in two mixtures series both dielectric friction and specific solute solvent interaction play important role. For alexafluor 430 in aqueous DMSO friction due to hydrogen bonding is negligible and dielectric friction is also less. But in aqueous 2-propanol dielectric friction and friction due to specific solute-solvent interaction both are possible reasons. For alexafluor 488 in both the mixture series dielectric friction is less and friction due to hydrogen bonding is dominant.

Table 2. Theoretically calculated τ_r values of Alexa flour dyes in aqueous DMSO using hydrodynamic (stick and slip) and dielectric friction theories

MF of DMSO in water	AF-350				AF-430				AF-488			
	Hydrodynamic friction theory		Dielectric friction theory		Hydrodynamic friction theory		Dielectric friction theory		Hydrodynamic friction theory		Dielectric friction theory	
	τ_r^{stick} (ps)	τ_r^{slip} (ps)	τ_r^{NZ} (ps)	τ_r^{vdZH} (ps)	τ_r^{stick} (ps)	τ_r^{slip} (ps)	τ_r^{NZ} (ps)	τ_r^{vdZH} (ps)	τ_r^{stick} (ps)	τ_r^{slip} (ps)	τ_r^{NZ} (ps)	τ_r^{vdZH} (ps)
0	127.25	6.36	0.98	6.30	206.95	5.85	0.29	4.25	271.30	9.25	0.68	0.99
0.0274	156.84	7.84	1.43	8.95	255.08	7.21	0.43	6.41	334.40	11.40	0.99	1.39
0.0596	193.73	9.68	2.40	14.75	315.07	8.90	0.72	10.49	413.04	14.08	1.66	2.30
0.0980	240.91	12.04	3.30	19.71	391.80	11.07	0.99	14.32	513.64	17.51	2.29	3.19
0.1446	308.11	15.39	4.28	24.48	501.09	14.16	1.28	18.07	656.90	22.39	2.97	4.09
0.2023	379.17	18.94	5.38	31.00	616.65	17.43	1.61	22.54	808.40	27.55	3.74	5.16
0.2756	445.93	22.28	6.70	36.45	725.24	20.50	2.00	28.76	950.76	32.40	4.65	6.35
0.3718	470.52	23.51	7.78	40.71	765.23	21.63	2.32	32.48	1003.19	34.19	5.40	7.37
0.5036	432.49	21.61	8.48	44.64	703.38	19.88	2.53	34.84	922.11	31.43	5.88	7.94
0.6954	344.28	17.20	6.92	35.10	559.92	15.82	2.07	28.93	734.03	25.02	4.81	5.11
1	261.93	13.09	5.81	27.97	425.98	12.04	1.74	23.62	558.45	19.03	4.03	2.41

Table 3. Experimentally determined values of viscosity (η), Dielectric constant (ε), Debye relaxation time (τ_D) of solutions of indicated mole fraction of 2-Propanol in water along with experimentally determined anisotropy (r) and fluorescence lifetime (τ_f) and rotational reorientation time τ_r^{Obs} of the Alexa flour dyes at different mole fractions of 2-Propanol in water

| MF of 2-propanol in water	Viscosity (η) (mPa.s)	ε	τ_D (ps)	Alexa flour-350			Alexa flour-430			Alexa flour-488		
				r	τ_f (ns)	τ_r^{Obs} (ps)	r	τ_f (ns)	τ_r^{Obs} (ps)	r	τ_f (ns)	τ_r^{Obs} (ps)
0	0.89	77.29	8.7	0.00925	4.09	115.62	0.01395	3.10	148.80	0.01141	2.93	121.63
0.0255	1.08	68.76	10.2	0.01074	4.65	153.23	0.01987	3.45	241.13	0.01597	2.91	171.77
0.0556	1.44	60.81	12.2	0.01449	4.32	194.32	0.02199	3.73	290.54	0.02214	3.46	289.67
0.0917	1.75	55.90	14.6	0.01744	4.09	223.27	0.02516	3.94	354.99	0.02643	3.47	353.21
0.1357	2.11	50.40	17.6	0.02522	4.50	264.45	0.03243	4.19	399.63	0.03494	3.48	483.88
0.1907	2.46	42.94	22.6	0.02633	3.80	322.35	0.03178	4.22	491.53	0.0401	3.33	542.89
0.2611	2.70	36.07	29.6	0.02984	3.56	346.49	0.03209	4.35	512.40	0.04694	3.50	686.17
0.3547	2.61	30.67	42.1	0.03408	3.41	384.55	0.0318	4.37	509.97	0.05283	3.40	768.27
0.4852	2.43	25.47	65.4	0.03234	3.38	358.99	0.02974	4.40	496.14	0.05489	3.09	732.00
0.6795	2.05	20.37	115.0	0.03458	3.35	383.00	0.02983	4.61	500.42	0.06752	3.35	1033.62
1	1.77	16.64	245.0	0.03518	3.21	374.25	0.02308	4.60	577.25	0.07228	3.32	1121.46

Prajakta S. Kadolkar and Sanjeev R. Inamdar
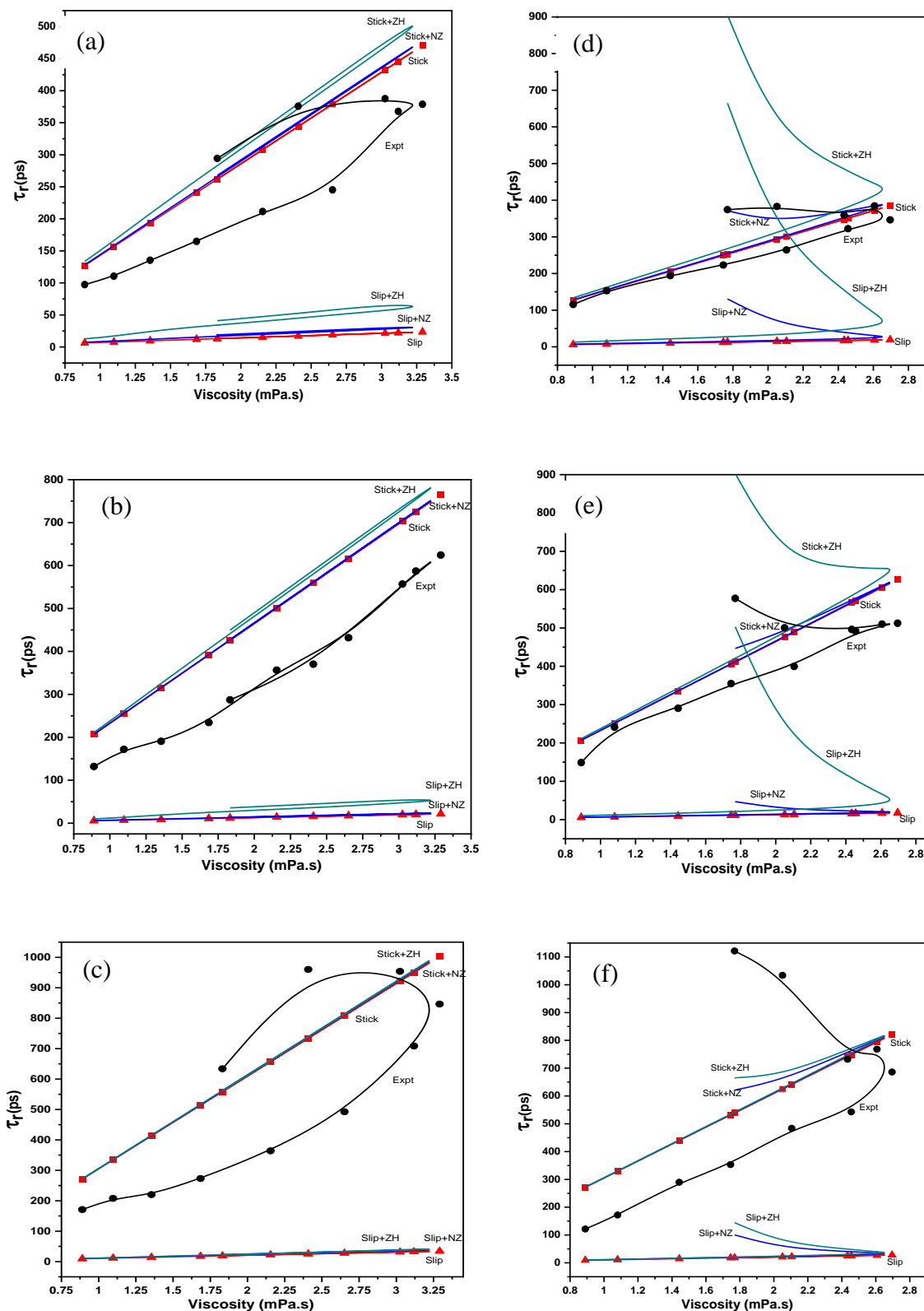
Figure 4. Rotational reorientation time (τ_r) vs. viscosity (η) profiles (Experimental (●), Stick (■), Stick+NZ, Stick +ZH, Slip (▲), Slip+NZ, Slip+ZH) for (a) Alexa flour-350 (b) Alexa flour-430(c) Alexa flour-488 in aqueous DMSO and (d) Alexa flour-350 (e) Alexa flour-430(f) Alexa flour-488 in aqueous 2-Propanol.

Prajakta S. Kadolkar and Sanjeev R. Inamdar

Table 4. Theoretically calculated τ_r values of Alexa flour dyes in aqueous 2-Propanol using hydrodynamic (stick and slip) and dielectric friction theories

MF of 2-Propanol in water	AF-350				AF-430				AF-488			
	Hydrodynamic friction theory		Dielectric friction theory		Hydrodynamic friction theory		Dielectric friction theory		Hydrodynamic friction theory		Dielectric friction theory	
	τ_r^{stick} (ps)	τ_r^{slip} (ps)	τ_r^{NZ} (ps)	τ_r^{vdZH} (ps)	τ_r^{stick} (ps)	τ_r^{slip} (ps)	τ_r^{NZ} (ps)	τ_r^{vdZH} (ps)	τ_r^{stick} (ps)	τ_r^{slip} (ps)	τ_r^{NZ} (ps)	τ_r^{vdZH} (ps)
0	127.25	6.34	0.98	6.42	206.95	5.85	0.29	4.25	271.30	9.25	0.68	0.99
0.0255	154.41	7.71	1.29	8.33	251.13	7.10	0.39	5.43	329.21	11.22	0.90	1.28
0.0556	206.31	10.31	1.78	11.50	335.53	9.48	0.53	7.07	439.87	14.99	1.23	1.74
0.0917	249.49	12.47	2.31	14.55	405.75	11.47	0.69	9.53	531.93	18.13	1.60	2.30
0.1357	300.96	15.04	3.09	19.37	489.46	13.83	0.92	12.19	641.66	21.87	2.15	3.03
0.1907	351.14	17.54	4.65	29.39	571.08	16.14	1.39	17.63	748.66	25.52	3.23	4.62
0.2611	385.46	19.26	7.19	43.58	626.88	17.72	2.15	29.16	821.82	28.01	4.99	7.50
0.3547	372.73	18.62	11.92	71.94	606.19	17.13	3.56	48.56	794.69	27.08	8.27	12.46
0.4852	347.99	17.39	21.91	135.78	565.96	15.99	6.55	91.23	741.95	25.29	15.21	23.86
0.6795	293.24	14.65	46.96	290.07	476.91	13.48	14.04	200.22	625.20	21.31	32.59	50.94
1	252.91	12.64	118.24	652.12	411.33	11.62	35.34	491.23	539.24	18.38	82.07	125.94

Conclusion:

In general the experimentally determined rotational reorientation times of most non polar probes could be described with Hydrodynamic (SED) theory [58-77]. For some molecules showing superstick or subslip behavior, Gierer-Wirtz (GW) theory and Dote-Kivelson-Schwartz (DKS) theory was quite successful. For very large molecules rotational reorientation time (τ_r) doesn't scale linearly with size of solute and τ_r values are less sensitive to solvent at high viscosities [78, 79] which all the three above theories fail to explain. Temperature dependent rotational diffusion studies are also done using non polar probes[80-85] but this needs to be explored more by using polar molecule in polar solvent. For polar molecules rotating in polar solvents dielectric friction theories can be used to explain the increased friction than predicted by SED theory [86-89]. This additional friction increases even more if probe is dissolved in hydrogen bonding solvents such as alcohols. In this case both dielectric friction and friction due to specific solute-solvent interaction is considered responsible along with hydrodynamic friction. Rotational diffusion studies of polar probes in binary solvent mixtures yield hook type profile giving different τ_r values at isoviscous points [90-97]. Situation becomes more complicated when binary mixtures of Alcohol-water is used. This is quite apparent in our studies of Alexa flour dyes in aqueous 2-Propanol mixtures.

While calculating dieletric friction using NZ and ZH theories excited state dipole moment of a solute is an important parameter. But finding excited state dipole moment accurately is difficult which affects the τ_r values calculated using dielectric friction. The theoretical models, hydrodynamic as well as dielectric friction model are not adequately precise in describing the experimental results. Also quantitative explaination of friction due to specific solute solvent interaction is necessary to understand the slower rotation of the solute than predicted by hydrodynamic theory. In conclusion, the theoretical framework for solute-solvent interactions is yet to evolve.

References:

[1] G. R. Fleming, Chemical Applications of Ultrafast Spectroscopy, Oxford University Press, New York, 1986, and references therein.
[2] Rotational Dynamics of Small and Macromolecules (Eds.: Th. Dorfmuller, R. Pecora), Springer-Verlag, Berlin, 1987.

Prajakta S. Kadolkar and Sanjeev R. Inamdar

[3] D. H. Waldeck in Conformational Analysis of Molecules in Excited States (Ed.: J. Waluk), Wiley-VCH, New York, 2000.

[4] P. Debye, Polar Molecules, Dover Publications, London, 1929.

[5] F. Perrin, J. Phys. Radium 7 (1936) 1-11.

[6] Chuang, T.J. & Eisenthal, K.B., J. Chem. Phys. 57 (1972) 5094-97.

[7] Hu, C.M. & Zwanzig, R., J. Chem. Phys. 60 (1974) 4354-57.

[8] Youngren, G.K. & Acrivos, A., J. Chem. Phys. 63 (1975) 3846-48.

[9] Zwanzig, R. & Harrison, A.K., J. Chem. Phys. 83 (1985) 5861- 62.

[10] Lakowicz, J. R., Principles of fluorescence spectroscopy, Springer: New York, 2006.

[11] Fleming, G.R., Chemical Applications of Ultrafast Spectroscopy, Oxford University Press: New York, 1986.

[12] van der Zwan, G. & Hynes, J.T., J. Phys. Chem. 90 (1985) 4181-88.

[13] Barbara, P.F. &Jarzeba, W., Adv. in Photochem. 15 (1990) 1-68.

[14] Maroncelli, M., J. Molec. Liq. 57 (1993) 1-37.

[15] Dutt, G.B., Srivatsavoy, V.J.P. &Sapre, A.V., J. Chem. Phys. 110 (1999) 9623-29.

[16] Lakowicz, J.R., Principles of Fluorescence Spectroscopy, Plenum Press, New York, 1983.

[17] Stokes, G., Trans. Cambridge Philos. Soc. 9 (1956) 5.

[18] G.T. Evans, R.G. Cole and D.K. Hoffman, J. Chem. Phys. 77 (1982) 3209.

[19] G. Stokes, Trans. Cambridge Philos. Soc. 9 (1956) 5.

[20] Einstein, Ann. Phys. 19 (1906) 371.

[21] G. Porter, P.J. Sadkowski and C.J. Tredwell, Chem. Phys. Lett. 49 (1977) 416.

[22] von Jena and H.E. Lessing, Chem. Phys. Lett. 78 (1981) 187.

[23] S. Canonica, A.A. Schmid and U.P. Wild, Chem. Phys. Lett. 122 (1985) 529.

[24] L. A. Philips, S. P. Webb and J. H. Clark, J. Chem. Phys. 83 (1985) 5810.

[25] S.R. Inamdar, J.R. Mannekutla, B.G. Mulimani and M.I. Savadatti, Chem. Phys. Lett. 429 (2006) 141.

[26]Norikazu Ohtori, Yuta Kondo, Yoshiki Ishii, Journal of Molecular Liquids 314 (2020) 113764.

[27] Gierer and K. Wirtz, Z. Naturforsch. A8 (1953) 532.

[28] J. L. Dote, D. Kivelson and R.N. Schwartz, J. Chem. Phys. 85 (1981) 2169.

[29] S. R. Inamdar, J. R. Mannekutla, M. S. Sannaikar, M. N. Wari, B. G. Mulimani, M. I. Savadatti, Journal of Molecular Liquids 268 (2018) 66.

[30] Hubbard, J.B. & Onsager, L., I. J. Chem. Phys. 67 (1977) 4850-57.

[31] Hubbard., J.B., J. Chem. Phys. 69 (1978) 1007-09.

[32] Dote, J.L., Kivelson, D. & Schwartz, R.N., J. Phys. Chem. 85 (1981) 2169-80.

[33] Felderhof, B.U., Mol. Phys. 48 (1983) 1283-88.

[34] Alavi, D.S., Hartman, R.S. & Waldeck, D.H., J. Chem. Phys. 95 (1991c) 6770-83.

[35] Kumar, P.V. & Maroncelli, M., J. Chem. Phys. 112 (2000) 5370-81.

[36] Nee, T.W. & Zwanzig, R., J. Chem. Phys. 52 (1970) 6353-63.

[37] Joseph B. Hubbard and Peter G. Wolynes, J. Chem. Phys. 69(3) (1978) 998-1006.

[38] van der Zwan, G. & Hynes, J.T., J. Phys. Chem. 90 (1985) 4181-88.

[39] Alavi, D.S., Hartman, R.S. & Waldeck, D.H., J. Chem. Phys. 94 (1991a) 4509-20.

[40] E. Lippert, Ber. Bunsenges. Phys. Chem. 61 (1957) 962.

[41] N. Mataga, Y. Kaifu, M. Koizumi, Bull. Chem. Soc. Japan 29 (1956) 465.

[42] L. Bilot and A. Kawski, Z. Naturforsch 17a (1962) 621.

[43] A. Kawski, Acta Phys. Polon. 29 (1966) 507.

[44] C. Richardt, "Solvents and solvent Effects in Organic Chemistry", third ed., Wiley-VCH, Weinheim Germany (2005)

[45] C. Richardt, Chem. Rev. 94 (1994) 2319.

Prajakta S. Kadolkar and Sanjeev R. Inamdar

[46] Gaussian 09, Revision D.01, M. J. Frisch, G. W. Trucks, H. B. Schlegel, G. E. Scuseria, M. A. Robb, J. R. Cheeseman, G. Scalmani, V. Barone, B. Mennucci, G. A. Petersson, H. Nakatsuji, M. Caricato, X. Li, H. P. Hratchian, A. F. Izmaylov, J. Bloino, G. Zheng, J. L. Sonnenberg, M. Hada, M. Ehara, K. Toyota, R. Fukuda, J. Hasegawa, M. Ishida, T. Nakajima, Y. Honda, O. Kitao, H. Nakai, T. Vreven, J. A. Montgomery, Jr., J. E. Peralta, F. Ogliaro, M. Bearpark, J. J. Heyd, E. Brothers, K. N. Kudin, V. N. Staroverov, T. Keith, R. Kobayashi, J. Normand, K. Raghavachari, A. Rendell, J. C. Burant, S. S. Iyengar, J.Tomasi, M. Cossi, N. Rega, J. M. Millam, M. Klene, J. E. Knox, J. B. Cross, V. Bakken, C. Adamo, J. Jaramillo, R. Gomperts, R. E. Stratmann, O. Yazyev, A. J. Austin, R. Cammi, C. Pomelli, J. W. Ochterski, R. L. Martin, K. Morokuma, V. G. Zakrzewski, G. A. Voth, P. Salvador, J. J. Dannenberg, S. Dapprich, A. D. Daniels, O. Farkas, J. B. Foresman, J. V. Ortiz, J. Cioslowski, and D. J. Fox, Gaussian, Inc., Wallingford CT, 2013.

[47] Roshmy Alphonse, Anitha Varghese, Louis George, Aatika Nizam, J. Mol. Liq. 215 (2016) 387–395.

[48] K B Akshaya, Anitha Varghese, Prajwal Lourdes Lobo, Rekha Kumari, Louis George, J. Mol. Liq. 224 (2016) 247–254.

[49] Mallikarjun K. Patil , M.G. Kotresh , Sanjeev R. Inamdar, Spectrochim. Acta A Mol. Biomol. Spectrosc. 215 (2019) 142–152.

[50] Chandra, A. & Bagchi, B., J. Chem. Phys. 94 (1991) 8367-77.

[51] Chandra, A., Chem. Phys. Lett. 235 (1995) 133-39.

[52] Skaf, M. & Ladanyi, B.M., J. Phys. Chem. 100 (1996) 18258-68.

[53] Day, T.J.F. & Patey, G.N., J. Chem. Phys. 106 (1997) 2782-91.

[54] Yoshimori, A., Day, T.J.F. & Patey, G.N., J. Chem. Phys. 109 (1998) 3222-31.

[55] Laria, D. & Skaf, M., J. Chem. Phys. 111 (1999) 300-09.

[56] G. S. Beddard, T. Doust & J. Hudales, Nature, 294 (1981) 145-146.

[57] P. S. Kadolkar, S. A. Patil, M. N. Wari, S. R. Inamdar, J. Mol. Liq. 312 (2020) 113452-63.

[58] A. Von Jena and H. E. Lessing , Chemical Physics 40 (1979) 245-256.

[59]Eva F. Gudgin Templeton, Edward L. Quitevis, and Geraldine A. Kenney-Wallace, J. Phys. Chem. 89 (1985) 3238-3243.

[60] G. J. Blanchard, J. Chem. Phys. 87 (1987) 6802-6808.

[61] G. J. Blanchard and C. A. Cihal, *J. Phys. Chem.* 92 (1988) 5950-5954.

[62] G. J. Blanchard, J. Phys. Chem. 93 (1989) 4315-4319.

[63] G. B. Dutt, S. Doraiswamy, N. Periaswamy & B. Venkataraman, J. Chem. Phys. 93 (1990) 8498-8513.

[64]G. J. Blanchard, J. Phys. Chem. 92 (1988) 6303-6307.

[65] Y. Jiang and G.J. Blanchard, J. Phys. Chem. 98 (1994) 6436-6440.

[66] Y. Jiang and *G*. J. Blanchard, J. Phys. Chem. 99 (1995) 7904-7912.

[67] Arvind Srivastava and S. Doraiswamy, J. Chem. Phys. 103 (14) (1995) 6197-6205.

[68] Steven De Backer, G. Bhaskar Dutt, Marcel Ameloot, Frans C. De Schryver, Klaus Mullen, and Frank Holtrup, J. Phys. Chem. 100 (1996) 512-518.

[69] M.L. Horng, J. A. Gardecki, and M. Maroncelli, J. Phys. Chem. A. 101 (1997) 1030-1047.

[70] R. S. Hartman, W. M. Konitsky, D. H. Waldeck, Y. J. Chang & E. W. Castner Jr., J. Chem. Phys. 106 (1997) 7920-7930.

[71] M. K. Singh, Photochemistry and Photobiology 72(4) (2000) 438–443.

[72] T. Gustavsson, L. Cassara, S. Marguet, G. Gurzadyan, P. van der Meulen, S. Pommeret& J. C. Mialocq., Photochem. Photobiol. Sci. 2 (2003) 329–341.

[73] G. B. Dutt, J. Chem. Phys. 121 (2004) 3625-3631.

[74] MiklosKubinyi, AndrasGrofcsik, TamasKarpati, W. Jeremy Jones, Chemical Physics 322 (2006) 247–253.

Prajakta S. Kadolkar and Sanjeev R. Inamdar

[75] J.R. Mannekutla, P. Ramamurthy, B.G. Mulimani, S.R. Inamdar, Chemical Physics 340 (2007) 149–157

[76] B.R. Gayathri& J.R. Mannekutla& S.R. Inamdar, J. Fluoresc. 18 (2015) 943–952.

[77] Radha Goudar, Ritu Gupta, Giridhar U. Kulkarni, Sanjeev R. Inamdar, J. Fluoresc. 25 (2015) 1671-1679

[78] S. A. Rice and G. A. Kenney-Wallace, Chem. Phys. 47 (1980) 161.

[79] W. Mikosch, Th. Dorfmuller, and W. Eimer, J. Phys. Chem. 101 (1994) 11044.

[80] G. J. Blanchard and M. J. Wirth, J. Phys. Chem. 90 (1986) 2521-2525.

[81] Marcia Levitus, R. Martin Negri, and Pedro F. Aramendia, J. Phys. Chem. 99 (1995) 14231-14239

[82] Kathy Wiemers and John F. Kauffman, J. Phys. Chem. A. 104 (2000) 451-457.

[83] G. B. Dutt and T. K. Ghanty, J. Chem. Phys. 121 (8) (2004) 3625-3631.

[84] K. S. Mali, G. B. Dutt, and T. Mukherjee, J. Chem. Phys. 128 (2008) 054504.

[85] K. H. Nagachandra, J. R. Mannekutla, M. A. Shivkumar, S. R. Inamdar, J. Lumin., 132 (2012) 570–578.

[86] R. S. Hartman, D. S. Alavi, and D. H. Waldeck, Phys. Chem. 1991, 95, 7872-7880

[87] EiraLaitinen, JoukoKorppi-Tommola, and JuhaLinnanto, J. Chem. Phys. 107 (19) (1997) 7601-7612.

[88] G. B. Dutt, Sumathi Raman, J. Chem. Phys. 114 (2001) 6702-6713.

[89] J. R. Mannekutla, Sanjeev R. Inamdar, B. G. Mulimani, and M. I. Savadatti, J Fluoresc (2010) 20:797–808

[90] Eva F. Gudgin Templeton and Geraldine A. Kenney-Wallace, J. Phys. Chem. 90 (1986) 2896-2900.

[91] G. B. Dutt, S. Doraiswamy & N. Periaswamy, J. Chem, Phys. 94 (1991) 5360-5368.

[92] G. B. Dutt & S. Doraiswamy, J. Chem. Phys. 96 (1992) 2475-2491.

[93] M. Krishnamurthy, Kishore Kumar Khan, and S. Doraiswamy, J. Chem. Phys. 98 (11) (1993) 8640-8646.

[94] Mischa Megens, Rudolf Sprik, Gerard H. Wegdam, and Ad Lagendijk. J. Chem. Phys. 107 (2) (1997) 493-498.

[95] G. B. Dutt, J. Chem. Phys., 113. 24. (2000) 11154- 11158.

[96] Sarah A. Stevenson and G. J. Blanchard, J. Phys. Chem. A 110 (2006) 3426-3431.

[97] S.R. Inamdar, B.R. Gayathri, J.R. Mannekutla, J. Fluoresc. 19 (2009) 693-703.

Growth of Biocompatible Ag$_2$O Nanoparticles by Co-precipitation Method

B. Saraswathi[1], V. S. Patil[1], G. H. Nagaveni[1], S. V. Halse[1*] and M. N. Kalasad[1*]

[1]Department of Studies in Physics, Davangere University, Davangere - 577 007, India.

***Corresponding author:** mnkalasad@gmail.com; drsvhalse@rediffmail.com*

ARTICLE INFO	ABSTRACT
Article history: Received: 4 May 2021; Revised: 12 May 2021; Accepted: 17 May 2021 **Keywords:** Ag$_2$O; Nanoparticles; Size; Preparation; Passivation; L-cysteine;	The Biocompatible Ag$_2$O nanoparticles have been prepared using L-cysteine molecules by co-precipitation method. Optical, structural and compositional measurements were carried out, the role of L-cysteine as a capping molecule was significant, because of better surface passivation and stability of Ag$_2$O nanoparticles. The estimated particle size was around 20 to 25 nm. The present method of synthesis of Ag$_2$O nanoparticles is simple, ecofriendly and used for photocatalytic and biomedical applications.

1. Introduction:

Recent developments in the field of nanostructured materials have opened up novel opportunities for various applications such as energy, catalysis, electronics and sensing materials. Materials at the nanometer scale often exhibit different properties as compared to bulk phase. Metal oxides play a very important role in many areas of chemistry, physics and materials science. The metal elements are able to form a large diversity of oxide compounds, these materials can adopt a large number of structural geometries with an electronic structure exhibit metallic, semiconductor or insulator features. In the modern technological applications, these oxide materials are used in the design of sensors, piezoelectric devices, microelectronic circuits, fuel cells and catalysts. Among these, oxide nanocrystals exhibit unique chemical properties due to their limited size and a high density of surface sites at the edges. In recent years, large

number of methods have been developed for the growth of novel metal oxides nanocrystals [1-6].

Metal oxide nanoparticles have many probable applications including use in biomedical [7], sensing [8], optoelectronic [9] and catalytic systems [10], which bond to their size and shape dependent properties. Environmental pollution is one the main global challenge having its related dangers that are rising day by day [11]. Owing to the increased industrialization and human population. There are many technologies are applied to reduced pollution occurs in environment in that a potential remedy is the semiconductor photocatalysis utilizes the solar energy, which has gained considerable attention [12-14]. As per the literature survey, semiconductor metal oxide nanocrystals such as CeO$_2$, ZnO, NiO, Cr$_2$O$_3$, Ag$_2$O, TiO$_2$ etc. [6, 8] are attracted more attention and been proven to be successful in degrading organic pollutants in an environment. The development of metals and their oxide by

means of protected and economical process have drawn the attention of researchers globally. The challenging task is to develop, an effective process to develop well defined nanocrystals with controlled shape and sizes, used for application in various fields [15-16]. Several research groups already reported the various techniques for the synthesis of metal oxide nanoparicles such as solid –liquid phase, ultraviolet irradiation, electrochemical, photosensitized reduction, simple chemical, sol-gel, hydrothermal and arc discharge methods [17-20], microwave assisted method [21] and solvothermal method [22]. Here, we report the preparation of Ag_2O nanoparticles by co-precipitation technique using L-Cysteine as capping molecule to produce stable sols with spherical shape.

2. MATERIALS AND EXPERIMENTAL METHODS:

2.1 Materials:

All chemicals used in synthesis work were of analytical grade, SD Fine Chemicals. The chemicals used in the preparation were silver nitrate (Ag_2NO_3), sodium hydroxide (NaOH) and L-Cysteine.

2.2 Experimental Methods:

L-Cysteine has been receiving attention because of its non-toxic and environmentally benign capping molecules for the growth of Ag_2O nanoparticles. Initially, 50 mM Silver nitrate was dissolved in doubled distilled water. 5 mM L-Cysteine was added to the water and stirred for about 30 minutes to completely soluble in water. Known quantity of L-Cysteine solution was slowly added to the silver nitrate solution and stirred for about 20 minutes. Later, sodium hydroxide solution was added drop wise to the silver nitrate solution. The brownish colored colloidal silver oxide nanoparticles was formed, later material was washed and collected for further process. Optical absorption measurements were carried out using V-760 UV-Visible Spectrophotometer. Photoluminescence (PL) spectra were collected using Horiba fluromax-4 spectrofluorometer and

FTIR spectra were recorded using Thermo Scientific, NICOLET iN10.

3. RESULTS AND DISCUSSIONS:

The synthesis of Ag_2O nanoparticle by L-Cysteine molecules forms a high affinity metal-ligand clusters with metal ions, due to the strong tendency of its active functional groups (-SH, -NH_2, and -COOH) to coordinate with metals and to prevent agglomeration. Figure 1 shows the optical absorption spectrum of Ag_2O nanoparticles, the unaffected nature of spectrum shows that the prepared Ag_2O nanoparticles are stable in nature. The absorption lies in the range of
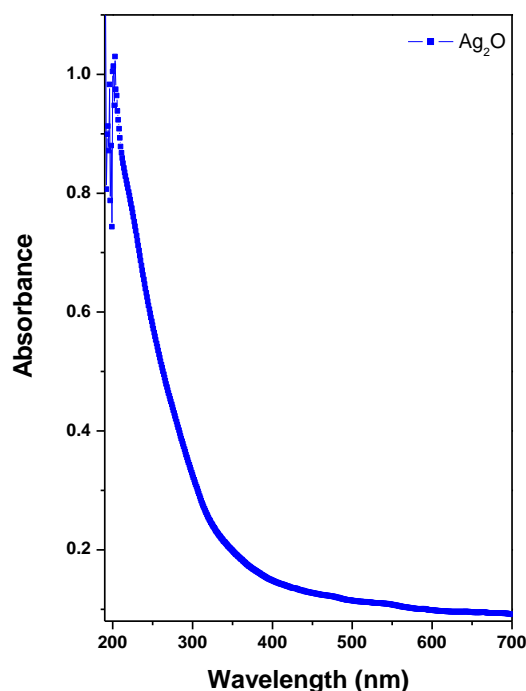
Figure 1: Optical absorption spectrum of Ag_2O nanoparticles.

367- 398 nm indicates that there is a transition of nonbonding electrons present in the p-orbital of the silver oxide nanoparicles to the higher sigma and pi antibonding orbitals. The shifting to visible absorption shows that the surface plasmon resonance absorption. Figure 2 shows the photoluminescence spectrum of colloidal Ag_2O nanoparticle, the emission peak around 375 nm indicates that there is an deexcitation of antibonding vibrational level electrons to the

B. Saraswathi et al.,
highest vibrational level of the nonbonding orbital of the silver oxide nanocrystals indicates
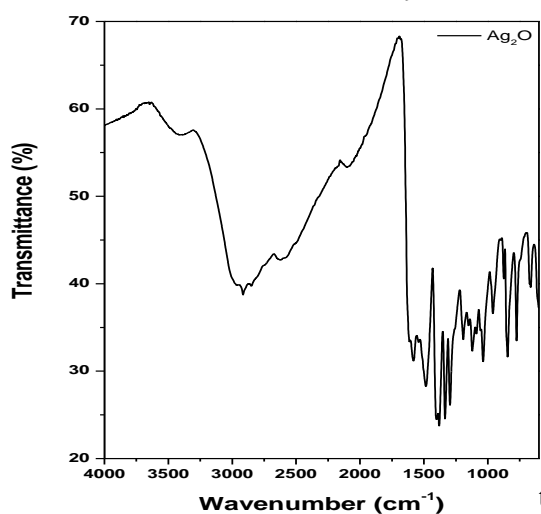
that vibration of the surface particles among lower and higher vibrational levels of the antibonding and nonbonding orbitals of silver oxide molecule.

Figure 2: Photoluminescence spectrum of Ag$_2$O nanoparticles.
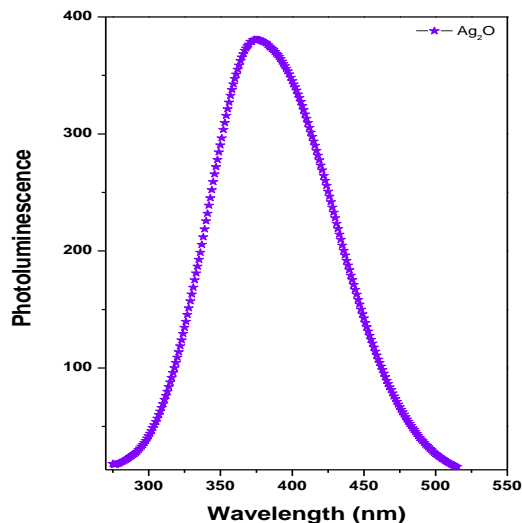
Figure 3: FTIR spectrum of Ag$_2$O nanoparticles.

Figure 3 illustrates the FTIR spectrum of Ag$_2$O nanoparticles in the wavenumber range of 4000 of Ag$_2$O nanoparticles in the wavenumber range of 4000 - 400 cm^{-1}. The characteristic transmission band at 534 cm^{-1} corresponds to the Ag-O stretching vibration mode. The band observed around 2900 cm^{-1} is due to C-H stretching vibrations. The clear absence of S-H

stretching band at 2550 cm^{-1} indicates the binding of L-cysteine molecules to the Ag. The band at 1400 cm^{-1} is due to the stretching vibration of C-O. The band at 1590 cm^{-1} is due to carboxylate group. But Ag-O bond was vibrating in 534 cm^{-1} wavenumber indicates that L-Cysteine molecules are strongly bind to the Ag$_2$O particles. On the basis of x-ray diffraction measurement Phase and particle was observed from the x-ray diffraction measurement, patterns of Ag$_2$O nanoparticles shows cubic phase. The estimated particle size using Debye-Scherrer formula was around 20 to 25 nm.

4. Conclusions:

In conclusion, the L-Cysteine functionalized Ag$_2$O nanoparticle are obtained by a facile co-precipitation method. Their optical and structural properties reveals that L-cysteine as act as effective passivating molecule. The particle size is controlled by varying the volume of the concentration of precursor and capping molecules. The present method of synthesis is simple and cost effective.

References:
[1]M. Fernandez-Garcıa, A. Martınez-Arias, J. C. Hanson and J. A. Rodriguez, Nanostructured Oxides in Chemistry: Characterization and Properties, Chem. Rev. (ACS), 104, 4063-4104, (2004).
[2]M. C. Daniel, D. Astru, Gold Nanoparticles: Assembly, Supramolecular Chemistry, Quantum-Size-Related Properties, and Applications toward Biology, Catalysis, and Nanotechnology. Chem. Rev. (ACS), 104, 293−346, (2004).
[3]N. Satoh, T. Nakashima, K. Kamikura, K. Yamamoto, Quantum size effect in TiO$_2$ nanoparticles prepared by finely controlled metal assembly on dendrimer templates. Nat. Nanotech. (Nature Publ.), 3, 106−111, (2008).
[4]Wells, A. F. Structural Inorganic Chemistry, 6th ed.; Oxford University Press: New York, (1987).
[5]S. Matussin, M. H. Harunsani, A.L. Tan, M.M. Khan, Plant-Extract-Mediated SnO$_2$ Nanoparticles: Synthesis and Applications, ACS

B. Saraswathi et al.,
Sustainable Chemistry & Engineering, (ACS) 8, 3040-3054. (2020).

[6] X. Pang, L. Zhao, Z. Lin, A general and robust strategy for the synthesis of nearly monodisperse colloidal nanocrystals. Nat. Nanotech. (Nature Publ.), 8,426-431, (2013).

[7] L. J. Schierholz, A. Lucas, A. Rump and G. Pulverer, J. Hosp. Infect., 40, 257. (1998).

[8] R. Molavi, M. H. Sheikhi, Facile wet chemical synthesis of Al doped CuO nanoleaves for carbon monoxide gas sensor applications. Materials Science in Semiconductor Processing (Elsevier) 106, 104767, (2020).

[9] M. N. Kalasad, M. K. Rabinal and B. G. Mulimani, Ambient synthesis and characterization of high-quality CdSe quantum dots by an aqueous route. Langmuir (ACS), 25, 12729–12735, (2009).

[10] B. C. Zhu, P. F. Xia, Y. Li, W.K. Ho, J.G. Yu, Fabrication and photocatalytic activity enhanced mechanism of direct Z-scheme g-C_3N_4/Ag_2WO_4 photocatalyst, Appl. Surf. Sci. 391, 175–183, (2017).

[11] M. Mohammed, Rahman, S. B. Khan, A. Jamal, M. Faisal, A. M. Asiri, Fabrication of highly sensitive acetone sensor based on sonochemically prepared as-grown Ag_2O nanostructures. Chemical Engineering Journal. (Elsevier) 192, 122-128, (2012).

[12] Y. Li, X.Y. Xiao, Z. H. Ye, Fabrication of $BiVO_4$/RGO/Ag_3PO_4 ternary composite photocatalysts with enhanced photocatalytic performance. (Elsevier) Appl. Surf. Sci. (Elsevier) 467-468, 902–911, (2019).

[13] L. N. Ma, G. H. Wang, C. J. Jiang, H. L. Bao, Q. C. Xu, Synthesis of core-shell TiO_2@gC_3N_4 hollow microspheres for efficient photocatalytic degradation of rhodamine B under visible light, Appl. Surf. Sci. (Elsevier) 430 263–272, (2018).

[14] J.X. Low, B. Cheng, J.G. Yu, Surface modification and enhanced photocatalytic CO_2 reduction performance of TiO_2: a review, Appl. Surf. Sci. (Elsevier) 392, 658–686, (2017).

[15] A. Ito, M. Shinkai, H. Honda, and T. Kobayashi, J. Biosci. Bioeng. Medical application of functionalized magnetic nanoparticles. (Elsevier), 100, 1-11, (2005).

[16] S. Guo and E. Wang, Synthesis and electrochemical applications of gold nanoparticles. Anal. Chim. Acta (Elsevier), 598, 181-192, (2007).

[17] C. Fang, A.V. Ellis and N. H. Voelcker, Graphene masks as passivation layers in the electrochemical etching of silicon. Electrochimica Acta (Elsevier), 59, 346-353 (2012).

[18] S. Jradi, L. Balan, X. H. Zeng, J. Plain, D. J. Lougnot, P. Royer, R. Bachelot, S. Akil, O. Soppera and L. Vidal, Spatially controlled synthesis of silver nanoparticles and nanowires by photosensitized reduction. Nanotechnology (IOP), 21, 95605 (2010).

[19] K. K. Caswell, C. M. Bender and C. J. Murphy, Seedless, surfactantless wet chemical synthesis of silver nanowires. Nano Lett. (ACS), 3, 667-669 (2003).

[20] R. J. Chimentao, I. Kirm, F. Medina, X. Rodriguez, Y. Cesteros, P. Salagre, J. E. Sueiras, Different morphologies of silver nanoparticles as catalysts for the selective oxidation of styrene in the gas phase, Chem. Comm. (RSC) 846–847, (2004).

[21] M. Hasanpoor, M. Aliofkhazraei, M. Hosseinali, Electrophoretic deposition of ZnO–CeO_2 mixed oxide nanoparticles, J. Am. Ceram. Soc. (ACS), 100, 901–910, (2017).

[22] M. Hasanpoor, H. Liu, H. Liu, X. Han, Core–shell CeO2 micro/nanospheres prepared by microwave assisted solvothermal process as high-stability anodes for Li-ion batteries. J. Solid State Electrochem. (Springer) 21, 291–295, (2017).

Karnatak University Journal of Science

Ameliorative effect of Cissus quadrangularis extract on carbosulfan induced splenic damage and hematological alterations in male albino rats (Rattus norvegicus)

Lokeshkumar P, M. David*

Department of Zoology, Karnatak University, Dharwad-580003
*Corresponding author: davidkcd@gmail.com

ARTICLE INFO

ABSTRACT

Carbosulfan is a major insecticide causing toxicological implication in mammals. Several studies estimated the consequences posed by this insecticide. The present study designed to investigate the possible ameliorative effects of Cissus quadrangularis on carbosulfan induced hematological alterations and splenic damage in male albino rat. The rats were subjected to 60 days exposure to sublethal concentration of carbosulfan. Hematological analyses revealed alterations in blood indices including red blood cells, white blood cells, hematocrit, hemoglobin, and platelet count. However, increased calcium level in plant extract treated groups was significant in the present study. This might be attributed to calcium enhancing property of plant extract in the animal physiology. Histological examination of spleen resulted in rarefication of white pulp, damaged marginal zone, decreased periarteriolar lymphoid sheath (PALS) and number of lymphoid follicles in high concentration of carbosulfan group. However, co-treatment of plant extract significantly recovered low concentration carbosulfan treated group than high concentration treated group. This indicates the ameliorative property of plant extract on immunomodulatory effects of carbosulfan. Results of the present study suggest that Cissus quadrangularis extract has potential key role in hematological and immunomodulatory processes that might be implemented in future for drug developmental purposes.

Introduction

A variety of pesticides used in agricultural industry contributed successfully to control harmful pests. However, the negative impact of pesticide residues on non-target organisms including fishes, amphibians and humans is a growing concern in recent years [1]–[4]. Apart from beneficial aspects of pesticides, people are using it as an alternative suicidal material in villages. As estimated by WHO, 1/3rd of suicidal cases all over the world occur due to pesticide intoxication which is a major public health issue in agricultural workers [5], [6]. Increased pesticide residues in rivers and waterbodies owed to lack of awareness in public and easy access to pesticides in the market [7]–[9]. Recent studies revealed that the vegetables, soil, human blood and breast milk were found to be having traces of pesticide residues that are harmful to human being and in some cases suspected to be a factor that leads to pregnancy loss in human beings [10]–[13]. Spleen is an important, largest and secondary lymphoid organ with compact structure that protects from blood-borne infections by the initiation of effective immune response. Immune response through phagocytosis, T- cell mediated immunity and B- cell mediated humoral immunity are the most important functions of spleen. Any biological alterations in the spleen will cause adverse effect on the organism [14]–[16]. Several studies indicated the effect of pesticides including carbosulfan was found to be spleenotoxic and modulates the normal function of spleen [17]–[19]. However, there is a void in literature related to spleen and needs attention in this research area. Hence, it is necessary to evaluate the adverse effect of carbosulfan and ameliorative properties of *Cissus quadrangularis* in spleen of male wistar rats. Carbosulfan [2,3-dihydro-2,2-dimethyl-7-benzofuranyl [(dibutylamino)thio] methylcarbamate belongs to carbamate group of insecticides. It has been widely applied to maize, coffee and rice crops to control various types of pests including nematodes, thrips and aphids. It was found to be highly effective in control of pests by the inhibition of AChE activity [20], [21]. Aquatic fauna was significantly affected by the insecticide carbosulfan and was found to be an oxidative stress inducer, mutagenic and genotoxic in nature [22]–[24]. Studies on carbosulfan revealed that it is a potential AChE inhibitor in *Oncorhynchus mykiss* and metabolism disruptor in *Danio rerio* [25], [26]. Although investigations regarding toxicity effects of carbosulfan on mammalian models are meagre, recent studies explained the significant changes in antioxidant enzymes, biochemical activities and haematological indices of male Sprague dawley rats exposed to carbosulfan [27]. Developmental disabilities including changes in AChE activity, oxidative markers and neurobehavioral changes were observed in rats during embryonic period [28]. Altered enzyme activities and testicular biochemical parameters were reported and was suspected to be a possible genotoxic inducer in male albino mice [29]. Physiological and histological impairments were reported in the liver of albino mice exposed to carbosulfan (Ksheerasagar and Kaliwal, 2006). Nuclear abnormalities and genotoxic effects were dominant in the fish *Channa punctatus* exposed to mixture of pesticides including carbosulfan [30].

Cissus quadrangularis (CQ) is a perennial climber, historically known as bone setter for its bone healing capacity. It belongs to vitaceae family and distributed throughout India especially tropical regions. The growth of the plant mainly depends on warm tropical climate that accelerates quadrangular stem propagation in the month of June and July [31]. The plant was mentioned in Ayurveda for its medicinal properties such as anthelminthic, digestive, analgesic in ear and eye diseases, asthma and irregular menstrual cycle. Studies reported antibacterial and inhibitory activity against leukemic cells and also used to prepare natural cellulosic fibre which can be used as an alternative to artificial fibre [32]–[34]. Anti-inflammatory effect, anti-arthritic activity, anti-ulcer activity, antiosteoporosis activity and amelioration of hyperglycaemic mediated antioxidative stress was revealed by recent studies [35]–[39].

It has been noted that *Cissus quadrangularis* extract was safe and examined no-observed-adverse-effect level (NOAEL) at 2500mg/ kg bw/day [40]. However, a few studies have attempted to investigate the ameliorative property of *Cissus quadrangularis* on pesticide induced

Lokeshkumar P and M. David

toxicity. A number of researchers have demonstrated the ameliorative effects of different plant extracts on pesticide induced toxicities. Ginger extract had preventative effect on lambda-cyhalothrin induced toxic effects in rats [41], *Beta vulgaris* root extracts ameliorated chlorpyriphos induced oxidative stress, inflammation and liver injury [42], *Cyperus rotundus* L. tuber extract exhibited neuroprotective effect against esfenvelerate damage in rats [43], *Citron limon* fruit extract found to be hepatoprotective against carbofuran induced toxicity [44]. Aqueous extract of *Cissus quadrangularis* was found to be effective in ameliorating quinalphos induced reproductive toxicity in albino mice [45]. However, there is a lacuna in relation to therapeutic effects of *Cissus quadrangularis*, hence the present study carried out to investigate the protective effects of ethanolic extracts of *Cissus quadrangularis* on carbosulfan induced splenic damage and haematological alterations in male wistar albino rat.

1. Materials and methods

a. Plant collection and preparation of ethanolic extract

Fresh stems of *Cissus quadrangularis* was collected from local habitats of Nelamangala taluk, Bengaluru district, Karnataka State, India. The specimen was shade dried for 30 days, powdered and sewed to get fine powder of the plant material. The resulting powder was subjected to Soxhlet apparatus containing ethanol and distilled water (75:25 ml v/v). The extraction was continued for 10 hours and then it was processed in rotary evaporator (BUCHI rotavapor R-210) to get final ethanolic extract. The final dosing concentration of 1000mg/kg BW of rat was prepared using distilled water and DMSO (Dimethyl sulfoxide) (99:1 ml v/v) as a vehicle.

b. Chemicals

Carbosulfan (Marshall 25% EC) was procured from FMC corporation India Pvt, Ltd. Mumbai, Maharashtra. Benzene, Xylene, paraffin wax and all other chemicals were of analytical grade and purchased from SRL Pvt. Ltd.

c. Animal maintenance

About 7-8 week old adult male albino rats of wistar strain (*Rattus* norvegicus) was obtained from the animal house facility, Department of Zoology, Karnatak university, Dharwad (No. 693/GO/Re/S/02/CPCSEA). They were maintained in polypropylene cages with free access to feed (VRK nutritional solutions, Sangli, Maharashtra) and water. rats were allowed to acclimatize to laboratory environment of temperature 25 ± 4 °C, 12/12h day and night cycle and relative humidity of $34 \pm 5\%$.

d. Experimental design

For the present study *Cissus quadrangularis* plant extract of 1000 mg/ kg BW was selected as an ameliorative drug concentration and the carbosulfan (Marshall 25% EC) concentrations of 6.37mg/ kg BW (high dose) and 3.4mg/ kg BW (low dose) was selected. The experimental period was 60 days and the dosing done during daylight. Post acclimatized male albino rats were randomly selected and divided into 6 groups (n=6). First group served as control with the administration of 1% DMSO/ kg BW, second group received plant extract only (1000 mg/ kg BW), third and fourth group received carbosulfan alone high and low dose (6.37mg and 3.4mg/ kg BW) respectively. fifth and sixth groups administered with plant extract (1000 mg/ kg BW) plus carbosulfan concentrations of 6.37mg and 3.4mg/kg BW respectively.

e. Hematology

Post experimental animals were sacrificed on completion of 60th day and the blood were collected in EDTA (helico HI-Nvac K_3 EDTA, 2ml) and clot activator vacutainers via cardiac puncture. The collected blood was subjected to centrifugation (3000 rpm, 5 minutes) to obtain clear serum and stored in deep freezer until further analyses. Hematological parameters such as Hemoglobin (Hb), Platelet count, Serum calcium, Cholesterol, Red blood cells (RBC), White blood cells (WBC), Hematocrit, Blood urea, Sugar, Creatinine, Neutrophils, Eosinophils and Lymphocytes were analyzed using auto hematology analyzer (UBM, Fx-19). Mean corpuscular volume (MCV), Mean

Lokeshkumar P and M. David

corpuscular hemoglobin concentration (MCHC) was calculated by following formulae.

$$1)\ MCV = \frac{Hematocrit\ (\%)\ X\ 10}{RBC\ count\ (10^6\ cells\ per\ mm^3)}$$

$$2)\ MCHC = \frac{Hemoglobin\ (g\ per\ 100ml)X\ 100}{Hematocrit\ (\%)}$$

f. Histology

Rats were autopsied on 60th day of experiment and the organs were isolated washed with PBS (1X, pH 7.0) and fixed in formalin (10%) for 24 hours. Post fixed organs were subjected to dehydration process with alcohol gradients and embedded in paraffin wax [46]. Thin sections (5µm) of spleen were obtained using automated microtome (Leica RM 2255). The sections were then stained with Hematoxylin & eosin and photographed using Olympus phase contrast microscope (Olympus BX51, Tokyo, Japan) with attached photographic camera (ProgRes C3, Jenoptic-Germany). The slides were analyzed in x100 magnification for better histopathological findings.

g. Ethical statement

All experiments performed in the present study followed the guidelines of the Institutional Animal Ethics Committee (IAEC). The experimental animals used in the study were handled with care according to the guidelines provided by the Committee for the Purpose of Control and Supervision of Experiments on Animals (CPCSEA), New Delhi, India.

h. Statistical analyses

All the data presented in the study was performed using Origin pro 2019b statistical package. The data were subject to one-way analyses of variance (ANOVA) with Tukey's post-hoc test and the data are presented as mean ± SD values with significance value set at $p < 0.05$.

2. Result

a. Haematology

Haematological data analysed in the present study was tabulated in Table 1. Haematological indices such as RBC, WBC, haemoglobin and haematocrit indicates overall health of the animal. In the present study red blood cell (RBC) level was found to be low in high dose and low dose treated animals and were significantly different ($p < 0.05$). White blood cells (WBC) were manifested elevated levels in high dose group compare to all other groups. Haemoglobin, haematocrit and platelet count was maintained normal in plant plus insecticide treated group and was reduced in high dose group. There was no significant change in MCV values except high dose group. MCHC was significantly different ($p < 0.05$) except plant plus high dose group. Blood sugar, serum calcium levels and total cholesterol levels were considerably different compare to control group ($p < 0.05$). Variation in blood urea, serum creatinine, neutrophils, lymphocytes and eosinophils were tabulated in Table 1.

3.2 Histopathology

The present study focused on spleen histopathology to analyze overall health of the organ. Histopathological alterations were photographed (Fig.1) and analyzed using available literature [47], [48]. There were no visible external signs of toxicity observed both in carbosulfan and plant extract treated group. In the figure 1 A, Control tissue of spleen of male albino rat exhibited normal histoarchitecture with sufficient amount of red pulp (R), white pulp (W), lymphoid follicle (LF) and marginal zone (MZ). In detail histological observation were tabulated in Table 2. The plant extract treated group indicated well demarcated histological structures as that of control group. In high dose insecticide treated group the red pulp has shown decreased cellularity and white pulp was markedly destructed, there were no proper lymphoid follicle and marginal zone. Low dose carbosulfan group manifested destructed cellular integrity in white pulp and red pulp. In contrast to this plant treated group including high and low dose revealed remarkable recovery of histological structures. White pulp was well recovered in plant plus insecticide low dose treatment group compare to plant plus high dose group.

Table 1: Effect of *Cissus quadrangularis* on carbosulfan induced hematological alterations in male wistar rats.

Parameters	Control	Plant	High dose	Low dose	Plant+ High dose	Plant+ Low dose
RBC (10⁶ cells/ mm³)	7.15 ± 0.16ᵃ	6.55 ± 0.33ᵇ	5.21 ± 0.23ᶜ	5.73 ± 0.37ᵈ	6.21 ± 0.17ᵉ	6.58 ± 0.31ᶠ
WBC (10³ cells/ mm³)	4.28 ± 0.23ᵃ	4.08 ± 0.11ᵃ	6.16 ± 0.21ᵇ	5.33 ± 0.28ᶜ	5.08 ± 0.21ᵈ	4.26 ± 0.25ᵃ
Hemoglobin (%)	15.35 ± 0.50ᵃ	10.18 ± 0.54ᵇ	10.2 ± 0.21ᶜ	10.95 ± 0.24ᵈ	12.83 ± 0.148ᵉ	11.91 ± 0.61ᵉ
Hematocrit (%)	45.16 ± 0.12ᵃ	43.48 ± 0.29ᵇ	36.53 ± 0.35ᶜ	38.51 ± 0.34ᵈ	40.08 ± 0.17ᵉ	42.25 ± 0.71ᶠ
Platelet count (lakhs/ cu mm)	3.84 ± 0.09ᵃ	3.12 ± 0.20ᵇ	2.24 ± 0.16ᶜ	2.54 ± 0.30ᵈ	2.49 ± 0.24ᵉ	3.22 ± 0.15ᶠ
MCV (μm³)	63.19 ± 1.38ᵃ	66.52 ± 3.25ᵃ	70.12 ± 2.52ᵇ	67.41 ± 4.34ᵃ	66.58 ± 5.32ᵃ	64.31 ± 3.68ᵃ
MCHC (g/ dl)	33.98 ± 1.11ᵃ	23.39 ± 1.24ᵇ	27.91 ± 0.51ᶜ	28.42 ± 0.46ᵈ	32 ± 1.16ᵃ	28.22 ± 2.01ᵉ
Blood Urea (mg/ dl)	35.05 ± 0.82ᵃ	35.15 ± 0.28ᵃ	25.05 ± 0.42ᵇ	34.15 ± 0.63ᵃ	30.64 ± 0.45ᶜ	31.4 ± 0.71ᵈ
Blood sugar (mg/ dl)	144.83 ± 2.13ᵃ	127.16 ± 3.06ᵇ	80 ± 1.41ᶜ	98 ± 1.78ᵈ	95.83 ± 2.31ᵉ	116.83 ± 2.92ᶠ
Serum Creatinine (mg/ dl)	1.25 ± 0.10ᵃ	1.68 ± 0.19ᵇ	0.88 ± 0.17ᶜ	1.41 ± 0.14ᵃ	1.21 ± 0.26ᵃ	1.36 ± 0.18ᵃ
Serum Calcium level (mg/ dl)	9.28 ± 0.31ᵃ	11.11 ± 0.47ᵇ	6.38 ± 0.34ᶜ	7.91 ± 0.24ᵈ	8.1 ± 0.23ᵉ	10.06 ± 0.32ᶠ
Neutrophils (%)	54.33 ± 2.06ᵃ	66.5 ± 2.88ᵇ	56.5 ± 2.58ᵃ	61.83 ± 1.72ᶜ	63.83 ± 2.48ᵈ	74.16 ± 2.48ᵉ
Lymphocytes (%)	36.16 ± 2.31ᵃ	23 ± 1.78ᵇ	35.83 ± 2.31ᵃ	40 ± 1.41ᶜ	28.83 ± 1.72ᵈ	22.16 ± 1.47ᵉ
Eosinophils (%)	5 ± 1.41ᵃ	6 ± 1.89ᵃ	5 ± 1.41ᵃ	5.16 ± 1.94ᵃ	4.83 ± 1.94ᵃ	2.16 ± 1.16ᵃ

All data represented as the mean ± SD (n=6). Values in the row with different superscript are significantly different at $p<0.05$

Table 2: Effect of *Cissus quadrangularis* on carbosulfan induced histoarchitectural changes in spleen tissues of male wistar rats.

Histological observation		Control	Plant (1000mg/ kg BW)	High dose (6.37mg/ kg BW)	Low dose (3.4mg/ kg BW)	Plant (1000mg/ kg BW) + High dose (6.37mg/ kg BW)	Plant (1000mg/ kg BW) + Low dose (3.4 mg/ kg BW)
Number of Follicles		0	0	(↓) 3	(↓) 2	(↓) 2	(↓) 1
Marginal Zone	Size	0	0	(↓) 4	(↓) 2	(↓) 2	(↓) 1
	Lymphocytes	0	0	(↑) 2	(↑) 1	0	0
Red pulp	Size	0	0	(↓) 4	(↓) 2	(↓) 2	(↓) 1
	Hematopoietic cells	0	0	(↓) 3	(↓) 2	(↓) 1	(↓) 1

*Note: 0 = normal, 1 = minimal, 2 = mild, 3 = moderate, 4 = marked, (↑) increased, (↓) decreased.
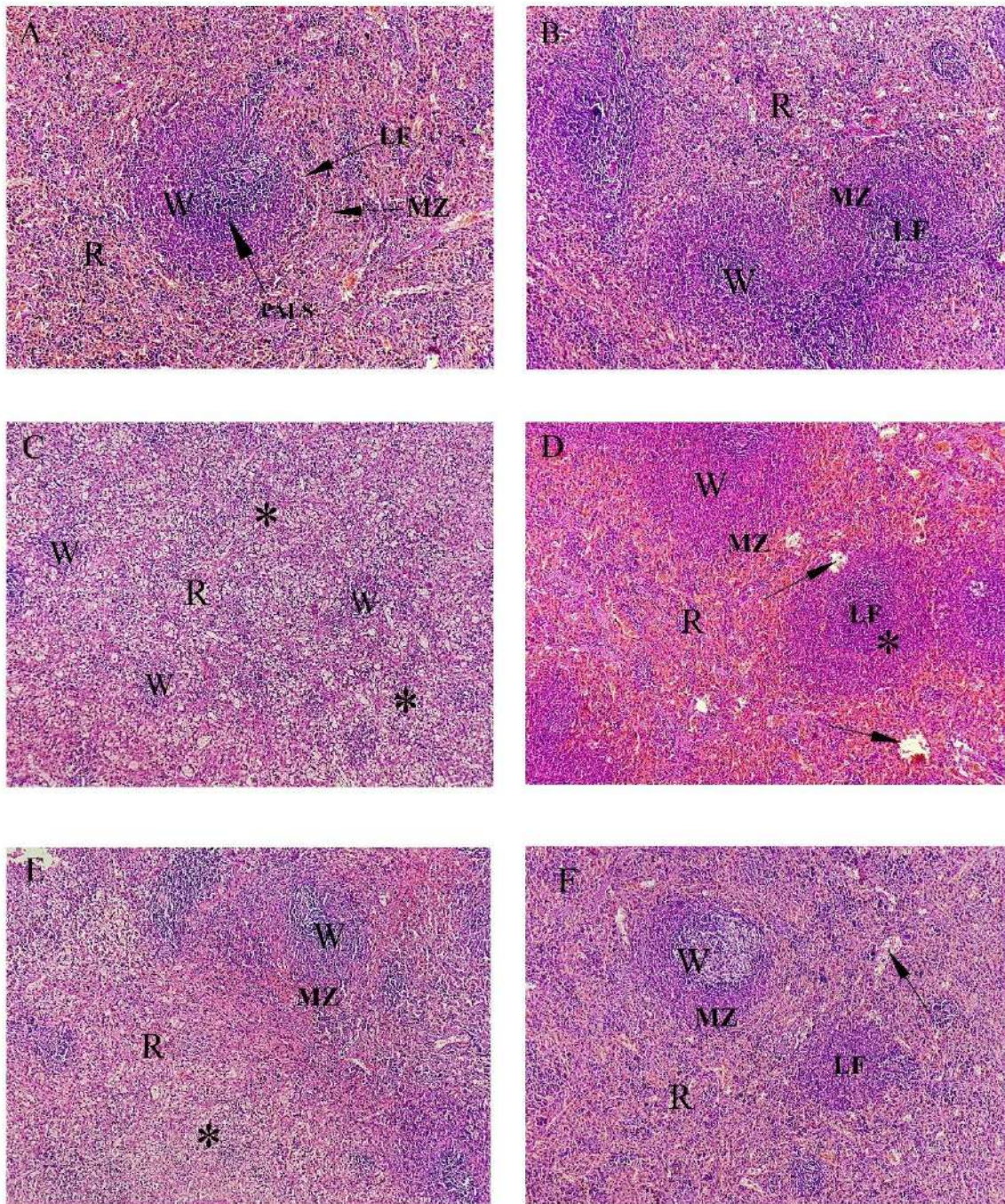
Fig. 1: (A) Spleen sections of control rats: (R) red pulp; (W) white pulp; (LF) lymphoid follicle; (MZ) marginal zone; (PALS) Periarteriolar lymphoid sheath. H&E, x100. (B) Spleen structure of rat treated with plant alone (1000mg/ kg BW) shows normal histoarchitecture. (C) & (D) Spleen sections of rats treated with carbosulfan (6.37 & 3.4 mg/ kg BW) respectively: arrow head ($\rightarrow$) shows thin damaged marginal zone (MZ), asterisk (*) indicates decreased cellularity (rarefication) and altered structural integrity of white pulp. H&E, 100x. (E) & (F) spleen tissues of plant plus carbosulfan treated (6.37mg/ kg, 3.4mg/ kg, 1000mg/ kg BW) respectively: ($\rightarrow$) shows damaged tissue region, marginal zone (MZ) & lymphoid follicles (LF) are significantly recovered. H&E, 100x.

3. Discussion

Carbosulfan is applied for a wide range of agricultural crops to avoid pest attack on crops and to improve the yield. Inhibition of acetylcholinesterase is a characteristic feature of carbosulfan that leads to aggregation of acetylcholine (neurotransmitter) in synapses. Overstimulation of postsynaptic cholinergic

receptors in neuromuscular junction induce muscle fasciculation in which at the end leads to paralyses of organism [49]. Carbosulfan was found to be a potential hemotoxic drug that elicits micronuclei formation in aquatic animals [22], [50]. It was also notably hemotoxic in mammalian model male Sprague dawley rats [27]. In the present study carbosulfan instigated hematological and histological alterations. Hematological studies revealed that RBC levels was significantly decreased in high dose carbosulfan treated group, indicating insecticide induced anemic condition in the animal. However, treatment of *Cissus quadrangularis* against insecticide treated animal remarkably recovered from low RBC count. The low count of RBC might be attributed to toxicity induced by the carbosulfan as it was demonstrated to effect bone marrow cells [51]. Elevated levels of WBC in high insecticide dose treatment group might indicates the onset of infection and defense mechanism in the animal [52]. Hemoglobin and hematocrit levels were slightly varied compared to control but recovered in case of plant treatment. Increased levels in MCV was observed in the group treated with carbosulfan high dose which could be a possible cause of anisocytosis.

Raised levels of MCV might indicate the presence of immature RBC that owing to compensatory mechanism to serve carbosulfan induced loss in RBC concentration [53]. MCHC values indicates the concentration of hemoglobin, the high concentration of insecticide dose showed low level of MCHC values compared to control and that in turn indicates the reduced level of hemoglobin concentration. Other hematological parameters such as blood sugar, urea, creatinine, neutrophils, lymphocytes and eosinophils altered due to insecticide intoxication. Attenuation of lymphocytes in the plant plus carbosulfan treated group may indicate the immunomodulatory effect of *Cissus quadrangularis* [54]. Increased level of serum calcium in plant extract treated group including carbosulfan and plant extract treated group illustrates the calcium promoting activity of *Cissus quadrangularis*. Previous studies also obtained similar kind of results in which the level of calcium was found to be high and accelerate the bone healing capacity [35], [55]. Our results are concordant with the previous hematological results of Ambali et al., 2011; Aroonvilairat et al., 2018; Rahman and Siddiqui, 2006; Savithri et al., 2010.

Therefore, the plant was effective in ameliorating the hematological changes elicited by the insecticide. Histopathological examination reveals the internal structure of an organ and aid in toxicity evaluation. Histology of spleen contains white pulp, red pulp, lymphoid follicle and periarteriolar lymphoid sheath (PALS). It plays an important role in elimination of weak, degenerate and aged red blood cells and also the bacteria from the blood supply [59]. Interpretation of histological changes in the spleen tissue was carried out with the aid of available literature [47], [48], [59]–[61]. Figure 1 represents the histological photographs of spleen of control, carbosulfan treated and plant plus carbosulfan treated groups. Control group and plant (*Cissus quadrangularis* 1000mg/ kg bw) treated group exhibited normal histological structures with compact parenchymal tissue, lymphoid follicle and periarteriolar lymphoid sheath (PALS). Carbosulfan high concentration treated group showed various histological alterations, white pulp was inspected with severely decreased cellularity, lymphoid follicle and periarteriolar lymphoid sheath. Similar symptoms but with extensive expansion of red pulp was observed in the spleen of rats treated with cisplatin [62]. Moderate to severe atrophy in white pulp was observed in the spleen tissues of male rats treated with Bisphenol-A [63].

In another study carbosulfan was found to implicate immunomodulatory effect by cytokine production in spleen cells [18]. In low dose carbosulfan treatment group the spleen was characterized by rarefication of marginal zone. This might be due to the immunomodulatory effect of carbosulfan, as the marginal zone was found to produce neutrophils and immunoglobulin, elevation of neutrophil levels could be related to the activation of defensive system in the animal [64]. Distortion of marginal zone was major histopathological symptom in the spleen of methimazole treated rats [65]. Cadmium treatment produced conflicting data regarding spleen, suppressing as well as stimulating effects were obtained in high doses of cadmium whereas in low dose treatment it expressed only proinflammatory effects of T-cells [66]. *In vivo* administration of Flubendiamide induced separation of splenocytes

Lokeshkumar P and M. David

and rarefication of the tissue in the spleen. Further the rarefication was found in white pulp and in lymphoid follicle [67]. Excess fluoride exposure on female rat found to be exacerbated with splenocyte apoptosis and abnormal cytokine expression [68]. Sodium fluoride treated rats spleen examined with degeneration of red pulp and lymphocyte infiltration [69]. In our study the number and size of lymphocytes in the marginal zone was depleted in high & low concentration of carbosulfan treated groups and recovered on protective treatment of ethanolic extract of *Cissus quadrangularis* (Table 2). Recovery of number of follicles in white pulp and hematopoietic cells in red pulp was evident in the study. Our study agrees with the studies of Hafez, 2013 where the *Ginkgo biloba* extract was able to recover splenic damage induced by the noise stress in adult albino rat.

4.   Conclusion

The aim of the present study was to investigate ameliorative effect of *Cissus quadrangularis* plant extract on carbosulfan induced toxicity. Hematological studies revealed the altered hematological indices including red blood cells (RBC), white blood cells (WBC), hemoglobin, hematocrit and platelet count in carbosulfan treated groups. However, protective treatment of CQ extract (1000mg/ kg bw) effectively normalized the haemotoxicity induced by carbosulfan. The results of this study evidenced elevated levels of serum calcium which might be owing to the calcium promoting capacity of CQ extract. Histopathological examinations such as rarefication of white pulp, decreased and damaged marginal zone, decreased number of lymphoid follicles were noticeable in carbosulfan treated groups. In contrast the CQ plant extract treated group showed recovery of the above said pathological symptoms. This suggests immunoprotective effect of CQ extract in carbosulfan intoxicated rats. This investigation might assist to future research related to exploration of possible key drug involved calcium promoting activity.

Conflict of interest

Authors claims no conflict of interest.

References

[1] M. David, S. R. Marigoudar, V. K. Patil, and R. Halappa, "Behavioral, morphological deformities and biomarkers of oxidative damage as indicators of sublethal cypermethrin intoxication on the tadpoles of D. melanostictus (Schneider, 1799)," *Pestic. Biochem. Physiol.*, vol. 103, no. 2, pp. 127–134, Jun. 2012, doi: 10.1016/j.pestbp.2012.04.009.

[2] M. David and R. M. Kartheek, "Malathion acute toxicity in tadpoles of Duttaphrynus melanostictus, morphological and behavioural study," *J. Basic Appl. Zool.*, vol. 72, pp. 1–7, Oct. 2015, doi: 10.1016/j.jobaz.2015.01.004.

[3] J. Gao *et al.*, "A full evaluation of chiral phenylpyrazole pesticide flufiprole and the metabolites to non-target organism in paddy field," *Environ. Pollut.*, vol. 264, p. 114808, Sep. 2020, doi: 10.1016/j.envpol.2020.114808.

[4] C. D. Milam, J. L. Farris, and J. D. Wilhide, "Evaluating Mosquito Control Pesticides for Effect on Target and Nontarget Organisms," *Arch. Environ. Contam. Toxicol.*, vol. 39, no. 3, pp. 324–328, Sep. 2000, doi: 10.1007/s002440010111.

[5] J. M. Bertolote, A. Fleischmann, M. Eddleston, and D. Gunnell, "Deaths from pesticide poisoning: a global response," *Br. J. Psychiatry*, vol. 189, no. 3, pp. 201–203, Sep. 2006, doi: 10.1192/bjp.bp.105.020834.

[6] L. Vijayakumar, L. Jeyaseelan, S. Kumar, R. Mohanraj, S. Devika, and S. Manikandan, "A central storage facility to reduce pesticide suicides - a feasibility study from India," *BMC Public Health*, vol. 13, no. 1, p. 850, Dec. 2013, doi: 10.1186/1471-2458-13-850.

[7] A. Agarwal, R. Prajapati, O. P. Singh, S. K. Raza, and L. K. Thakur, "Pesticide residue in water—a challenging task in India," *Environ.*

Lokeshkumar P and M. David

Monit. Assess., vol. 187, no. 2, p. 54, Feb. 2015, doi: 10.1007/s10661-015-4287-y.

[8] A. Kaushik, H. R. Sharma, S. Jain, J. Dawra, and C. P. Kaushik, "Pesticide pollution of River Ghaggar in Haryana, India," *Environ. Monit. Assess.*, vol. 160, no. 1–4, pp. 61–69, Jan. 2010, doi: 10.1007/s10661-008-0657-z.

[9] M. K. Mohanty *et al.*, "Knowledge attitude and practice of pesticide use among agricultural workers in Puducherry, South India," *J. Forensic Leg. Med.*, vol. 20, no. 8, pp. 1028–1031, Nov. 2013, doi: 10.1016/j.jflm.2013.09.030.

[10] T. P. Swarnam and A. Velmurugan, "Pesticide residues in vegetable samples from the Andaman Islands, India," *Environ. Monit. Assess.*, vol. 185, no. 7, pp. 6119–6127, Jul. 2013, doi: 10.1007/s10661-012-3012-3.

[11] A. Sharma, J. P. S. Gill, and J. S. Bedi, "Monitoring of Pesticide Residues in Human Blood from Punjab, India," *Bull. Environ. Contam. Toxicol.*, vol. 94, no. 5, pp. 640–646, May 2015, doi: 10.1007/s00128-015-1522-8.

[12] A. Pandey *et al.*, "Pesticide Risk and Recurrent Pregnancy Loss in Females of Subhumid Region of India," *Niger. Med. J. J. Niger. Med. Assoc.*, vol. 61, no. 2, pp. 55–59, 2020, doi: 10.4103/nmj.NMJ_117_18.

[13] J. S. Bedi, J. P. S. Gill, R. S. Aulakh, P. Kaur, A. Sharma, and P. A. Pooni, "Pesticide residues in human breast milk: Risk assessment for infants from Punjab, India," *Sci. Total Environ.*, vol. 463–464, pp. 720–726, Oct. 2013, doi: 10.1016/j.scitotenv.2013.06.066.

[14] M. Laukova, P. Vargovic, I. Rokytova, G. Manz, and R. Kvetnansky, "Repeated Stress Exaggerates Lipopolysaccharide-Induced Inflammatory Response in the Rat Spleen," *Cell. Mol. Neurobiol.*, vol. 38, no. 1, pp. 195–208, Jan. 2018, doi: 10.1007/s10571-017-0546-5.

[15] G. Tarantino, S. Savastano, D. Capone, and A. Colao, "Spleen: A new role for an old player?," *World J. Gastroenterol. WJG*, vol. 17, no. 33, pp. 3776–3784, Sep. 2011, doi: 10.3748/wjg.v17.i33.3776.

[16] R. Zhou *et al.*, "A New Role for the Spleen," *Am. J. Pathol.*, vol. 189, no. 11, pp. 2233–2245, Nov. 2019, doi: 10.1016/j.ajpath.2019.07.008.

[17] I. B. Dhouib, M. M. Lasram, M. Abdeladhim, N. Gharbi, M. B. Ahmed, and S. El-Fazaa, "Immunosuppression and oxidative stress induced by subchronic exposure to carbosulfan in rat spleen: immunomodulatory and antioxidant role of N-acetylcysteine," *Toxicol. Mech. Methods*, vol. 24, no. 6, pp. 417–427, Sep. 2014, doi: 10.3109/15376516.2014.928764.

[18] I. El-Bini Dhouib, M. M. Lasram, A. Annabi, N. Gharbi, and S. El-Fazaa, "A comparative study on toxicity induced by carbosulfan and malathion in Wistar rat liver and spleen," *Pestic. Biochem. Physiol.*, vol. 124, pp. 21–28, Oct. 2015, doi: 10.1016/j.pestbp.2015.03.012.

[19] A. Medjdoub, S. A. Merzouk, H. Merzouk, F. Z. Chiali, and M. Narce, "Effects of Mancozeb and Metribuzin on in vitro proliferative responses and oxidative stress of human and rat spleen lymphocytes stimulated by mitogens," *Pestic. Biochem. Physiol.*, vol. 101, no. 1, pp. 27–33, Sep. 2011, doi: 10.1016/j.pestbp.2011.06.002.

[20] P. Guillet, R. N'Guessan, F. Darriet, M. Traore-Lamizana, F. Chandre, and P. Carnevale, "Combined pyrethroid and carbamate 'two-in-one' treated mosquito nets: field efficacy against pyrethroid-resistant Anopheles gambiae and Culex quinquefasciatus," *Med. Vet. Entomol.*, vol. 15, no. 1, pp. 105–112, 2001, doi: https://doi.org/10.1046/j.1365-2915.2001.00288.x.

[21] C.-H. Hsu, C.-C. Hu, and T.-C. Chiu, "Analysis of carbofuran, carbosulfan, isoprocarb, 3-hydroxycarbofuran, and 3-ketocarbofuran by micellar electrokinetic chromatography," *J. Sep. Sci.*, vol. 35, no. 10–11, pp. 1359–1364, 2012, doi: https://doi.org/10.1002/jssc.201101108.

[22] I. Altinok, E. Capkin, and H. Boran, "Mutagenic, genotoxic and enzyme inhibitory effects of carbosulfan in rainbow trout Oncorhynchus mykiss," *Pestic. Biochem. Physiol.*, vol. 102, no. 1, pp. 61–67, Jan. 2012, doi: 10.1016/j.pestbp.2011.10.011.

[23] E. Capkin and I. Altinok, "Effects of chronic carbosulfan exposure on liver antioxidant enzyme activities in rainbow trout," *Environ. Toxicol. Pharmacol.*, vol. 36, no. 1, pp. 80–87, Jul. 2013, doi: 10.1016/j.etap.2013.03.022.

Lokeshkumar P and M. David

[24] M. David, "Studies on carbosulfan induced oxygen deprivation and behavioral anomalies in freshwater fish Cyprinus carpio," *J Adv Sci Res*, vol. 11, no. 4, pp. 1–8, 2020.

[25] E. Capkin and H. Boran, "Response of Acetylcholinesterase (AChE) in the Erythrocyte and Liver of Rainbow Trout Exposed to Carbosulfan," *Turk. J. Fish. Aquat. Sci.*, vol. 14, pp. 1–2, Sep. 2014, doi: 10.4194/1303-2712-v14_3_06.

[26] J. Cui *et al.*, "Bioaccumulation and Metabolism of Carbosulfan in Zebrafish (*Danio rerio*) and the Toxic Effects of Its Metabolites," *J. Agric. Food Chem.*, vol. 67, no. 45, pp. 12348–12356, Nov. 2019, doi: 10.1021/acs.jafc.9b03674.

[27] C. D. Nwani *et al.*, "Toxicological effects of carbosulfan in rats: Antioxidant, enzymological, biochemical, and hematological responses," *Toxicol. Ind. Health*, vol. 32, no. 7, pp. 1335–1343, Jul. 2016, doi: 10.1177/0748233714564243.

[28] D. Banji, O. J. F. Banji, M. Ragini, and A. R. Annamalai, "Carbosulfan exposure during embryonic period can cause developmental disability in rats," *Environ. Toxicol. Pharmacol.*, vol. 38, no. 1, pp. 230–238, Jul. 2014, doi: 10.1016/j.etap.2014.05.009.

[29] R. L. Ksheerasagar and B. B. Kaliwal, "Temporal effects of carbosulfan on testicular biochemical parameters and enzyme activities in albino mice," pp. 1–9, 2013.

[30] C. D. Nwani, N. S. Nagpure, R. Kumar, B. Kushwaha, P. Kumar, and W. S. Lakra, "Induction of micronuclei and nuclear lesions in *Channa punctatus* following exposure to carbosulfan, glyphosate and atrazine," *Drug Chem. Toxicol.*, vol. 37, no. 4, pp. 370–377, Oct. 2014, doi: 10.3109/01480545.2013.866138.

[31] R. P. Rastogi and B. N. Mehrotra, *Compendium of Indian medicinal plants*. Central Drug Research Institute, 1990.

[32] S. Dhanasekaran, "Phytochemical characteristics of aerial part of Cissus quadrangularis (L) and its in-vitro inhibitory activity against leukemic cells and antioxidant properties," *Saudi J. Biol. Sci.*, vol. 27, no. 5, pp. 1302–1309, May 2020, doi: 10.1016/j.sjbs.2020.01.005.

[33] V. Gopinath, S. Priyadarshini, N. Meera Priyadharsshini, K. Pandian, and P. Velusamy, "Biogenic synthesis of antibacterial silver chloride nanoparticles using leaf extracts of Cissus quadrangularis Linn," *Mater. Lett.*, vol. 91, pp. 224–227, Jan. 2013, doi: 10.1016/j.matlet.2012.09.102.

[34] S. Indran and R. E. Raj, "Characterization of new natural cellulosic fiber from Cissus quadrangularis stem," *Carbohydr. Polym.*, vol. 117, pp. 392–399, Mar. 2015, doi: 10.1016/j.carbpol.2014.09.072.

[35] U. M. Aswar, V. Mohan, and S. L. Bodhankar, "Antiosteoporotic activity of phytoestrogen-rich fraction separated from ethanol extract of aerial parts of Cissus quadrangularis in ovariectomized rats," *Indian J. Pharmacol.*, vol. 44, no. 3, pp. 345–350, 2012, doi: 10.4103/0253-7613.96310.

[36] M. Jainu, K. Vijaimohan, and K. Kannan, "Cissus quadrangularis L. extract attenuates chronic ulcer by possible involvement of polyamines and proliferating cell nuclear antigen," *Pharmacogn. Mag.*, vol. 6, no. 23, p. 225, 2010, doi: 10.4103/0973-1296.66941.

[37] O. Karimi-Khouzani, E. Heidarian, and S. A. Amini, "Anti-inflammatory and ameliorative effects of gallic acid on fluoxetine-induced oxidative stress and liver damage in rats," *Pharmacol. Rep.*, vol. 69, no. 4, pp. 830–835, Aug. 2017, doi: 10.1016/j.pharep.2017.03.011.

[38] R. Kumar, Y. K. Gupta, S. Singh, and S. Arunraja, "Cissus quadrangularis attenuates the adjuvant induced arthritis by down regulating pro-inflammatory cytokine and inhibiting angiogenesis," *J. Ethnopharmacol.*, vol. 175, pp. 346–355, Dec. 2015, doi: 10.1016/j.jep.2015.08.058.

[39] R. K. Lekshmi, R. Rajesh, and S. Mini, "Ethyl acetate fraction of Cissus quadrangularis stem ameliorates hyperglycaemia-mediated oxidative stress and suppresses inflammatory response in nicotinamide/streptozotocin induced type 2 diabetic rats," *Phytomedicine*, vol. 22, no. 10, pp. 952–960, Sep. 2015, doi: 10.1016/j.phymed.2015.06.014.

[40] S. C. Kothari *et al.*, "Safety assessment of Cissus quadrangularis extract (CQR-300):

Lokeshkumar P and M. David

Subchronic toxicity and mutagenicity studies," *Food Chem. Toxicol.*, vol. 49, no. 12, pp. 3343–3357, Dec. 2011, doi: 10.1016/j.fct.2011.09.029.

[41] W. M. Al-Amoudi, "Toxic effects of Lambda-cyhalothrin, on the rat thyroid: Involvement of oxidative stress and ameliorative effect of ginger extract," *Toxicol. Rep.*, vol. 5, pp. 728–736, 2018, doi: 10.1016/j.toxrep.2018.06.005.

[42] G. Albasher, R. Almeer, F. O. Al-Otibi, N. Al-Kubaisi, and A. M. Mahmoud, "Ameliorative Effect of Beta vulgaris Root Extract on Chlorpyrifos-Induced Oxidative Stress, Inflammation and Liver Injury in Rats," *Biomolecules*, vol. 9, no. 7, Art. no. 7, Jul. 2019, doi: 10.3390/biom9070261.

[43] J. S. Hussein *et al.*, "Amelioration of neurotoxicity induced by esfenvalerate: impact of Cyperus rotundus L. tuber extract," *Comp. Clin. Pathol.*, vol. 30, no. 1, pp. 1–10, Feb. 2021, doi: 10.1007/s00580-020-03182-0.

[44] S. K. Jaiswal, V. K. Gupta, N. J. Siddiqi, R. S. Pandey, and B. Sharma, "Hepatoprotective Effect of *Citrus limon* Fruit Extract against Carbofuran Induced Toxicity in Wistar Rats," *Chin. J. Biol.*, vol. 2015, pp. 1–10, Nov. 2015, doi: 10.1155/2015/686071.

[45] P. Kokilavani *et al.*, "Antioxidant mediated ameliorative steroidogenesis by Commelina benghalensis L. and Cissus quadrangularis L. against quinalphos induced male reproductive toxicity," *Pestic. Biochem. Physiol.*, vol. 109, pp. 18–33, Feb. 2014, doi: 10.1016/j.pestbp.2014.01.002.

[46] J. D. Bancroft, *Theory and Practice of Histological Techniques*. Elsevier Health Sciences, 2008.

[47] S. A. Elmore, "Enhanced Histopathology of the Spleen," *Toxicol. Pathol.*, vol. 34, no. 5, pp. 648–655, Aug. 2006, doi: 10.1080/01926230600865523.

[48] R. E. Mebius and G. Kraal, "Structure and function of the spleen," *Nat. Rev. Immunol.*, vol. 5, no. 8, pp. 606–616, Aug. 2005, doi: 10.1038/nri1669.

[49] B. E. Mileson, A. T. Eldefrawi, A. G. Karczmar, R. J. Richardson, and L. G. Sultatos, "Common Mechanism of Toxicity: A Case Study

of Organophosphorus Pesticides," vol. 41, p. 13, 1998.

[50] C. D. Nwani, W. S. Lakra, N. S. Nagpure, R. Kumar, B. Kushwaha, and S. K. Srivastava, "Mutagenic and genotoxic effects of carbosulfan in freshwater fish Channa punctatus (Bloch) using micronucleus assay and alkaline single-cell gel electrophoresis," *Food Chem. Toxicol.*, vol. 48, no. 1, pp. 202–208, Jan. 2010, doi: 10.1016/j.fct.2009.09.041.

[51] S. Giri, A. Giri, G. D. Sharma, and S. B. Prasad, "Mutagenic effects of carbosulfan, a carbamate pesticide," *Mutat. Res. Toxicol. Environ. Mutagen.*, vol. 519, no. 1–2, pp. 75–82, Aug. 2002, doi: 10.1016/S1383-5718(02)00114-6.

[52] M. E. A. Elhalwagy, N. S. Darwish, and E. M. Zaher, "Prophylactic effect of green tea polyphenols against liver and kidney injury induced by fenitrothion insecticide," *Pestic. Biochem. Physiol.*, vol. 91, no. 2, pp. 81–89, Jun. 2008, doi: 10.1016/j.pestbp.2008.01.006.

[53] S. F. Ambali, J. O. Ayo, K. A. N. Esievo, and S. A. Ojo, "Hemotoxicity Induced by Chronic Chlorpyrifos Exposure in Wistar Rats: Mitigating Effect of Vitamin C," *Vet. Med. Int.*, vol. 2011, p. e945439, Apr. 2011, doi: 10.4061/2011/945439.

[54] C. I. Acker, A. C. G. Souza, M. P. dos Santos, C. M. Mazzanti, and C. W. Nogueira, "Diphenyl diselenide attenuates hepatic and hematologic toxicity induced by chlorpyrifos acute exposure in rats," *Environ. Sci. Pollut. Res.*, vol. 19, no. 8, pp. 3481–3490, Sep. 2012, doi: 10.1007/s11356-012-0882-4.

[55] H. R. Brahmkshatriya, K. A. Shah, G. B. Ananthkumar, and M. H. Brahmkshatriya, "Clinical evaluation of Cissus quadrangularis as osteogenic agent in maxillofacial fracture: A pilot study," *Ayu*, vol. 36, no. 2, pp. 169–173, 2015, doi: 10.4103/0974-8520.175542.

[56] S. Aroonvilairat, C. Tangjarukij, T. Sornprachum, P. Chaisuriya, T. Siwadune, and K. Ratanabanangkoon, "Effects of topical exposure to a mixture of chlorpyrifos, cypermethrin and captan on the hematological and immunological systems in male Wistar rats," *Environ. Toxicol. Pharmacol.*, vol. 59, pp. 53–60, Apr. 2018, doi: 10.1016/j.etap.2018.02.010.

Lokeshkumar P and M. David

[57] M. F. Rahman and M. K. J. Siddiqui, "Hematological and Clinical Chemistry Changes Induced by Subchronic Dosing of a Novel Phosphorothionate (RPR-V) in Wistar Male and Female Rats," *Drug Chem. Toxicol.*, vol. 29, no. 1, pp. 95–110, Jan. 2006, doi: 10.1080/01480540500408697.

[58] Y. Savithri, P. R. Sekhar, and P. J. Doss, "Changes in hematological profiles of albino rats under chlorpyrifos toxicity.," *Int. J. Pharma Bio Sci.*, vol. 1, no. 3, 2010, Accessed: Mar. 31, 2021. [Online]. Available: https://www.cabdirect.org/cabdirect/abstract/2011 3372389.

[59] A. W. Suttie, "Histopathology of the Spleen," *Toxicol. Pathol.*, vol. 34, no. 5, pp. 466–503, Aug. 2006, doi: 10.1080/01926230600867750.

[60] M. F. Cesta, "Normal Structure, Function, and Histology of the Spleen," *Toxicol. Pathol.*, vol. 34, no. 5, pp. 455–465, Aug. 2006, doi: 10.1080/01926230600867743.

[61] P. M. Treuting, S. M. Dintzis, D. Liggitt, and C. W. Frevert, *Comparative Anatomy and Histology: A Mouse and Human Atlas (Expert Consult)*. Academic Press, 2011.

[62] I. A. Okafor, U. S. Nnamah, and J. Nnaka, "Liver Function Analyses and Spleen Histology Assessment Following the Co-administration of Cisplatin and Methanolic Extract of Portulaca Oleracea in Wistar Rats: An Experimental Study," *Nat. Prod. Sci.*, vol. 26, no. 3, p. 7, 2020.

[63] A. J. Hussein, "Histopathological study of lung, kidney, spleen and prostate in adult male rats treated with Bisphenol A.," *Basrah J. Vet. Res.*, vol. 14, no. 2, pp. 74–86, 2015.

[64] I. Puga et al., "B cell–helper neutrophils stimulate the diversification and production of immunoglobulin in the marginal zone of the spleen," *Nat. Immunol.*, vol. 13, no. 2, pp. 170–180, Feb. 2012, doi: 10.1038/ni.2194.

[65] E. Cano-Europa, V. Blas-Valdivia, M. Franco-Colin, C. A. Gallardo-Casas, and R. Ortiz-Butrón, "Methimazole-induced hypothyroidism causes cellular damage in the spleen, heart, liver, lung and kidney," *Acta Histochem.*, vol. 113, no. 1, pp. 1–5, Jan. 2011, doi: 10.1016/j.acthis.2009.07.004.

[66] J. Demenesku et al., "Acute cadmium administration to rats exerts both immunosuppressive and proinflammatory effects in spleen," *Toxicology*, vol. 326, pp. 96–108, Dec. 2014, doi: 10.1016/j.tox.2014.10.012.

[67] R. Mandil et al., "In vitro and in vivo effects of flubendiamide and copper on cyto-genotoxicity, oxidative stress and spleen histology of rats and its modulation by resveratrol, catechin, curcumin and α-tocopherol," *BMC Pharmacol. Toxicol.*, vol. 21, no. 1, p. 29, Dec. 2020, doi: 10.1186/s40360-020-00405-6.

[68] J. Liu, H. Wang, W. Zhao, X. Li, L. Lin, and B. Zhou, "Induction of pathological changes and impaired expression of cytokines in developing female rat spleen after chronic excess fluoride exposure," *Toxicol. Ind. Health*, vol. 35, no. 1, pp. 43–52, Jan. 2019, doi: 10.1177/0748233718809773.

[69] A. Kumar and S. Kumari, "Histopathology of spleen of rat (Rattus norvegicus) fed on doses of sodium fluoride," p. 6, 2013.

[70] M. S. Hafez, "Histological and immunohistochemical study on the effect of noise stress on the spleen of adult albino rat and the possible role of Ginkgo biloba extract:," *Egypt. J. Histol.*, vol. 36, no. 3, pp. 546–555, Sep. 2013, doi: 10.1097/01.EHX.0000431731.50366.dc.

Biogenic Synthesis of Iron Oxide Nanoparticles Using Moringa olifera leaf extract

Kotresh M. G[a]*, Mallikarjun K. Patil[b], Darukaswamy T. H[c]. M[c] and Sanjeev R. Inamdar[b]

[a]Department of Studies in Physics, Vijayanagara Sri Krishnadevaraya University, Ballari-583 105, India.
[b]Laser Spectroscopy Programme, Department of Physics, Karnatak University, Dharwad-580 003, India.
[c]Department of Physics, Govt. First Grade College, Koppal-583 231.
Corresponding author: kotreshm26@gmail.com

ARTICLE INFO

ABSTRACT

The present study is an effort on green synthesis of iron oxide nanoparticles (NPs) by using Moringa olifera leaf extract as reducing agent. Crystalline nature, size, morphology, chemical composition and its optical features were analysed using X-ray diffraction (XRD), Scanning electron microscope (SEM), Fourier transform infrared (FTIR) and UV-Visible absorption spectroscopic measurements, respectively. XRD spectrum manifests the cubic phase of the NPs with average size of about 24nm. SEM analysis confirms the spherical shape of NPs with agglomeration. FTIR spectrum reveals the occurrence of Fe-O vibrational bond. The NPs are optically active and can be utilized in light harvesting and biosensor applications.

1. Introduction:

Recently, research on nanoparticles (NPs) gained a wide range of interest among the scientific community due to its applications in biology, medicine, and engineering [1]. NPs exhibit unique optical, electrical and magnetic properties upon changing their size, shape and composition, respectively [1, 2]. Currently, there is a large number of NPs are extensively applied in biomedical studies in particularly antimicrobial, antioxidant, and drug delivery agents. The development in nanoscience has

to lead to the production of NPs by various chemical and physical techniques. Conversely, these techniques have a negative impact on the environment and living organisms because an un-reacted chemicals are discharged in the environment [3].

The introduction of NPs in biomedicine and drug delivery has turned out to be a source of urge therefore it is also essential to develop hygienic, safe, simple and non-toxic materials through eco-friendly synthesis [4]. There are various synthesis methods are available to

Kotresh M. G. et al.,

synthesize the NPs such as sol-gel, chemical vapour deposition, Hydrothermal, co-precipitation methods etc. however green synthesis method is an alternative for above said chemical and physical methods which is simple, harmless, ease of preparation and eco-friendly which reduces the use of toxic chemical components, solvents, precursors and uses naturally available eco-friendly materials like yeast, bacteria, fungi, plant leaves, root, stem, viruses as reducing agents to synthesize the NPs [4]. Ismat Bibi et al. [3] has synthesized the iron oxide NPs using pomegranate seeds extract and studied photocatalytic activity evaluation for the degradation of textile dye. S. Saranya et al. [5] has studied the synthesis of Iron nanoparticles using aqueous extract of Musa ornata flower sheath tested for antimicrobial activity against pathogenic organisms. T. Vandhana et al. [4] synthesized Mn-Ag co-doped FeO NPs and studied in vitro anticancer and antibacterial activity of the NPs using MCF-7 and HeLa cancer cells.

Further, Moringa oleifera is a versatile tropical tree belonging to the family of Moringaceae, a native to the Indian subcontinent and is in use for almost five thousand years. It is very well known due to its medicinal, nutritional, commercial, and therapeutic properties. The leaves of Moringa oleifera are important sources of vitamin C, protein, beta-carotene iron, and potassium. The plant contains various fatty acids, vitamins, amino acids and nutrients, glucosinolates and phenolics which are responsible for capturing the metal ion. Various parts of Moringa oleifera such as leaves, flowers, roots, gums, fruits, and seeds of Moringa oleifera are widely used in the treatment of inflammation, cardiovascular dysfunction, liver disease, hematological and renal malfunction. Insight of aforesaid facts, the present study was focused on the biogenic synthesis of Fe_3O_4 NPs using Moringa olifera leaf extract as reducing and stabilizing agent [2].

2. Material and experimental methods

2.1 Chemical, reagents and sample collection

The Moringa oleifera leaves were collected in the local area of Ballari city, India. The leaves were separated from the stem and used for extract preparation. The AR grade Ferrous sulfate heptahydrate ($FeSo_4.7H_2O$) salt was obtained from Fisher Scientific chemical company and used without further purification. Double distilled water was used for extraction and solution preparation purposes.

2.2 Preparation of leaf extracts of Moringa oleifera

The collected Moringa oleifera leaves were washed with double distilled water and then, 20g leaves are added in 250ml of distilled water and heated for 30 minutes at 80°C. Then the solution was cooled for 10min and filtered using Whatmann filter paper. Further, the filtered solution was stored at 4°C and used for the preparation of Fe_3O_4 NPs.

2.3 Prepartion of Iron oxide Nanoparticles

1N of $FeSO_4.7H_2O$ was prepared in 100ml of distilled water under constant stirring conditions. After complete dissolution of the mixture, Moringa oleifera leaf extract was added drop-wise to the $FeSO_4.7H_2O$ solution under constant stirring until the colour changes from yellowish to dark green colour and the pH of the solution was maintained 7 during the entire reaction. Then the mixture was stirred continuously for 4 hours at room temperature and kept for few hours to obtain precipitation. The resulting precipitation was filtered with Whatmann filter paper number 42 and washed repeatedly with double distilled water (about 2 liters) finally with ethanol in order to remove ionic impurities. The obtained sample was dried at room temperature for 24 hours and annihilated at 500°C for two hours. The annihilated sample was ground with mortar and pestles to obtain a homogeneous powder sample then stored in an airtight container for further characterization studies using various spectroscopic techniques.

2.4 Characterization

The crystalline structure of the biosynthesized Fe_3O_4 NPs was investigated by using Rigaku X-ray diffractometer (model: SmartLab SE, Rigaku Corporation), XRD spectrum was recorded from 10° to 80° angles using CuKα radiation operated at 10kV and 30mA. The optical properties of the synthesized NPs were evaluated using a Shimadzu-Pharmaspec double beam UV-Vis spectrophotometer within the wavelength range of 200-700nm. Fourier Transformer infrared (FTIR) spectra of the synthesized NPs were recorded in the range of 4000-400cm⁻¹ at room temperature using Perkin Elmer spectrometer in order to analyse and detect functional groups. The surface morphology and elemental analysis of Fe_3O_4 NPs were characterized by JSM-IT500 scanning electron microscope (model: JSM-IT500 LA InTouchScope™).

3 Results and Discussion

3.1 X-ray Diffraction analysis

The structural properties of the Fe_3O_4 NPs are charcterized by using powder X-ray diffraction analysis. The XRD pattern of biosynthesized Fe_3O_4 NPs is shown in fig.1 which displayed number of diffraction peaks at 15.77°, 22.7°, 36.5°, 50.7° and 58.37° corresponds to peak index (220), (311), (400), (511) and (440) reflection lines, respectively. All the peaks are confirmed Fe_3O_4 cubic phase (Fd-3m space group) by comparison with JCPDS card number 96-101-1033 taken from Match2 software. The sharp and narrow diffraction peaks indicate that the synthesized sample is well crystalline in nature and has a smaller crystalline size. The mean crystalline size of the particles was determined from the Debye-Scherrer equation given by

$$D = \frac{K\lambda}{\beta cos\theta} \qquad (1)$$

Where D is the crystallite size, K is Scherrer's constant of value 0.9 for spherical particles, λ is the wavelength of X-ray used (λ= 0.15406 nm), θ is Bragg's angle and β is the full width half

maximum of Fe_3O_4 NPs XRD peaks. The average crystalline size of the synthesized particle is obtained to be 24 nm. The average values of lattice constant *a* is obtained to be 8.33Å which is in good comparison with the
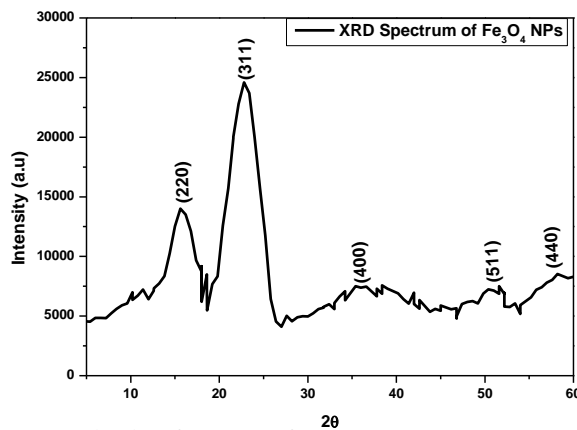
standard reference of XRD spectrum [6].

Figure 1: XRD spectrum of biosynthesized Fe_3O_4 NPs (Smoothed at a scale of 50 using Origin Pro 8.5)
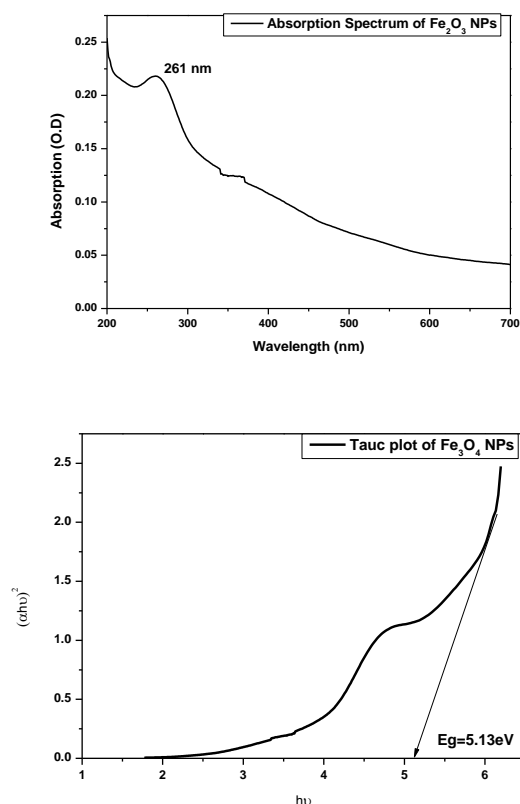
3.2 Uv-visible absorption spectroscopic analysis

The optical absorption features of Fe_3O_4 NPs was investigated using UV-visible absorption spectroscopy over the wavelength range of 200-700nm. The room temperature UV-Vis absorption spectra of biosynthesized Fe_3O_4 NPs is shown in fig. 2a. From the graph, it is confirmed that the sample exhibits a typical excitonic absorption peak at 261nm and reveals the formation of optically active Fe_3O_4 NPs.

Further, the energy bandgap of the synthesized NPs was calculated by using Tauc's relation.

$$(\alpha h\nu)^n = K(h\nu - Eg) \qquad (2)$$

Where, α is the absorption coefficient, hν is the photon energy, Eg is the bandgap of sample and n denotes the nature of the transitions. The value of n is taken 2 for direct allowed transition [7]. The graph has been plotted between $(\alpha h\nu)^2$ as a function of photon energy, extrapolating the linear portion of the curve which gives the direct bandgap of synthesized Fe_3O_4 NPs. From fig. 2b the value bandgap was found to be 5.13eV.

Figure 2: (a) Uv-visible absorption spectrum of synthesized Fe_3O_4 NPs; (b) Tauc plot of Fe_3O_4 NPs to estimate the energy bandgap.

3.3 Fourier Transformer Infrared Spectrum (FTIR) analysis

The FTIR analyses were carried out for synthesized Fe_3O_4 NPs in the frequency range 4000 to 400 cm^{-1} using the KBr pellet method and shown in fig. 3. The synthesized Fe_3O_4 NPs exhibit broadband at 3410 cm^{-1} due to the stretching vibration of O-H groups. An intense peak at 1630cm^{-1} and 1117.9 cm^{-1} denotes the existence of imino group and C-O-CN stretch, respectively. The characteristic sharp absorbance peak observed at 588 cm^{-1} corresponded to Fe-O stretching vibration for Fe_3O_4 NP in the sample. The high frequency band ranging from 540 to 590 cm^{-1} is a characteristic band of spinel cubic structure of Fe_3O_4 crystalline structure and confirms the formation of Fe_3O_4 NPs [8-9].
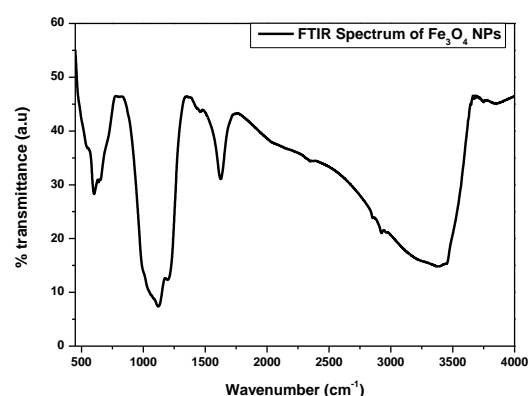
Figure 3: FTIR spectrum of biosynthesized Fe_3O_4 NPs

3.4 SEM and EDS spectroscopic analysis
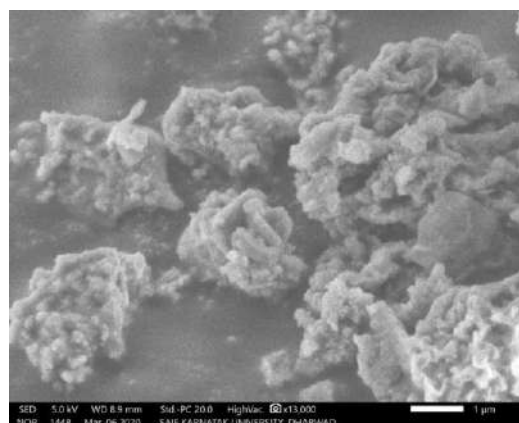
Figure 4: SEM image of synthesized Fe_3O_4 NPs

Scanning Electron Microscope (SEM) and Energy-dispersive X-ray spectroscopy (EDS) analysis were carried out for the synthesized Iron oxide NPs. Fig. 4 shows the SEM image of the Fe_3O_4 NP and it indicates that synthesized NPs are in spherical in shape with agglomeration. Further, from the EDS analysis it is confirmed that formation of Iron oxide NPs with some minor impurities such as Carbon, Silicon and Sulfur elements in smaller quantity. The atomic and mass percentage of elements present in the sample is shown in table 1. Further, EDS analysis confirms the formation Fe_3O_4 NPs with minor impurity elements.

Table 1: Elemental concentration in synthesized Fe_3O_4 NPs estimated using EDS analysis

Element	Mass%	Atom%
Carbon	6.74±0.14	13.46±0.28
Oxygen	40.96±0.35	61.44±0.52
Silicon	0.36±0.05	0.31±0.04
Sulfur	7.75±0.12	5.80±0.09
Iron	44.19±0.45	18.99±0.19
Total	100	100

4. Conclusion

The present study confirms the formation of good quality Fe_3O_4 NPs using Moringa olifera leaf extract as reducing and capping agent. The XRD spectrum reveals the formation of cubic spinel structured Fe_3O_4 NPs with the average size of about 24nm estimated using Debye-scherrer method. The FTIR analysis confirms the presence metal oxygen vibration within the region of 500-600cm^{-1} and confirms the formation Iron oxide NPs. SEM analysis reveals the formation of spherical NPs with agglomeration. The EDS analysis additionally confirms the formation Iron oxide NPs with minor impurities. The UV-Visible analysis shows that, these biosynthesized NPs are optically active and will be utilized in light harvesting and biosensor application in future.

References

[1] Green synthesis and characterization of silver nanoparticles from Moringa oleifera flower and assessment of antimicrobial and sensing properties. Bindhu M.R, Umadevi M, Galal A. E, Naif A.A.D, Mariadhas V.A. J. Photochem. Photobiol. B, 205, 111836, (2020).

[2] Green synthesis of NiO nanoparticles using Moringa oleifera extract and their biomedical applications: Cytotoxicity effect of nanoparticles against HT-29 cancer cells, Angel E, Vijaya J. J, Kaviyarasu K, Maaza M, Ayeshamariam A, John Kennedy L, J. Photochem. Photobiol. B, 164, 352-360, (2016).

[3] Green synthesis of iron oxide nanoparticles using pomegranate seeds extract and photocatalytic activity evaluation for the degradation of textile dye, Ismat B, Nosheen N, Sadia A, Misbah S, Abid A, Ansar A, Kashif J, Shagufta K, Fazli M. S, M. Iftikhar K, Fatima J, Munawar I, J. Mater. Res. Technol., 8, 6115-6124, (2019).

[4] Biogenic Synthesis of Mn-Ag co-doped FeO ($Fe_{1-2x}Mn_xAg_x$) Nanoparticles: As an effective disinfectant and anticancer agent, Vandhana T, Lourduraj A.J.C, Inorg. Chem. Commun., 112, 107712, (2020).

[5]Green Synthesis of Iron Nanoparticles using Aqueous Extract of *Musa ornata* Flower Sheath against Pathogenic Bacteria, Saranya S, Vijayarani K, Pavithra S, Indian J. Pharm. Sci .79, 688-694 (2017).

[6]X-ray diffraction analysis by Williamson-Hall, Halder-Wagner and size-strain plot methods of CdSe nanoparticles- a comparative

Kotresh M. G. et al.,

study, Debojyoti N, Fouran S, Ratan D, Mater. Chem. Phys. 239 (2020) 122021.

[7]Photoluminescence properties of SnO_2 nanoparticles: Effect of solvents, Horti N.C, Kamatagi M. D, Patil N.R, Wari M.N, Inamdar S.R, Optik, 169 (2018) 314-320.

[8]Green synthesis of iron oxide nanoparticles using Hibiscus rosa-sinensis for fortifying wheat biscuits, Sirajunnisa A.R, Abishek S, Sanjay S, Geethalakshmi R, Shanmugavel S, Manivasagan V, Ramesh B.N, Renganathan S, SN Applied Sciences 2 898 (2020).

[9]In vitro toxicity assessment of chitosan oligosaccharidecoated iron oxide nanoparticles. Shukla S, Jadaun A, Arora V, Sinha R.K, Biyani N, Jain V. Toxicol. Rep. 2:27-39, (2015).

Biosynthesis of Nano-silver using *Withania coagulans* and analysis of physical and therapeutic properties

Jarnain R. Naik[a] and M. David[a]*

[a]Enivronmental Biology and Molecular Toxicology Laboratory, Department of Zoology Karnatak University, Dharwad 580 003, India

***Corresponding author:** davidkcd@gmail.com; Phone: +91-9845709815*

ARTICLE INFO

ABSTRACT

In folk medicines, *Withania coagulans* berries has been used to treat diabetes, *asthma*, ulcers, rheumatism, bronchitis. In the present study, the silver nanoparticles (AgNPs) were synthesized using *Withania coagulans* berries extract that act as reducing and capping agent. The AgNPs were characterized using different techniques such as UV-Visible spectroscopy, FTIR, XRD, FESEM, EDS, zeta-sizer and zeta potential. UV-Visible spectroscopy of fabricated AgNPs showed absorption maximum at 413nm. FTIR studies illustrated the phytoconstituent that are involved in the biogenesis of nanoparticles. FESEM analysis revealed that AgNPs are spherical in shape. The In-vitro antidiabetic activity of fabricated Silver nanoparticles were analyzed and the results showed significant enhancement of Glucose uptake rate and inhibition of Carbohydrate digestive enzyme α-Amylase. Additionally, the AgNPs showed potential anticancer activity against MCF-7 cell line with IC50 150μg/ml. Hence, the synthesis of silver nanoparticles using plant metabolites that forms the surface coating on silver will give great potential applications in the field of therapeutics.

Introduction

Nanotechnology is one of the most fascinating area for research as it describes the synthesis and utilization of materials with at least one dimension in the range of 1-100nm that results in high surface area to volume ratio [1]. Nanoparticle not only display high surface area to volume ratio but they also exhibit better physical, chemical and biological properties depending upon their size and morphology compared to as that of their bulk counterparts [2]. Last few years due to their unique properties, nanomaterials are used for various applications like information technology, healthcare industry, electronics, catalyst, cosmetics, biosensors, biomedicine and pharmaceutical applications. The metal nanoparticles have been reported to contain medicinal properties [3]. Specially, metal and metal oxide nanoparticles like gold, silver, iron oxide, zinc oxide are used for drug delivery, antibacterial, antimicrobial activities and cancer therapy [4]. Especially the silver nanoparticles have gained more attention due to

Jarnain R. Naika and M. David

their anti-cancer, anti-bacterial, antimutagenic, antidiabetic, antifungal and anti-oxidant properties. Due to unique physicochemical and optoelectronic properties there are used in the medicinal field for diagnostics, drug delivery and tissue engineering [5]. There are various methods available for the synthesis of nanoparticles via physical, chemical, and biological techniques. Various approaches such as thermal decomposition, electrochemical, sol-gel, microwave-assisted and green chemistry for fabrication of nanoparticles[6]. Among the various methods biological technique is most popular for the synthesis using plant, algae, and microbes [7]. Leaf, fruits, bark, callus, and root are the various parts of the plant that are used in the synthesis of metal and metal oxide nanoparticles of various shapes and size. As the plant-based fabrication of nanoparticles are considered as better because it is not only environmentally friendly, least toxicity for human health, cost effective and also, they can be fabricated in single step method [8].

In human health care management medicinal plants are used for centuries as a primary source of treatment. There is high demand for the medicinal plants in herbal-based drugs, food products and cosmetics [9]. The medicinal plants are rich source of bioactive compounds that includes various secondary metabolites such as alkaloids, flavonoids, phenols, saponins, terpenoids, tannins, etc that has various medicinal properties such as anti-diabetic, anticancer, anti-bacterial, immunomodulatory. Use of these natural based compounds is much safer than synthetic drugs [10]. These bioactive compounds help in the synthesis of silver nanoparticles by reducing silver ions into silver nanoparticles and acts as capping and stabilizing agent which is responsible for better biological activity of nanoparticles. Nevertheless, the preparation of new bioactive active compound conjugated with silver nanoparticles will give a new material with exclusive biological properties that associate

both the properties of Nanoparticles as well as of bioactive compounds [11].

Withania coagulans Dunal, commonly known as Indian rennet, Indian cheese maker, belonging to family Solanaceae, is distributed in drier parts of India. The berries of this plant are reddish brown globose and have enclosed leathery calyx. They are rich in withanolides that is steroidal-lactones, they also contain esterase, free amino acids, and fatty oils [12]. There are more than 12 alkaloids and 40 different types of withanolids that are responsible for the pharmaceutical applications of this plant [13]. They are said to be having antihyperglycemic, anti-dyslipidemia, free radical scavenging, anti-inflammatory, hepatoprotective and antifungal activities [14]. Thus, the present study evaluated the synthesis of silver nanoparticles (WC-AgNPs) using *Withania coagulans* berries extract along with inhibition of alpha amylase enzyme, glucose uptake by yeast cells was studied for anti-diabetic analysis and MTT assay was carried out to study the anticancer activity against MCF-7 cells.

2. Materials and Methods

2.1. Preparation of Withania coagulans berries extract

Withania coagulans berries were purchased from the commercial market. The berries were frozen at -24°C for 24h. The frozen berries were placed as a single layer on metal pans and placed on the tray of a freeze dryer (CoolSafe PRO, LaboGene™) and the freeze-drying process was performed for 24 h under high vacuum (13–55 Pa), with isothermal (heating) plate temperatures of 20 °C. The freeze-dried berries were pulverized using electronic grinder, and stored in an airtight container. For extraction, 5 g of powder was boiled in 100 ml of distilled water for 15 min at 60 ^{0}C. The extract was filtered using Whatman filter paper – number 1, and stored in a sterile state.

2.2. Synthesis of silver nanoparticles and characterization

Jarnain R. Naika and M. David

The source of silver used for the synthesis of nanoparticles in present study was silver nitrate (AgNO₃) (Himedia, Mumbai, India). An aqueous 1×10^{-3} M solution of AgNO₃ was prepared in distilled water at room temperature and stocked in an amber-colored glass bottle in a dark cabinet to elude photoactivation of AgNO₃ under static conditions. The 10 ml *Withania coagulans berries* extract was added to 90 ml of AgNO₃ solution and was kept under direct sunlight and gradually the color starts turning brown, which is a visual observation representing the synthesis of WC-AgNPs. The synthesized nanoparticles were centrifuged at 10,000 rpm (Remi R–8C) and the pellet was re-disposed in distilled water. The process was repeated four times to ensure complete separation of silver nanoparticles. Isolated WC-AgNPs were transferred into watch glass and kept in oven for drying. The dried nanoparticles were stored in dark container for further use.

The synthesized silver nanoparticles were confirmed by using UV–Visible spectroscopy. The reduction of silver ions was monitored from 300 to 700 nm by UV-spectrophotometer (Hitachi–2800) operated at a resolution of 0.5 nm. The measurements were carried out at room temperature and the wavelength was plotted against absorbance. The FTIR analysis is performed, in order to understand the role of biomolecules in the synthesis of silver nanoparticles. Dried WC-AgNPs powder was mixed with potassium bromide (KBr 1:100), pelletized, and analyzed at a range from 4000 to 500 cm⁻¹ with 4 cm⁻¹ resolution (Thermo scientific Nicolet–6700 with DTGS detector). The shape of the synthesized AgNPs were analyzed using FESEM at a voltage of 15 kV along with the energy dispersive X-ray Spectroscopy (EDX) by mounting nanoparticles on the stub and were coated with gold with Eiko IB. 3 Ion Coater. The crystallinity and average particle size were analyzed via powder X-ray diffraction using Philips X'Pert powder diffractometer at a potential of 40 kV and a current of 30 mA with Cu-Ka radiation (λ = 1.54056 Å). The X-ray diffraction of sample were scanned over a 2 θ angle ranging from 20° to 90°. The particles size analyzer (Horiba scientific nanoparticles analyzer SZ-100) to determine the hydrodynamic diameter and zeta potential. The silver nanoparticles were determined at 25°C at 90° detection angle.

2.3. *In-Vitro* Antidiabetic activity

2.3.1. *Glucose Uptake Assay by Yeast Cells.*

The glucose uptake by yeast cells assay was performed by method describe by Cirillio [15]. Commercial baker's yeast was used and dissolved in distilled water to prepare 1% yeast suspension and was incubated overnight at room temperature. The suspension was centrifuged at 4200rpm for 5 min on the next day. The pallet was washed with distilled water repeatedly till the clear supernatant was attained. The process was repeated by the addition of distilled water to the pallet until a clear supernatant was obtained. Exactly 10 parts of the clear supernatant fluids were mixed with 90 parts of distilled water to get a 10% v/v suspension of the yeast cells. 10% w/v of the yeast cell suspension was prepared by using a clear supernatant. Samples (*Withania coagulans berries* extract, Silver nanoparticles and metformin) of different concentrations were prepared in DMSO and 1 ml of 5 mM glucose for 10 min at 37° C. 100µl yeast suspension was added in the reaction mixture to start the reaction. After 60 min of incubation at 37° C, centrifugation was done at 3800 rpm for 5 min and the amount of glucose in the supernatant was measured at 520 nm by UV-Visible spectrophotometer. The effective concentration (EC50) was obtained from the percentage activity curve. The (%) increase in glucose uptake was calculated according to the following formula:

% Increase in glucose uptake = $\frac{Abs\ of\ Control - Abs\ of\ Sample}{Abs\ of\ Control} * 100$

Metformin was used as the standard drug, and control contains all reagents except sample.

2.3.2. Inhibition of α-amylase Assay

The Inhibition of α-amylase Assay was performed by method describe by O. Ganiyu [16] with slight modification. Different concentration of sample (*Withania coagulans berries* extract, Silver nanoparticles and metformin) was dissolved in 10% DMSO and it is further dissolved in 20Mm Sodium Phosphate buffer (ph-6.9). A volume of 500μl of α-amylase (Sigma Aldrich) (2Units/ml) was added to the 500μl of samples and was incubated for 10 minutes at 30°C. Further, 500μl of (1%) starch solution was added to each test tubes and incubated for 3minutes. The reaction was terminated by adding 500μl of DNSA reagent and was boiled for 10minutes in a water bath at 85°C. The mixture was cooled at room temperature and was diluted with distilled water. The absorbance is measured using UV-Visible spectroscopy (Hitachi–2800) at 540nm. The α-amylase inhibitory activity was expressed as % inhibition and was calculated using equation given below:

% of α-amylase inhibition= $\frac{Abs\ of\ Control - Abs\ of\ Sample}{Abs\ of\ Control} * 100$

2.4. *In vitro* Anticancer activity

The *in vitro* anti-cancer activity of *Withania coagulans* berries extract and biosynthesized WC-AgNPs was evaluated on breast cancer MCF-7 cell lines through MTT assay, as described by Mosmann T [17]. MCF-7 cell lines were maintained at 37oC and 5% CO2 in incubator. The cell lines were plated in 96-well plates at a concentration of 1×10^4 cells and incubated for 24 hours. After 24 hours, cells were treated with different test samples (50-250 μg/ml) of *Withania coagulans* berries extract or AgNPs were added to the respective wells and incubated for 24 h at 5% CO2. After incubation, in each well MTT reagent was added and incubated at 37 ºC in a CO2 incubator for4 h. Then, the formed crystals were dissolved in 100 μl of DMSO and mixed well. Absorbance was measured in a microplate reader at a wavelength of 570 nm. Cisplatin (15 μg/ml) was used as the reference drug. Each experiment was performed in triplicates, the IC50 Inhibition of viability was determined

graphically, and the effect of samples was calculated by using the following formula:

% Cell viability = [At/Ac] × 100

where At is absorbance of test sample, and Ac is absorbance of control.

Statistical analysis

The results were expressed as mean ± SD. One-way ANOVA was used to analyze the variation and level of statistical significance between groups. $P<0.05*$ was considered statistically significant.

3. Results and Discussion

### 3.1. Synthesis and Characterization of AgNPs

UV-Visible spectroscopy has sensitivity towards the presence of metal nanoparticles. So, it is used for the confirmation of formation and stability of nanoparticles based on the optical properties of nanoparticles [18]. Metal nanoparticles such as silver, gold and iron exhibit an intense absorbance peak due to excitation of localized surface plasmon resonance of the electrons [19]. The absorption peak of typical silver nanoparticles exists in the range of wavelength 350-450 nm [20]. The UV–Visible spectrum analysis reveals an intense absorption peak at 413nm that confirms the biogenesis of AgNP (Figure 1A). The reduction of silver metal ions into AgNPs is due to the active biomolecules present in the plant extract. In previous studies, Absorption spectra of silver nanoparticles synthesized from *Euphorbia hirta* leaf extract have been reported to have an absorbance peak at 430 nm that supports the current study [21].

FT-IR analysis was done to determine the bioactive functional groups of phytoconstituents present in aqueous extract of *Withania coagulans* berries and to identify the possible compounds responsible for reduction and capping of silver nanoparticles [22]. FT-IR spectrum as shown in the (figure 2B) of extract showed intense broad band at 3264.62 cm^{-1} corresponding to O–H group, weak band at 2933.17 cm^{-1} corresponding to asymmetric stretching vibrations of CH group that is

correlated to presence of alkanes in extract [23], intense peak at 1582.06 cm^{-1} depicts C-C Stretching due to the presence of aromatic group of flavonoids, the intense peak at 1035.61 cm^{-1} is due to the C-O Stretching of phenolic compounds [4]. The IR spectrum of AgNPs showed there is deviation in peak at 3260.99 cm^{-1} (O–H group), and bands at 2926.53 cm^{-1}, 1528cm^{-1}, 1390.03 cm^{-1}, 1032.76 cm^{-1} that corresponds Stretching of CH group, C-C group, C-O group, respectively. Hence, the FTIR spectra depicts that the involvement of the amides, flavonoids, alkaloids, phenolic present in the *Withania coagulans* berries extract, that confirms they are most likely involved in the reduction of silver ions and are adsorbed on the surface of AgNPs and act as reducing, capping, and stabilizing agents. The shift in the IR bands suggests the reaction between silver ions and the extract [24, 25, 26]. Thus, the FT-IR studies propose that the phytoconstituents present in the *Withania coagulans* berries extract have the efficacy to interact with the metal ions to facilitate the formation of nanoparticles in bottom-up approach.

To analyze the surface morphology of the synthesized silver nanoparticles using *Withania coagulans* berries extract was done by using Field Emission Scanning Electron Microscope (FESEM). The FESEM images (Figure 1C) reveals that the nanoparticles are spherical in shape. The images were scanned at different magnifications. Previously many research studies have been reported the synthesis of silver nanoparticles using different plant extracts. The biogenic of silver nanoparticles from *Hypericum scabrum* seed extract were spherical in shape [27]. The silver nanoparticles synthesized using *Ipomoea asarifolia* were spherical [28]. The chemical composition of the nanomaterials was quantified using Energy dispersive spectroscopy (EDX). As observed in the EDX spectra (Figure 1D) the presence of Silver nanoparticles was confirmed by a strong optical absorption peak at the 3 KeV, which confirms
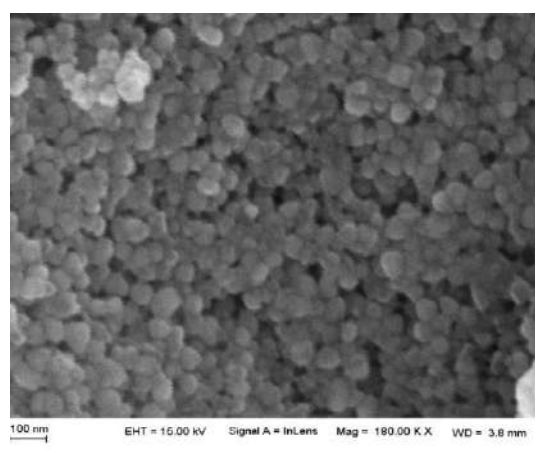
the silver as a major element. The biogenesis of WC-AgNPs is 59.94%. Additionally, the EDX analysis showed other weak peaks of C, Cl, and O are due to the phytoconstituents of *Withania coagulans* berries extract that are responsible for the fabrication of resultant AgNPs [29].
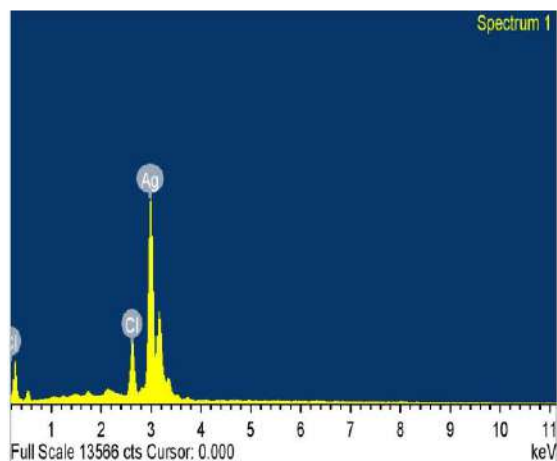
(A)

(B)

(C)

Jarnain R. Naika and M. David
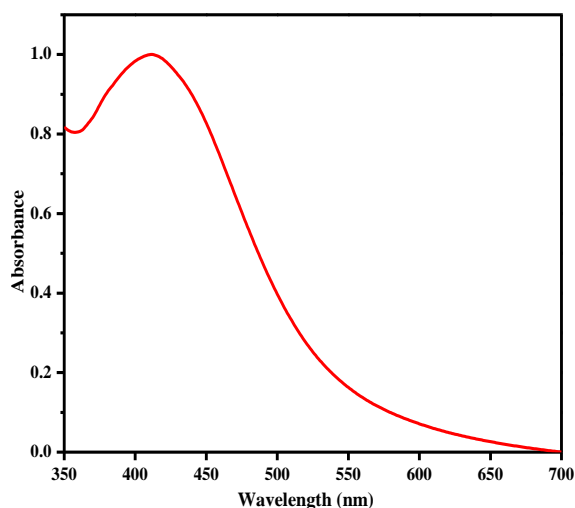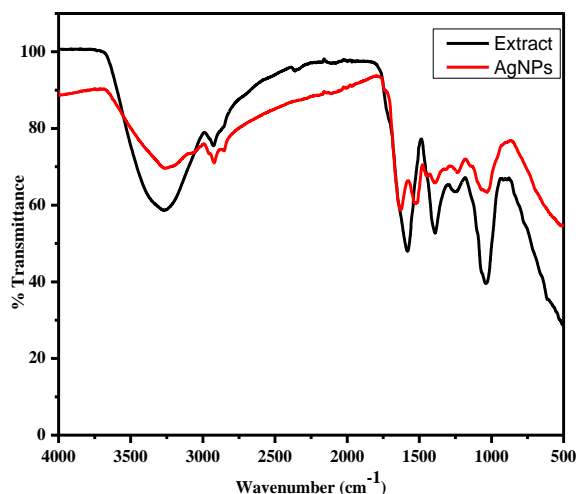
(D)

Figure 1. (A) UV-vis absorption spectra of synthesized WC-AgNPs (B) FTIR Spectra of *Withania coagulans berries* extract and WC-AgNPs (C) FESEM image of WC-AgNPs at 100nm (D) EDS spectrum of WC-AgNPs

The powder WC-AgNPs was used to characterize to know the crystalline nature and structural details of synthesized silver nanoparticles using extract. The XRD pattern of AgNPs has been seen in Figure 2A. The characteristic diffraction peaks at 2θ values 38.14, 44.17, 64.59, 77.07, 81.28 are attributed to (111), (200), (220), (311) and (222) planes of silver metal, respectively, and confirms the face centered cubic structure of the WC-AgNPs. The X-ray diffraction patterns of WC-AgNPs were matched with ICDD Card number 03-065-8428. In the diffractogram, other peaks are also been observed which are due the biomolecules or other constituents present in plant extract in the tracer amount involved in the synthesis of nanoparticles by acting as reducing and stabilizing agents [30]. The average size of the silver nanoparticles was estimated by using Debye–Scherrer equation, $D = k\lambda/\beta cos\theta$, where D is average particle size, k is constant equal (0.9), λ is the incident wavelength (0.154nm), β is full width of half maximum (FWHM), θ is the diffraction angle corresponding to the lattice plane (111). The average crystalline size according to Debye–Scherrer equation calculated is found to be 12.54nm [31].

The hydrodynamic size and zeta potential of biogenic silver nanoparticles was shown in figure 2B and C. The average hydrodynamic size is 86.2nm. the size obtained by the particle sizer is higher than that of XRD due to the sample preparation. In XRD the particle size was determined at the dry state of the sample that actually represents the diameter of the nanoparticles whereas in zeta sizer method the obtained diameter of nanoparticles is hydrodynamic diameter due to which the particle will show hydrodynamic volume because of solvent effect in hydrated state [32]. The zeta potential of green synthesized AgNPs was measured to be -22.1 mV as a measure of stability of the nanoparticles. Due to the negative charge on the surface of AgNPs there is increase in the electrostatic repulsive forces that prevents from aggregation of AgNPs and thereby increase in the stability of the silver nanoparticles [33].

(A)
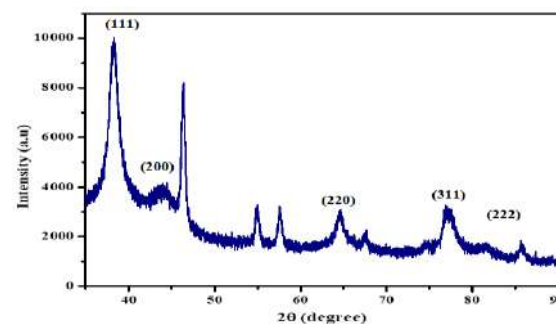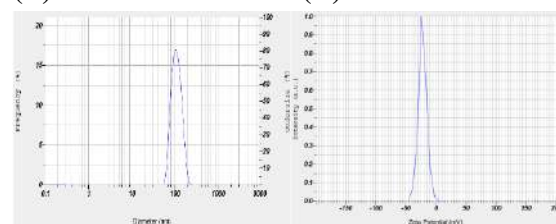
(B) **(C)**

Figure 2. (A) XRD pattern of WC-AgNPs (B) Particle diameter of WC-AgNPs (C) Zeta potential of WC-AgNPs.

3.2. *In vitro* antidiabetic activities
3.2.1. Glucose Uptake by Yeast Cells

The antidiabetic activity of *Withania coaguans* berries extract and fabricated WC-AgNPs has been evaluated by the glucose uptake by yeast cells. The WC-AgNPs

enhanced glucose uptake in yeast cell was compared with that of *Withania coaguans* berries extract and standard drug metformin. The amount of glucose uptake was decided by the presence of unused glucose present in medium. The rate of glucose uptake of Extract and WC-AgNPs was at 50μg/ml >30% and >35% which has reached almost ≥70% and ≥80% respectively at 250μg/ml as seen in the figure 3A it is seen that the increase in concentration of WC-AgNPs correspondingly the glucose uptake percentage also increases ultimately increasing the glucose uptake by yeast cells. The transport of glucose across the yeast cell is aided by the facilitated diffusion process. As the glucose transporters are stereospecific allows the entry of glucose down the gradient into the cell. With the entry of glucose, the phosphorylation occurs inside cell [34]. Thus, concentration of glucose decreases as most of the glucose is converted into other metabolites in the cell [35]. As the glucose is readily converted into other metabolites, ultimately the concentration of glucose inside cell is decreased and facilitate diffusion will favor increase in uptake of glucose into the cell [36]. The phytoconstituents adsorbed on the surface on WC-AgNPs may act on the glucose transporters that are present on the cell membrane and elevating the glucose metabolism inside cell. Nevertheless, it will be interesting if metabolite-based nanoparticles are explored more in vivo that enhances uptake by adipose and muscle cells of the body that helps binding and transporting glucose efficiently across the cell membrane and boosting the glucose metabolism. Hence, increasing the uptake of the glucose by the cells and converting into other metabolites and decreasing the blood glucose levels.

3.2.2. α-Amylase inhibition activity

Alpha-amylase is an essential enzyme that is required in carbohydrate metabolism by breaking the starch and glycogen into simpler forms such as glucose by hydrolysing α- D - (1 –4) glycosidic bond [37]. Inhibition of the pancreatic amylase will lead to delay in the carbohydrate metabolism and glucose absorption that decreases the post-prandial hyperglycaemia which is an effective approach for the management of type II diabetes. However, the commercially available drugs such as acarbose are said to have the several side effects [38,39]. So, it is necessary to search the more potential drug with the least side effects. The silver nanoparticles synthesized using *Withania coagulans* berries extract has exhibited higher level of α-amylase inhibition activity when compared with extract alone. The percentage of inhibition showed that as the concentration of nanoparticles increases the inhibition percentage also as shown in figure 3B. The percentage inhibition of alpha-amylase enzyme of Extract and WC-AgNPs at 50μg/ml was ≥10% and ≥20% which has at 250μg/ml reached almost ≥50% and ≥65% respectively. The results obtained depicts that the biosynthesized WC-AgNPs inhibit activity than the extract and metformin.

(A)

(B)
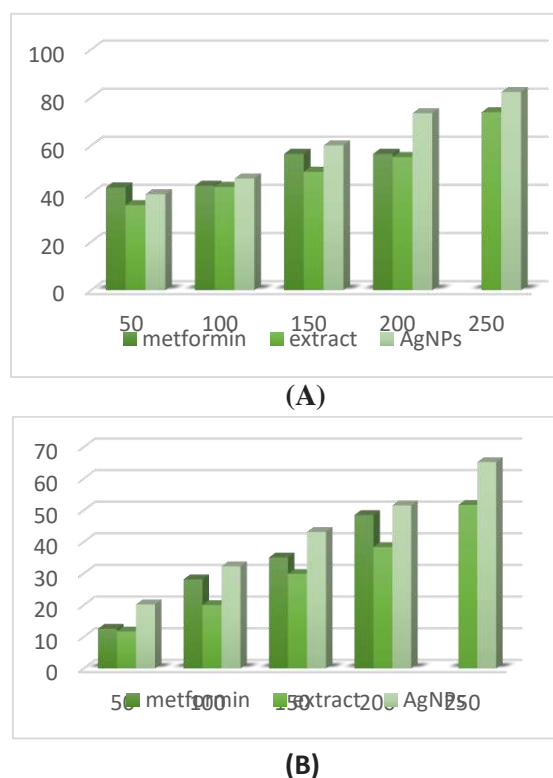
Figure 3. (A) Glucose uptake by yeast cell of metformin, *Withania coagulans* berries extract, and WC-AgNPs (B) Inhibition Alpha-amylase

enzyme of metformin, *Withania coagulans* berries extract, and WC-AgNPs.

(A)

(B)

(C)

(D)
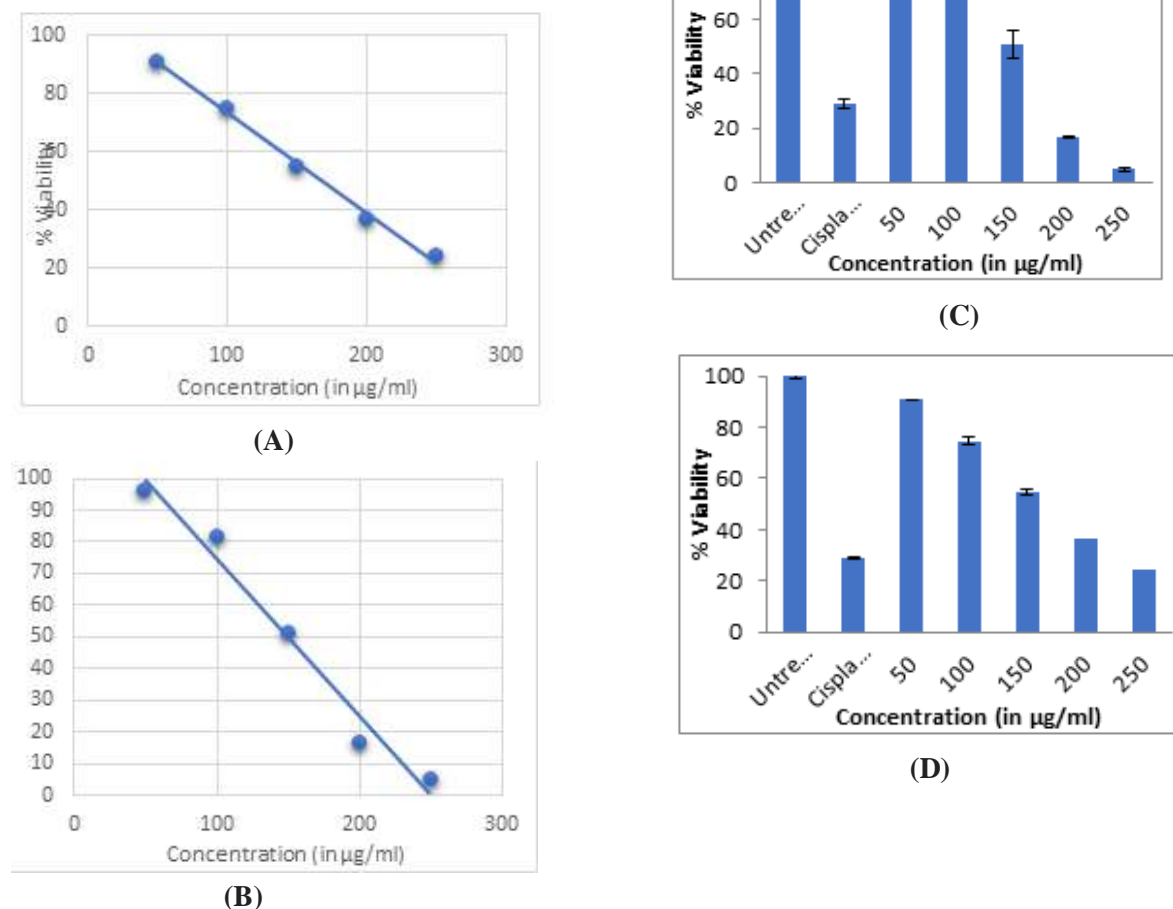
Figure 4. A and B Anticancer activity of WC-AgNPs against MCF-7 cell line. **C and D** Anticancer activity of *Withania coagulans* berries extract against MCF-7 cell line.

3.3. *In vitro* anticancer activity

Results obtained from the MTT assay revealed that both *Withani coagulans* berries extract and WC-AgNPs showed promising cytotoxic activity against human breast carcinoma cell lines (MCF-7) after 24 hours of incubation at lower concentrations. The cell culture showed 50% inhibition of proliferation (IC_{50}) is 150μg/ml concentration of WC-AgNPs as seen in Figure 4A and B Cell mortality increased further with an increasing concentration of silver nanoparticles, whereas the aqueous extract IC_{50} 162.57μg/ml concentration against MCF-7 cells as seen in Figure 4B and C. Morphological alterations were observed in the treated cells. Normal cellular morphology was distorted as compared to the control. Exposure to WC-AgNPs caused significant reduction in both cell size and number. A loss of typical morphology was evident along with the loss of adhesive property. Many cells formed clumps on treatment with WC-AgNPs. Microscopic examination suggested that treatment with silver nanoparticles can induce severe morphological alterations as well as cell death in MCF-7 Cells as shown in figures 5A and B. Recently; silver nanoparticles are finding widespread applications in anticancer therapy to treat and control several types of cancer. Multiple reports are available on previous studies done in this domain. The synthesized silver nanoparticles using aqueous extract of *Rosa damascena* petals and the nanoparticles exhibited profound anticancer activity against Human lung adenocarcinoma epithelial cell

lines (A549) [40]. Similarly, the anticancer activity of nanoparticles synthesized using *Mounda pubescens* plant leaf extract against HEP G2 cells (Human liver cancer epithelial cells) [41].
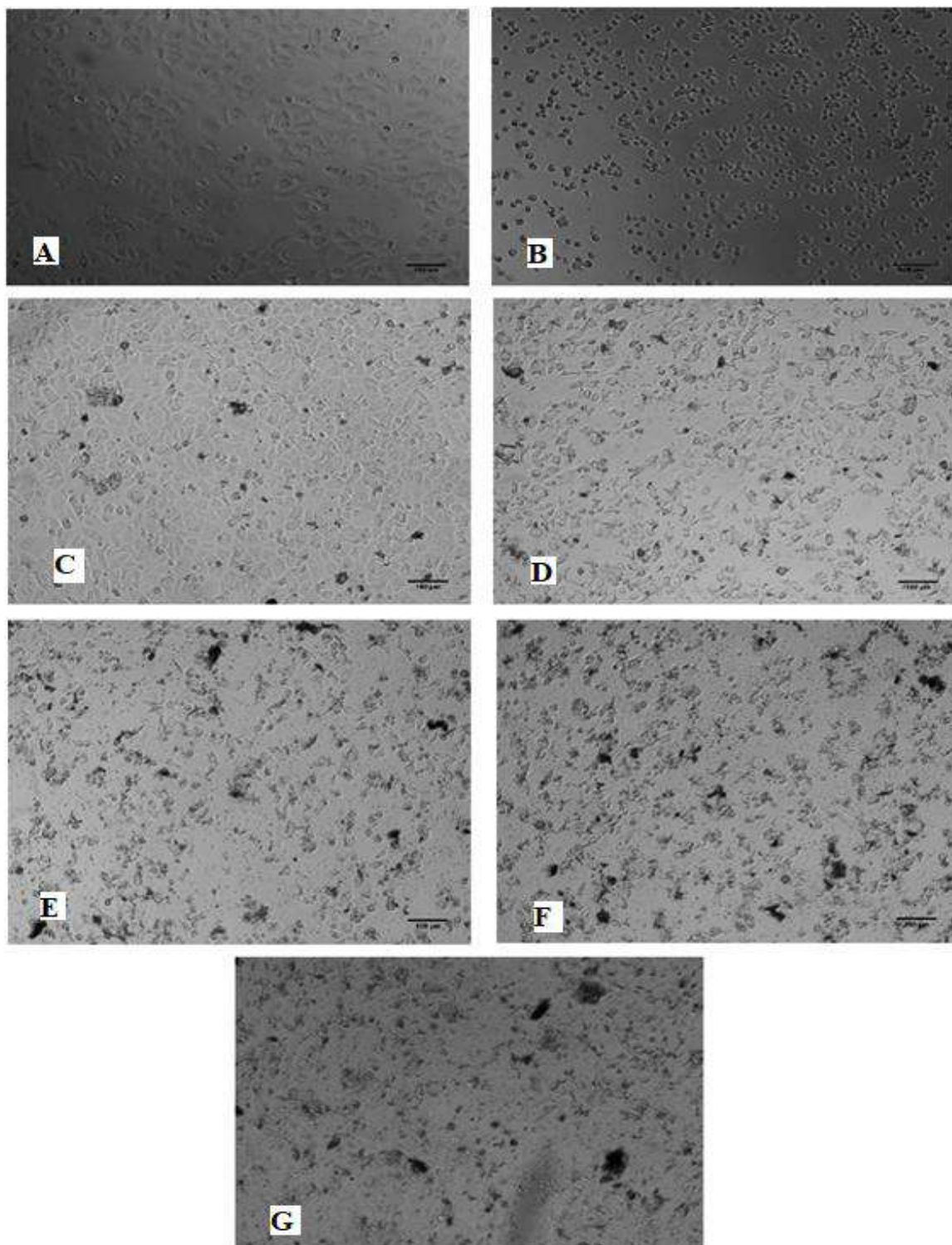
Figure 5. A. Plate showing the cytotoxic activity of *Withania coagulans* berries extract (A) Untreated breast cancer cells, (B) Cells treated with standard drug cisplatin, (C) Cells treated with extract 100 µg/ml, (D) 200 µg/ml, (E) 300 µg/ml, (F) 400 µg/ml, (G) 500 µg/ml.
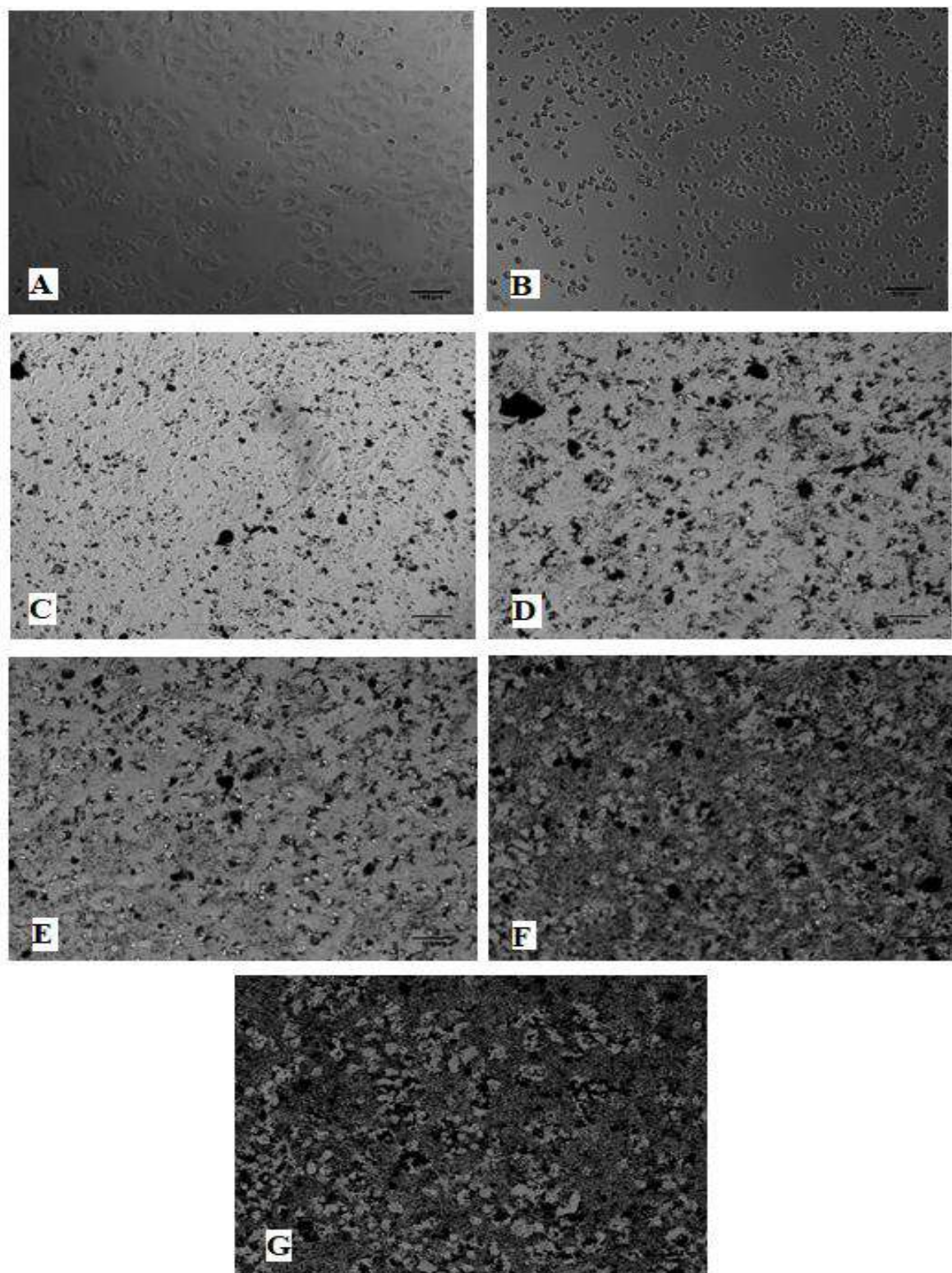
Figure 5. B. Plate showing anti-cancer activity of WC-AgNPs (A) Untreated breast cancer cells, (B) Treated with cisplatin, (C) Treated with WC-AgNPs 100 µg/ml, (D) 200 µg/ml, (E) 300 µg/ml, (F) 400 µg/ml, (G) 500 µg/ml.

The silver nanoparticles synthesized from leaf extract of *C. maxima, M. oleifera,* and *A. calamus* showed anticancer activity against epidermoid A431 carcinoma cells [42]. Cancer is an abnormal growth of living tissue in which cells exhibit uncontrolled division and proliferation autonomously, foremost to a progressive amplification in the number of

actively dividing cells. The probable mechanism involved in the anti-cancer activity of AgNPs may be attributed to their immense potential for selective disruption of mitochondrial respiratory chain, and release of Cytochrome C, which in turn leads to the production of reactive oxygen species (ROS), interruption of adenosine triphosphate (ATP), and causes ultimate damage to the cellular components. This chain of events subsequently leads to programmed cell death – apoptosis [43]. As the nanoparticles are smaller in size, they efficiently enter the cell. Thus, nanoparticles modify the mechanism of proliferation of cancer cell and causes damage to the cell ultimately leading to death of cancerous cell. Hence, shape, size, and phytoconstituents that are capped on the surface of the nanoparticles plays an important role in cellular uptake mechanism and apoptosis of cancerous cells [44].

4. Conclusion

In conclusion, the aqueous berries extract of *Withania coagulans* was used for the synthesis of silver nanoparticles by green chemistry method in a bottom-up synthesis approach. The method is simple, cost-efficient, and eco-friendly. It eliminated the requirement of usage of hazardous and toxic chemicals in the synthesis pathway, and natural compounds present in the plant extract served as reducing and stabilizing agents during the nanoparticle synthesis. Physical characterization of the obtained WC-AgNPs was carried out by UV-visible spectroscopy with the SPR value of nm. Studies using analytical techniques such as, Fourier-transform infrared spectroscopy, XRD, FESEM, EDS, Zeta potential revealed the irregular structure, 12.54nm size, Stability, and phytochemical groups involved in the reduction mechanism. The synthesized nanoparticles showed promising therapeutic applications – antidiabetic activity by increasing the glucose uptake in the yeast cells and by inhibiting the Alpha-amylase enzyme and anti-cancer action by significantly inhibiting the proliferation of human breast cancer cells. Hence, silver nanoparticles in conjugation with *Withania coagulans* berries extract showed impressive antidiabetic and anticancer activity which can hold immense potential for industrial and medicinal applications.

References:
[1] A. Saxena, R. M. Tripathi, F. Zafar, P. Singh, Green synthesis of silver nanoparticles using aqueous solution of Ficus benghalensis leaf extract and characterization of their antibacterial activity. *Materials letters*, *67*(1), 91-94 (2012).

[2] S. Pirtarighat, M. Ghannadnia, S. Baghshahi, Green synthesis of silver nanoparticles using the plant extract of Salvia spinosa grown in vitro and their antibacterial activity assessment. *Journal of Nanostructure in Chemistry*, *9*(1), 1-9 (2019).

[3] A. Aygün, F. Gülbağça, M. S. Nas, M. H. Alma, M. H. Çalımlı, B. Ustaoglu, F. Şen, Biological synthesis of silver nanoparticles using Rheum ribes and evaluation of their anticarcinogenic and antimicrobial potential: a novel approach in phytonanotechnology. *Journal of pharmaceutical and biomedical analysis*, *179*, 113012 (2020).

[4] U. P. Manik, A. Nande, S. Raut, S. J. Dhoble, Green synthesis of silver nanoparticles using plant leaf extraction of Artocarpus heterophylus and Azadirachta indica. *Results in Materials*, *6*, 100086 (2020).

[5] S. F. Hashemi, N. Tasharrofi, M. M. Saber, Green synthesis of silver nanoparticles using Teucrium polium leaf extract and assessment of their antitumor effects against MNK45 human gastric cancer cell line. *Journal of Molecular structure*, *1208*, 127889 (2020).

Jarnain R. Naika and M. David

[6]A. C. Gomathi, S. X. Rajarathinam, A. M. Sadiq, S. Rajeshkumar, Anticancer activity of silver nanoparticles synthesized using aqueous fruit shell extract of Tamarindus indica on MCF-7 human breast cancer cell line. *Journal of Drug Delivery Science and Technology*, *55*, 101376 (2020).

[7]K. Logaranjan, A. J. Raiza, S. C. Gopinath, Y. Chen, K. Pandian, Shape-and size-controlled synthesis of silver nanoparticles using Aloe vera plant extract and their antimicrobial activity. *Nanoscale research letters*, *11*(1), 1-9 (2016).

[8]S. S. Dakshayani, M. B. Marulasiddeshwara, S. Kumar, R. Golla, S. R. H. K. Devaraja, R. Hosamani, Antimicrobial, anticoagulant and antiplatelet activities of green synthesized silver nanoparticles using Selaginella (Sanjeevini) plant extract. *International journal of biological macromolecules*, *131*, 787-797 (2019).

[9]B. Venkatadri, E. Shanparvish, M. R. Rameshkumar, M. V. Arasu, N. A. Al-Dhabi, V. K. Ponnusamy, P. Agastian, Green synthesis of silver nanoparticles using aqueous rhizome extract of Zingiber officinale and Curcuma longa: In-vitro anti-cancer potential on human colon carcinoma HT-29 cells. *Saudi Journal of Biological Sciences*, *27*(11), 2980-2986 (2020).

[10] V. Sharma, S. Kaushik, P. Pandit, D. Dhull, J. P. Yadav, S. Kaushik, Green synthesis of silver nanoparticles from medicinal plants and evaluation of their antiviral potential against chikungunya virus. *Applied microbiology and biotechnology*, *103*(2), 881-891 (2019).

[11] K. Ranoszek-Soliwoda, E. Tomaszewska, K. Małek, G. Celichowski, P. Orlowski M. Krzyzowska, J. Grobelny, The synthesis of monodisperse silver nanoparticles with plant extracts. *Colloids and Surfaces B: Biointerfaces*, *177*, 19-24 (2019).

[12] R. Maurya, Akanksha, Jayendra, Chemistry and pharmacology of Withania coagulans: an Ayurvedic remedy. *Journal of pharmacy and pharmacology*, *62*(2), 153-160 (2010).

[13] D. Tripathi, A. Modi, G. Narayan, S. P. Rai, Green and cost effective synthesis of silver nanoparticles from endangered medicinal plant *Withania coagulans* and their potential biomedical properties. *Materials Science and Engineering: C*, *100*, 152-164 (2019).

[14] S. K. Prasad, R. Kumar, D. K. Patel, S. Hemalatha, Wound healing activity of *Withania coagulans* in streptozotocin-induced diabetic rats. *Pharmaceutical Biology*, *48*(12), 1397-1404 (2010).

[15] V. P. Cirillo, Mechanism of glucose transport across the yeast cell membrane. *Journal of bacteriology*, *84*(3), 485-491 (1962).

[16] O. Ganiyu, A. O. Ademiluyi, A. J. Akinyemi, T. Henle, J. A. Saliu, and U. Schwarzenbolz, Inhibitory effect of polyphenol-rich extracts of jute leaf (Corchorus olitorius) on key enzyme linked to type 2 diabetes (α-amylase and α-glucosidase) and hypertension (angiotensin I converting) in vitro, *Journal of Functional Foods* 4 (2012).

[17] T. Mosmann Rapid Colorimetric Assay for Cellular Growth and Survival: Application to Proliferation and Cytotoxicity Assays Tim. *J of lmmunologica*l *Methods*. *65*. 55–63 (1983).

[18] B. Adebayo-Tayo, A. Salaam, A. Ajibade, Green synthesis of silver nanoparticle using Oscillatoria sp. extract, its antibacterial, antibiofilm potential and cytotoxicity activity. *Heliyon*, *5*. (2019).

[19] U. K. Sur, B. Ankamwar, S. Karmakar, A. Halder, P. Das, Green synthesis of Silver nanoparticles using the plant extract of Shikakai and Reetha, *Materials Today: Proceedings*, *5*(1), 2321-2329 (2018).

[20] M. U. Rashid, M. K. H. Bhuiyan, M. E. Quayum, Synthesis of silver nano particles (Ag-NPs) and their uses for quantitative analysis of vitamin C tablets, *Dhaka Univ J Pharm Sci*, *12*, 29–33 (2013).

[21] E. K. Elumalai, T. N. V. K. V. Prasad, J. Hemachandran, S. V. Therasa, T. Thirumalai, E. David, Extracellular synthesis of silver nanoparticles using leaves of Euphorbia hirta and their antibacterial activities, *J Pharm Sci*

Jarnain R. Naika and M. David

Res, *2*, 549–54 (2010).

[22] M. S. Aref, S. S. Salem, Bio-callus synthesis of silver nanoparticles, characterization, and antibacterial activities via Cinnamomum camphora callus culture. *Biocatal Agric Biotechnol*, *27*, (2020) https://doi.org/10.1016/j.bcab.2020.101689.

[23] A. C. Gomathi, S. X. Rajarathinam, A. M. Sadiq, S. Rajeshkumar, Anticancer activity of silver nanoparticles synthesized using aqueous fruit shell extract of Tamarindus indica on MCF-7 human breast cancer cell line, *Journal of Drug Delivery Science and Technology*, *55*, 101376 (2020).

[24] A. R. Phull, Q. Abbas, A. Ali, H. Raza, S. J. Kim, M. Zia, I. U. Haq, Antioxidant, cytotoxic and antimicrobial activities of green synthesized silver nanoparticles from crude extract of Bergenia ciliata *Futur J Pharm Sci*, *2*, 31-6 (2016). http://dx.doi.org/10.1016/j.fjps.2016.03.001.

[25] B. Kumar, K. Smita, L. Cumbal, A. Debut, Green synthesis of silver nanoparticles using Andean blackberry fruit extract, Saudi Journal of Biological Sciences, 24(1), 45–50 (2017).

[26] A. Nouri, M. T. Yaraki, A. Lajevardi, Z. Rezaei, M. Ghorbanpour, M. Tanzifi, Ultrasonic-assisted green synthesis of silver nanoparticles using Mentha aquatica leaf extract for enhanced antibacterial properties and catalytic activity, *Colloid and Interface Science Communications*, *35*, 100252, (2020).

[27] Z. Nazari, A. Shafaghat, Biological synthesis and antimicrobial activity of nano silver using Hypericum scabrum seed extract, *Inorg Nano-Metal Chem*, *47*, 870-5 (2017).

[28] J. M. Khaled, N. S. Alharbi, S. Kadaikunnan, A. S. Alobaidi, M. N. Al-Anbr, K. Gopinath, A. Aurmugam, M. Govindarajan, G. Benelli, Green Synthesis of Ag Nanoparticles with Anti- bacterial Activity Using the Leaf Extract of an African medicinal plant, Ipomoea asarifolia (Convolvulaceae), *J Clust Sci*, *28*, 3009–19 (2017).

[29] N. Bibi, Q. Ali, Z. I. Tanveer, H. Rahman, M. Anees, Antibacterial efficacy of silver nanoparticles prepared using Fagonia cretica L. leaf extract, *Inorg Nano-Metal Chem*, 49 (2019).

[30] E. E. Elemike, D. C. Onwudiwe, A. C. Ekennia, Eco-friendly synthesis of silver nanoparticles using Umbrella plant, and evaluation of their photocatalytic and antibacterial activities, *Inorg Nano-Metal Chem*, 50 (2020).

[31] M. M. H. Khalil, E. H. Ismail, K. Z. El-Baghdady, D. Mohamed, Green synthesis of silver nanoparticles using olive leaf extract and its antibacterial activity, *Arab J Chem* (2014).

[32] S. Pattanayak, M. M. Mollick, D. Maity, S. Chakraborty, S. K. Dash, S. Chattopadhyay, S. Roy, D. Chattopadhyay, M. Chakraborty, Butea monosperma bark extract mediated green synthesis of silver nanoparticles: Characterization and biomedical applications, *J Saudi Chem Soc, 21* (2017).

[33] K. Jyoti, A. Singh, Green synthesis of nanostructured silver particles and their catalytic application in dye degradation, *J Genet Eng Biotechnol*, *14*, 311–7 (2016).

[34] U. R. Shwetha, M. S. Latha, C. R. Rajith Kumar, M. S. Kiran, V. S. Betageri, Facile synthesis of zinc oxide nanoparticles using novel Areca catechu leaves extract and their in vitro antidiabetic and anticancer studies, *Journal of Inorganic and Organometallic Polymers and Materials*, 1-8 (2020).

[35] V. Varadharaj, A. Ramaswamy, R. Sakthivel, R. Subbaiya, H. Barabadi, M. Chandrasekaran, M. Saravanan, Antidiabetic and antioxidant activity of green synthesized starch nanoparticles: an in vitro study, *Journal of Cluster Science*, 1-10 (2019).

[36] R. Gauhar, M. Hamayun, A. Iqbal, S. U. Islam, S. Arshad, K. Zaman, A. Ahmad, A. Shehzad, A. Hussain, and I. J. Lee, "In vitro antidiabetic effects and antioxidant potential of Cassia nemophila Pods," *BioMed research international* 2018 (2018).

[37] S. B. Nasab, A. Homaei, L. Karami, Kinetic of α-amylase inhibition by Gracilaria corticata and Sargassum angustifolium extracts

Jarnain R. Naika and M. David

and zinc oxide nanoparticles, *Biocatalysis and Agricultural Biotechnology*, *23*, 101478 (2020).

[38] D. Jini, S. Sharmila, S. Green synthesis of silver nanoparticles from Allium cepa and it's in vitro antidiabetic activity, *Materials Today: Proceedings*, *22*, 432-438 (2020).

[39] D. Rehana, D. Mahendiran, R. S. Kumar, A. K. Rahiman, In vitro antioxidant and antidiabetic activities of zinc oxide nanoparticles synthesized using different plant extracts, *Bioprocess and biosystems engineering*, *40*(6), 943-957 (2017).

[40] B. Venkatesan, V. Subramanian, A. Tumala, E. Vellaichamy, Rapid synthesis of biocompatible silver nanoparticles using aqueous extract of Rosa damascena petals and evaluation of their anticancer activity, *Asian Pac J Trop Med* (2014).

[41] L. Inbathamizh, T. M. Ponnu, E. J. Mary, In vitro evaluation of antioxidant and anticancer potential of Morinda pubescens synthesized silver nanoparticles, *J Pharm Res* (2013).

[42] D. Nayak, S. Pradhan, S. Ashe, P. R. Rauta, B. Nayak, Biologically synthesised silver nanoparticles from three diverse family of plant extracts and their anticancer activity against epidermoid A431 carcinoma, *J Colloid Interface Sci* (2015).

[43] S. M. Husseiny, T. A. Salah, H. A. Anter, Biosynthesis of size controlled silver nanoparticles by Fusarium oxysporum, their antibacterial and antitumor activities, *Beni-Suef Univ J Basic Appl Sci* (2015).

[44] D. B. Manikandan, A. Sridhar, R. K. Sekar, B. Perumalsamy, S. Veeran, M. Arumugam, P. Karuppaiah, and T. Ramasamy, Green fabrication, characterization of silver nanoparticles using aqueous leaf extract of Ocimum americanum (Hoary Basil) and investigation of its in vitro antibacterial, antioxidant, anticancer and photocatalytic reduction, *Journal of Environmental Chemical Engineering*, *9*(1), p.104845 (2021).

Karnatak University Journal of Science

Temperature effects of Bandgap in Core Cadmium Selenide quantum dots: Spectroscopic Approach

K.S. Adarsh*

Department of Physics, Jain College of Engineering and Technology, Sainagar, Unkal, Hubballi-58003, India.
***Corresponding author:** shettiadarsh@gmail.com*

ARTICLE INFO

ABSTRACT

The temperature dependence of absorption, fluorescence spectra, and Photoluminescence (PL) decay dynamics for core Cadmium Selenide (CdSe) quantum dots (QDs) is recorded using fluorescence and Time-resolved spectroscopy techniques. The quenching of fluorescence intensities and shrinking related to the bandgap of peak wavelength about 3-4 nm towards the redder-region are discussed. The shrinking of the core CdSe QD, the bandgap is analyzed under the Varshni Law by varying the temperature ranging from, 300-343 K. This law is widely used to explain the bulk semiconductor bandgap but has also been found to apply to QDs as well. Varshni's coefficients are known as, and in the temperature range, 300-343K. Obtained result reveals a nearly matching value of is compared with bulk semiconductors, suggesting improve the thermal stability of the QD. Further, the PL lifetime decay dynamics of core CdSe QD have been studied concerning temperature. We observe that the longer lifetime component highly depends on temperature and it shows the formation of a red tail which is due to the surface defect state of QD.

1. Introduction

Semiconductor nanocrystals (NCs) are beneficial materials for lasing and optical advantages because of their size and composition tunable emission [1-3]. Owing to the discrete number of states, in Zero-Dimension quantum dot (QD) methods were anticipated to occur at the low thresholds of temperature sensitivity. The study on the dependence of temperature on energy and broadening of electronic interband transitions can provide significant information with the interaction of electron-phonon, charge carrier properties, etc., [4]. For scientific applications such as biomedical fluorescent markers [5], optically pumped lasers [6] light-emitting diodes [7], and solar cells [8, 9] core CdSe QD was explored as a potential candidate. These properties are not present in the single molecules or bulk crystals, mainly because of the quantum containment effect. This is caused by the position of an electron-hole in a confined space. That results in the measurable quantization of the level of electron energy and increases the bandgap energy when the particle size falls below a critical size known as a Bohr radius [10]. Comprehensive research [11, 12] has been carried out to a detailed comparison of experiments with theories of quantum-confined electronic states in semiconductor NCs and provides a more precise

K.S. Adarsh

description of the difference between NC bandgap variation and the size of the particle.

Research has concentrated in recent years on group BII-VI of semiconducting materials, namely CdSe, CdS, ZnSe, ZnS, and so on. However, elements like CdS and CdSe QDs exhibits some surface trap states and lower the photoluminescence (PL) quantum efficiencies. Currently, research on the temperature characteristics of the QDs has centered on the measurement of lower energy levels of the QD structures at temperatures between 15 and 300 K [13-15]. However, this temperature is technically best suited to optoelectronics, since the real working condition typically has a higher temperature [16]. Therefore, we need to examine the nanoscale semiconductor bandgap variation against temperature. A few experiments on thermal stability at the QDs at ambient temperature and above room temperature have also been performed.

In this paper, we studied the temperature dependence of bandgap in CdSe QD and luminescence lifetimes in the range 300–343 K. Varshni's law that is widely applied for bulk semiconductors refers to the QD in the present work to determine the relationship between bandgap fluctuation and temperature change. For the temperature range 300–343K, Varshni's coefficients of α and β for the QD are calculated.

To validate the obtained values of α and β, a comparison is made between the theoretical and experimental estimation. This focus provides new insight into the process of exciton recombination.

2. Experimental
2.1 Material and Methods
Toluene solutions of core CdSe QD (Lumidot) purchased from Sigma-Aldrich Chemicals Co. USA. Using a UV – visible spectrophotometer (Hitachi, U2800) the absorption spectra of the core CdSe QD are recorded and the fluorescence spectra were recorded by setting the excitation wavelength as 375nm through scanning wavelength ranging from 400–700 nm using the Hitachi F7000 spectrofluorometer. A thermostatic circulating water bath (CB 2000, Cyberlab Instrument, USA)

is used as a heater to heat the toluene solution of Core QDs. Once the temperature has been in a steady-state, spectral calculations are applied. The fluorescence lifetimes are calculated by using a picosecond time-domain spectrometer based on the time-correlated Single Photon Counting (TCSPC) technique (Horiba DeltaPro). CdSe QD samples were excited with a diode laser at 375 nm. The instrument response function for this system is $\sim$862 ps. An iterative. Fitting program provided by IBH (DAS-6) analyzed the fluorescence decay curves.

2.2 Quantum Yield
The fluorescence quantum yield of a core CdSe QD (φ_S) was determined by comparing it with a standard dye. PL quantum yields(φ_S) were obtained by comparison with standard dye using equation (1) [3]. This method involves the measurement of two absorbance and two emission spectrum values. The element of absorption must be precisely determined for solutions with a low absorbance, typically A<0.08. Under these conditions, there is a linear relationship was formed between absorbance and total integral emission and therefore no corrections for inner filter effects were conducted

$$\varphi_S = \left(\frac{F_s \cdot A_r \cdot n_S^2}{F_r \cdot A_S \cdot n_r^2} \right) * \varphi_R \qquad (1)$$

where F_s and F_r are the integrated fluorescence emission of the sample (QD) and the standard dye (coumarin 307 ($\varphi = 56\%$) in ethanol) [17], respectively. A_s and A_r, respectively, are the absorbance's at the excitation wavelength of the sample and the reference, φ_S and φ_R, respectively, are the quantum yields of the sample and the reference and n is the refractive index. The values of F_s and F_r are determined from the photoluminescence spectra corrected for the instrumental response, by integrating the emission intensity over the desired spectral range. Only the band-edge luminescence peak was integrated (any other luminescence bands, such as defect associated luminescence or solvent fluorescence, were discarded as background) The Quantum yield of core CdSe QD is listed in Table1.

**Table 1.** Photophysical parameters of core CdSe QDs

QDs	Size (nm)	Emission (nm)	Ref. dye	φ_R a	φ_S b
CdSe 480	2.5	480	Coumarin 307	0.56	0.38

a: Quantum yield of a reference dye

b: Quantum yield of a sample (QDs)

3. Results and discussion

3.1 Steady-state absorption and fluorescence spectra of core CdSe QD.

The optical absorption and Fluorescence spectra of the core CdSe quantum dot as a function of the temperature range 300–343 K are reported as shown in Fig. 1 (A & B) and Fig 2 (A& B).
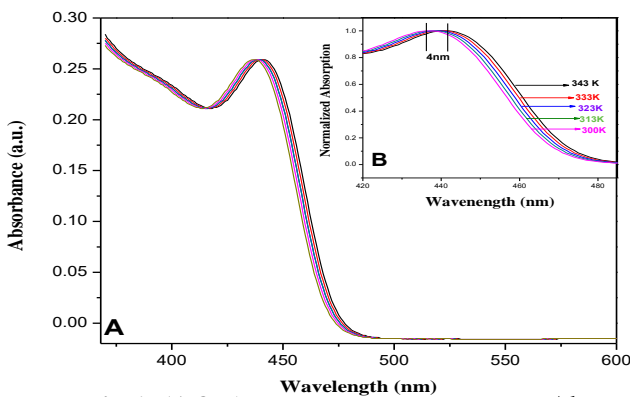
Fig.1 (A&B): Absorption spectra of Core CdSe QD (A) and Normalised Absorption spectra of the CdSe QD (B).
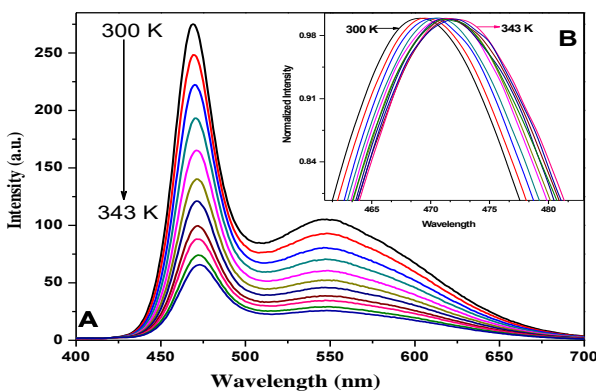
Fig.2 (A&B): Emission spectra of CdSe QD (A) and Normalised Emission spectra of the CdSe QD (B) at different temperatures (excitation is at 375 nm).

The normalized absorption and Fluorescence peaks are highlights the impact on peak-wavelength shift with increasing temperature. In Fig. 2 (A) we noticed that the fluorescence intensity variation is a function of temperature, as fluorescence intensity decreases with increasing temperature this quenching of Fluorescence intensity is due to increased molecular collision that occurs more frequently at the higher temperature. This report however, does not discuss whether the temperature has an impact on the peak fluorescence intensity, because several unknown considerations such as the pH of the samples, volatilization, remained concentration, as well as potential degradation of the solution, may affect the intensity of the spectrum. The redshifts of 3-5 nm of the emission peak have been seen, when the temperature increasing from 300 to 343K. This means that the band-gap in the core CdSe QD and temperature are negatively correlated.

3.2 Experimental determination of the bandgap of core CdSe QD.

Varshni's law describes temperature-dependent energy gaps in bulk semiconductor materials, which is given as [18]

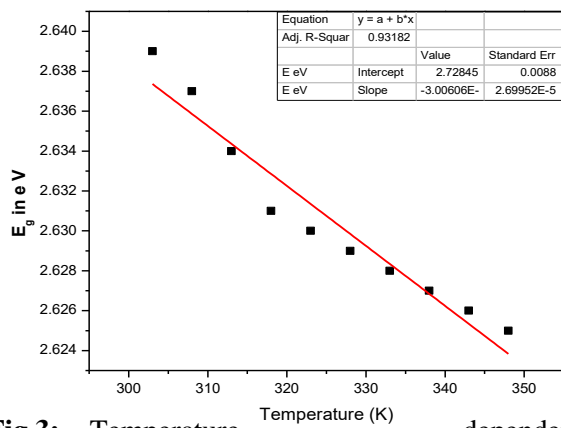$$E_g = E_0 - \frac{\alpha T^2}{(T + \beta)} \qquad (2)$$

where E_g is the energy gap that can be direct or indirect E_0 is the energy transition at 0K, α and β are the Varshni's coefficients depending on the materials. Generally, Varshin's Law is widely referred to the bandgap of bulk semiconductors but it has also been found to be applicable for QDs [15-19]. By using the experimental value of emission spectra Fig. 2(A) we can obtain the Varshini's coefficients are listed in Table2. This shows the comparative values of Varshini's coefficients for the QD at low temperature and the bulk semiconducting material at ambient temperature [20].

Table 2. Varshni's coefficients.

Varshni's coefficients	For Core QD (T =300–343 K)	For bulk (room temperature) [29]
$\alpha(eV / K)$	3×10^{-4}	$(2.8 - 4.1) \times 10^{-4}$

$\beta(K)$	220 ± 30	181-315

By substituting α and β value in Eq. (2), the energy gap is calculated as vary with temperature, as shown in Fig. 3. The observed band shift is 2.7285eV when the temperature varying from 300 to 343K.

Fig. 3 also indicates the Temperature-dependent bandgap of the core CdSe QD fitted by a least square method, with a slope of $\Delta E_g / \Delta T = -0.3006 meV / K$, suggests a linear variation of the bandgap as a function of temperature.

| Equation	y = a + b*x	
Adj. R-Squar	0.93182	
	Value	Standard Err
E eV Intercept	2.72845	0.0088
E eV Slope	-3.00606E-	2.69952E-5

Fig.3: Temperature- dependent bandgap of the core CdSe QD.

The relative bandgap is calculated by Eq. (2) and obtained α and β values are $3 \times 10^{-4} eV / K$, and $220 \pm 30 K$ respectively, in comparison to bulk CdSe [19]. From Eq. (2), and observed the lower the value of α and this related to bandgap fluctuation. In other words, the influence of temperature on the fluctuation of the bandgap energy is weaker for the discrete states of the QD than the continuous states in bulk semiconductors. As a result, QD has certain benefits on the better thermal stability over bulk-semiconductor materials as an applied device in usual temperature environments.

3.3 Time-resolved measurements

The PL lifetimes were estimated by using a time-domain spectrometer by employing the time-correlated single-photon counting (TCSPC) technique. The time-resolved fluorescence decay curves of core CdSe QDs with temperatures 300K
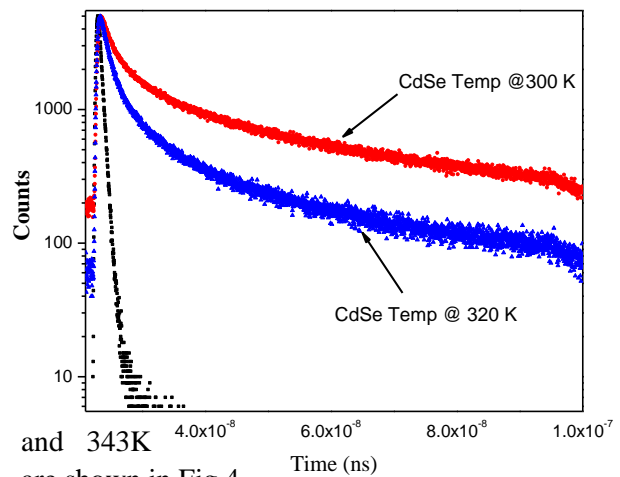
and 343K are shown in Fig 4.

Fig. 4: Semi log scale plot of time-resolved PL traces for core CdSe QD at temperature 300K and 320K

The decay profile of core CdSe QD is analyzed with a multi-exponential function [21].

$$I(t) = \left(A_1 \tau_1 + A_2 \tau_2 + A_3 \tau_3 \right) \qquad (3)$$

where τ_1, τ_2, τ_3 represents the shorter, longer, and longest lifetime components with their normalized pre-exponential factors A_1, A_2 and A_3, respectively.

Table 3. Time-resolved measurements for CdSe QDs at room temperature 300K and 320K

QDs	τ_1(ns)	τ_2(ns)	τ_3(ns)	A_1	A_2	A_3	$<\tau>$ (ns)
CdSe 480 @ Temp 300K	0.49	4.2	50.4	0.01	0.04	0.95	48.05
CdSe 480 @ Temp 320 K	0.50	4.3	42.0	0.03	0.09	0.88	37.36

The ratio of pre-exponential factors depends on the quality of the QD surface. The shortest lifetime τ_1 represents emission from radiative relaxation of an excited electron to ground state and can be attributed to the initially populated core–shell recombination and the possible origin of the longest lifetime component remains relatively uncertain [22-24]. A distribution of PL decay times is predicted by change in the non-radiative decay

K.S. Adarsh

rates of different QD is due to variation in the type and number of the quenching centers. By applying all of these processes, along with the difference between the populations of the individual NCs move towards multiexponential emission dynamics for different QD. The PL lifetime (τ) is calculated by using [25, 26]

$$\tau = \frac{\sum A_i \tau_i^2}{\sum A_i \tau_i} \tag{4}$$

where A_i is the normalized pre-exponential factor and τ_i the fluorescence lifetime.

One can be seen from Fig. 2(A) the core CdSe QD having two emission bands. The Peak wavelength of 480 nm corresponding to band-edge luminescence and the red tail (600 nm) corresponds to surface related emission. The fluorescence lifetimes values of CdSe at 300K and 320 K are listed in Table 3. It is reported that a broad dispersion in the energy splitting is due to the size and shape distribution of the QD [14]. Although, higher-size QDs exhibit multi-exponential PL decay at low temperatures on a longer lifetime scale. The surface trap states may also have a strong influence on the relaxation mechanisms of QD. This describes the large relative distribution of longer lifetime is observed at very low temperatures and this suggests the surface-related emission. As temperature increases the PL lifetimes also decrease. These observations indicate that the emission occurs from two thermally populated states, a weekly emitting short-lived ground state, and a strongly emitting upper one.

4. Conclusion

In summary, we studied the temperature behaviour of the PL studies of the core CdSe QD by employing steady-state and time-resolved spectroscopy Techniques. The emission wavelengths of the core CdSe QD show a red-shift of 3- 5 nm as the temperature increases from 300 to 343K. This indicates that as the temperature increases the bandgap of QD decreases. Generally, Varshni's law is used to describe the bandgap of bulk semiconductors and is also suitable for the QD in a lower temperature range. Varshni's coefficients for the QD have been determined by spectrum analysis and thermal property estimation. The PL lifetime decay dynamics of core CdSe QD

reveals the formation of a red tail which is due to the surface defect state of QD.

References

[1] S. V. Gaponenko, Optical Properties of Semiconductor Nanocrystals; Cambridge University Press: Cambridge, (1998).

[2] Synthesis, properties and perspectives of hybrid nanocrystal structures, P. D. Cozzoli, T. Pellegrino and L. Manna Chem. Soc. ReV. 35, 1195- 1208 (2006)

[3] Composition-dependent energy transfer from alloyed ternary CdSeS/ ZnS quantum dots to Rhodamine 640 dye K.S.Adarsh, M.G. Kotresh, M.A. Shivakumar and S.R. Inamdar J. Nanophoton. (SPIE) 12(4), 046016 (2018)

[4] Temperature dependence of the dielectric function and interband critical points in silicon P. Lautenschlager, M. Garriga, L. Vina, and M. Cardona Phys. Rev. B 36, 4821 –30 (1987)

[5] Semiconductor Nanocrystals as Fluorescent Biological Labels M. Bruchez, M. Moronne, P. Gin, S. Weiss, A.P. Alivisatos, Science 81, 2013-16(1998).

[6] High-Efficiency Green Phosphorescent Organic Light-Emitting Diode Based on Simplified Device Structures Z. Hong-Mei, W. Dan-Bei, Z. Wen-Jin and Yan Min-Nan CHIN. PHYS. LETT. IOP Science) Vol. 32, No. 9 , 097803(2015)

[7] Lasing from Semiconductor quantum Rods in a cylindrical microcavity M. Kazes, D.Y. Lewis, Y. Ebenstein, T. Mokari, U. Bannin, Adv. Mater. (Wiley online Library) 14 317 (2002).

[8] Feng Gao, Advanced Nanomaterials for Solar Cells and Light Emitting Diodes 1st Edition (Elsevier) 12th April (2019)

[9] Photoluminescence studies of CdS thin films annealed in CdCl$_2$ atmosphere J. A. Hernández, J. S. Hernández, R. M. Pérez, G. C. Puente, M. C.

K.S. Adarsh

García, J. O. López, Sol. Energy Mater. Sol. Cells (Elsevier) 90 704-712 (2006).

[10]   Electronic wave functions in semiconductor clusters: experiment and theory L.E. Brus, J. Phys. Chem.(ACS Publication) 90, 6 2555-60 (1986).

[11] Exciton   light   absorption   by   CuCl microcrystals growth in a glass matrix. Sov Phys Chem Glass A.I. Ekimov, A.A. Onushchenko, A.V. Tzehomskii, Sov. Phys. Chem. Glass 6 (1980) 511

[12] Photo-Degradation and Fluorescence of Colloidal-Cadmium Sulfide in Aqueous Solution A. Henglein, Ber. Bunsen-Ges. Phys. Chem. (Wiley online Library) 86 301-305(1982)

[13] Temperature dependence of the exciton transition in semiconductor quantum dots J.P. Thomas, J.R. Rajeev, Appl. Phys. Lett. 89 223132(2006).

[14]   Temperature   Dependence   of   the Luminescence Lifetime of Single CdSe/ZnS Quantum Dots O. Labeau, P. Tamarat, and B. Lounis Physical Review Letters 90, 257404-4 (2003)

[15] Temperature-dependent photoluminescence of vertically stacked self-assembled CdSe quantum dots in ZnSe   X. Liu, M. Dobrowolska, J.K. Furdyna, S. Lee, Physica E (Elsevier) 32 65-68 (2006).

[16]   Characteristics of bandwidth, gain and noise of a PbSe quantum dot-doped fiber amplifier C. Cheng, H. Zhang, Opt. Commun. (Elsevier) 277, 372-78 (2007).

[17]   Novel multi-branched organic compounds with enhanced two-photon absorption benefiting from the strong electronic coupling Y. Ren, Q. Xin, X. T. Tao,, L. Wang, X. Qiang Y. J. X. Yang and M.H. Jiang Chem. Phys. Lett. (Elsevier) 414, 253–258 (2005).

[18] Temperature Dependence Of The Energy Gap In Semiconductors P. Varshni, Physica 34 149-154 (1967).

[19] Temperature   effects   on   the   spectral properties of colloidal CdSe nanodots, nanorods,

and tetrapodsA. Al Salman, A. Tortschanoff, M.B. Mohamed, D. Tonti, F. Van Mourik, M. Chergui, Appl. Phys. Lett. 90 093104(2007)

[20]   K.H.Hellwege,Landolt-Bo¨   rnstein, NumericalDataandFunctionalRelation-   ship inScienceandTechnology,NewSeries,GroupIII,Vol .17(Pt.B),Springer, Berlin,1982.

[21]   Quantum dot based FRET to cresyl violet: Role of surface effects M.A. Shivkumar, K.S. Adarsh and S.R. Inamdar, J. Lumin. 143 680–686 (2013).

[22]   Experimental   Determination   of   the Extinction Coefficient of CdTe, CdSe, and CdS Nanocrystals X. Wang, L. Qu, J. Zhang, X. Peng, and M. Xiao, Chem. Mater.(ACS Publication) 15, 2854-2860 (2003)

[23]   Electronic Energy Transfer in CdSe Quantum Dot Solids C.R. Kagan, C.B. Murray, M. Nirmal, M.G. Bawendi, Phys. Rev. Lett.(APS Physics) 76 (1996) 9, 1517-1520.

[24]   FRET from core and core–shell quantum dots to laser dye: A comparative investigation K.S. Adarsh, M.K.Singh, M.A. Shivkumar, M.K. Rabinal,   B.N.Jagatap,   B.G.   Mulimani M.I.Savadatti   and   S.R.Inamdar   J. Lummi.(Elsevier) 160216–222(2015)

[25]   Fluorescence enhancement via aggregation effect due to microenvironmental alterations in human hemoglobin protein in presence of carbon quantum dots (CQD): Comparative spectroscopic approach, M. Chakraborty, I. Mitra, K. Sarkar, M. Bardhan, S. Paul , .S Basu, A Goswami, A.Saha, B. Show, T. Ganguly Spectrochimica Acta Part A 215, 313-326 (2019)

[26]   Effects of Carbon Quantum Dots (CQDs) on the energy storage capacity of a novel synthesized short-chain dyad. Mitra, S. Paul, M.Bardhan, S Das, M Saha, A Saha,T. Ganguly Chem Phys Letts 276, 1-6   (2019)

Karnatak University Journal of Science

Determination of effective atomic number of acetate compounds using Am-Be neutron source

Prashant N. Patil[1], A. Vinayak[1], G. B. Hiremath[1], M. M. Hosamani[1], A. S. Bennal[1], and N. M. Badiger[1, 2*]

[1]Department of Studies in Physics, Karnatak University, Dharwad -580003

[2]School of Advanced Sciences, KLE Technological University, Hubli, Karnataka -580031.

Corresponding author: nbadiger@gmail.com

ARTICLE INFO

ABSTRACT

An elementary experiment has been carried out to determine the effective atomic number of nuclear reactor shielding materials such as Manganese acetate, Cobalt acetate, Nickel acetate, and Cadmium acetate using NaI(Tl) gamma ray spectrometer and Am-Be neutron source through (n, γ) reaction. The effective atomic number of above acetates is determined by using the plot of intensity ratio of 2.2 MeV neutron induced gamma to 4.43 MeV gamma of Am-Be for different elemental targets. The experimentally determined effective atomic number has been compared with theoretical values.

Introduction

The neutron interaction with matter is an area of current research due to significant role of neutrons and their activity in the development of nuclear reactors and nuclear weapons. In case of fissioning of nuclei ^{235}U and ^{239}Pu the essential knowledge of neutrons absorption is required. While penetrating into the matter, neutron may undergo elastic and inelastic scattering or trigger nuclear reactions like neutron capture and fission [1]. In case of neutrons interaction with matter, one of the primary objectives is to moderate the speed of neutrons to increase the interaction probability in region of sample of interest or in region of detector or in regions of both. Since neutron interaction is high for low atomic number (Z) materials, neutron can be moderated by low Z

moderators such as paraffin and heavy water. On the other hand, the interaction of gamma rays is high for high Z materials and can be moderated by high Z materials [2]. The simultaneous analysis of neutrons and gammas is of great interest as it provides information about materials suitable for the reactor engineering. A variety of techniques have been performed to detect and analysis the neutron and gamma simultaneously [3, 4]. More recently, M. M. Hosamani and N. M. Badiger et al., have shown that the effective atomic number (Z_{eff}) of composite materials can be determined by beta-ray backscattering [5]. With these motivations an elementary experiment has been carried out to determine the effective atomic number (Z_{eff}) for the acetate compounds using NaI(Tl) detector and

Am-Be neutron source through (n, γ) reaction. In the present investigation, intensity ratio of 2.2 MeV neutron induced gamma to 4.43 MeV gamma of Am-Be is measured as a function of different thickness of laboratory available C, Al, Cu, Ni, Zn and Pb elemental targets. Next, the slope of above intensity ratio is normalized by an effective atomic mass (A) of above acetate compounds. From the plot of slope/A as a function of Z of the elemental targets the Z_{eff} of above acetate compounds is determined. The measured Z_{eff} values are compared with WINXCOM and GEANT4 predictions [6-8]. A good agreement between experimental values and theoretical model predictions has been found. The present experiment is simple and low cost and can be implemented to determine Z_{eff} of any unknown composite material. Therefore present technique can be adapted in the research laboratories deprived by neutron detector.

1. **Theory**
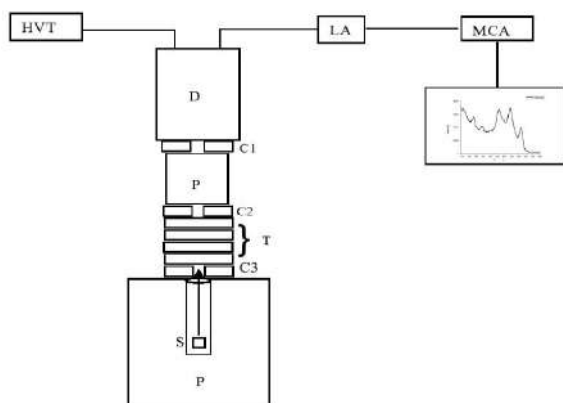
Figure 1. Experimental arrangement to determine the effective atomic number of acetate compounds.

The probability of an event through interaction of a neutron with a nucleus is expressed in terms of cross section. The magnitude of cross section is dependent on the neutron energy [9]. The total cross section (σ_t) is the sum of scattering cross section (σ_s) and absorption cross section (σ_a) [10]. In elastic scattering the total kinetic energy (TKE) of the nucleus and neutron is unchanged by the interaction where in case of inelastic scattering

the TKE of the exit channel is less than the TKE of the entrance channel. Instead of scattering, neutron may absorbed by the nucleus. During absorption phase the nucleus may rearrange its internal structure and may release one or more gammas or emits light charged particles like α, proton, deuteron or it may emits excess neutrons or may undergo fission by splitting into two nearly similar mass fragments. Because of photon interaction cross-section for elements of composite material, a single atomic number being a characteristic of element will not describe the atomic number of composite material in the all energy ranges and hence a new number of composite materials called to be effective atomic number (Z_{eff}) , suggested by Hine [11]. Since, 'Z' has been associated with the fundamental properties of the elements and 'Z_{eff}' has been employed in the composite media [12]. By definition, the Z_{eff} is the weighted arithmetic mean of the atomic number of the constituent atoms [13]. This weighing factor accounts for the type of radiation, material and interaction cross section. Since Z_{eff} varies with the type and energy of radiation with which it interacts, determination of Z_{eff} got prominent importance especially in the fields of technological applications and nuclear medicine for the calculation of dose in radiation therapy and medical imaging. In the present experimental investigation, the Z_{eff} is determined simply by a slope of intensity ratio of 2.2 MeV neutron induced gamma to 4.43 MeV gamma of Am-Be to atomic mass of the moderating medium for the average neutron energy ~ 4.2 MeV of Am-Be.

2. **Experimental details**

The experimental arrangement to measure the effective atomic number of Manganese acetate tetra hydrate, Nickel acetate tetra hydrate, Cobalt acetate tetra hydrate and Cadmium acetate dihydrate is shown in figure 1. The neutrons are generated from Am-Be neutron source of flux 10^5 n/cm^2.s kept in a paraffin container of 20 inch height and 10 inch

diameter covered with a lead sheet to shield the isotropic emission of radiations from the source [3].

Table 1. Comparison of experimentally determined Z_eff with theoretical values.

Name of the target	Z_{eff}		
	This expt.	Geant4	WinXCOM
Manganese acetate tetrahydrate	13.85 ± 2.07	11.539	11.539
Cobalt acetate tetrahydrate	14.64 ± 2.19	12.484	12.457
Nickel acetate tetrahydrate	14.16 ± 2.12	12.747	12.751
Cadmium acetate dehydrate	25.42 ± 3.81	27.862	27.801

The generated neutrons have the distributions from thermal to fast neutrons with average neutron energy ~ 4.2 MeV [3, 4].
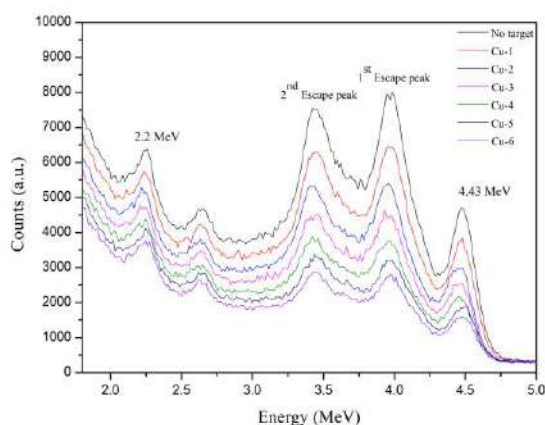
Figure 2. Typical captured neutron gamma yield at various thicknesses as a function of neutron energy in case of Cu elemental target.

Along with neutrons, γ rays of 4.4 MeV also emitted from the nuclear de-excitation of $^{12}C^*$ indicating that generation of neutrons and γ rays are correlated [14]. The above acetate and elemental targets of various thicknesses were placed on the Am-Be neutron source with 2π geometry for the interaction of collimated radiation through lead collimator (C1) of 2 cm diameter and 2 cm thick. After this, the interacted/non-interacted collimated radiation is allowed through lead collimator (C2) of diameter 2 cm and 2 cm thick to interact with 7 cm paraffin wax placed before collimator (C3) of similar dimension of C1 and C2. The prompt γ-rays of 4.38 MeV and neutron induced gammas resulting from (n, γ) reaction are acquired using 2" × 2" energy calibrated NaI(Tl) gamma ray spectrometer coupled to 8k multi-channel analyser. The NaI(Tl) gamma ray spectrometer was operated at 750 volts. The typical spectrum of Am-Be radioactive source acquired by NaI(Tl) detector for the Cu elemental target at various thicknesses is shown in figure 2. The peak at 4.4 MeV corresponds to prompt gammas, 1st and 2nd escape peaks appeared near to 3.9 MeV and 3.4 MeV due to the crystal size [15, 16], a minute peak observed at 2.65 MeV due to the effective contributions of decay of ^{24}Na from detector [17] and ^{208}Tl from ^{232}Th series of ^{241}Am [15] and the peak observed at 2.2 MeV due to (n,γ) reaction [3]. From the obtained intensity spectra ratio at different thicknesses of elemental targets the Z_{eff} for above acetate compounds has been determined.

3. **Results and Discussion**

The present experimental investigation is has been carried out to determine the Z_{eff} of the above mentioned acetate compounds which are commonly used as nuclear reactor shielding materials. A typical captured neutron gamma yield at various thicknesses as a function of neutron energy in case of Copper elemental target is shown in figure 2. Figure indicates that intensity ratio of 2.2 MeV to 4.4 MeV gamma yield increases gradually as a function of thickness of the target and confirms the neutron captured gammas resulting from (n, γ) reaction. The (n, γ) reaction cross section in the targets for hydrogen composites is itself taken care

during extraction phase of intensity ratio. The plot of intensity ratio as a function of target thickness for laboratory available C, Al, Fe, Cu, Zn and Pb elemental targets at various thicknesses gives a straight line as shown in figure 3
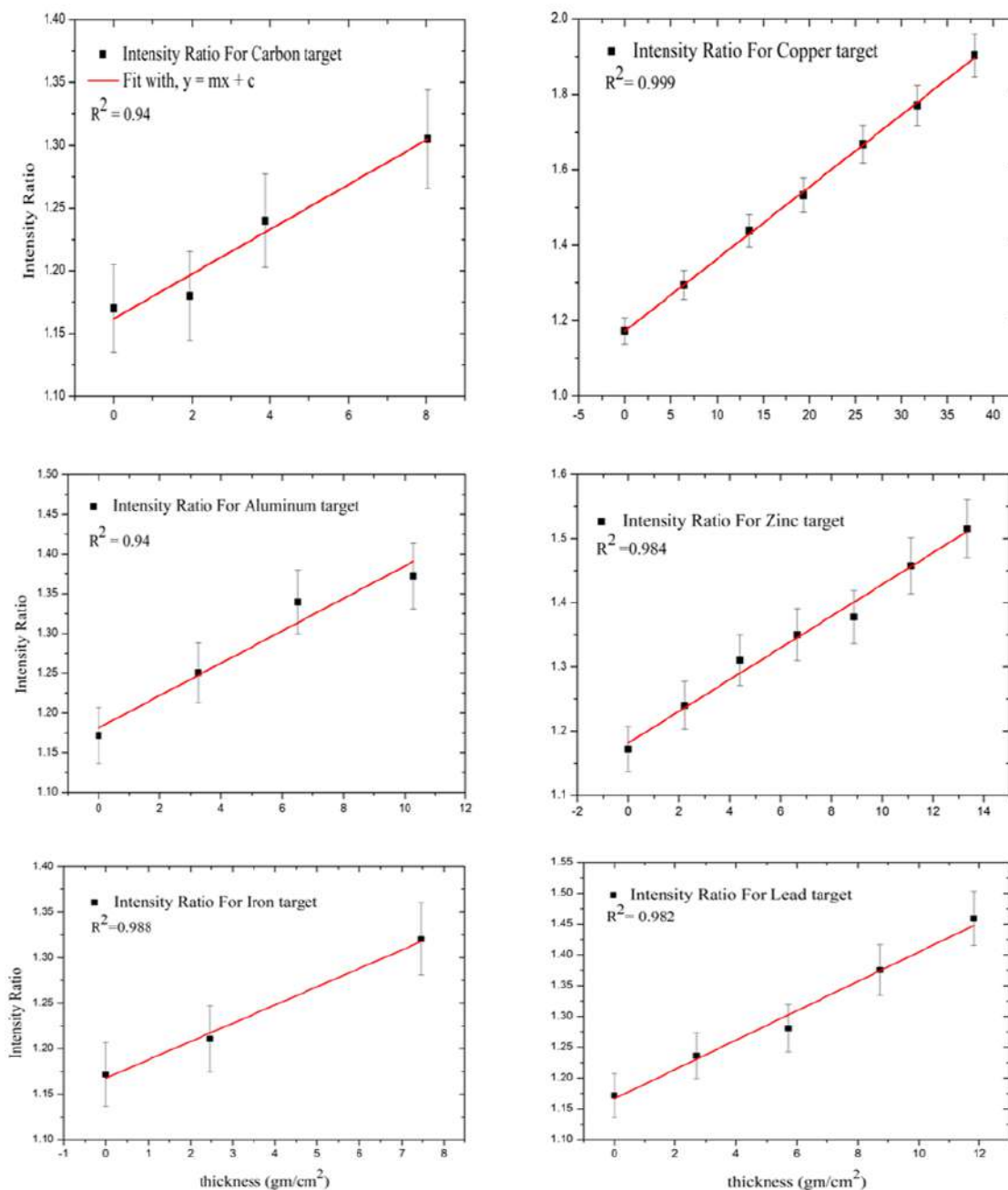
**Figure 3.** Intensity ratio as a function of various thicknesses of different elemental targets.
.

The slope thus obtained is normalized by dividing the corresponding effective atomic mass of the acetate compounds and plotted as a function of Z of the elemental targets at various thicknesses as shown in figure 4 to determine the Z_{eff}. The effective atomic mass of the above acetate compounds can be determined by using simple formulation; $\Sigma f_i A_i$. The term 'f_i' represents weight fraction in the compound and 'A_i' represents the atomic weight element [18]. The present technique is useful to understand the concept of moderation of fast neutrons into thermal neutrons in specified materials and facilitates to determine the Z_{eff} of any unknown composite material. The experimentally observed Z_{eff} values are compared with the

GEANT4 Monte Carlo simulation code [7, 8] and WinXCOM code [6] predictions and are tabulated in table 1. The experimentally observed Z_{eff} values are in good agreement with theoretical model predictions/simulations indicating that present simple technique is reliable to study the radiation interaction phenomenon in any multifunctional composite targets for neutron physics.
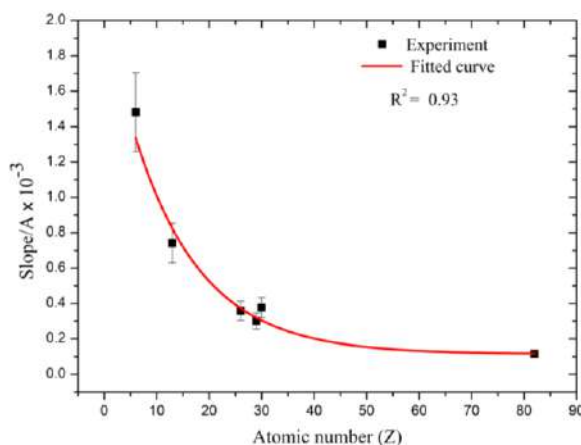
Figure 4. Experimentally determined slope/A versus atomic number (Z) of the elemental targets.

4. Summary and Conclusion

Objective of the present investigation is to determine the one of the important radiation interaction properties such as the effective atomic number of nuclear reactor shielding materials namely Manganese acetate tetra hydrate, Cobalt acetate tetra hydrate, Nickel acetate tetra hydrate and Cadmium acetate dihydrate through (n, γ) reaction. The NaI(Tl) gamma ray spectrometer has been used to detect 2.2 MeV and 4.4 gamma ratio for elemental targets such as C, Al, Cu, Ni, Zn and Pb. The plot of slope/A as a function of Z for elemental targets has been treated as calibration curve. Using such calibration curve the Z_{eff} of nuclear reactor materials have been determined and compared with theoretical values. The experimentally observed Z_{eff} values are in good agreement with theoretical model predictions/simulations. The present experiment is simple and low cost and also facilitates to determine the Z_{eff} of the any unknown composite material. Therefore present technique can be adapted in the research laboratories deprived by neutron detectors.

Acknowledgment

References:

[1] D. L. Garber and R. R. Kinsey Neutron Cross Sections, Vol. II, Curves, Brookhaven National Laboratory report, BNL p325 (1976).

[2] Measurement of the Effective Atomic Number of some Transition and Rare Earth compounds using the Rayleigh to Compton Scattering ratio of gamma radiation Mutturaj Hosamani, S Ramesh Babu, Santosh Mirji, N. M. Badiger Spectroscopy Letters, 50 (7), 370-374 (2017).

[3] Binding energy of the deuteron: A laboratory experiment T. S. Mudhole and N. Umakantha American Journal of Physics 43, p104 (1975).

[4] Determination of the thermal neutron flux by measuring gamma radiations with high and low resolution detectors M. M. Hosamani, A.

Prashant N. Patil et al.,

S. Bennal and N. M. Badiger J. Nucl. Phys. Mat. Sci. Rad. A. 6(2), p178 (2019).

[5]Determination of Effective Atomic Number of Multifunctional Materials Using Backscattered Beta Particles–A Novel Method M. M. Hosamani, A. Vinayak, S. Mangeshkar, S. Malode, S. Bhajantri, V. Hegde, G. B. Hiremath, N. M. Badiger Spectroscopy Letters 53 p132 (2020).

[6]XCOM: Photon Cross Section Database (version 1.5). [Online] http://physics.nist.gov/xcom [2020, October 7].

[7]Geant4 Developments and Applications J. Allison, K. Amako, J. Apostolakis, H. Araujo, . P. Arce Dubois, M. Asai,G. Barrand, R. Capra, S. Chauvie,R. Chytracek et al., IEEE Transactions on Nuclear Science 53 p270 (2006).

[8]Recent Developments in GEANT4 J. Allison, K. Amako, J. Apostolakis, P. Arce, M. Asai, T. Aso, E. Bagli, A. Bagulya, S. Banerjee, G. Barrand et al., Nucl. Instrum. Methods Sec. A 835 p186 (2016).

[9]The investigation of the neutron total cross section & measurement of the nuclear radius with comparison of Ramsauer model Abdelrazig Mohmed and Abdelbagi International Journal of Pure and Applied Physics 13(3) p 495 (2017).

[10] Robley D. Evans, The Atomic Nucleus Tata Mcgraw-Hill Publishing Company Ltd, Bombay – New Delhi p95, 1955.

[11] The effective atomic numbers of materials for various gamma ray interactions Hine, G. J. Phys. Rev. 85, p725 (1952).

[12] The high frequency spectra of the elements H. Moseley Phil. Mag. 26 p1024 (1913).

[13] Determination of effective atomic number of some bimolecules for electron interaction S. Ramesh Babu, M. M. Hosamani, S. Mirji, N. M. Badiger IOSR Journal of Applied Physics 8 p23 (2016).

[14] Tagging fast neutrons from an 241Am/9Be source J. Scherzinger, J.R.M. Annand, G. Davatz, K.G. Fissum, U. Gendotti, R. Hall-Wilton, A. Rosborg, E. Håkansson, R. Jebali, K. Kanaki, M. Lundin, B. Nilsson, H. Svensson Applied Radiation and Isotopes, 98 p74 (2015).

[15] The 4.438 Mev gamma To neutron ratio For the Am–Be neutron source Zhenzhou Liu, Jinxiang Chen, Pei Zhu, Yongming Li, Guohui Zhang Applied Radiation And Isotopes 65 p1318 (2007).

[16] Nonlinear Response Function Of A 3" × 3" NaI Scintillation Detector Hashem Miri Hakimabad, Hamed Panjeh, Alireza Vejdani-Noghreiyan Asian J. Exp. Sci., 21 p1 (2007).

[17] Table of Isotopes G. T. Seaborg and I. Perlman Rev. Mod. Phys. 20 p585 (1948).

[18] Effective Atomic Weight, Effective Atomic Numbers and Effective Electron Densities of Hydride and Borohydride Metals for Fusion Reactor Shielding Vishwanath P. Singh, N. M. Badiger, J Fusion Energy 33 p386 (2014).

Karnatak University Journal of Science

Bounds for Complementary Distance Eigenvalue and Complementary Distance Energy of Graphs

H. S. Ramane[1], S. S. Shinde[2] and S. Sedghi[3]

[1]Department of Mathematics, Karnatak University Dharwad - 580003, India
[2]Department of Mathematics, KLE Technological University Hubbali – 580031, India
[3]Department of Mathematics, Islamic Azad University, Qaemshahr Branch, Qaemshahr, Iran
Corresponding author: *hsramane@yahoo.com*

ARTICLE INFO

ABSTRACT

The complementary distance matrix of a connected graph is a square matrix whose (i,j)-th entry is $1+D - d_{ij}$ if $i \neq j$ and zero, otherwise, where D is the diameter of a graph and d_{ij} is the distance between the vertices v_i and v_j in the graph. The complementary distance energy of a graph is defined as the sum of the absolute values of the eigenvalues of its complementary distance matrix. In this paper we obtain a lower bound for the maximum eigenvalue and bounds for complementary distance energy.

1. Introduction:

Let G be a simple, connected graph with n vertices and m edges. The distance between the vertices v_i and v_j, denoted by $d_{ij} = d(v_i, v_j)$ is the length of a shortest path joining them. The diameter of a graph G is the maximum distance between any pair of vertices of G and is denoted by $diam(G)$ [1]. The complementary distance matrix [3] of a connected graph G is a square matrix of order n defined as $CD(G) = [c_{ij}]$, in which $c_{ij} = 1+D - d_{ij}$ if $i \neq j$ and $c_{ij} = 0$, otherwise, where D is the diameter of G and $d_{ij} = d(v_i, v_j)$.

In chemistry, the structural descriptors calculated from this matrix are used to develop the structure-property models for the normal boiling temperature, molar heat capacity, refractive index, vaporization enthalpy and the density of alkanes [3, 4].

The eigenvalues of the complementary distance matrix denoted by $\mu_1, \mu_2, ..., \mu_n$ are said to be the CD-eigenvalues of G. Since the complementary distance matrix is symmetric, its eigenvalues are real and can be arranged as $\mu_1 \geq \mu_2 \geq \cdots \geq \mu_n$.

The complementary distance energy of a graph G is defined as,

H. S. Ramane

$$CDE(G) = \sum_{i=1}^{n} |\mu_i|. \qquad (1.1)$$

The Eq. (1.1) is in full analogy to the ordinary graph energy [2, 5]. In [7], line graphs of some regular graphs having equal complementary distance energy were reported. The construction of graphs having equal complementary distance energy for $n \geq 6$ have been done in [6]. In this paper we obtain a lower bound for the maximum CD-eigenvalue and bounds for the complementary distance energy of graphs.

We need the following results.

Lemma 1.1 [8]: Let a_1, a_2, ... , a_n be non-negative numbers. Then

$$n \left[\frac{1}{n} \sum_{i=1}^{n} a_i - \left(\prod_{i=1}^{n} a_i \right)^{1/n} \right] \leq n \sum_{i=1}^{n} a_i - \left(\sum_{i=1}^{n} \sqrt{a_i} \right)^2$$

$$\leq n(n-1) \left[\frac{1}{n} \sum_{i=1}^{n} a_i - \left(\prod_{i=1}^{n} a_i \right)^{1/n} \right]$$

.

2. Complementary distance eigenvalues

Lemma 2.1: For a connected graph on n vertices with CD-eigenvalues μ_1, μ_2, ... , μ_n,

$$\sum_{i=1}^{n} \mu_i = 0 \text{ and}$$

$$\sum_{i=1}^{n} \mu_i^2 = 2 \sum_{1 \leq i < j \leq n} (1 + D - d_{ij})^2 .$$

Proof: (i) Since trace$(CD(G)) = 0$, $\sum_{i=1}^{n} \mu_i = 0$.

(ii) Also $\sum_{i=1}^{n} \mu_i^2 = \text{trace}((CD(G))^2)$

$$= \sum_{i=1}^{n} \sum_{j=1}^{n} (1 + D - d_{ij})((1 + D - d_{ji})$$

$$= \sum_{i=1}^{n} \sum_{j=1}^{n} (1 + D - d_{ij})^2$$

$$= 2 \sum_{1 \leq i < j \leq n} (1 + D - d_{ij})^2 .$$

Corollary 2.2: For a connected graph on n vertices and m edges,

(i) if $diam(G) = 1$, then $\sum_{i=1}^{n} \mu_i^2 = 2m$

(ii) if $diam(G) = 2$, then $\sum_{i=1}^{n} \mu_i^2 = n^2 - n + 6m$

.

Proof: Let D be the diameter of G. If $diam(G) \leq 2$, then in a graph G there are m pairs of vertices at distance one and remaining $n(n - 1)/2 - m$ pairs of vertices are at distance 2. Therefore, from Lemma 2.1,

$$\sum_{i=1}^{n} \mu_i^2 = 2 \left[m(1 + D - 1)^2 + \left(\frac{n(n-1)}{2} - m \right)(1 + D - 2)^2 \right]$$

$$= 2mD^2 + (n(n - 1) - 2m)(D - 1)^2.$$

$$(2.1)$$

Now the conclusion is immediate by choosing either $D = 1$ or $D = 2$.

Theorem 2.3: For a connected graph on n vertices and m edges with $diam(G) = 2$,

$$\mu_1 \geq \left(\frac{n^2 - n + 2m}{n} \right).$$

Equality holds if and only if G is a regular graph.

Proof: Let v_1, v_2, ..., v_n be the vertices of G and let d_i be the degree of a vertex v_i, $i = 1, 2, ... , n$. As $diam(G) = 2$, we observe that the i-th row of $CD(G)$ consists of one zero, d_i number of 2's and $n - d_i - 1$ number of 1's. Let $x = [1, 1, ..., 1]$ be the all one vector. Then by Rayleigh's principle we have

$$\mu_1 \geq \frac{x(CD(G))x^T}{xx^T} = \frac{1}{n} \sum_{i=1}^{n} (2d_i + n - d_i - 1)$$

$$= \frac{1}{n} \sum_{i=1}^{n} (d_i + n - 1)$$

$$= \frac{1}{n} (2m + n^2 - n) .$$

For equality:

If G is a regular graph, then $d_i = r$ for all $i = 1, 2, ... , n$. Therefore each row sum of $CD(G)$ is

H. S. Ramane

equal to $2d_i + (n - d_i - 1) = n + r - 1$. If $CD(G)$ has eigenvalue $\mu_1 > 0$, there exist a vector $x > 0$ such that $CD(G)x = \mu_1 x$. Since G is an r-regular, $CD(G)\mathbf{1} = (n + r - 1)\mathbf{1}$, where $\mathbf{1} = [1, 1, \dots, 1]'$. Hence $\mathbf{1}'CD(G)x = (n + r - 1)(\mathbf{1}'x)$. And also $\mathbf{1}'CD(G)x = \mu_1(\mathbf{1}'x)$. Therefore $\mu_1 = n + r - 1$.

Conversely, if equality holds then, x is the eigenvector corresponding to μ_1 and this happens only when all the row sums of $CD(G)$ are equal to $d_i + n - 1$. This occurs only when d_i has the same value for each i, that is only when G is regular.

3. Bounds on complementary distance energy

Theorem 3.1: For a connected r-regular graph on n vertices with $diam(G) = 2$,

$2(n + r - 1) \le CDE(G) \le 2n - 2 + E_\pi(G)$,

where $E_\pi(G)$ is the ordinary energy of G.

Proof: Let $r = \lambda_1, \lambda_2, \dots, \lambda_n$ be the eigenvalues of the adjacency matrix of G. Then the CD-eigenvalues of G are $n + r - 1, \lambda_2 - 1, \dots, \lambda_n - 1$ [7]. Therefore

Lower bound:

$$CDE(G) = |n + r - 1| + \sum_{i=2}^{n} |\lambda_i - 1|$$

$$\ge (n + r - 1) + \left| \sum_{i=2}^{n} (\lambda_i - 1) \right|$$

$$= (n + r - 1) + |-r - (n - 1)|$$

since $\sum_{i=2}^{n} \lambda_i = -r$

$$= 2(n + r - 1).$$

Upper bound:

$$CDE(G) = |n + r - 1| + \sum_{i=2}^{n} |\lambda_i - 1|$$

$$\le (n + r - 1) + \sum_{i=2}^{n} (|\lambda_i| + |-1|)$$

$$= (n + r - 1) + E_\pi(G) - r + (n - 1)$$

$$= 2n - 2 + E_\pi(G).$$

Theorem 3.2: For a connected r-regular graph on n vertices with $diam(G) = 2$, if $\lambda_1, \lambda_2, \dots, \lambda_n$

are the eigenvalues of its adjacency matrix and if $\lambda_i \le 1$ for $i = 2, 3, \dots, n$, then $CDE(G) = 2(n + r - 1)$.

Proof: The proof is analogous to the first part of the proof of Theorem 3.1.

Theorem 3.3: For a connected graph on n vertices,

$$\sqrt{2 \sum_{1 \le i < j \le n} (1 + D - d_{ij})^2} \le CDE(G) \le \sqrt{2n \sum_{1 \le i < j \le n} (1 + D - d_{ij})^2}$$

.

Proof: By Cauchy-Schwarz inequality, we get

$$\left(\sum_{i=1}^{n} |\mu_i| \right)^2 \le n \sum_{i=1}^{n} \mu_i^2$$

$$(CDE(G))^2 \le 2n \sum_{1 \le i < j \le n} (1 + D - d_{ij})^2$$

$$CDE(G) \le \sqrt{2n \sum_{1 \le i < j \le n} (1 + D - d_{ij})^2} ,$$

Which is an upper bound.

Now for the lower bound we consider

$$(CDE(G))^2 = \left(\sum_{i=1}^{n} |\mu_i| \right)^2 \ge \sum_{i=1}^{n} |\mu_i|^2$$

$$= 2 \sum_{1 \le i < j \le n} (1 + D - d_{ij})^2$$

$$CDE(G) \ge \sqrt{2 \sum_{1 \le i < j \le n} (1 + D - d_{ij})^2} .$$

This leads to the lower bound of $CDE(G)$.

If $diam(G) = 2$, then from Lemma 2.1 and Corollary 2.2

$$\sum_{1 \le i < j \le n} (1 + D - d_{ij})^2 = \frac{n^2 - n + 6m}{2} .$$

Substituting this in Theorem 3.3 we get following corollary.

Corollary 3.4: For a connected graph on n vertices and m edges with $diam(G) = 2$,

$$\sqrt{n^2 - n + 6m} \le CDE(G) \le \sqrt{n^3 - n + 6m} .$$

H. S. Ramane

Corollary 3.5: For a connected graph on n vertices,

$$CDE(G) \geq \sqrt{n(n-1)}$$

Proof: As $1 + D - d_{ij} \geq 1$ for $i \neq j$ and there are $n(n-1)/2$ pairs of vertices, from the lower bound of Theorem 3.3 we have

$$CDE(G) \geq \sqrt{2 \sum_{1 \leq i < j \leq n} (1 + D - d_{ij})^2} \geq \sqrt{2 \frac{n(n-1)}{2}} = \sqrt{n(n-1)}$$

Theorem 3.6: For a connected graph on n vertices with Δ as the absolute value of the determinant of the complementary distance matrix of G, we have

$$\sqrt{2 \sum_{1 \leq i < j \leq n} (1 + D - d_{ij})^2 + n(n-1)\Delta^{2/n}} \leq CDE(G)$$
$$\leq \sqrt{2(n-1) \sum_{1 \leq i < j \leq n} (1 + D - d_{ij})^2 + n\Delta^{2/n}}$$

.

Proof: Let

$$X = n\left[\frac{1}{n} \sum_{i=1}^{n} \mu_i^2 - \left(\prod_{i=1}^{n} \mu_i^2 \right)^{1/n} \right]$$

$$= n\left[\frac{2}{n} \sum_{i=1}^{n} (1 + D - d_{ij})^2 - \left(\prod_{i=1}^{n} |\mu_i| \right)^{2/n} \right]$$

$$= 2 \sum_{1 \leq i < j \leq n} (1 + D - d_{ij})^2 - n\Delta^{2/n} .$$

By Lemma 1.1, if $a_i = \mu_i^2$, $i = 1, 2, \ldots, n$, then

$$X \leq n \sum_{i=1}^{n} \mu_i^2 - \left(\sum_{i=1}^{n} |\mu_i| \right)^2 \leq (n-1)X$$

that is,

$$X \leq 2n \sum_{i=1}^{n} (1 + D - d_{ij})^2 - (CDE(G))^2 \leq (n-1)X$$

Simplifying this we get the required result.

If $diam(G) = 2$, then from Lemma 2.1 and Corollary 2.2

$$\sum_{1 \leq i < j \leq n} (1 + D - d_{ij})^2 = \frac{n^2 - n + 6m}{2} .$$

Substituting this in Theorem 3.6 we get the following corollary.

Corollary 3.7: For a connected graph on n vertices and m edges with $diam(G) = 2$,

$$\sqrt{n(n-1) + 6m + n(n-1)\Delta^{2/n}} \leq CDE(G)$$
$$\leq \sqrt{(n-1)(n^2 - n + 6m) + n\Delta^{2/n}}$$

.

Theorem 3.8: For a connected graph on n vertices and m edges with $diam(G) = 2$,

$$CDE(G) \leq \mu_1 + \sqrt{(n-1)(n^2 - n + 6m - \mu_1^2)}$$

.

Proof: By Cauchy-Schwarz inequality, we have

$$\left(\sum_{i=2}^{n} |\mu_i| \right)^2 \leq (n-1) \sum_{i=2}^{n} |\mu_i|^2$$

$$(CDE(G) - |\mu_1|)^2 \leq (n-1)\left[2\sum (1 + D - d_{ij})^2 - |\mu_1|^2 \right]$$

. (3.1)

Since $diam(G) = 2$, from Lemma 2.1 and Corollary 2.2, the Eq. (3.1) becomes

$$CDE(G) \leq \mu_1 + \sqrt{(n-1)(n^2 - n + 6m - \mu_1^2)}$$

If G is an r-regular graph, then $\mu_1 = n + r - 1$. Therefore from Theorem 3.8 we have the following corollary.

Corollary 3.9: For an r-regular connected graph on n vertices and m edges with $diam(G) = 2$,

$$CDE(G) \leq (n + r - 1) + \sqrt{(n-1)[n(r+1) - (r-1)^2]} .$$

References

[1] F. Buckley, F. Harary, Distance in Graphs, Addison-Wesley, Redwood, 1990.

[2] I. Gutman, The energy of a graph, Ber. Math. Stat. Sekt. Forschungsz. Graz, 103 (1978), 1-22.

[3] O. Ivanciuc, T. Ivanciuc, A. T. Balaban, The complementary distance matrix, a new

H. S. Ramane

molecular graph metric, ACH-Models Chem., 137 (2000), 57-82.

[4]D. Jenezic, A. Milicevic, S. Nikolic, N. Trinajstic, Graph Theoretical Matrices in Chemistry, Uni. Kragujevac, Kragujevac, 2007.

[5]X. Li, Y. Shi, I. Gutman, Graph Energy, Springer, New York, 2012.

[6]H. S. Ramane, M. M. Gundloor, On complementary distance energy of the join of certain graphs, Discr. Math. Lett., 2 (2019), 57 – 64..

[7]H. S. Ramane, K. C. Nandeesh, Complementary distance spectra and complementary distance energy of line graphs of regular graphs, J. Indones. Math. Soc., 22 (2016), 27-35.

[8]B. Zhou, I. Gutman, T. Aleksic, A note on the Laplacian energy of graphs, MATCH Commun. Math. Comput. Chem., 60 (2008), 441-446.

Impact of Irrigation on Regional Development in Haveri District of Karnataka

M. G. Nayak*

Department of Geography, Karnatak University, Dharwad.
Corresponding author: maheshgnayak16@gmail.com

ARTICLE INFO

ABSTRACT

The regional disparities of irrigation development in the Haveri district were analyzed based on the score value of the regional variation of seven indicators with the help of the Z score and composite index method. The main objective of this paper is to analyse the development scenario in the irrigation sector of Haveri district over a decade (2006-07 and 2016-17) and to identify the changes in the development of irrigation in seven taluks of the study region. Based on the results of statistical methods it is analysed that as per the 2016-17 dataset shows that, out of seven taluks, the Hangal and Haveri taluks are fall in the 'highly developed category', whereas Ranebennur and Hirekerur taluks are found in the medium developed category. But remaining three taluks namely Shiggaon, Savanur and Byadagi taluks are found in the 'low development category'. The study region has well-drained by Varada and Tungabhadra rivers boosting the irrigation activities in the study region, especially in Varada river flows Hangal, Haveri and Savanur taluks. In the study region, the other sources of irrigation activities are also boon to sustainable development..

INTRODUCTION

Irrigation has contributed significantly to the alleviation of poverty, food security and improving the quality of life for rural populations. However, the sustainability of irrigated agriculture is being questioned, both economically and environmentally. The increased dependence on irrigation has not been without its negative environmental effects. Irrigation is the application of controlled amounts of water to plants at the needed interval. Irrigation helps to grow crops, maintain landscapes and re-vegetate disturbed soils in dry areas and during periods of less than average rainfall. Irrigation enhances the productivity of crops per unit area and facilitates the former to bring land under multiple cropping. Irrigation system affects agriculture in various ways such as: helps to improve the yields of crops, impact on cropping pattern leading to shift from less to more productivity and help to enhance the overall productivity of crops.

STUDY AREA

The Haveri district was formed in the year 1997 by dividing the earlier Dharwad district into Haveri, Gadag and Dharwad districts. The districts encompass an area of 4, 85,156 hectares lying between the latitudinal parallels of 14°19′

M. G. Nayak

North to 15° 09′ North and the longitudes of 75° 01′ East to 75° 50′ East. The district is administratively divided into two sub-division with seven taluks. Shiggaon, Hangal, Savanur coming under the Savanur sub-division and Haveri, Hirekerur, Byadagi and Ranebennur coming under the Haveri sub-division (Map No:1). The district is bounded on the North by the districts of Dharwad and Gadag, on the South by the districts of Davanagere and Shimoga and West by the district of Uttar Kannada. In the Haveri district, Varada River flows west to east direction about 128 kms on the north-east and southern part and the river Tungabhadra flows in between Haveri, Gadag and Shimoga districts and also the Kumadavathi river flows in rainy season in the study region. The total population in the district is 15,97,668 as per the 2011 census.

OBJECTIVES

The main objectives of this paper are enunciated here:

- to assess the regional variation of irrigation development in 2006-07 and 2016-17.
- to identify the irrigation development disparities (high, medium and low) in the study region.

DATABASE AND METHODOLOGY

The study is synthesized based on the taluk-wise secondary sources of data that has been considered as the smallest unit area for analysis. The data has been collected from various sources like the Department of Economics and Statistics of Haveri District for the year 2006-07 and 2016-17.

By using this data set the regional irrigation development has been calculated by using the composite Z-score method for two different periods i.e. 2006-07 and 2016-17. To identify the disparities assess the irrigation development by using 7 indices has been taken (Table No. 1). In the present study, all the seven indicators of irrigation development are analyzed with the help of the Z-score method (Smith- 1979).

$$Z_{ij} = \frac{X_{ij} - X_i}{\delta X_i}$$

Where:

Z_{ij} - Standardize the value of the variable i in taluka j,

X_{ij} - Actual value of variable i in taluka j,

X_i - Means value of variable i in all the taluks,

δX_i - Standard deviation of variables i in all taluks.

To assess overall taluka-wise levels of agricultural development in the study area based on the results of the standard score by using the weighted aggregated method and obtained the weights of all seven indicators are added and finally find out the taluka-wise composite standard score (CSS) value of each taluka and formula is algebraically expressed as:

$$C.S = \frac{\sum Z_{ij}}{N}$$

Where:

$C.S$ = Composite Score,

$\sum Z_{ij}$ = 'z' score of all variables i in district j, and

N = No. of variables.

All data has been arranged in a standardized manner used zero mean for interpretation purpose. The positive values show a high level of irrigation development and the negative values shown a low level of irrigation development. To measure the irrigation development of the Haveri district are grouped into three categories based on the logical method as high, medium and low (Table No. 2).

IRRIGATION DEVELOPMENT

The disparity of irrigation development indices calculated with the help of the Z score technique by considering the 7 indicators. The obtained results have been grouped into 3 major categories like High, Medium and Low Development regions (Table No. 3).

High Irrigation Development Regions:

During 2006-07, the irrigation development index of Z score values above +0.5 are shown in 2 taluks namely, Hangal (0.6973) and Ranebennur (0.9388). These taluks are located in the North West and South-East part of the study region. Out of the seven indicators, five indicators namely Net cropped area (X_3), net irrigated area (X_4), Percentage Irrigation

M. G. Nayak

intensity (X_5), Total irrigated area (In Sq.km) (X_2) and Percentage Net irrigated areas to the net cropped area (X_6) are highly correlated to the high irrigation development index.

During 2016-17 the high category of irrigation development index recorded in 2 taluks namely, Hangal (1.1053) and Haveri (0.6434) located in North West and Eastern part of the study region. The reason for gaining a high irrigation development score in these taluks are highly supported by the following six indicators Total cropped area (X_1), Total irrigated area (X_2), net irrigated area (X_4), Net cropped area (X_3), Percentage Net irrigated areas to the net cropped area (X_6) and Percentage Irrigation intensity (X_5).

Medium Irrigation Development Regions:

In this development category total of 3 taluks are recorded during 2006-07, they are Shiggaon (-0.4692), Haveri (0.4573) and Hirekerur (-0.4692) which are located in the North-west, North-east and Southern part of the study area. Over a period of time, the number of taluks decreased from 3 (2006-07) to 2 in 2016-17 namely: Ranebennur (0.2954) and Hirekerur (0.0563). The main reason for decreased the irrigation development intensity in these taluks are: the percentage of net irrigated areas to the net cropped area (X_6), percentage irrigation intensity (X_5) and percentage of tube-wells irrigation to the net irrigated area (X_7) are the main reason for decreasing in the intensity of irrigation development.

Low Irrigation Development Regions:

Two taluks fall under the low level of irrigation development during 2006-07 such as Savanur (-0.5293) and Byadagi (-0.7532). The number of taluks in the category of low level of irrigation development increased from 2 (2006-07) to 3 (2016-17) namely, Shiggaon (-0.6858), Savanur (-0.7475) and Byadagi (-0.6673) (Map No. 2). Decreased in the 40 per cent of annual rainfall in these taluks during 2016-17is the main reason for the adverse impact on decreasing the intensity of the following indicators namely total irrigated area (X_2), net irrigated area (X_4), net

cropped area (X_3), percentage net irrigated areas to the net cropped area (X_6) and percentage irrigation intensity (X_5) and percentage of tube-wells irrigation to the net irrigated area (X_7) in the Shiggaon, Savanur and Byadagi.

CONCLUSION

The present study of regional analysis indicates the irrigation development is not uniform in the study area. The study highlights that the Hangal and Haveri taluks are well developed in the present scenario, because of Varada river flows through these region boosting irrigation activities. But the Shiggaon and Ranebennur taluks are decreased their pace of development indices because of the drought-hit in 2016-17 and also the impact of urbanization, that's why they lose their agricultural land. The remaining three taluks namely Savanur, Byadagi and Hirekerur maintain the status for over a decade due to the slow development of irrigation activities compare to Hangal and Haveri region. In the future need to increase the irrigation area and its intensity by proper utilization of the available surface and groundwater resource in the study region and also create awareness among the farmers regarding the benefits for increasing the irrigation activities in agriculture area for local and regional sustainable development.

REFERENCE

[1]Haveri District At A Glance: 2006-07 and 2016-17, Published by Government of Karnataka, Bangalore.

[2]R. Rangaswamy (2016). A Textbook of Agriculture Statistics. New Age International Publishers, New Delhi, India.

[3]Sharma Rajni (2014). Regional Disparities in the Level of Agricultural Development in Aligarh District of Western Uttar Pradesh. International Journal of Scientific and Research Publication, Vol.4, Issue 8, August-2014, pp.1-7.

[4]Singh Satbir and Mehala Vinay (2016). Agricultural Development Level Disparities in the Indian States. International Journal of Agriculture Science, Vol. 8, Issue 62, pp. 3533-3535.

An Efficient and Greener FRET System based on PEG-InP/ZnS QDs and Fluorescent Dyes

M. S. Sannaikar, Shivaraj A. Patil, and S. R. Inamdar*

Laser Spectroscopy Programme, Department of Physics, Karnatak University, Dharwad-580 003, India.

Corresponding author: *him_lax3@yahoo.com*

ARTICLE INFO

ABSTRACT

The present study demonstrates that greener PEG-InP/ZnS QD-dye pairs can be used to design very sensitive chemical/biological sensors. The higher potential of the toxic free QDs-dye nano assembly combination than the typical organic donor–acceptor dye pairs enhances the scope of FRET analysis particularly in biological applications. To the best of our knowledge, this is the first report on FRET from green emitting and toxic free InP/ZnS core shell QDs (546 nm) to fluorescent organic dyes (Crysel Violet and Rhodamine 6G). Steady state and time-resolved spectroscopic studies are used to understand the quenching process. We observed range of critical transfer distances for donor-acceptor pairs designed in the study. Noticed reduction in both the decay time and PL quenching of donor-QDs with increasing acceptor successfully confirms non-radiative energy transfer (FRET) between D-A. Interestingly, FRET pairs constituting InP/ZnS QDs and Rh-6G dyes showed superior results among other studied pairs. Enhanced transfer efficiencies and rates with increasing spectral overlap integral of D-A pairs follows the FRET formalism.

1. Introduction

Traditional fluorophores such as fluorescent dyes have several drawbacks such as photobleaching and high sensitivity to environmental factors. In the era of nanotechnology, fluorescent nanomaterials are emerged as an integrated research field because they offer superior optical properties, Semiconductor quantum dots (QDs) are bright fluorescence emitters with high quantum yields, high molar extinction coefficients, size-dependent tunable emission, and high photostability [1–3]. One often-used strategy towards the development of QD nanosensors is based on fluorescence resonance energy transfer (FRET) with the QDs as the FRET donor. FRET is very appealing for bioanalysis because of its simpleness of building ratiometric fluorescent systems. Fluorescence Resonance Energy Transfer (FRET) is essentially the non-radiative transfer of electronic excitation energy from a donor molecule to the unexcited acceptor molecule, therefore the signature of FRET is quenching of the low energy fluorophore followed by emission from the acceptor fluorophore.

M. S. Sannaikar et al.,

Recently, FRET based sensing has become most effective method for the detection of ions in environment. FRET based sensors have been widely used in metal ion detection [4-6], sensing of the fluorophores [7, 8], Silica, and polymer particles [9, 10].

Colloidal semiconductor nanocrystals, referred as quantum dots (QDs) offer several advantages over organic fluorophores in the FRET studies. Quantum dots have a broader excitation spectra and a narrow, more sharply defined emission peak. Due to these properties, a single light source can be used to excite multicolor quantum dots simultaneously without signal overlap [11, 12]. The brightness of quantum dots compared to organic dyes are 10-20 times brighter [13]. Currently most of the employed core shell semiconductor nanocrsyatals are containing one or more heavy metal like Hg, Pb, Cd, Se, etc. The toxicity of these quantum dots to cells is a major issue. For example, *Hardman et al.,* reported that the coating of quantum dots can be cytotoxic such as mercaptoacetic acid [14]. And *Alivisato et al.,* observed a damaging effect of these QDs on cells becomes visible at concentrations above ~6μM for mercaptoacetic acid and above 30μM for PEG-silica coated quantum dots [15].

Therefore to minimize these aforementioned drawbacks of QDs, progressive research has been underway to produce promising visible emitters such as of type III–V and I–III–VI. particularly, Polyehtylene glycol (PEG) surface modified InP/ZnS core shell QDs have proven to be potential class of QDs which have remarkably minimized the above listed drawbacks of heavy metal based QDs like improved quantum efficiency, enhanced stability, minimised toxicity, more specific binding, minimizing the risk of leaching and improved serum half life of PEG modified particles [16-20]. Thus PEG surface functionalized InP/ZnS QDs have found footprints in biological oriented applications. In the present paper, we have studied the fluorescence resonance energy transfer between the PEG surface modified non toxic InP/ZnS core shell QDs (InP/ZnS-550) as donors and two fluorescent organic dyes Crysel violet and Rhodamine-6G as acceptors. These FRET pairs are designed for the purpose of bio and chemical sensors which will be studied in the near future.

2. Materials and Methods

Colloidal aqueous solution of heavy metal free (HMF) PEG functionalized InP/ZnS QDs of core size 3–4 nm, hydrodynamic size 30–40 nm and surface charge -15mV to -23mV were purchased from Mesolight Inc. (Little Rock, AR, USA) and used without further alteration and organic dyes namely Cresyl violet (CV) and Rhodamine 6G (Rh-6G) were received in powder form from Excitone Chemical Co. Inc. (USA). The optical absorption spectra were recorded using UV–VIS–NIR spectrophotometer (JASCO V670). The fluorescence spectra were measured using a FluoroMax-4 spectrofluorometer (Horiba, JY), with the excitation wavelength of 300 nm. Fluorescence decay lifetime measurements of the FRET samples were carried out using time correlated single photon counting technique (TCSPC) and decay profiles were fitted by using DAS6 fitting software. Our investigations are, in particular, directed towards the possible effect of fluorescence resonance energy transfer of QDs and organic dyes.

3. Quantitative analysis of FRET

The simplified equation of FRET efficiency is illustrated as follows,

$$E = \frac{R_0^6}{r^6 + R_0^6} \qquad (1)$$

where r is the distance between donors and acceptors, and R_0 is the fluorescent distance of donors and acceptors when the transfer efficiency is 50%. The energy transfer efficiency (E) is inversely proportional to the sixth power of the distance between donors and acceptors. The rate of transfer is about to reach the maximum with the decreasing distance r (less than R_0). From following Eqn. (2) the necessary spectral overlap integral $J(\lambda)$ is estimated by using corrected fluorescence intensity of donor, $F_D(\lambda)$, molar extinction

coefficient of an acceptor, $\varepsilon_A(\lambda)$ and wavelength, λ,

$$J(\lambda) = \int_0^\infty F_D(\lambda)\varepsilon_A(\lambda)\lambda^4 d\lambda \qquad (2)$$

We can estimate the FÖrster distance (R_0) between donor and acceptor in angstrom using Eqn. (3), where n is the refractive index of the medium, κ^2 is orientation factor (2/3 for randomly oriented dipoles) and Q_D quantum yield of the donor.

$$R_0 = 0.211 \times 10^8 (n^{-4}\kappa^2 Q_D J(\lambda))^{\frac{1}{6}} \qquad (3)$$

It is well known that FRET is long-range dipole-dipole interaction phenomena vary inversely as a function of distance (as r^{-6}) between donor and acceptor. And hence donor-acceptor distances (r) for donor-acceptor were evaluated from following Eqn. (4).

$$r = R_0 \left[\frac{1}{E} - 1 \right]^{\frac{1}{6}} \qquad (4)$$

Further, the energy transfer rates (k_T) were approximated from lifetime of donor alone (τ_D), FÖrster distance (R_0) and donor to acceptor distances (r) were determined from equations as given in Eqn. (5).

$$k_T = \frac{1}{\tau_D}\left(\frac{R_0}{r}\right)^6 \qquad (5)$$

4 Results and Discussion

4.1 Steady State Spectral Analysis

Emission spectroscopy is a powerful tool to get detailed information of excited state energies and lifetime of emitting species. Accordingly, for the study of deactivation of excited states such as electron and energy transfer processes, donor–acceptor pair needs to be carefully chosen. In this work we have chosen PEG-InP/ZnS-550(QD-1) as donor and Crysel Violet, Rhodamine-6G as acceptor pair because there is a good spectral overlap between the emission spectra of the donor QD-1 and the absorption spectra of both the acceptors (CV and Rh-6G) as shown in Fig.1. Generally, FRET rates depend strongly on the overlap between donor emission and acceptor

absorption spectra and the spectral overlap is constant for a given donor/acceptor system. Spectral overlap integral values and FÖrster distances for the FRET pairs were determined and listed in Table 1. The absorption spectra of CV and Rh-6G dyes have a peak at 584 nm.
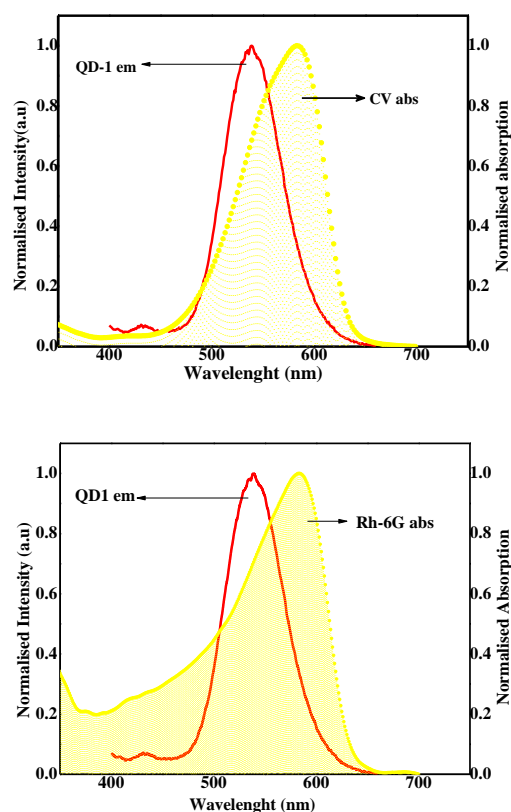
Fig.1: Spectral overlap of FRET pairs.

Fluorescence peak of QD-1 at 540 nm, (Fig.2) reduces with gradual addition of CV and Rh-6G acceptor, reduction in fluorescence intensity of QD-1is observed with noticeable enhancement in the fluorescence intensities of CV and Rh-6G dyes. This reduction in the fluorescence intensities of donor QD-1 resulting in enhancement of fluorescence of both the acceptors CV and Rh-6G as the molar ratio of acceptor dyes to QDs increases. The quenching of QDs emission and simultaneous enhancement in acceptors emission intensities validates and confirms the non-radiative resonance energy transfer from PEG-InP/ZnS-550 to CV and Rh-6G dyes.

M. S. Sannaikar et al.,

QD1 with CV

QD1 with Rh-6G
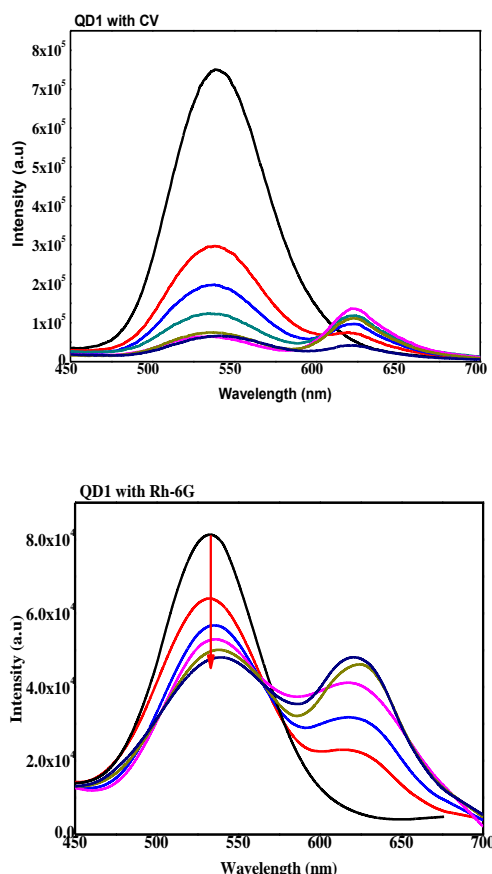
Fig. 2: Typical fluorescence spectra of QD-1 (donors) in absence and presence of acceptor dyes at various concentrations.

**Table 1** Spectral overlap integrals and Förster distances for FRET pairs.

Sample	$J(\lambda)$ $M^{-1}cm^{-1}nm^4$	R_0 in Å
QD1+CV	1.68×10^{16}	74.22
QD1+Rh-6G	8.65×10^{14}	45.27

4.2 Time-Resolved Fluorescence Study

To confirm the energy transfer from semiconducting nanoparticles to dye molecules, time-correlated single-photon counting (TCSPC) study was performed because decay time measurements are more sensitive than PL quenching efficiencies where errors originates from the fluctuations in the lamp intensity. We used pulsed excitation (296 nm) to measure the decay times of these nanoparticles at their maximum PL peak. Fig. 3 shows the time-resolved fluorescence decay curves of PEG-InP/ZnS QDs without and with

CV and Rh-6G dyes. The decay profiles are well fitted with bi and tri-exponential functions,

$$I(t) = R_1 \exp(-t/\tau_1) + R_2 \exp(-t/\tau_2) + R_3 \exp(-t/\tau_3) \quad (6)$$

QD1 with CV

QD1 with Rh-6G
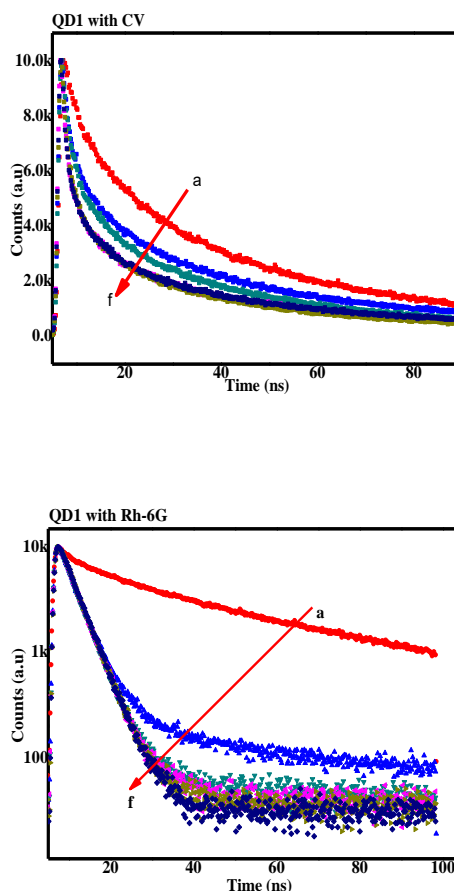
Fig. 3: Time-resolved fluorescence decay curves of PEG-InP/ZnS QDs without and with CV and Rh-6G dyes.

The average decay time 33.42 ns for QD-1 in the absence of acceptor dyes, and the average decay times are shortening upon addition of acceptors dyes (Table 2 (a-b)). It clearly reveals that a significant shortening of the decay time of nanocrystals in the presence of dye which is one of the hallmarks of efficient FRET between donor-acceptor molecules. The reduction in lifetime also heralds the quenching of the QDs emission by the acceptor dye molecule. The decrease in lifetime further confirms the non radiative resonance energy transfer from PEG-InP/ZnS nanoparticles to CV and Rh-6G dyes.

4.3 Energy Transfer Efficiencies and Transfer Rate

M. S. Sannaikar et al.,

After establishing the occurrence of the dynamic quenching in the PEG-InP/ZnS-CV, PEG-InP/ZnS-Rh-6G and system, we have calculated the efficiency of the energy transfer process for FRET pairs. The efficiency of FRET (E) is the fraction of the energy absorbed by the donor that is transferred to the acceptor. Similar to the rate of energy transfer (k_T), E falls off with sixth power of the distance between the donor and acceptor molecules, leading to a large change in its value over the range of 0.5 R_0 to 1.5 R_0. Below 0.5 R_0, energy transfer efficiency remains 98–100%, and there would be not much change to see. Beyond 1.5 R_0, the efficiency of energy transfer is very low. The energy transfer efficiencies (E) obtained for QD1-CV and QD1-Rh-6G FRET determined based on steady state fluorescence measurements are listed in Table 2 (a-b). In addition, the energy transfer efficiencies for the FRET pairs are calculated from measured decay time values of the donor (QDs) in the absence and presence of the acceptor.

Knowledge of R_0 and E determined from both steady state and time resolved measurements for each donor-acceptor pair, helps to find out the distance of separation between donor and acceptor molecule for each FRET pair.

Table 2a: Experimentally calculated FRET parameters for CV and QD-1.

Sample (QD1+CV)	r_s (nm)	r_t (nm)	E_s (%)	E_t (%)	K_s (s^{-1})	K_t (s^{-1})	τ (ns)
QD1+00	---	---	---	---	---	---	33.42
QD1+0.2	9.66	11.2	17.05	7.66	6.15×10^6	2.48×10^6	30.86
QD1+0.4	8.31	10.8	33.70	9.56	1.52×10^7	3.16×10^6	30.22
QD1+0.6	7.02	10.6	58.24	10.38	4.17×10^7	3.44×10^6	29.97
QD1+0.8	6.23	9.46	74.05	18.91	8.54×10^7	6.99×10^6	27.09
QD1+1.0	5.97	9.40	78.63	19.57	1.10×10^8	7.26×10^6	26.90

Table 2b: Experimentally calculated FRET parameters for Rh-6G and QD-1.

Sample (QD1+Rh-6G)	r_s (nm)	r_t (nm)	E_s (%)	E_t (%)	K_s (s^{-1})	K_t (s^{-1})	τ (ns)
QD1+00	---	---	---	---	---	---	33.42
QD1+0.2	5.64	5.86	21.11	17.50	8.01×10^6	6.36×10^6	26.91
QD1+0.4	5.21	5.55	29.98	22.86	1.28×10^7	8.84×10^7	25.8
QD1+0.6	5.03	5.32	34.63	27.63	1.59×10^7	1.14×10^7	24.21
QD1+0.8	4.90	5.20	38.43	30.41	1.87×10^7	1.31×10^7	23.93
QD1+1.0	4.77	5.02	42.23	34.98	2.19×10^7	1.61×10^7	21.74

5 Conclusions

Steady state and time-resolved spectroscopic studies are used to understand the quenching process. Shortening of both the decay time and PL quenching of QDs in the presence of acceptor dye is adequate confirmation of efficient FRET between D-A. We observed that the energy transfer from QDs to dye increases with increasing spectral overlap integral. The estimated energy transfer rates are of the order 10^7 to 10^8 s^{-1}. The FRET pairs constituting InP/ZnS QDs and Rh-6G dyes showed excellent results among other studied pairs. The present study demonstrates that successful construction of toxic free FRET pairs which can

be further utilised in designing chemical/biosensors for in vitro and in vivo studies. And also designed pairs can be used as spectroscopic ruler for biomedical applications. The possibility of their use in biological application is being explored in near future.

5. References

[1]Quantum dots for live cells, in vivo imaging, and diagnostics, X. Michalet, F. F. Pinaud, L. A. Bentolila, J. M. Tsay, S. Doose, J. J. Li, G. Sundaresan, A. M. Wu, S. S. Gambhir, S. Weiss, Science (Wiley), 307, 538 (2005).

[2]Quantum dot bioconjugates for imaging, labelling and sensing, I. L. Medintz, H. T. Uyeda, E. R. Goldman, H. Mattoussi, Nat. Mater (Nature), 4, 435 (2005).

[3]The use of nanocrystals in biological detection, P. Alivisatos, Nat.Biotechnol (Nature). 22, 47 (2004).

[4]J. R Lakowicz, Principles of Fluorescence Spectroscopy (3rd ed.), Springer, New York (2006).

[5]Gold nanorods-based FRET assay for ultrasensitive detection of Hg^{2+}, G. Chen, Y. Jin, L. Wang, J. Deng, and C. Zhang, Chem. Commun. (RSC), 47, 12500 (2011).

[6]FRET-based sensor for imaging chromium(III) in living cells, Z. Zhou, M. Yu, H. Yang, K. Huang, F. Li, T. Yi, and C. Huang, Chem. Commun.(RSC), 29, 3387 (2008).

[7]Molecular Engineering of DNA: Molecular Beacons, K. Wang, Z. Tang, C. J. Yang, Y. Kim, X. Fang, W. Li, Y. Wu, C. D. Medley, Z. Cao, J. Li, P. Colon, H. Lin, and W. Tan, Angew. Chem. (Wiley), 48, 856 (2009).

[8]Gold nanoparticle-fluorophore complexes: sensitive and discerning "noses" for biosystems sensing, U. H. F. Bunz, and V. M. Rotello, Chem. Int. Ed. (Wiley), 49, 3268 (2010).

[9]Ratiometric pH sensor based on mesoporous silicananoparticles and Förster resonance energy transfer, J. Lei, L. Wang, and J. J. Zhang, Chem. Commun. (RSC), 46, 8445 (2010).

[10] Ratiometric Fluorescence Detection of Mercury Ions in Water by Conjugated Polymer Nanoparticles, E. S. Childress, C. A. Roberts, D. Y. Sherwood, C L. M. LeGuyader, E. J. Harbron (ACS), 84, 1235 (2012).

[11] Nanotechnology, nanomedicine, and the development of new, effective therapies for cancer, E.S. Kawasaki, A. Player, Nanomedicine: Nanotechnology, Biology, and Medicine. (Elsevier) 1, 101 (2005).

[12] Quantum dots as cellular probes, A.P. Alivisatos, W. Gu, C. Larabell, Annu. Rev. Biomed. Eng. (Annual Reviews), 7, 55 (2005).

[13] In vivo molecular and cellular imaging with quantum dots, X. Gao, L. Yang, J.A. Petros, F.F. Marshall, J.W. Simons, S. Nie, Current opinion in biotechnology. (Elsevier), 16, 63 (2005).

[14] A toxicologic review of quantum dots: toxicity depends on physicochemical and environmental factors, R. A. Hardman, Environmental Health Perspectives., 114, 165 (2006).

[15] Semiconductor Clusters, Nanocrystals, and Quantum Dots, A.P. Alivisatos, Science. (AAAS), 271, 933 (1996).

[16] Poly(ethylene glycol)-modified nanocarriers for tumor-targeted and intracellular delivery, L. E. Van Vlerken, T. K. Vyas and M. M. Amiji, Pharm. Res. (Springer), 24, 1405 (2007).

[17] Lasing from colloidal InP/ZnS quantum dots, S. Gao, C. Zhang, Y. Liu, H. Su, L. Wei, T. Huang, N. Dellas, S. Shang, S. E. Mohney, J. Wang and J. Xu, Opt. Express, (OSA) 19, 5528 (2011).

[18] Near-infrared fluorescent type II quantum dots for sentinel lymph node mapping, S. Kim, Y. T. Lim, E. G. Soltesz, A. M. De Grand, J. Lee, A. Nakayama, J. A. Parker, T. Mihaljevic, R. G. Laurence, D. M. Dor, L.H.

M. S. Sannaikar et al.,

Cohn and M. G. Bawendi, Nat. Biotechnol. (npg), 22, 93 (2004).

[19] P. Jie, Multifunctional nanoparticles of biodegradable polymers for diagnosis and treatment of cancer, National University of Singapore, 2009.

[20] A fluorescence resonance energy transfer-derived structure of a quantum dot-protein bioconjugate nanoassembly, I. L. Medintz, J. H. Konnert, A. R. Clapp, I. Stanish, M. E. Twigg, H. Mattoussi, J. M. Mauro and J. R. Deschamps, PNAS, 101, 9612 (2004).

Karnatak University Journal of Science
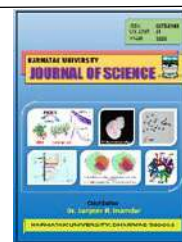
Potential of *Gloriosa superba* extract as a novel oral contraceptive for males: *in vivo* study on Wistar albino rats

Suraj S. Dabire[a] and M. David[a,*]

[a]Environmental Biology and Molecular Toxicology Laboratory, Department of Zoology, Karnatak University, Pavate Nagar, Dharwad – 580 003, India.

***Corresponding author:** davidkcd@gmail.com*

ARTICLE INFO

ABSTRACT

Gloriosa superba, known by its English vernacular glory lily, is a medicinal plant traditionally used for a wide range of therapeutic applications. Tubers and seeds of glory lily are rich in colchicine, an alkaloid known to interfere with microtubule polymerization by binding to tubulin, and thus inhibit cell division. Few reports are available pertaining to the reproductive toxicity of *Gloriosa superba* in female rats but reports on male reproductive toxicity are meagre. The present study was undertaken to establish the role of *Gloriosa superba* extract in regulation of male reproductive capacity. Oral administration of ethanolic *Gloriosa superba* tuber extact (GSTE) at doses 20, 40 and 60 mg/kg body weight was found to alter the normal male reproductive physiology, causing significant reduction in cauda epididymal sperm count, ductal sperm motility, and blood testosterone levels. Morphological abnormalities in sperm samples obtained from cauda epididymis of GSTE-treated animals were increased. Fewer females were impregnated by treated males as compared to control ones, and pregnant females delivered fewer pups which indicated reduced rate of conception after insemination. Parallel analysis of hepatic and renal toxicity of the extract revealed no significant dose-related biochemical and structural alterations in these vital organs, which may be an indication of prospect of *Gloriosa superba* as a source of safe and effective oral contraceptive for males.

1. Introduction

Advances in medical science have resulted in significantly improved public health, decline in mortality, and increased life expectancy. The extraordinary growth of world population has become the most important of all biosocial and medical problems confronting humankind today [1]. Fertility control and regulation has been promoted through several methods of contraception. Steroid-based oral contraceptives have long been the most common and preferred form of contraceptive agents. Though effective, they are accompanied with serious adverse effects and risks [2]. Also, oral contraceptives are currently meant for use only by women, mechanical barriers being the only form of contraception available to males. There is a need for developing suitable products from herbal

sources that could be effectively used in place of synthetic steroidal pills, and to explore the possibility of similar oral contraceptives for males too (the male pill).

From times immemorial, humans have relied on plants and their products for healthcare. A variety of plants and plant-derived substances has been in use for the regulation of fertility since ancient times, and herbal formulations have been documented as remedies for problems related to reproductive health of both males and females [1]. Screening and developing prospective fertility-regulating agents from indigenous herbal sources is an attractive research domain because of their effectiveness, reversible nature, nil to minimum adverse secondary effects, and evident history of their therapeutic use in traditional medicine. Modern research is crucial in establishing the effectivenenss and acceptability of folk remedies in modern medical science. Many authors have previously reported the anti-fertility activities of variety of plants and their different solvent extracts on male reproductive health. These effects include cessation of spermatogenesis, degenereation of seminiferous tubules, regression of Leydig cells, and atrophy of accessory sex organs [3, 4], suppression of sperm count and motility [5], long-term reversible azoospermia [6], structural and functional damage to testis and spermatozoa, and reduction in serum testosterone [7, 8]. The nature of anti-fertility activity has been suggested to be post-testicular in few reports and did not affect libido [5].

Fig. 1. *Gloriosa superba* in its natural habitat (Banavasi, Uttar Kannada, Karnataka)

Gloriosa superba (family Colchicaceae) is a semi-woody herbaceous climber, native of tropical Africa and grows in many parts of tropical Asia including India, Burma, Malaysia and Sri Lanka up to an altitude of 2100 m above mean sea level [9]. It is known as 'Malabar glory lily' and 'flame lily' in English, '*Agnishikha*' in Sanskrit, '*Kalihari*' in Hindi, and '*Gourihoovu/Gourigadde*' in Kannada [10, 11]. It is commercially grown in many parts of southern India (mainly in parts of Tamil Nadu) for its high colchicine content. Both its tuber and seeds have similar medicinal properties [9]. Its beautiful flame-shaped flowers have placed glory lily as an ornamental plant in gardens too [12].

Gloriosa superba finds mention in various traditional systems of medicine and is well-documented for a variety of purposes– from pacifying *kapha* and *vata* to relieving indigestion, inflammation, abdominal pain, fever, arthritis, piles, obstructed labor, and skin disorders [9, 13, 14]. Higher doses of any part of this plant, especially tuber, are highly poisonous and may prove fatal. The tuber is described as pungent, bitter, acrid, heating, anthelmintic, laxative, alexiteric and abortifacient in nature [9, 13]. The alkaloid colchicine from the plant is used in modern medicine for the treatment of gout, rheumatism and cancer. Tribal and rural people largely depend on natural agents for various health-related issues [15, 16]. Indigenous populations in many states across India have been reported to make use of *Gloriosa* tubers (topically or orally) for purposes such as inducing labour, easing childbirth, relieving pain during parturition, inducing abortion at early stages of pregnancy, and expulsion of retained placenta [9, 13, 17-19].

2. Materials and methods

2.1 Plant material and preparation of extract

Tubers of *Gloriosa superba* were purchased from commercial supplier (Sri Murugan Impex, Tiruppur, Tamil Nadu), and authenticated by Dr. K. Kotresha, Associate Professor, Dept. of Botany, Karnatak Science College, Dharwad. A plant specimen collected from Banavasi, Uttar Kannada district, Karnataka was submitted to the herbarium of Dept. of Botany, Karnatak University, Dharwad (Accession No. KUD/Zoo/2020-21/1-3). The tubers were checked for microbial infestation, washed thoroughly under tap water, sliced, and shade-dried for one

Suraj S. Dabire and M. David

week. Dried material was pulverized using electronic grinder, sieved, weighed, and stored in airtight container until extraction.

50 g of tuber powder was extracted with 350 ml of 70% ethanol by hot extraction in Soxhlet apparatus. Obtained extract was filtered using Whatman grade 1 filter paper, evaporated in a rotary evaporator, and dried in laboratory oven at 40 °C [20, 21]. The sticky, semi-solid extract so obtained was stored in refrigerator until further use. Yield was 5.6%
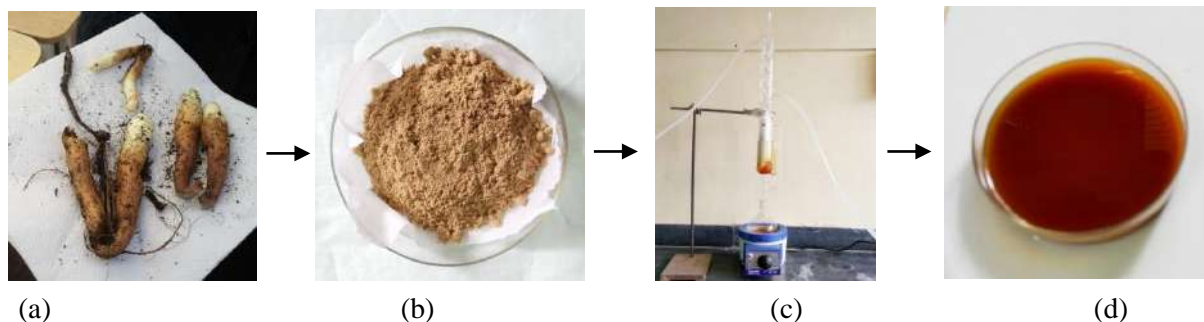

Fig. 2. (a) *Gloriosa superba* tubers, (b) Dried tuber powder, (c) Soxhlet extraction, (d) Crude extract

2.2 Qualitative phytochemical analysis

A small amount of dried extract was reconstituted in 10 ml of ethanol and subjected to chemical tests for the primary analysis of phytochemical groups present in GSTE. The following tests were performed according to the standard protocols: Mayer's test and Wagner's test (alkaloids), ferric chloride test (phenols), Shinoda's test (flavonoids), lead acetate test (tannins), Keller-Kiliani test (cardiac glycosides), Borntrager's test (anthraquinones), foam test (saponins), Benedict's test and iodine test (carbohydrates), biuret test (proteins), Salkowski's test (phytosteroids), and tests for terpenoids and phlobatannin [22-26].

2.3 Procurement and maintenance of animals

Healthy adult male and female albino rats (strain Wistar, age 6-8 months, weight about 300-350 g) were obtained from the animal house facility of Department of Zoology, Karnatak University, Dharwad (No. 639/GO/Re/S/02/CPCSEA). The animals were housed in polypropylene cages containing paddy husk as bedding material, and fed with commercial rat feed (VRK Nutritional Solutions, Sangli) and tap water *ad libitum*. The animals were maintained under 12/12 hours light/dark cycle and temperature 28 ± 2 °C. All the experimental protocols were in accordance with the CPCSEA (New Delhi) guidelines for the care and use of laboratory animals, and approved by the Institutional Animal Ethics Committee (IAEC) of Karnatak University, Dharwad.

2.4 14-day repeated dose oral toxicity

14-day repeated dose oral toxicity testing was done to determine the safe dose of extract (GSTE) as described by [27]. The extract was safe up to dose concentration of 120 mg/kg body weight. However, it caused mild diarrhoea which recovered in 48-72 hours.

2.5 Analysis of anti-fertility potential in males

Rats were randomly divided into four groups of three animals each (n=3). The doses were selected based on the results of 14-day repeated dose oral toxicity study (1/6, 1/3, and ½ of the highest safe dose). The experimental design was as follows: group I received 20 mg/kg b.w. GSTE orally once daily for 56 days (duration of one spermatogenic cycle in ra*t).* Group II and group III received 40 mg/kg and 60 mg/kg GSTE respectively once daily for 56 days. Another group received only vehicle for the same duration and served as control. All the animals were monitored daily before and after dosing for clinical signs of toxicity. Weight gain and feed intake were recorded. 24 hours after the last dose, the animals were weighed and sacrificed by cervical dislocation under inhalation anaesthesia. Autopsy

Suraj S. Dabire and M. David

was performed and testicles, epididymis, and seminal vesicles were dissected out, separated from adherent tissue and weighed to the nearest milligram on an electronic balance.

2.5.1 Sperm count, morphology and motility

Cauda epididymis was selected as the sampling site for assessment of sperm count and sperm morphology according to the protocols described by [28]. Cauda epididymis was weighed and homogenized in 10 ml of PBS, and 1 ml of the resulting sperm suspension was diluted 10 times before counting the spermatozoa. The data was obtained in triplicates for each animal and average was taken. Sperm count was reported as number of sperm per mg cauda epididymal tissue using formula $(0.25 \times N \times 10^6)$/weight of cauda epididymis (in mg), where N = total number of spermatozoa counted in four counting squares of Neubauer chamber.

Sperm morphology was assessed by supravital staining technique and spermatozoa were evaluated for various morphological abnormalities of the head and the tail, as per the criteria described by [29] and [30]. For reporting purpose, the sperm were classified into only two categories – normal and abnormal, and the data reported as percent abnormal spermatozoa = (Number of abnormal spermatozoa × 100)/Total number of spermatozoa

Vas deferens was selected as sampling site for the assessment of sperm motility by diffusion method as described by [28]. A drop of sperm suspension was placed on a Neubauer slide with coverslip and observed under the microscope. The percentage of motile sperm was calculated by the formula = (Number of motile spermatozoa × 100)/Total number of spermatozoa

2.5.2 Male reproductive performance

Eight days prior to the completion of dosage schedule, all the males of all dosage groups were housed with normal, adult females exhibiting normal estrous cycle for mating (1M : 2F) to assess the reproductive capacity and fertility of males. Insemination was confirmed by examining the vaginal smear in the morning hours. After eight days (two estrous cycles) the females were separated, and all the inseminated females were

housed singly and allowed to deliver at term. Litter size and number of live/dead pups were recorded for females that delivered.

2.6 Hormone assay

About 5.0 ml of blood was drawn from each animal immediately following euthanasia by cardiac puncture for assay of testosterone levels. Blood samples were allowed to clot at room temperature for about 30 minutes, and centrifuged at 3000 rpm for 2 minutes to separate the serum. Serum samples were analyzed for the levels of male sex hormone by fully automated bidirectionally interfaced chemiluminescent immuno-assay (CLIA, sensitivity 0.15 ng/ml).

2.7 Histopathological studies

Testes, liver and kidney from each animal were separated from adherent tissue, weighed to the nearest milligram, and fixed in 10% NBF for 48 hours. The organs were processed for histological preparation according to the procedure described by [31].

2.8 Statistical analysis of experimental data

Arithmetic means were calculated for individual data groups obtained from the experiments and results were expressed as mean ± standard error. Results were subjected to one-way analysis of variance (ANOVA) using IBM SPSS Statistics software package (version 21.0). Statistically significant change was considered at p less than 0.05 ($p < 0.05$).

3. Results and discussion
3.1 Qualitative phytochemical analysis

Results obtained from qualitative phytochemical analysis of the extract revealed the presence of alkaloids, phenols, phytosteroids, and saponins as the major components of ethanol extract of *Gloriosa superba* tuber. Moderate presence of flavonoids, glycosides, carbohydrates, and proteins was detected as well while tannins were present in trace amounts. These results are summarized in table 1. Presence of these phytochemicals accounts for the widespread use of flame lily tubers for a variety of purposes in traditional medicine. However, presence of high

Suraj S. Dabire and M. David

amount of alkaloids makes it toxic at the same time. *G. superba* is a major commercial source of colchicine which is widely used in modern medicine for the treatment of gout, Behçet's disease and cancer.

3.2 Health status of the animals during dosage period

No experimental animals showed any serious or long-term clinical manifestations arising from GSTE administration. Body weight gain and food consumption were normal in group I males as compared to control. However, in other two groups, few animals exhibited diarrhoea accompanied by lethargy and reduced food consumption during the initial days of dosing, which was recovered within 2 to 3 days. These animals gained weight more slowly.

Table 1. Qualitative biochemical tests for identification of phytochemical groups in ethanolic GSTE

S. No.	Qualitative test	Presence (+)/absence (-) in ethanolic GSTE
1.	*Tests for alkaloids*: Mayer's test/ Wagner's test	+++ / +++
2.	*Test for phenols*: Ferric chloride test	+++
3.	*Test for flavonoids*: Shinoda's test	++
4.	*Test for tannins*: Lead acetate test	+
5.	*Test for cardiac glycosides*: Keller-Kiliani test	++
6.	*Test for anthraquinones*: Borntrager's test	_
7.	*Test for saponins*: Foam test	+++
8.	*Tests for carbohydrates*: Benedict's test/ Iodine test	++ / +
9.	*Test for proteins*: Biuret test	++
10.	*Tests for phytosteroids*: Salkowski's test	+++
11.	*Test for terpenoids*	_
12.	*Test for phlobatannin*	_

3.3 Sperm parameters (count, morphology, and motility)

Administration of GSTE resulted in significantly reduced cauda epididymal sperm count in all the treatment groups as compared to control in a dose-dependent manner. Similar trend was observed for sperm motility. Proportion of abnormal spermatozoa showing various abnormalities of the head, tail, and neck region was significantly high in GSTE-treated males (table 2). Residual cytoplasm droplets was the most frequently observed sperm abnormality in the experimental animals and this suggests possible interference of the extract with sperm maturation (spermiogenesis). Other frequently observed abnormal morphologies include twisted/coiled tail, amorphous head, and hookless head. This also affected motility, with significant number of sperm exhibiting rotational motion without any net displacement.

Possible anti-fertility efficiency of *Gloriosa superba* in males is very less reported in the literature and nominal data is available regarding its use for the regulation of male fertility. Ethanol extract of *Gloriosa superba* tubers given orally to male gerbils caused significant reduction in sperm count and viability, reduction in the diameter of seminiferous tubules and Leydig cells, and reduction in testosterone levels [32]. In another study, ethanol extract of *Gloriosa superba* bark given orally to male rats at concentrations 100 and 200 mg/kg for 45 days resulted in significant reduction in the weight of seminal vesicles and decrease in sperm count over control in a dose-dependent manner. However, all the effects of the extract were reversible after a recovery period of 30 days [33].

3.4 Male reproductive performance

All the females cohabited with control, group I and group II males were mated (mating here refers to insemination which was confirmed by the

Suraj S. Dabire and M. David

presence of sperm in the vaginal smear). However, one female was not inseminated in group III during the 8 day cohabitation period, which may be due to reduced libido of that particular male. All the inseminated females of control and group I delivered pups at the end of gestation. In groups II and III, only four and three females delivered pups respectively. Also, there was a marked decrease in the number of pups born to the females impregnated by GSTE-treated males of all groups when compared to control. Reduction in litter size exhibited a dose-dependent trend. These results are summarized in table 4. However, the delivered pups were healthy and showed normal growth and development.

revious studies have reported that ethanol extract of *G. superba* bark caused reduction in the ratio of delivered and inseminated females, which means all the cohabited females were inseminated by extract-treated males, but only few females delivered pups. However, there was no significant reduction in litter size of delivered females [33]. The reduction in litter size in present study is in agreement with the altered sperm parameters i.e., reduced sperm count and motility, and increased sperm abnormalities. Reduced count and motility of spermatozoa may ultimately lead to some of the ova released during the reproductive cycle remaining unfertilized while ova fertilized by abnormal spermatozoa may result in spontaneous reabsorption of abnormal embryos during early stages of pregnancy. Litter size is represented as mean ± SE (n= 6), where $p = 0.00015$ (< α) as analysed by one-way ANOVA. Significant change between control and treatment groups has occured.

Table 2. Effect of GSTE on sperm count, motility and morphology.

	Control	Group 1	Group 2	Group 3
Sperm Count (in millions)	0.2419 ± 0.0021	0.2165 ± 0.0056	0.1620 ± 0.0087	0.1370 ± 0.0037
% Motile Spermtozoa	84.33 ± 1.1547	80.67 ± 1.5745	72.33 ± 1.1547	62.33 ± 0.5773
% Abnormal Spermatozoa	14.66 ± 1.5275	19.67 ± 1.5632	28.00 ± 2.8867	36.33 ± 1.1547

All values are represented as mean ± SE (n= 3), where $p = 0.0027$ (< α) as analysed by one-way ANOVA. Significant change between control and treatment groups has occured.

**Table 3.** Effect of GSTE on weight (in grams) of testis and accessory reproductive organs.

	Control	Group 1	Group 2	Group 3
Testis	1.410 ± 0.0435[a]	1.515 ± 0.0256[a]	1.637 ± 0.0321[a]	1.350 ± 0.010[a]
Epididymis	0.457 ± 0.0205[a]	0.468 ± 0.065[a]	0.477 ± 0.0152[a]	0.457 ± 0.0115[a]
Seminal vesicle	0.563 ± 0.02[a]	0.429 ± 0.05[b]	0.383 ± 0.01[c]	0.290 ± 0.07[d]

Table 4. Number of pups delivered by females mated with males of different treatment groups.

	No. of females inseminated/ No. of females cohabited	No. of females delivered/ No. of females inseminated	Mean litter size of delivered females
Control	6/6	6/6	9.33 ± 0.5773
Group I	6/6	6/6	8.33 ± 0.4682
Group II	6/6	4/6	4.66 ± 0.5773
Group III	5/6	3/5	2.66 ± 1.1509

3.5 *Hormone assay*

Serum testosterone levels were significantly reduced in all the three experimental groups over control (396.78 ng/dl) in a dose-dependent manner. The results obtained from testosterone assay are illustrated in figure 3. This suggests that the ethanol extract of *Gloriosa superba* tuber demonstrates significant antiandrogenic activity by suppressing the secretion of testosterone from the interstitial cells of testis.
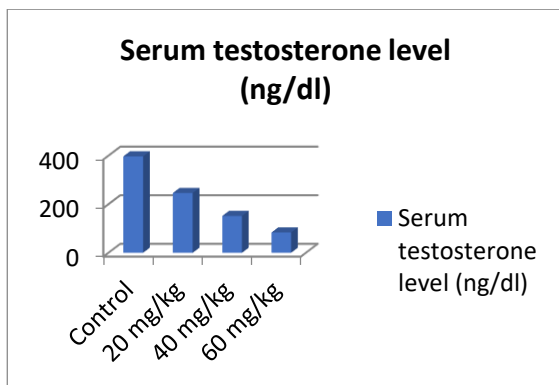

Fig. 3. Serum testosterone levels in control and experimental male rats at the end of dosage period.

3.6 *Histopathological studies*

Histopathological analysis of kidney and liver did not reveal any significant damage or alteration in the histoarchitecture of these vital organs in GSTE-dosed animals. These results were consistent with the results obtained from RFT and LFT, where no treatment-related alterations were observed. However, histoarchitecture of testes was found to be altered by GSTE administration. The interference of the extract with spermatogenesis in seminiferous tubules was evident from histopathological examination of testicular tissue (fig. 4). Active spermatogenesis was evident in tissues from control animals and testicular cells representing all the different stages of spermatogenic cycle were noticeable, whereas tissues from dosed animals showed mild lesions and deterioration of the germinal epithelium. Degeneration of spermatogonial cells was evident as well. These observations were dose dependent and damage was higher at highest dose i.e., 60 mg/kg. Sperm concentration in the lumen of seminiferous tubules appeared to be reduced at high dose.
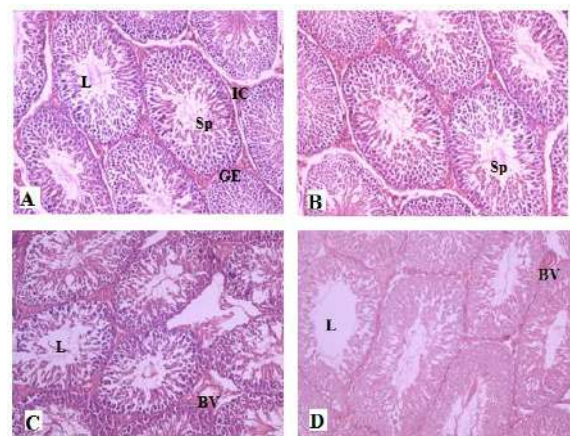
Fig. 4. **A.** TS of Control testis showing seminiferous tubules and interstitium (100x), **B.** TS of testis of group I (20 mg/kg) (100x), **C.** TS of testis of group II (40 mg/kg) (100x), **D.** TS of testis of group III (60 mg/kg) (100x). Legend: L- lumen, Sp- spermatozoa, GE- germinal epithelium, IC- interstitial cell, BV- blood vessel.

4. Conclusion

Suraj S. Dabire and M. David

Ethanol extract of *Gloriosa superba* tuber was found to have significant fertility-suppressing activity in male rats. The extract was safe up to 120 mg/kg concentration when given orally. Three concentrations (20, 40, 60 mg/kg) of the extract were tested for anti-fertility activity and all of them caused significant reduction in the level of male sex hormone testosterone in a dose-dependent manner. Sperm health was affected and sperm concentration was reduced in the cauda epididymis, with increased proportion of morphologically abnormal spermatozoa. This subsequently affected motility too. Fewer female rats were impregnated by treated males as compared to control, and pregnant females delivered fewer pups at term which indicated reduced fertility rate post-insemination. Analysis of hepatic and renal toxicity revealed no significant adverse effects at any of the three test concentrations which may be seen as a sign of safety of the extract and its potential to be developed as a prospective male contraceptive.

Acknowledgement

References

[1]Jain S, Choudhary G P, Jain D K (2015) Medicinal plants with potential anti-fertility activity: a review. International Journal of Green Pharmacy; 9(4): 223-228.

[2]Pradhan D. K., Mishra M. R., Mishra A. et al. (2013) A comprehensive review of plants used as contraceptives. *Int J Pharm Sci Res*; 4(1): 148-155.

[3]Akbarsha M. A., Manivannan B., Hamid K. S., Vijayan B. (1990) Antifertility effect of *Andrographis paniculata* (Nees) in male albino rats. Indian J. Exp. Biol; 28(5): 421-426.

[4]Murugavel T., Akbarsha M. A. (1991) Antispermatogenic effect of *Vinca rosea* Linn. Indian J Exp Biol; 29: 810-812.

[5]Lohiya N. K., Goyal R. B. (1992) Antifertility investigations on the crude chloroform extract of *Carica papaya* Linn. seeds in male albino rats. Indian J Exp Biol; 30: 1051-1055.

[6]Lohiya N. K., Manivannan B., Mishra P. K., *et al.* (2002) Chloroform extract of *Carica papaya* seeds induces long-term reversible azoospermia in langur monkey. Asian J Androl; 4(1): 17-26.

[7]Shaikh P. D., Manivannan B., Pathan K. M., *et al.* (1993) Antispermatic activity of *Azadirachta indica* leaves in albino rats. Current Science; 64(9): 688-89.

[8]Kasturi M., Manivannan B., Ahamed R. N. *et al.* (1995) Changes in epididymal structure and function of albino rat treated with *Azadirachta indica* leaves. Indian J Exp Biol; 33(10): 725-729.

[9]Sonali Jana, G S Shekhawat (2011) Critical review on medicinally potent plant species: *Gloriosa superba*. Fitoterapia; 82: 293–301.

[10] Pulliah T (2002) Medicinal plants in India, Vol. I, Regency Publications, New Delhi. p. 269–70.

[11] Warrier P K, Nambiar V P K, Ramankutty C (1995) Indian Medicinal Plants Vol. 3 (editor Arya Vaidua Sala, Kottakkal), Orient Longman; p.76–81.

[12] Kavithamani D, Umadevi M, Geetha S (2013) A review on *Gloriosa superba* L as a medicinal plant. Indian Journal of Research in Pharmacy and Biotechnology; 1(4): 554-557.

[13] H Badwaik, T K Giri, D K Tripathi et al. (2011) A review on pharmacological profile for phytomedicine known as *Gloriosa superba* Linn. Research J. Pharmacognosy and Phytochemistry; 3(3): 103-107.

[14] Singh V K (1993) Selected Indian folk medicinal claims and their re levance in primary health care programme. Glimpses Plant Res; 10:147–52.

[15] Yadav J. P., Kumar S., Siwach P. (2006) Folk medicine used in gynaecological and other related problems by rural population of Haryana. Indian Journal of Traditional Knowledge; 5(3): 323-326.

[16] Husain N., Chauhan D., Trak T. H. (2017) Some ethno-medicinally important plants from Chattisgarh, India, with caution stigma in reference to their abortifacient activity. Int J Sci Res; 6(7): 2046-2050.

Suraj S. Dabire and M. David

[17] Prakash J W, Anpin Raja R D, Anderson N A et al. (2008) Ethnomedicinal plants used by Kani tribes of Agasthiyarmalai biosphere reserve southern Western Ghats. India J Trad Knowl; 7(3): 410–3.

[18] Augustine J, Sreejesh K R, Bijeshmon P P (2010) Ethnogynecological uses of plants prevalent among the tribes of Periyar tiger reserve, Western Ghats. India J Trad Knowl; 9(1):73–6.

[19] Mali R G, Hundiwale J C, Gavit R S et al. (2006) Herbal abortifacients used in North Maharashtra. Nat Prod Radia; 5:315–8.

[20] Mariappan Senthilkumar (2013) Phytochemical Screening of *Gloriosa superba* L.- from different Geographical Positions. International Journal of Scientific and Research Publications; 3(1): 1-5.

[21] G. Ragupathi (2016) Phytochemical and antioxidant screening of *Gloriosa superba* L. from different geographical positions of south India. International journal of botany studies; 1(4): 13-19.

[22] Rahman Gul, Syed Umer Jan, Syed Faridullah et al. (2017) Preliminary phytochemical screening, quantitative analysis of alkaloids, and antioxidant activity of crude plant extracts from *Ephedra intermedia* indigenous to Balochistan. Hindawi: The Scientific World Journal; 1-7. https://doi.org/10.1155/2017/5873648

[23] Rufai Y, Isah Y, Isyaka M S (2016) Comparative phyto-constituents analysis from the root bark and root core extractives of *Cassia ferruginea* (Schrad D. C) plant. Sch J Agric Vet Sci; 3(4): 275-283. doi: 10.21276/sjavs.2016.3.4.1

[24] H O Edeoga, D E Okwu, B O Mbaebie (2005) Phytochemical constituents of some Nigerian medicinal plants. African Journal of Biotechnology; 4(7): 685-688.

[25] M A Mir, S S Sawhney, M M S Jassal (2013) Qualitative and quantitative analysis of phytochemicals of *Taraxacum officinale*.

Wudpecker Journal of Pharmacy and Pharmocology; 2(1): 1-5.

[26] Chandrashekar K, Santanu S, Prasanna K (2010) Phytochemical studies of aerial parts of the plant *Leucas lavandulifolia*. Der Pharma Chemica; 2(5): 434-437.

[27] Jun-Won Yun, Euna Kwon, Yun-Soon Kim *et. al* (2018) Assessment of acute, 14-day, and 13-week repeated oral dose toxicity of *Tiglium* seed extract in rats. BMC Complementary and Alternative Medicine, 18:251.

[28] Jennifer Seed, Robert E. Chapin, Eric D. Clegg et al. (1996) Methods for assessing sperm motility, morphology, and counts in the rat, rabbit, and dog: a consensus report. Reproductive Toxicology; 10(3): 237-244.

[29] Filler R. (1993) Methods for evaluation of rat epididymal sperm morphology. In Heindel J. & Chapin R. E. (editors) Male Reproductive Toxicology, Part A. Academic Press; New York. 334-343.

[30] Wyrobek A. J. and Bruce W. R. (1975) Chemical induction of sperm abnormalities in mice. Proc. Nat. Acad. Sci. USA; 72(11): 4425-4429.

[31] Humason G. L. (1972) Animal tissue techniques. 3rd Edition, W. H. Freeman and Company, San Francisco.

[32] Dixit V P, Joshi S, Kumar A (1983) Possible antispermatogenic activity of *Gloriosa superba* (ETOH extract) in male gerbil (*Meriones hurrianae* Jerdon): a preliminary study. Comp physiol ecol, 8:17-22.

[33] Gupta H, Sharma D K, Maheshwari K K (2018) Reversible germ cell toxicity of ethanolic extract of *Gloriosa superba* in male rats. International journal of current advanced research, 7(1G):9215-9217.

Karnatak University Journal of Science

ij-Generalized δb-Closed Sets

J.B.Toranagatti

Department of Mathematics, Karnatak University's, Karnatak College, Dharwad-580 001,Karnataka State, India.

Corresponding author: jagadeeshbt2000@gmail.com

ARTICLE INFO

ABSTRACT

In this paper, a new class of ij-generalized closed sets in bitopological spaces called ij-generalized δb-closed sets, is defined and its properties are studied and investigated. Finally, we defined and obtained the characterizations of ij-gδb-continuous functions.

1. Introduction:

The triple (X,τ_1,τ_2) where X is a set and τ_1 and τ_2 are topologies on X is called a bitopological space (briefly, BTS) and Kelly [7] initiated the study of such spaces. In 1985, Fukutake [6] introduced the notion of g-closed set in bitopological spaces and after that several authors turned their attention towards generalizations of various concepts of topology by considering bitopological spaces. Recently, Raman [9] introduced and studied the notion of ij-gb-closed set as a generalization of ij-g-closed set.

The purpose of this paper is to introduce the concepts of ij-gδb-closed set and ij-gδb-continuity for bitopological spaces and investigate some of their properties.

2. Preliminaries

Let us recall the following definitions which are useful in the sequel:

Definition 2.1 A subset A of a bitopological space (X,τ_1,τ_2) is called,

(i) ij-semi-open[3] if $A \subseteq i\text{-cl}(j\text{-int}(A))$.

(ii) ij-pre-open[8] if $A \subseteq i\text{-int}(j\text{-cl}(A))$.

(iii) ij-b-open[1] if $A \subseteq i\text{-cl}(j\text{-int}(A)) \cup j\text{-int}(i\text{-cl}(A))$.

(iv) ij-regular open[10] if $A = i\text{-int}(j\text{-cl}(A))$.

The complement of an ij-semiopen (resp. ij-pre-open, ij-b-open, and ij-regular open) subset of (X,τ_1,τ_2) is called an ij-semiclosed(resp.,ij-pre-closed,ij-b-closed, and ij-regular closed) subset of (X,τ_1,τ_2).

Definition 2.2 [1,3,8] For any BTS (X,τ_1,τ_2) and $A \subseteq X$, the ij-semi closure,

ij-b closure and i-closure of A are denoted and defined as follows:

(1) $scl_{ij}(A) = \cap \{F \subseteq X : F \in ij\text{-}SC(X), A \subseteq F\}$;

(2) $bcl_{ij}(A) = \cap \{F \subseteq X : F \in ij\text{-}BC(X), A \subseteq F\}$;

(3) $cl_i(A) = \cap \{F \subseteq X : F \in i\text{-}C(X), A \subseteq F\}$.

Definition 2.3 [2] A subset A of a BTS (X,τ_1,τ_2) is called ij-δ-closed if A=ij-cl_δ(A) where

ij-cl_δ(A)={$x \in X$:$int_i(cl_j(U)) \cap A \neq \phi, U \in \tau_i$, $x \in U$}

Definition 2.4 A subset A of a BTS (X,τ_1,τ_2) is called,

(i) ij-g-closed [6] if $cl_j(A) \subseteq G$ whenever $A \subseteq G$ and $G \in \tau_i$.

(ii) ij-gb-closed [9] if $bcl_{ji}(A) \subseteq G$ whenever $A \subseteq G$ and $G \in \tau_i$.

(iii) ij-rg-closed [5] if $cl_j(A) \subseteq G$ whenever $A \subseteq G$ and $G \in ij\text{-}RO(X)$.

(iv) ij-gbr-closed [9] if $bcl_{ji}(A) \subseteq G$ whenever $A \subseteq G$ and $G \in ij\text{-}RO(X)$.

(iv) ij-gδs-closed [4] if $scl_{ji}(A) \subseteq G$ whenever $A \subseteq G$ and $G \in ij\text{-}\delta O(X)$.

The complements of the above mentioned closed sets are their respective open sets.

3. ij-Generalized δb-Closed Sets.

Definition 3.1 Let (i, j) ∈ {1,2} where i≠ j. A subset M of a BTS (X,τ_1,τ_2) is said to be:

(1) ij-generalized δb-closed (briefly, ij-gδb-closed) if $M \subseteq G, G \in ij\text{-}\delta O(X) \Rightarrow bcl_{ji}(M) \subseteq G$.

(2) ij-generalized δ-closed (briefly, ij-gδ-closed) if $M \subseteq G, G \in ij\text{-}\delta O(X) \Rightarrow cl_j(M) \subseteq G$.

The family of all ij-gδb-closed(resp.,ij-gδ-closed) subsets of a BTS (X,τ_1,τ_2) will be as always denoted by ij-GδBC(X)(resp., ij-GδC(X)).

Example 3.2 Consider X={a,b,c,d} with topologies
τ_1={X,φ,{a},{b},{a,b},{a,c},{a,b,c}} and
τ_2 ={X,φ,{a},{b},{a,b},{a,b,c}}.Then

12-GδBC(X)={X, φ, {a},{b},{c},{d},{a,c},{a,d},{b,c},{b,d},{c,d},{a,b,d},{a,c,d},{b,c,d}}.

Remark 3.3 The following diagram holds for any subset M of a BTS (X,τ_1,τ_2) :

j-C(X) $\dashrightarrow$ ij-GC(X) $\dashrightarrow$ ij-GδC(X) $\dashrightarrow$ ij-RGC(X).

$\downarrow$ $\qquad$ $\downarrow$ $\qquad$ $\downarrow$ $\qquad$ $\downarrow$

ji-BC(X)$\dashrightarrow$ij-GBC(X)$\dashrightarrow$ij-GδBC(X)$\dashrightarrow$ij-GBRC(X)
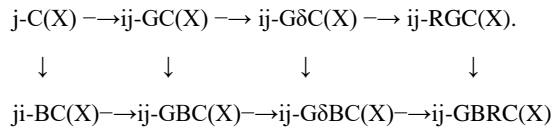
None of these implications are reversible as shown in the following example.

Example 3.4 Consider (X,τ_1,τ_2) as in Example 3.2 .Then

(1) {a}∈ 12-GδBC(X) but {a}∉ 12-GBC(X)∩12-GδC(X)

(2) {a,b}}∈ 12-GBRC(X) but {a,b}∉ 12-GδBC(X).

Theorem 3.5 For any BTS (X,τ_1,τ_2), M⊆X, the following are holds:

(1) If M∈ ij-GδBC(X)∩ij-δO(X), then M∈ ji-BC(X).

(2) If M∈ ij-GδBC(X) and τ_i=ij-δO(X), then M∈ij-GBC(X).

(3) If M∈ ij-GδBC(X) and j-C(X)=ji-BC(X), then M∈ij-GδC(X).

(4) If M∈ ij-GBRC(X) and ij-RO(X)=ij-δO(X), then M∈ij-GδBC(X).

Proof: Obvious

Theorem 3.6 If M ∈ ij-GδBC(X) and M ⊆ N ⊆ bcl_{ji}(M), then N ∈ ij-GδBC(X).

Proof: Suppose that M ∈ ij-GδBC(X) and M ⊆ N ⊆ bcl_{ji}(M). Let N ⊆ U and U∈ij-δO(X). Since M ⊆ N and N ⊆ U, we have M ⊆ U then bcl_{ji}(M))⊆ U as M ∈ ij-GδBC(X).

Now N ⊆ bcl_{ji}(M) which implies bcl_{ji}(N) ⊆ bclji(bcl_{ji}(M)) ⊆ bcl_{ji}(M) ⊆ U.

Therefore N ∈ ij-GδBC(X).

Theorem 3.7 If M∈ ij-GδBC(X), then bcl_{ji}(M)-M contains no non empty ij-δ-closed set.

Proof: Let M be a ij-gδb-closed set and O be a ij-δ-closed set in X such that

O⊆bcl$_{ji}$(M)-M,then O⊆bcl$_{ji}$(M) and O⊆X-M implies M⊆X-O. Since M ∈ ij-GδBC(X),

we have bcl$_{ji}$(M)⊆O^c and thus O⊆bcl$_{ji}$(M)∩(X-bcl$_{ji}$(M))=φ.

The converse of the above theorem need not be true as seen from the following example

Example 3.8 In Example 3.2, let M={a} then bcl$_{12}$(M)-M ={c} does not contain any non empty 21-δ-closed set but M ∉ 21-GδBC(X).

Corollary 3.9 If M is ij-gδb-closed in $(X,τ_1,τ_2)$ then M is ji-b-closed if and only if bcl$_{ji}$(M)-M is ij-δ-closed.

Proof: Let M be ji-b-closed then bcl$_{ji}$(M)=M.That is,bcl$_{ji}$(M)-M=φ which is ij-δ-closed.

Conversely, let bcl$_{ji}$(M)-M is ij-δ-closed then by Theorem 3.7, bcl$_{ji}$(M)-M=φ,as

M∈ij-GδC(X).Therefore M is ji-b-closed .

Theorem 3.10 If A is ij-gδb-closed and A⊆B⊆bcl$_{ji}$(A),then B is ij-gδb- closed.

Proof: Let G be a ij-δ-open set in X such that B⊆G,then A⊆G. Since A

is ij-gδb-closed,then bcl$_{ji}$(A)⊆ G. Now, bcl$_{ji}$(B)⊆bcl$_{ji}$(bcl$_{ji}$(A))=bcl$_{ji}$(A)⊆G.

Therefore bcl$_{ji}$(B)⊆G. Hence B is ij-gδb-closed.

The converse of the above theorem need not be true as seen from the following example

Example 3.11 Consider $(X,τ_1,τ_2)$ as in Example 3.2. Let A={a,b} and B={a,b,d},then A⊆B⊆bcl$_{21}$(A) and B is ij-gδb-closed but A ∉ 12-GδBC(X).

Theorem 3.12 Let A⊆Y⊆X and suppose A is ij-gδb-closed in X ,then A is ij-gδb-closed relative to Y.

Proof: Let A⊆Y∩G,where G is ij-δ-open in X. Since A is ij-gδb-closed in X and A⊆G,

then bcl$_{ji}$(A)⊆G. This impels that Y∩bcl$_{ji}$(A)⊆Y∩G. Thus A is ij-gδb-closed relative to Y.

Theorem 3.13 [9] If j-D(A)⊆ij-D$_b$(A) where ij-D$_b$(A) denotes ij-b-derived set of A

then bcl$_{ij}$(A∪B)= bcl$_{ij}$(A)∪ bcl$_{ij}$(B) .

Theorem 3.14 If A and B are ij-gδb-closed sets such that i-D(A)⊆ji-D$_b$(A) and

i-D(B)⊆ji-D$_b$(B), then A∪B is ij-gδb-closed.

Proof: It follows from the Theorem 3.13

Remark 3.15 The union of two ij-gδb-closed sets need not be ij-gδb-closed

set in general, as seen from the following example.

Example 3.16 In example 3.2, the subsets {a} and {b} are ij-gδb-closed but their union

{a, b} is not ij-gδb-closed.

Theorem 3.17 For a BTS $(X,τ_1,τ_2)$, the following statements are equivalent:

(i) ij-δO(X)⊆{B⊆X: B is ji-b-closed};

(ii) Every subset of X is ij-gδb-closed.

Proof: (i)→(ii): Let M be any subset of X such that M⊆G where G is

ij-δ-open in X.Then by (i), G is ji-b-closed and hence bcl$_{ji}$(M)⊆G which implies

M is ij-gδb-closed.

(ii)→(i): Let G be a ij-δ-open set in X .Then by(ii), G is ij-gδb-closed and since G⊆G,

then bcl$_{ji}$(G)⊆G but G⊆bcl$_{ji}$(G) is always true. Therefore bcl$_{ji}$(G)=G and hence G is

ji-b-closed.

Theorem 3.18 For a BTS $(X,τ_1,τ_2)$, the following statements are equivalent:

(i) Every ij-gδb-closed set is ij-gδs-closed;

(ii) Every ji-b-closed set is ij-gδs-closed.

Proof: (i)→(ii) :Obvious

(ii)→(i) : Let M be a ij-gδb-closed set in X such that M ⊆ G where G is ij-δ-open in X.

Then $bcl_{ji}(M) \subseteq G$ and since $bclji(M)$ is ji-b-closed, then by (ii), $bcl_{ji}(M)$ is ij-gδs-closed.

So that $scl_{ji}(M) \subseteq scl_{ji}(bclji(M) \subseteq G$. Therefore $scl_{ji}(M) \subseteq G$.

Theorem 3.19 For any p∈X ,the set $\{p\}^c$ is ij-gδb-closed or ij-δ-open.

Proof: Suppose that $\{p\}^c$ is not ij-δ-open,then $\{p\}^c$ will be ij-gδb-closed.As X

is the only ij-δ-open set containing $\{p\}^c$. This implies $bcl_{ji}(X-\{p\}) \subseteq X$.

Hence $\{p\}^c$ is ij-gδb-closed.

Theorem 3.20 If N is ij-gδb-closed,then ij-$cl_\delta\{x\} \cap N \neq \varphi$ for every $x \in bcl_{ji}(N)$.

Proof: Let $x \in bcl_{ji}(N)$.Suppose that ij-$cl_\delta\{x\} \cap N = \varphi$, then $N \subseteq X$-ij-$cl_\delta\{x\}$ and

ij-$cl_\delta\{x\}^c$ is ij-δ-open. Since $N \in$ij-GδC(X), then $bcl_{ji}(N) \subseteq X$-ij-$cl_\delta\{x\}$ so that

$x \notin bcl_{ji}(N)$ which is a contradiction. Therefore ij-$cl_\delta\{x\} \cap N \neq \varphi$.

Definition 3.21 For any BTS (X,τ_1,τ_2) and A ⊆ X, the ij- gδb-closure of A is

denoted and defined as $g\delta bcl_{ij}(A) = \cap \{F \subseteq X : F \in$ ij-GδBC(X), $A \subseteq F\}$.

Theorem 3.22 Let A and B be subsets of a BTS (X,τ_1,τ_2) .Then

(i) $A \subseteq bcl_{ji}(A) \subseteq gbcl_{ij}(A) \subseteq g\delta bcl_{ij}(A)$.

(ii) If A⊆B,then $g\delta bcl_{ij}(A) \subseteq g\delta bcl_{ij}(B)$.

(iii) $g\delta bcl_{ij}(A) \cup g\delta bcl_{ij}(B) \subseteq g\delta bcl_{ij}(A \cup B)$.

(iv) $g\delta bcl_{ij}(A \cap B) \subseteq g\delta bcl_{ij}(A) \cap g\delta bcl_{ij}(B)$.

(v) If A is ij-gδb-closed,then $g\delta bcl_{ij}(A)=A$.

Remark 3.23 The equalities do not hold in results (iii) and(iv) as seen from the following example.

Example 3.24 Consider $(X,\tau_1,\tau_2$) as in Example 3.2

(iii)Let A = {a} and B = {b}.Then

$g\delta bcl_{12}(A)=\{a\}$, $g\delta bcl_{12}(B)=\{b\}$ and $g\delta bcl_{12}(A \cup B)=\{a,b,d\}$. Thus we have $g\delta bcl_{12}(A \cup B)=\{a,b,d\}$

$$\neq \{a,b\} = g\delta bcl_{12}(A) \cup g\delta bcl_{12}(B) .$$

(iv) Let A={a,b} and B={c.d}.Then $g\delta bcl_{12}(A)=\{a,b,d\}$, $g\delta bcl_{12}(B)=\{c,d\}$ and $g\delta bcl_{12}(A \cap B)=\varphi$. Then we have

$g\delta bcl_{12}(A \cap B)=\varphi \neq \{d\} = g\delta bcl_{12}(A) \cap g\delta bcl_{12}(B)$

Definition 3.25 The intersection of all ij-δ-open subsets of X containing M is called the

ij-δ kernel of M and it is denoted by ij-$ker_\delta(M)$.

Theorem 3.26 A is ij-gδb-closed if and only if $bcl_{ji}(A) \subseteq$ij-$ker_\delta(A)$.

Proof: Let A be a ij-gδb-closed set in X such that $x \in bcl_{ji}(A)$. Suppose that

$x \notin$ij-kerδ(A),then there exists a ij-δ-open set G in X such that A⊆G and x∉G.

Since A ∈ ij-GδBC(X), $bcl_{ji}(A) \subseteq G$ implies $x \notin bcl_{ji}(A)$ which is a contradiction.

Conversely,let $bcl_{ji}(A) \subseteq$ij-$ker_\delta(A)$ and G is a ij-δ-open set containing A, then

ij-$ker_\delta(A) \subseteq G$ which implies $bcl_{ji}(A) \subseteq G$ and hence A is ij-gδb-closed.

Definition 3.27 A subset A of a BTS (X,τ_1,τ_2) is called a ij-generalized δb-open

(briefly, ij-gδb-open) set if A^c is ij-gδb-closed.

Theorem 3.28 A subset A of a BTS (X,τ_1,τ_2) is ij-gδb-open if and only

if M ⊆ $bint_{ji}(A)$ whenever M is ij-δ-closed and M ⊆ A.

Proof: Let A be a ij-gδb-open set and suppose M⊆A where M is ij-δ-closed.

Then A^c is a ij-δgb-closed set contained in the ij-δ-open set M^c. Hence

$bcl_{ji}(X-A) \subseteq (X-M)$ which implies X-$bint_{ji}(A) \subseteq X$-M. Thus M⊆$bint_{ji}(A)$.

Conversely, let M⊆ $bint_{ji}(A)$ be true whenever M⊆A and M is ij-δ-closed.

J.B.Toranagatti

Then $X-bint_{ji}(A)\subseteq(X-M)$. That is,$bcl_{ji}(X-A)\subseteq X-M$. Hence X-A is ij-gδb-closed

and A is a ij-gδb-open set.

Theorem 3.29 If A is ij-gδb-open and B is any set in X such that $bint_{ji}(A)\subseteq B\subseteq A$,

then B is ij-gδb-open in X.

Theorem 3.30 If A is ij-gδb-open and B is any set in X such that $bint_{ji}(A)\subseteq B$,

then A∩B is ij-gδb-open in X.

Proof: Let A be a ij-gδb-open set of X and $bint_{ji}(A)\subseteq B$ then $A\cap bint_{ji}(A)\subseteq A\cap B\subseteq A$.

Since $bint_{ji}(A)\subseteq A$,then $bint_{ji}(A)\subseteq A\cap B\subseteq A$ and by Theorem 3.29, A∩B is ij-gδb-open.

Theorem 3.31 Let (X,τ_1,τ_2) be a BTS and $A\subseteq X$.Then $x\in g\delta bcl_{ij}(A)$ if and only if

U ∩ A ≠ φ for every ij-gδb-open set U containing x.

Proof: Let $x\notin g\delta bcl_{ij}(A)$ ↔ there exists a ij-gδb-closed set N containing A such that $x\notin N$

↔ there exists a ij-gδb-open set N^c containing x such that $N^c\cap A=\varphi$.

4. ij-gδb-continuous functions

Definition 4.1 A function f: (Y,τ_1,τ_2) −→(X,η_1,η_2) is said to be G(i,j)-continuous if

$f^{-1}(M)$ is ij-gδb-open in X for each η_i-open set M of Y.

Theorem 4.2 Suppose that ij-GδBC(X) is closed under arbitrary intersections.

Then the following are equivalent for a function f: (X,τ_1,τ_2) −→(Y,η_1,η_2):

(i) f is G(i,j)-continuous;

(ii) for every x ∈ X and each i-open set B of Y containing f(x),there exists an

ij-gδb-open set A in X containing x such that $f(A)\subseteq B$.

(iii) for each x ∈ X and each i-closed set G of Y not containing f(x),there exists

an ij-gδb-closed set H in X not containing x such that $f^{-1}(G)\subseteq H$.

(iv) $f(g\delta bcl_{ij}(A))\subseteq cl_i(f(A))$ each $A\subseteq X$.

(v) $g\delta bcl_{ij}(f^{-1}(B))\subseteq f^{-1}(cl_i(B))$ for each $B\subseteq Y$.

Proof: (i)→(ii) Let B be an i-open set in Y containing f (x),then $x\in f^{-1}(B)$.By

(i), $f^{-1}(B)$ is ij-gδb-open set in X containing x.Let $A=f^{-1}(F)$,then $f(A)=f(f^{-1}(B))\subseteq B$.

(ii)→(i) Let F be any i-open set in Y containing f(x),then $x\in f^{-1}(F)$. By (ii),

there exists ij-gδb-open set G in X containing x such that $f(G)\subseteq F$ which implies

$G\subseteq f^{-1}(F)$. Thus $f^{-1}(F) = \cup\{G : x\in G\}$ which is ij-gδb-open.

Hence $f^{-1}(F)$ is ij-gδb-open set in X.

(ii)→(iii) Let G be any i-closed set of Y not containing f(x). Then Y-G is an

i-open set in Y containing f(x). Then by (ii), there exists

ij-gδb-open set F in X containing x such that $f(F)\subseteq(Y-G)$. This implies

$F\subseteq f^{-1}(Y-G) = X- f^{-1}(G)$.

Hence, $f^{-1}(G)\subseteq(X-F)$. Set H=X-F,then H is ij-gδb-closed set not containing

x in X such that $f^{-1}(G)\subseteq H$.

(iii)→(ii) Let F be any i-open set of Y containing f(x). Then (Y-F) is a i-closed

set in Y not containing f(x). By (iii), there exists ij-gδb-closed set K in X not containing

x such that $f^{-1}(Y-F)\subseteq K$.This implies $(X-K)\subseteq f^{-1}(F)$ That is, $f(X-K)\subseteq F$. Set U=(X-K),

then U is ij-gδb-open set containing x in X such that $f(U)\subseteq F$.

(i)→(iv) Let A be any subset of X. Suppose $y\notin cl_i(f(A))$,then there exists an i-open set F

in Y containing y such that f(A) ∩ F = φ. Hence we have A ∩ $f^{-1}(F) = \varphi$ and

J.B.Toranagatti

$g\delta bcl_{ij}(A) \cap f^{-1}(F) = \varphi$ which implies $f(g\delta bcl_{ij}(A)) \cap F = \varphi$ and hence

$y \notin f(g\delta bcl_{ij}(A))$.Therefore $f(g\delta bcl_{ij}(A)) \subseteq cl_i(f(A))$.

(iv)$\rightarrow$(v)Let $B \subseteq Y$,then $f^{-1}(B) \subseteq X$. By (iv),$f(g\delta bcl_{ij}(f^{-1}(B))) \subseteq cl_i(f(f^{-1}(B))) \subseteq cl_i(B)$.

Thus $g\delta bcl_{ij}(f^{-1}(B)) \subseteq f^{-1}(cl_i(B))$.

(v)$\rightarrow$(i) Let N be any i-closed subset of Y. Then by (v), $g\delta bcl_{ij}(f^{-1}(N) \subseteq f^{-1}(cl_i(N)) = f^{-1}(N)$ and since $f^{-1}(N) \subseteq g\delta bcl_{ij}(f^{-1}(N))$. Hence $g\delta bcl_{ij}(f^{-1}(N)) = f^{-1}(N)$.

Therefore $f^{-1}(N)$ is ij-gδb-closed set in X.

References

[1] T.Al-Hawary and A.Al-Omari, b-open and b-continuity in bitopological spaces, Al-Manarah, 13(3)(2007),89-101.

[2]G.K.Banerjee,On pairwise almost strongly Ɵ-continuous mappings, Bull. Calcutta Math.Soc.79(1987)314-320.

[3]S. Bose, Semi open sets, semi-continuity and semiopen mappings in bitopological spaces, Bull. Calcutta Math. Soc. 73(1981),237-246.

[4]A. Edward Samuel and D. Balan, ij-Generalized delta semi closed sets, Annals of Pure and Applied Mathematics,10(2)(2015), 255-266.

[5] O.A.El-Tantawy, H.M.Abu-Donia, Some bitopological concepts based on the alternative effects of closure and interior operator, Chaos, Solit. Fractals 19 (2004) 1119–1129.

[6]T.Fukutake, On generalized closed sets in bitopological spaces, Bull.. Fukuoka Uni Ed., Part III, 35(1986),19-28.

[7] J.C.Kelly, Bitopological spaces, Proc. London Math. Soc., 13 (1963) 71-89.

[8] S. S. Kumar, On a Decomposition of Pairwise Continuity, Bull. Cal. Math. Soc., 89 (1997), 441–446.

[9] T.C. K. Raman, On generalized b-closed sets in bitopological spaces, Int.J. Sci. Eng. and Tech.,5(2)(2016), 124-127.

[10]A.S.Singal and A.S.Arya,On pairwise almost regular spaces, Glasnik Mat. 6(26), (1971), 335-343.

Lipid peroxidation and anti-oxidant activity in brain and liver during variable stages of Diethylnitrosamine- induced hepatocarcinoma

Hariprasad Shetty[1,2], Monika Sadananda[1]*

[1]Brain Research Laboratory, Biotechnology Unit, Department of Biosciences, Mangalore University, Mangalagangothri 574 199, Karnataka.

[2]Department of Zoology, St. Aloysius College (Autonomous), Mangaluru 575003, Karnataka

Corresponding author: monikasadananda@gmail.com;
monikasadananda@mangaloreuniversity.ac.in

ARTICLE INFO

ABSTRACT

Hepatic carcinoma (HCC) is induced when Diethylnitrosamine (DEN) is metabolized to its active ethyl radical formthatcauses mutations. While single/multiple injections models exist, comparative analysis and the effect on the brain of a peripheral tumor remain to be studied. Here, we aim to observe the effect of single/multiple DEN injectionson brain and liver lipid peroxidation, anti-oxidants and interleukin-4 expression. Towards this, adult male Wistar rats were injected with DEN either once or once each month for three months. Controls received saline. After three months, liver histology and Ki-67 immunohistochemistry were conducted to establish development of HCC. Liver, brain lipid peroxidation (LPO), glutathione, Nitric oxide synthase (NOS) and plasma interleukin-4 levels were assayed. Histological changes were observed in the HCC liver as well as increased density of Ki-67 cells in single- and multiple-dose conditions. Liver LPO was increased in the multiple-dose condition, while brain LPO was not affected. Liver GSH was reduced in both conditions, while brain glutathione was increased in multiple-dose condition. NOSactivity was significantly increased in both single and multiple dose conditions. Plasma interleukin-4 levels were variably affected. LPO process manifests free-radical-based membrane damage and indicates altered homoeostasis. GSH blocks LPO formation, with the latter leading to depletion of GSH as observed here in HCC. NOS, which may be neuronal or inducible produces reactive nitrogen species leading to nitrosative stress and neuroinflammation. Thus, brain oxidative/nitrosative mechanisms are affected in HCC, and though the time point and turnover are unknown, the implications are detrimental to post-mitotic neurons.

Hariprasad Shetty and Monika Sadananda

1. Introduction

The liver and the brain interact towards supply of nutrients, removal of detrimental toxic substances including those generated in the brain and detrimental to post-mitotic neurons, such that liver malfunction could cause brain dysfunction [1]. Hepatic carcinoma (HCC), caused by hepatitis B/C viral infections, alcohol consumption and other liver disorders is ranked sixth in occurrence and fourth in death rate [2]. HCC is strongly correlated with immunosuppression, excessive release of pro-inflammatory cytokines with chronic inflammation increasing the progress of HCC [3].

Although causes of HCC are known, the molecular pathogenesis is still being unraveled. Primary hepatic cancers are of two main types: HCC derived from hepatocytes, and cholangiocarcinoma [4]. Different growth patterns are observed, while some spread tentacle-like growths throughout the liver, others develop into single tumors that spread to other parts of the liver or develop nodules. Triggers include colour fixatives, flavoring agents, nitrate and nitrite compounds added to meat and fish, whose intake in the presence of primary amines and gastric juices, forms nitroso compounds [4]. Use of tobacco, pharmaceutical products and agricultural chemicals also trigger preformation of nitrosoamines [5] by using multistep processes to thwart the cell cycle and develop into carcinomas [6].

One of the laboratory models for HCC is chemically induced by diethylnitrosamine (DEN) which results in liver damage manifested in histopathological and dysfunctional profiles. DEN undergoes metabolismto anactive ethyl radical form, [4,6] that interacts with DNA inducing mutations [7] and results in free radical generation ofreactive oxygen species (ROS), nitrogen species (NOS)etc, leading to oxidative stress and ensuing cell injuries [8-10]. Nitrosamines such as DEN have been shown to have diverse effects based on genetic background, sex and age [11]. As histopathological similarities of rodent liver tumors on DEN administration are comparable to human HCC [12], it is suitable to study chemical-induced HCC in experimental Wistar rats, but whether a single dose suffices to manifest the histopathology and altered physiology of HCC or whether multiple doses are required is still debated.

The harmful effects of ROS and RNS (RONS) induce lipid peroxidation (LPO), which is the manifestation of free radical based membrane damage produced by downstream fission molecules and endocyclization of fatty acids, is balanced by antioxidantGlutathione (GSH) and peroxidase [13]. Despite the activity of antioxidants, RONS have been implicated in neuronal cell damage and ensuing neurodegenerative disorders [14]. Besides mediating oxidative stress, ROS are also involved in immune regulation during tumor development and suppression of immune system. Specifically, ROS induce increase of IL-4 cytokine release by T_2 helper cells [15, 16]. And are involved in the development of inflammation with IL-13 with which IL-4 shares receptors [17].

In a neoplasm, there are cells in active phases of the cell cycle and resting cells, so Ki-67 expression was used as a marker [18-20] to indicate high rate of mitosis as its expression is more profound as HCC progresses temporally [20-22]. Ki-67 has been shown to be significantly higher in the non-malignant liver tissue with cirrhosis and hepatic cancer as compared with cirrhotic hepatic cancer [23]. Therefore, in the present study, an attempt has been made to study liver and brain enzyme activity in response to single vs. multiple doses of DEN in a Wistar rat model of HCC. Lipid peroxidation or membrane damage was assessed, and antioxidant activity assayed in liver and brain.

2. Materials and Methods
2.1 Animals and Treatment

Young adult male Wistar rats (100–160 g) were housed in polypropylene cages in groups of three, under standard laboratory conditions with food and water *ad libitum* (ambient

Hariprasad Shetty and Monika Sadananda

temperature of 24±2°C; 12-h: 12-h light/dark cycle). All animal experiments were conducted in accordance with the ethical regulations for animal care, use and experimentation laid by CPCSEA and cleared by the Institutional Animal Ethics Committee (SAC/IAEC/118/2012, 18/09/2012).

2.2 Administration of DEN

The rats were randomly divided into four groups of n=8 each. Diethylnitrosomine (DEN, Sigma) was dissolved in saline and administered at a dosage of 200mg/kg b.w.ip, either once (Single) and once per month for three months (Multiple). The control groups were administered vehicle.

2.3 Brain and liver tissue harvesting

After three months, rats were sacrificed; brain and liver were harvested, blood plasma was collected and frozen in liquid nitrogen and stored in -80°C deep freezer for further analysis.

2.4 Liver histology

A portion of the liver was cut into two to three pieces of approximately 6mm^3 size and fixed in phosphate buffered 10% formaldehyde solution. After embedding in paraffin wax, thin sections of 5μm thickness of liver tissues were cut and stained with haematoxylin-eosin.

2.5 Ki-67 Immunohistochemistry

Frozen liver samples were sectioned on a cryostat (Leica CM 1510S) and mounted on gelatine-coated slides. Sections were fixed in 10% methanol and incubated in 3% hydrogen peroxide. Sections were then incubated in primary antibody i.e. Ki-67 (H-300, Santacruz Biotechnology) overnight, incubated with biotinylated secondary antibody (anti-Goat IgG, made in Rabbit; Vectastain PK-6101, Vector laboratories) and incubated in Vectastain A-B complex before being immersed in Diaminobenzidine hydrochloride (DAB, Sigma) with 3% hydrogen peroxide in Tris-PBS. All the above steps were carried out with intermittent washing in 0.01M Phosphate buffered saline (PBS; pH 7.4). Sections were dehydrated in alcohol series, cleared in Xylene and coverslipped.

2.6 Microscopy

Sections were observed, and photomicrographs taken using LAS software and camera connected to a Leica DM2500 microscope. For quantitative analysis, the central vein of each liver section was located at the center of the visual field and darkly stained hepatocytes with immuno-positive nuclei were counted in an area of 160x120um. The average of ten measures of each liver tissue sample was taken for statistical analysis.

2.7Assays

Lipid Peroxidation (LPO) was measured [24] by estimating the formation of Thio-barbituric acid reactive substances (TBARS). Briefly, brain and liver tissues were homogenized in 0.25M sucrose and centrifuged at high speed for 5 minutes. To 1 ml of supernatant, 1.5ml of 20% TCA and 2.5ml of 0.67% TBA were added, boiled for 30 minutes and cooled, after which 2ml of butanol was added, then centrifuged again as above. The top layer formed was read at absorption maxima of 535nm.

Gluthathione (GSH) was assayed in liver and brain with modifications after Ellman. [25] Briefly, 0.2g of tissue was homogenized in 1:1 ratio of 10% TCA and 10mM EDTA, centrifuged at 4ºC at high speed for 15 min. To 200μl of the supernatant, 3ml of 0.2M Tris HCl and 50μl of 10mM DTNB dissolved in 1% Sodium citrate were added and incubated for 10 min at room temperature. Absorbance was read at 412nm and content expressed as μg/mg protein.

Brain tissue was homogenized in 50mM Tris HCl Buffer (pH 7.4) containing 2mM EDTA and centrifuged at high speed for 15min at 4°C and assayed for NADPH Diaphorase (nNOS) activity [26] Briefly, the reaction mixture which contained the supernatant, EDTA (5mM), NBT (0.5mM), NADPH (0.5mM) in 50mM Tris Buffer (pH 7.4) was incubated for 15min at 37°C and the colour developed was read at 585nm (Molar Extinction Coefficient of NBT is 16,000m/cm).

Total protein estimation of the liver and brain samples used for enzyme assays and

oxidative stress-related measures was carried out [27] using BSA as standard. UV-Vis spectrophotometer (Spectro 105, Systronics) was used for all the above enzyme assays.
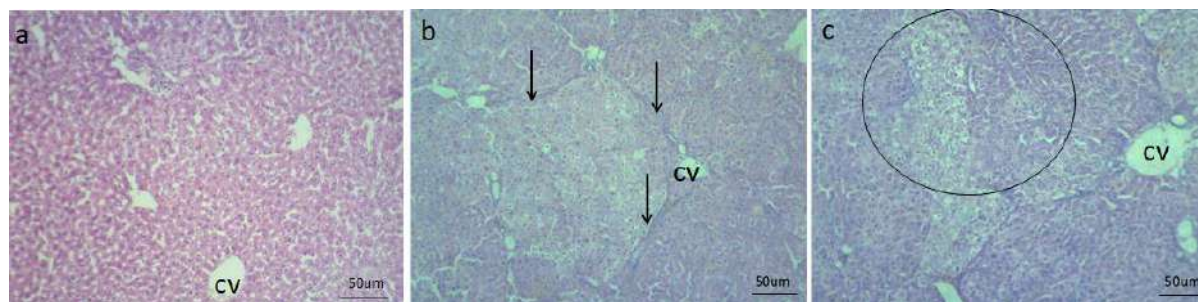
2.8 Plasma IL-4

The plasma was assayed for IL-4 using an ELISA kit (RayBio® Rat IL-4, ELR-IL-4). Standards ranged from 0.66-160pg. The minimum detectable dose of rat IL-4 was determined to be 1.5pg/ml. Absorbance was read at 450 nm using Thermo Scientific Multiskan GO.

2.9 Statistical analysis

All data were represented as mean ± SEM. A two-way ANOVA for single vs. multiple doses of DEN was used. Post-hoc Bonferroni tests were carried out to obtain significant differences between groups. Significance was set at $p < 0.05$.

3. Results

Two of the single dose animalsand four multiple dose animalsdid not survive for three months. Histological examination of liver sections of controls revealed normal architecture of cells with granulated cytoplasm and uniform nuclei. No effect was observed on the portal triad and mild peripheral steatosis.Single DEN dose induced loss of architectural, nodular hyperplasia with ballooning degeneration and bridging fibrosis as well as congested and dilated sinusoids. Pigment ingestion was also seen with bile pigment ingested by macrophages. Multiple doses of DEN induced a further loss of architecture with ballooning degeneration. Karyomegaly, hyperplasia, binary radical proliferation, patchy ballooning degeneration and ingestion of pigment could be seen, besides Kupffer cell hyperplasia with karyomegaly (fig.1).

Figure 1 Histology of liver tissue on DEN treatment: Control liver (a) Single dose DEN showing nodular hyperplasia (arrows) (b) Multiple dose DEN showed nodular hyperplasia with patchy ballooning degeneration (circled) (c). CV: Central Vein

Excessive tissue damage during immunohistochemistry did not enable good photomicrographs. However, immunopositive cells could be identified and quantified. Single dose DEN HCC liver depicted 84.80 ± 4.36 Ki-67 +ve cells vs. 57.50 ± 3.10 in vehicular controls. Multiple doses of DEN induced Ki-67 expression with 177.2 ± 11.88 +ve cells as compared to 59.90 ± 3.76 of vehicular controls. Two-way ANOVA for K-67+ve immune reactivity indicated an effect of DEN $F_{(1, 36)} = 113.69$; $p < 0.0001$), effect of the dose ($F_{(1, 36)} = 48.86$; $p < 0.0001$) and DEN x dose interaction ($F_{(1, 36)} = 44.04$; $p < 0.0001$). Post test results indicated that Ki-67 expression in the multiple

dose group was significantly higher ($p < 0.001$) than in the single dose group.

There was a significant effect of DEN ($F_{(1, 16)} = 117.45$; $p < 0.0001$) on liver MDA levels (Fig 2a), a significant effect also of dose ($F_{(1, 16)} = 174.80$; $p < 0.0001$) with significant DEN x dose interaction ($F_{(1, 16)} = 147.80$; $p < 0.0001$). Post tests revealed that DEN induced a significant increase in liver MDA levels in multiple dose group as compared to Controls ($p < 0.001$) and as compared to single dose group ($p < 0.001$).

A significant effect of DEN was observed ($F_{(1, 18)} = 275.90$; $p < 0.0001$) on liver GSH levels (Fig 2b) though there was no effect of the dose ($F_{(1, 18)} = 2.59$; $p > 0.05$; DEN x dose

interaction ($F_{(1, 18)} = 2.23$; $p > 0.05$). Post tests revealed significant differences at both doses tested between both Controls and DEN-treated groups ($p < 0.001$).

There was no effect of DEN ($F_{(1, 18)} = 0.12$; $p > 0.05$) on plasma IL-4 levels.

Significant differences however emerged in single vs. multiple dosage conditions with an increase in the latter ($F_{(1, 18)} = 40.23$; $p < 0.0001$). Due to significant DEN x dosage interaction ($F_{(1, 18)} = 10.71$; $p < 0.01$; fig 2c), post hoc tests did not reveal any group differences.
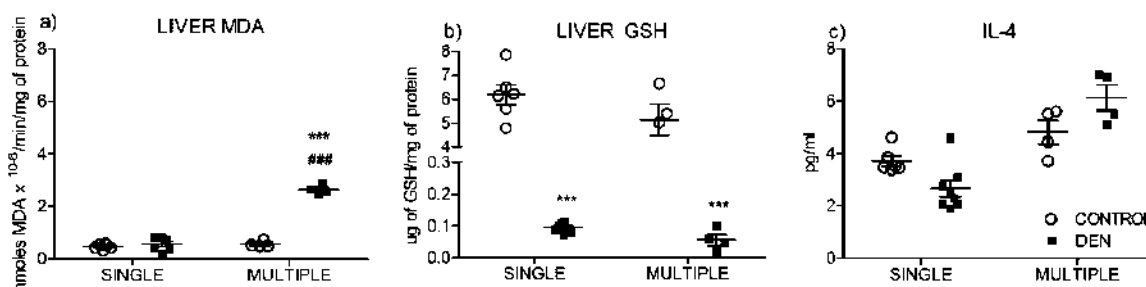
Figure 2: DEN induced effects on liver peroxidation, GSH and plasma IL-4 levels. Data are represented as mean ± SEM. a) Liver MDA in nmoles x 10^{-6}/min/mg of protein; b) Liver GSH in μg/mg of protein; c) plasma IL-4 in pg/ml of plasma. * Control vs. DEN; $p < 0.05$; # Single vs. multiple; $p < 0.05$; $p < 0.01$; $p < 0.001$.

DEN did not induce any effect on brain MDA levels ($F_{(1, 18)} = 1.11$; $p > 0.05$) and there were no differences between single vs. multiple dosed condition ($F_{(1, 18)} = 0.31$; $p > 0.05$) and no significant DEN x dosage interaction ($F_{(1, 18)} = 0.04$; $p > 0.05$; fig 3a).

Brain GSH was variably affected, with a lowering in the single dose group as compared to an increase in the multiple dose group. Two-way ANOVA demonstrated no effect of DEN per se on brain GSH levels ($F_{(1, 18)} = 2.49$; $p > 0.05$) in either of the groups as compared to controls, though it increased steadily in the multiple dosed group such that there was an

effect based on dosage ($F_{(1, 18)} = 12.24$; $p < 0.01$) with significant differences between single vs. multiple dose group ($p < 0.05$; DEN x dosage interaction ($F_{(1, 18)} = 12.03$; $p < 0.01$; fig 3b).

There was a significant effect of DEN ($F_{(1, 19)} = 36.35$; $p < 0.0001$) on NOS levels (fig 3c) in both single as well as multiple dosed conditions with post-tests revealing significant increase in NOS on DEN treatment in both single dosed ($p < 0.001$) as well as multiple dosed conditions ($p < 0.01$). However, there was no difference between single vs. multiple dosage conditions ($F_{(1, 19)} = 0.14$; $p > 0.05$) and no significant interaction of DEN x dose ($F_{(1, 19)} = 0.06$; $p > 0.05$).
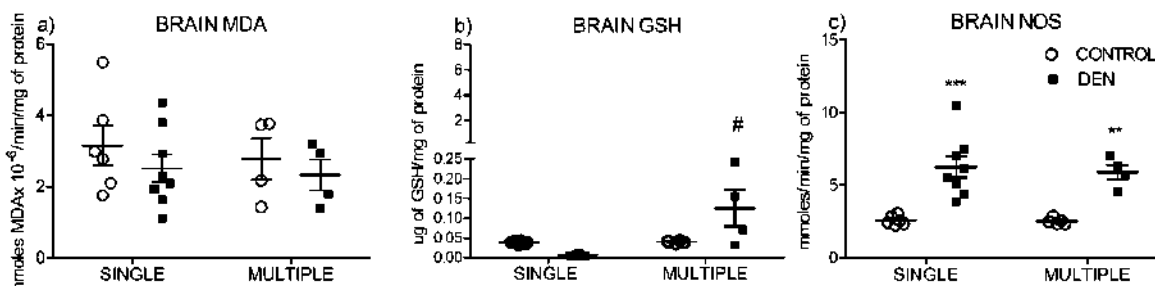
Figure 3: DEN induced effects on brain peroxidation, GSH and Nitric oxide synthase. Data are represented as mean ± SEM. a) Brain MDA in nmoles x 10^{-6}/min/mg of protein; b) Brain GSH in μg/mg of protein; e) nNOS in mmoles x 10^{-6}/min/mg of protein * Control vs. DEN; # Single vs. multiple; $p < 0.05$; $p < 0.01$; $p < 0.001$.

4. Discussion and Conclusion

From the histological sections it is evident that the multiple dose administration regimen demonstrated higher cell proliferation and structural changes associated with HCC. Ki-67 expression which demonstrated an increase in the multiple dose group is amarker for neoplasia as it is expressed during all active phases of the cell cycle [18]. Ki-67 has been found to be significantly higher in the non-malignant liver tissue with cirrhosis and hepatic cancer as compared with cirrhotic hepatic cancer [23].

Lipid peroxidation and GSH and are some of the important references widely used in animal studies to observe the development of hepatocarcinogenesis [20, 28]. In the present study, lipid peroxidation state as assessed by MDA levels in the liver was not affected on single dose administration. Liver MDA levels were increased only in the group that was administered multiple doses of DEN, indicating cellular damage. GSH, an important antioxidant, scavenger of free radicals and cofactor of many detoxifying enzymes against oxidative stress, was significantly reduced in both the DEN-treated groups.

Lipid peroxidation produces relatively stable decomposition end products like α, β-unsaturated reactive aldehydes, such as malondialdehyde, 4-hydroxy-2-nonenal, 2-propenal, and isoprostanes, which have been used as biomarkers of oxidative/nitrosative stress damage [29]. However, the effect of LPO levels is not very clearly understood. In DEN treatment, white nodules were macroscopically noted after the 10th week, with an increase in the numbers thereafter. After 12 weeks of the DEN treatment, hyperplastic nodules developed [30].

As an important antioxidant GSH is also considered the most important scavenger of free radicals and cofactor of many detoxifying enzymes against oxidative stress. Increased GSH levels are normally associated with the proliferative response and are essential for cell cycle progression. In fact, higher percentages of tumor cells with high GSH content were able to survive in the presence of nitrosamine and oxidative stress [31]. However, in this study, GSH levels were depleted in the liver. Whether the depletion indicates increased peroxidation and thereby deviation from homeostasis cannot be determined on the basis of this study.

The concentration of plasma IL-4 is due to the immunomodulatory actions of DEN on the immune cells. IL-4, which demonstrated no group-based differences in this study, is said to be interlinked with IFNγ production by inhibiting its secretion. This negative correlation between IL-4 and IFNγ and TNFα has been observed in response to exposure of xenobiotics such an Ethanol or Cadmium too [32].

The brain is extremely sensitive to RONS, due to high lipid content and increased tissue oxygen consumption, with a correlation between oxidative stress and lipid peroxidation products such as malondialdehyde etc. However, in this study brain MDA levels were not affected. Brain GSH which was in low concentrations in controls was increased only on multiple DEN administration and not from a single dose. DEN induced a significant increase in brain NOS at both doses tested. NOS produces NO, an important signaling molecule associated with neurodegenerative disorders with inducible NOS inhibitors being proposed asneurotherapeutic targets [33]. Expression of neuronal NOS and its downstream targets is shown to be highest in progressive HCC, with neuronal NOS levels being directlycorrelated with genomic instability, proliferation rate and micro vessel density of HCC, andinversely correlated with apoptosis and patients' survival [34].

Overall, elevated lipid peroxidation (LPO) in the multiple dose group is the result of oxidative stress, an indicator of altered homeostasis and occurs when the antiperoxidative processes collapse as observed here in depleted liver GSH. It is possible that other primary antioxidants such as Catalase and Superoxide dismutase are active. The brain with low baseline GSH levels demonstrated an

increase also only in multiple DEN group, indicating mechanisms underway to block LPO formation via peroxidases.

5. Acknowledgements:

6. References

[1] F.B. Roger (2004): Hepatic encephalopathy, https://pubs.niaaa.nih.gov/publications/arh27-3/240-246.htm. (The National Institute on Alcohol Abuse and Alcoholism (NIAAA))

[2] F. Bray, J.Ferlay, I. Soerjomataram, R. L. Siegel, L. A. Torre and A. Jemal (2018): Global cancer statistics 2018: GLOBOCAN estimates of incidence and mortality worldwide for 36 cancers in 185 countries, CA: A Cancer Journal for Clinicians (American Cancer Society) 68(6) 394–424 (2018)

[3] J. Song, W. Ding, B. Liu, D. Liu, Z. Xia, L. Zhang, L. Chiu, Y. Luo, J. Xiaobin, L. and Feng (2020): Anticancer effect of caudatin in diethylnitrosamine-induced hepatocarcinogenesis in rats. Molecular Medicine Reports (Spandidos) 22(2) 697-706 (2020)

[4] G. Ramakrishnan, H.R. Raghavendran, R. Vinodhkumar and T. Devaki (2006): Suppression of N-nitrosodiethylamine induced hepatocarcinogenesis by silymarin in rats. Chemico-biological Interactions (Elsevier) 161(2), 104–114 (2006)

[5] A. H. S. Nermin, A. E.L. Shohda and F.I. Manal (2008): Diethylnitrosamine-induced hepatocarcinogenesis in rats: possible chemoprevention by blueberries; African Journal of Biochemistry (Academic Journals) 2(3), 081-087(2008)

[6] M. Valko, C.J. Rhodes, J. Moncol, M. Izakovic and M. Mazur (2006): Free radicals, metals and antioxidants in oxidative stress-induced cancer. Chemico-biological Interactions (Elsevier) 160(1), 1–40. (2006)

[7] T. Chakraborty, A. Chatterjee, A. Rana, D. Dhachinamoorthi, P. A. Kumar and M. Chatterjee (2007): Carcinogen-induced early molecular events and its implication in the initiation of chemical hepatocarcinogenesis in rats: chemopreventive role of vanadium on this process. Biochimica et Biophysica Acta (Elsevier) 1772(1), 48–59. (2007)

[8] Y. Shirakami, M. E. Gottesman and W.S. Blaner (2012): Diethylnitrosamine-induced hepatocarcinogenesis is suppressed in lecithin:retinol acyltransferase-deficient mice primarily through retinoid actions immediately after carcinogen administration. Carcinogenesis (Oxford University Press) 33(2), 268–274. (2012)

[9] W. Lopaczynski and S. H. Zeisel (2001): Antioxidants, programmed cell death, and cancer. Nutrition Research (Elsevier); 21: 295–307. (2001)

[10] G. Poli, G. Leonarduzzi, F. Biasi and E. Chiarpotto (2004): Oxidative stress and cell signalling. Current Medicinal Chemistry (Bentham Science) 11(9), 1163–1182. (2004)

[11] R. Tolba, T. Kraus, C. Liedtke, M. Schwarz M and R. Weiskirchen (2015): Diethylnitrosamine (DEN)-induced carcinogenic liver injury in mice. Laboratory Animals (SAGE) 49 (1), 59–69. (2015)

[12] S. De Minicis, T. Kisseleva, H. Francis, G.S. Baroni, A. Benedetti, D. Brenner, D. Alvaro, G. Alpini and M. Marzioni (2013): Liver carcinogenesis: rodent models of hepatocarcinoma and cholangiocarcinoma. Digestive and Liver Disease: Official Journal of the Italian Society of Gastroenterology and the Italian Association for the Study of the Liver (Elsevier);(45(6), 450–459. (2013)

[13] B. Halliwell (1995): Antioxidant characterization. Methodology and mechanism. Biochemical Pharmacology (Elsevier) 49(10), 1341–1348. (1995)

[14] K. Rahman (2007): Studies on free radicals, antioxidants, and co-factors. Clinical Interventions in Aging (Dove Medical Press) 2(2), 219–236. (2007)

[15] V. Paul and P. Ekambaram (2011): Involvement of nitric oxide in learning & memory processes. The Indian Journal of Medical Research (Medknow Publications on behalf of ICMR) 133(5), 471–478. (2011)

Hariprasad Shetty and Monika Sadananda

[16] R.L. Coffman, B.W. Seymour, S. Hudak, J. Jackson and D. Rennick (1989): Antibody to interleukin-5 inhibits helminth-induced eosinophilia in mice. Science (Science New York, NY) 245(4915), 308–310. (1989)

[17] J. Zamorano, M. D. Rivas and M. Pérez-G (2003): Interleukin-4: A multifunctional cytokine. Inmunologia (Elsevier) 22 (2): 215-224. (2003)

[18] Y. Ito, N. Matsuura, M. Sakon, T. Takeda, K. Umeshita, H. Nagano, S. Nakamori, K. Dono, M. Tsujimoto, M. Nakahara, K. Nakaoand M. Monden (1999): Both cell proliferation and apoptosis significantly predict shortened disease-free survival in hepatocellular carcinoma. British Journal of Cancer (Nature) 81(4):747-51 (1999)

[19] G. Guzman, V. Alagiozian-Angelova, J.E. Layden-Almer, T.J. Layden, G. Testa, E. Benedetti, A. Kajdacsy-Balla, and S.J. Cotler (2005): p53, Ki-67, and serum alpha feto-protein as predictors of hepatocellular carcinoma recurrence in liver transplant patients. Modern Pathology: An Official Journal of the United States and Canadian Academy of Pathology, (Nature Inc) 18(11), 1498–1503. (2005).

[20] J. Pizem, V.F. Marolt, B. Luzar, and A. Cör (2001): Proliferative and apoptotic activity in hepatocellular carcinoma and surrounding non-neoplastic liver tissue. PflugersArchiv: European Journal of Physiology (Springer) *442*(6), 174–176. (2001)

[21] M.I. Youssef, H. Maghraby, E.A. Youssef and M.M. El-Sayed (2012): Expression of Ki 67 in hepatocellular carcinoma induced by diethylnitrosamine in mice and its correlation with histopathological alterations. Journal of Applied Pharmaceutical Science (Open Science) 02 (03): 52-59. (2012)

[22] T. Umemura, S. Kai, R. Hasegawa, K. Kanki, Y. Kitamura, A. Nishikawaand M. Hirose (2003): Prevention of dual promoting effects of pentachlorophenol, an environmental pollutant, on diethylnitrosamine-induced hepato- and cholangiocarcinogenesis in mice by green tea infusion. Carcinogenesis (Oxford University Press) 24(6):1105-9 (2003)

[23] J. Koskinas, K. Petraki, N. Kavantzas, I. Rapti, D. Kountouras and S. Hadziyannis (2005): Hepatic expression of the proliferative marker Ki-67 and p53 protein in HBV or HCV cirrhosis in relation to dysplastic liver cell changes and hepatocellular carcinoma. Journal of Viral Hepatitis (Wiley online publications) 12(6), 635–641. (2005)

[24] H. Ohkawa, N. Ohishi and K. Yagi (1979): Assay for lipid peroxides in animal tissues by thiobarbituric acid reaction. Analytical biochemistry (Elsevier) 95(2), 351–358. (1979)

[25] G.L. Ellman (1959): Tissue sulfhydryl groups. Archives of Biochemistry and Biophysics (Elsevier) 82(1), 70–77. (1959)

[26] T.M. Dawson, D.S. Bredt, M. Fotuhi, P.M. Hwang and S.H. Snyder (1991): Nitric oxide synthase and neuronal NADPH diaphorase are identical in brain and peripheral tissues. Proceedings of the National Academy of Sciences of the United States of America (United States National Academy of Sciences) 88(17), 7797–7801. (1991)

[27] O. H. Lowry, N. J. Rosebrough, A. L. Farr and R. J. Randall (1951): Protein measurement with the Folin phenol reagent. The Journal of Biological Chemistry (Elsevier) 193(1), 265–275. (1951)

[28] V. Kumar and K.D. Gill (2014): Oxidative stress and mitochondrial dysfunction in aluminium neurotoxicity and its amelioration: a review. Neurotoxicology (Elsevier) 41, 154–166. (2014)

[29] E.B. Kurutas (2016): The importance of antioxidants which play the role in cellular response against oxidative/nitrosative stress: current state. Nutrition Journal (Springer Nature) 25;15(1):71. (2016)

[30] R. Abe, J.I. Okano, R. Imamoto, Y. Fujise and Y. Murawaki (2012): Sequential analysis of diethylnitrosamine-induced hepatocarcinogenesis in rats. Experimental and therapeutic medicine (Spandidos) 3(3), 371-378 (2012).

[31] N. Traverso, R. Ricciarelli, M. Nitti, B. Marengo, A.L. Furfaro, M.A. Pronzato, U. M.

Hariprasad Shetty and Monika Sadananda

Marinari and C. Domenicotti (2013): Role of glutathione in cancer progression and chemoresistance. Oxidative Medicine and Cellular Longevity (Hindawi) 2013, 972913. (2013)

[32] J. Moniuszko-Jakoniuk, M. Jurczuk and M. Gałażyn-Sidorczuk (2009): Evaluation of Some Immunoregulatory Cytokines in Serum of Rats Exposed to Cadmium and Ethanol. Polish Journal of Environmental Studies (HARD) 18 (4): 673-680. (2009)

[33] P.S. Garry, M. Ezra, M.J. Rowland, J. Westbrook, and K.T. Pattinson (2015): The role of the nitric oxide pathway in brain injury and its treatment-from bench to bedside. ExperimentalNeurology (Elsevier) 26*3*, 235–243. (2015)

[34] R.M. Pascale, M. Frau and F. Feo, Prognostic Significance of iNOS in Hepatocellular Carcinoma. In: Bonavida B. (eds) Nitric Oxide (NO) and Cancer. Cancer Drug Discovery and Development. Springer, New York, New York, p3
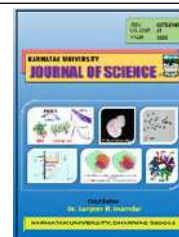
UNIQUES, EXCEPTIONS AND ANOMALIES

B Y M Gouder

Department of Zoology, Karnatak University, Dharwad, Karnataka, India -580003.

Corresponding author: bymgouder27@gmail.com

Uniques, exceptions and anomalies seem to have built this world-why! The Universe - it is said, exceptions prove the rule; the Universe with all its components - galaxies, stars, planets and several other celestial bodies - have come a long way that has taken billions of years to attain the present state. When one takes the broad retrospect how these were born, underwent evolution, one gets a feeling that it is all due mostly to the exceptions and uniques - in ways due to freaks rather than to general or common rules. Briefly speaking, the exceptions rule the roost. The Universe was born trillions of years ago. The particles condensed and compacted into ball, gained energy, attained criticality and exploded by the process of what we call Big Bang (BB). We are yet to find from where these, what we call Fundamental Particle (FP) also named Elementary Particles (EP) came from rather we do not know their source or origin, at least for the time being. The BB spewed out these FPs which went on spreading into a void called space. Thus the astronomical term was born. Thus far, the existence of 18 FPs has been recognised of which existence of 16 has been experimentally confirmed. The 17th FP is the last one added to the list. It is called

Higgs Boson named after the discoverers Peter Higgs and Satyendranath Bose - a mathematician from Kolakata of West Bengal, India-who later worked with Nobel Laureate, Albert Einstein – the Man of the Millennium 2000. Higgs Conceptualised the existence of this particle and Bose proved it mathematically. The particle in common parlance came to be known as the "God Particle"; it is an anomaly among the FPs. It is the only particle that has mass and is the lone basis for the creation of the Universe without which further development of the Universe, its galaxies, stars, planets; life as we witness today would not have been created; hence the nickname - GOD PARTICLE. Coming back, once again it is its unique and exceptional property that has created everything of the Universe that we have today. Of the total of 18 FPs that were theorised, only two of the total 18 FPs, only two have remained theoretically conjectured. All the subsequent changes that the Universe has undergone are solely due to this God Particle. Negatively speaking-Had this particle not been there or had it been like other FPs or had it not possessed mass, there would not have been the galaxies, stars, planets - for that

matter there would not have been the Universe what it is today!! We owe everything to this God Particle- which is an exception, unique and anomalous contrary to other fundamental particle. Our inverse has many Galaxies of which our galaxy - Milky Way is one. The galaxy nearest to ours is Andromeda about which we know very little. Our Galaxy Milky Way is so named because of the myth that Hera suckling her baby realised that the baby was not hers; she pulled out the baby in disgust and her breast milk splattered in the sky causing the Milky Way. As the legend goes, it is Hera's milk that caused our Galaxy. The neighboring Andromeda is moving nearer to Milky Way and the time will come when it passes through our galaxy - the catastrophic result of which is presently beyond comprehension. There are millions of stars in our galaxy alone and our Sun is one such star. It is hardly believable that the stars including our sun have finite span of life though the span of astronomical time is very large. Some stars in our galaxy are yet to be born, are just born, adolescents, youths, old ones, and also that have died and metamorphosed into other celestial bodies??. There are stars many times bigger than our Sun and the light they emit is incomprehensibly bright. The gravitational pull they exert is beyond one's imagination. In this background, the Sun is unique and exceptional. It's everything is ideal and tailor made to sustain Earth Planet which has no parallel or near parallel in the Universe so far known. Age of the sun is determined by means of carbon dating of the rocks obtained from moon, mars and the earth. It is estimated to be about 400-500 million years?? It was born by cleaving from the nebulous cluster??. The Sun has already spent 28% of its life-span; it is yet

to "live" a life of 72% before it "dies". All its traits are very precisely made to create life and man ultimately. A little deviation from its paradigms would not have created what our Earth Planet, had been and is today. Let us see how this is in brief: The Sun emits light energy as a result of nuclear fusion about which a huge international expensive project called CERN .for LHC (Council of European Nuclear Research or Large Hadron Collider) is presently under way. It is an internationally sponsored, the largest and the most expensive laboratory of Particle Physics. Nuclei of Hydrogen fuse; as a result; huge amount of energy - in the form of short, medium, long or heat waves and electromagnetic waves also called gamma rays are emitted into space in ideal quantity and intensity. If this is less or more the Planet Earth would not have been what it is today. If the Sun happened to be bigger than what it is now, it would by its gravity have pulled the Earth towards it and upset the Entire Solar System with all its planets and the moons moving around them. In case, the Sun were smaller than the present one, the composition of the atmosphere would have been different. Earth's gravity would have become far less. Light would have been very feeble. The Earth would become dark, lifeless, much bigger and burnt. A word of caution, The Sun will become old and things in the solar system would alter. In course of astronomical time, the Sun cools down from 90000° F to 3000°F becomes Red Giant and lasts only for 2 billion years. Briefly, nothing is permanent and indestructible as the scriptures claim. These are so unique and exceptional as well as tailor made keeping in view of some futuristic purpose, one cannot but accept that there is a Supernatural Entity which the

humans call God. Man as the human species has limitations to understand and use it to his advantage. His tribe is bound to perish; Earth conditions become harsh and hostile following his extinction that is bound to take place!!

Our planet Earth is not only ideal amongst the planets of the solar system through it, in a way, is a freak amongst the planets discovered so far. It's all parameters are ideal for creating life. Deviation of any one parameter would not have led to creation of life and subsequent changes that we witness today. Its size, distance, rotation, revolution-both spatial and temporal, 23° tilt of the rotational axis, nature of its orbit around the Sun• all these are so precisely set; slight deviation from them, would not have enabled our planet Earth what it is today. Just to cite consequence of only a few aberrations of these parameters: the tilt has enabled onset of seasons, duration of days and nights depends on rotation a condition ideal for plants and animals, distance from the Sun: if it is farther, temperature would be very cold and there would not be water in fluid or gaseous state; if it is nearer than earth now is, our planet would be too hot to sustain life. Take for instance its size: if it had been bigger, the force of gravity would have been more affecting the composition of the atmosphere; for all probability, earth would not have lost its hydrogen gas it held once upon a time and there would not have been atmospheric oxygen.

The next very vital chemical that is unique and exceptional is water H_2O There is no other chemical natural or synthesized similar to H_2O. Had there been no water, there would not have been life. Water exists in three states solid (ice) liquid (water) and gaseous (vapour air moisture) at room temperature. Ice expands when water is cooled from 4°C to 0°C) water; hence ice floats on water enabling the aquatic plants and animals to survive. It has the maximum latent heat; no other liquid is the solvent as ideal as water. Hence it is an ideal vehicle to transport materials in body functions. It has the maximum latent heat of evaporation not witnessed in other chemicals; there are many more exceptional qualities of water not cited here. Briefly speaking, it is the elixir of life without which our planet earth would have been barren and bland without life and greenery. No other planet in our galaxy has life. The planet bearing life is yet to be found though theoretically as many as 150 earth-like planets are inferred to exist. Some of them having very advanced civilization say - thousands of years ahead of what our earthly civilization would be. One freak evidence in support of the concept is that we are receiving weird signals from outer space; the aliens are probably trying.to contact us we, the earthly beings.

After all the elements, metallic as well as non-metallic came into existence, the organic substances began to be formed in water. Carbon appeared next to helium and Hydrogen as the temperature came down. The first important organic chemical in the context is the group of 20 amino-acids ($+NH_2$-COOH-) of which 9 are essential ones; they are to be obtained from outside diet and the other 11 are non-essential in a sense that they are synthesized in the body. They are the building blocks of the living body.

An Amino Acid is a freak, unique and exceptional compound having the

properties that no organic compound seems to have. It is these qualities that have paved the way towards creation of life. Negatively speaking, there would not have been life without amino acids!! Amino-(NH_2) has positive (+) charge at its free end and Hydroxy (COOH) group carried negative (-) charge. That means one amino acid at its NH_2 +ve end can bond with COOH-ve end of other amino acid; further, this compound possessing +ve and -ve charges at either ends can bond with other amino acid molecules, so that a long chain of any number of amino acids may be formed. The result: such long chains are the proteins. The bond between the two amino acids is weak, separable and reversible; they disintegrate if milieu (molarity, pH etc) change. Another property is that an enzyme, specific to amino acids in bonding, is a must. As a result of these traits of amino acids and proteins are very unstable and remain intact only under certain ambience called substrates?? or media (Milieu).There is no chemical natural or synthesized having these parameters. These -unique, exceptional and anomalous qualities paved the way towards creation of life subsequently. In other words, there is no chemical akin to or having these properties in the organic world.

Another unique or freak compound is nucleic acid which is of two types: DNA (De-oxy Ribose Nucleic Acid and RNA (Ribose Nucleic Acid). These are exceptional substances a precursor of living beings because they have the ability to build their own likes i.e. they have the ability to duplicate themselves a type of reproduction in biological language. Each molecule picks up its ingredients and builds its own kind. It is something like a fictional robot that repairs itself or builds its own like from picking machine parts from surrounding!!

Thus the Life began with two nucleic acids that went on producing variety of proteins, later viruses, bacteria, fungi……; Organic Evolution began and created microorganisms, plants and animals; the process of organic evolution virtually came to an end with the appearance of man. Man is an exception, unique, so to say a freak among the animals.

TILL HERE

Man stands alone and desolate amongst the animals of the animal kingdom. There is no living being like him in other planets, solar systems or galaxies or anywhere in the Universe! If one introspects at the 'nano' (10^{-9}) and 'giga' (10^{+9}) levels, he gets a weird and perplexed feeling. Compare his body size in terms of an electron or any elementary particle; he becomes bigger than the universe. Consider his body size as compared to the size of the Universe! He is smaller than an electron. Man's body is made of millions of cells; fosters trillions of microbes; more than 96% or so of these die and give rise to new ones; yet he continues to be an entity like the river Ganges that has been flowing from times immemorial but its water molecules changing every nanosecond! Consider man in Biological sense; there is nothing his own, like a flowing river, he inherits something from fore fathers and hands them to his progeny. Consider his age in terms of that of Universe time scale; it is beyond one's imagination. He is the lone animal of the animal kingdom having the faculty of reasoning, thinking, remembering, and learning. Man is the only animal that has the

speaking ability and uses a language. Man is the final product of bodily or somatic or structural evolution. It is also an onset of second phase of evoluion of learning.

The onset of man's speaking language is really a miracle amongst miracles - not encountered in animals. Zoologically speaking, man is also an animal of the animal kingdom; yet he is different from animals - unique, exceptional and freak; he stands alone desolate and so apart from animals. Other animals have languages of their own; but entirely different in a sense that they produce the sound and communicate by facial expression, body signs, changing the intensity i.e. pitch of the sound. In grammatical sense animals produce vowels: they cannot produce or pronounce consonants for which a complicated architecture of the tongue, internal ear, middle ear (columella auris) are required. At The most animals can produce only the vowels and vary the pitch, thereby the animals, namely the land vertebrates (Amphibians, Reptiles, Birds and Mammals excluding man). Man is able to produce not only vowels and consonants but also their combinations such as pra .cl, thr, shrou and so on.

Anatomy of language of humans is yet another freak amongst the means of communication of the animal world! The vocal chords vibrate and produce feeble sound, the sinuses m the skull amplify it; The tongue, palate, teeth, lips and the buccal cavity participate in unison and produce not only vowels but also consonants; besides the internal ear Cochlea?? and more importantly the hearing centre in the brain is evolved and tuned - rather - orchestrated to develop human language.

The somatic or structural evolution comes to an end with origin of man and "learning evolution" started from now on. Gene theory comes to a close paving way for Meme Theory that is: a new phrase that envisages organic, learning and behavioral changes!

God is not in human body shape; Sun is not God but a creation in the process of evolution; God created only a unique, exceptional, the only one of its kind - the "Boson" that was programmed by him to undergo progressive changes of which Man is the latest product. In a way Boson -the GOD Particle - is a "God's Stem Cell" programmed to do something which only the Future can decipher. In a way Man is produced to further something which we know not. We men are only a transient product fighting amongst ourselves and making the Earth inhabitable and fly to another planet ordained to reach its logical end. Everything that is born must perish some day or the other. Everything has the purpose ordained to do something; only the future can decipher. Amen!

Dr.BY M Gouder

bymgouder27@gmail.com

About the author:

Dr. B.Y. Mariappa Gouder, (now 95 years young) retired faculty from Department of Zoology, Karnatak University, Dharwad. He has been a popular teacher and researcher. A renowned teacher is always judged by the success of his/her students. Many of his students have served as the faculty in the Department of Zoology in K.U. and elsewhere. All his

students have made a mark in their respective fields. Dr. Gouder worked on Endocrinology and Reproductive Physiology and has guided many students for PhD. Dr. Gouder and myself were the first to initiate research on development of reptiles in India. These reptiles are the first amniotes among vertebrates. In fact development of amniotic eggs in reptiles enabled nature's most successful experiment in the evolution of land-dwelling vertebrates and the diversity of reptiles reached its zenith during the Mesozoic era ("Age of Reptiles"). Dr. Gouder and his student Prof. Shrimati Gaitonde were pioneers in introducing hypophysectormy (removal of pituitary) technique in these reptiles for the first time. I am fortunate to have been his student and associated with him for more than three decades now. Dr. Gouder has published research articles in national and international journals of repute. He has also presented his research work at national and international symposia and conferences. He was principal investigator of many research projects funded by the UGC, DOE, DOD and DST, Govt. of India, New Delhi.

Post retirement, he has taken up social cum community service and has been In-Charge of Sharada Girls' High School, Dharwad. He has been the key person in improving the academics of Sharada English and Kannada medium Nursery, Primary, High Schools. He has great passion for teaching and has excellent command over English language and grammar. He has been teaching English grammar to high school students since last 3 decades – free of charge. He has written a book "English Grammar: Learning through Kannada" which has become quite popular and has seen 2nd Edition recently. Even at the ripe age of 95 Dr. Gouder has great passion for science and keeps writing science articles. The present article depicts his analytical view of the "God particle" and its connection to everything that is there in the universe. Happy reading!!!

Prof. Laxmi S. Inamdar
Department of Zoology
Karnatak University
Dharwad 580 003

Science Education: Some Reflections and Ways

Prof. M. I. Savadatti

Today, Science and Scientificity have become of paramount importance in every field of our lives. In the field of school and college education, we just give importance to science teaching. Scientificity is an entirely different matter. There is a lot of difference between Science and Scientificity; Science is about scientific knowledge, Scientificity refers to the state of being scientific in education, science and technology.

Science Education is mainly comprised of:
1. Science Learners
2. Science Teachers
3. Well - equipped laboratories and other infrastructures needed for science teaching.

The question before us is how much importance we have given to Science in the kind of environment in which we have grown up. Mostly, talented students in their Pre-University Examinations with reasonably good financial background opt for Engineering and Medical career. As a result, the number of these students opting for the study of Science is very small. Some students enroll for Science courses with the intention of getting jobs in some sectors. For example, after BSc with Ed degree they may become High School teachers, and some after MSc may become lecturers in colleges. Today, Science thus has become a way of livelihood. We have not made serious attempts to ensure evolving of a system to teach and learn Science in an exciting way. We are stuck with an environment which is not conducive to kindle curiosity and fire the imagination of students, which are necessary, among other factors, for making the learning of Science interesting and exciting.

Historically, if one looks back over nearly hundred years ago, some students learnt science extremely well. In fact, during that time there were very few teachers and High Schools were not as good as the present ones. In spite of all the constraints the country produced a first Nobel Laureate in Science (Physics) – Sir C. V. Raman in 1930. Afterwards, we have not seen a second Nobel Laureate in science in the last ninety years of our history. Similarly, it may be noted that those who went abroad after 1960 were selected based on their academic credentials. Later, there were special aptitude-testing examinations for the selection of students for studying abroad. It so happened that many who went abroad particularly to USA did not return back to the country. There they found for themselves good jobs, positions, an ambience to excel and good life. Net result of this brain drain was that we lost talented scientists and the

country was left with largely second rate scientists.

The kinds of high-tech based equipment we employ in scientific research are imported from abroad. Further, many people who were sent abroad for training by Govt. of India did not return either to exploit experience for enhancing the work nor build scientific pool of people. One may ask for answers from the basic question as to why all this happened. The simplest and the well-thought answer one can give is that, in our system we have not given enough importance to Science Education which it deserves. Today, teachers do not get the respect in the society. They do not get enough salary and as a result they consider 'teaching' as a mere 'job' for livelihood. The net result is teachers have lost interest in knowing/learning more about the subjects they teach. Further, my own experience is that when I told a teacher, who was teaching a subject for more than ten years continuously, to choose another subject in its place, his simple answer was - "Sorry Sir. I cannot. It is not possible". Such teachers simply presented the same topic insipidly before the students, year after year, till they retired from job. This is the situation in many schools, colleges and universities in our country. In this context, let us look at an interesting and enlightening case from Caltech, one of the best American universities in the world. A physics professor, who was a Nobel Laureate too, was asked to teach students at the PU level (Freshman and Sophomore classes) during 1961 -63. Initially he said it was not possible for him as it was a full-time assignment involving a good deal of preparation. When persuaded by Caltech, he accepted and taught students for 3 years with commitment, dedication and preparation

with full of insights, making it an interesting and exciting. It may be noted that during those three years he could not carry out his research work. Lectures were meant for enthusiastic students. The personality of the lecturer was so interesting that a large number of students (and some of his colleagues) used to attend the classes, filling the class room all the while. Many used to sit in the windows and on the floor of the hall. Two of the colleagues took down notes of his lectures (and also video recorded lectures). All of this culminated in a three-volume set of books based on the lectures and were published under the title, "Feynman Lectures on Physics". The professor who accomplished this feat was Richard P. Feynman. The three books bear the name of Feynman, Leighton and Sands (the two were his colleagues who attended the lectures). The three books rank among the classics of our times. Some of those students who attended the lectures went on to become very fine scientists including winning Nobel Prizes. However, none of those students matched Feyman, the great teacher.

One important lesson we learn from Feynman's experiment is that teachers in the US, UK, and few other countries study deeply the subject they teach and enjoy the subject as well as teaching process. Unfortunately, this kind of situation does not prevail much in our country. Also, parents in our country, always, think whether their children get jobs paying higher salaries. Hardly, we teach Science in an exciting way so that students really learn Science. Also, few teachers who are capable of better teaching will not teach with interest and dedication. The reasons for all the mess in teaching-learning Science are the irregularities in the appointments of

teachers. We need teachers who are competent and capable of studying the subjects themselves in depth, which they teach. The monitoring mechanisms, as to how teachers teach and what they really teach, are very weak. Even these are not seriously implemented. Teachers Training Programs are organized but nobody bothers about the effectiveness of the programs. We do not have meaningful data about the percentage of teachers enhancing their competencies. We seem not to bother whether the training of teachers has made any impact on the learning of students and whether the trained teachers are attracting large number of students for the study of science. Another important issue which bothers is that students after completing their prescribed PU courses, whether they learn or not join for tuition classes which prepare them for Entrance Examinations to get admissions in Engineering and Medical colleges. Getting ranks is the only aim through rote learning and not the learning leading to understanding of the subjects. As colleges do not allot courses to students as per their liking but based on the basis of marks students secure, students resort to malpractices to secure ranks. In this way Education has become a commercial commodity. People may ask then, how come we have done so well in the fields of Atomic Energy and Space Science & Technology. The answer for this lies in finding out whether concerned scientists and technologists had been abroad for training or were trained in India itself. This is important. For, those who go abroad have the opportunity of interacting with scientists in those countries. Similarly, if we say we are using second grade scientific equipments it means that we are modifying the technology got from developed countries and use for our

requirements. All this, in no way means that we are not intelligent or competent. But at the same time we note that no important discoveries/inventions/innovations are taking place as we expect. If we say otherwise, then the question arises why there are no new Nobel Laureates in the field of Science and Technology. S. Chandrashekar the great astrophysicist got Nobel Prize when he went abroad and worked there. The other Nobel Prizes went to the persons of Indian origin who had settled abroad.

For those who are staying in India, as said earlier, job has become much more important. They do not feel the necessity of doing quality research and have no urge to strive for developing our own science and technology for our own needs. The root cause of this apathy lies in the fact that, in our Education System, the full control lies with the Education Ministry, not with enlightened and educated citizens. Competent and qualified persons have not much freedom to accomplish things of value. It is interesting to note, in this context, Russia (earlier Union of Socialist Soviet Republic or USSR), during the reign of Joseph Stalin, had no contact/communication with the external world. Iron curtain was drawn. Scientific achievements of USSR were not known to the outside world. When the iron curtain was lifted after nearly four years, four Nobel Prizes went to Russian scientists. When the reasons for these achievements were investigated, it was found that, though Russia was a Communist country, the scientists received higher salaries compared to others, even compared to some important officials. Top scientists were provided with two houses – one in their work place and the other one in the region where they could spend their holidays. Importantly, the

scientists were respected. What this illustrates is that how one can attract and retain persons who are competent and interested in teaching and research. Until and unless this kind of strategy/policy is adopted we cannot progress in the field of science and technology and cannot emerge as a developed nation. We see that while many have become millionaires at the time of their retirement, the tragedy is that we are not realizing that development of the country will not take place with such people.

To understand the subtelities of developments of Science and Technology, we need to be well educated. For this to happen teachers who are motivated and interested in life- long learning be appointed. Teaching should be a passion for them. For example, while appointing teachers for high schools, we should not only consider their qualifications but also dedication and love for teaching profession. Most of us have heard the name of Michael Faraday. He did not go to any college. But his contributions as a scientist are amazing and invaluable. Royal Society of London honored him for his phenomenal research work. What Faraday's example illustrates is that advances in science and technology take place where scientists are valued for their merit/competence and quality contributions.

Education can be compared to nurturing the growth of a tree. It involves supplying right manure and watering properly. Most important of all is that the planted sapling should be disease free, that is to say, remain healthy. This is what is needed to happen in our institutions of science. However, it appears to be a remote possibility as the educational institutions have already been bereft of the spirit of motivation, passion and dedication. We are in a situation of not knowing where to start

and who has to improve whom. Further, if we look at the academic grades students secure at SSLC (10th class) and PUC (12th class) examinations, one gets the feeling that they must be geniuses. Instead, the reality is that students never read anything beyond books prescribed and many teachers never teach anything beyond the syllabus clearly marked. As a result of all this the Educational System has stagnated. It is a Herculean task to improve or reform it.

India is a big country with great heritage. Only way for the improvement of the Education System is that it requires a kind of revolution and countrymen be educated. We may give suggestions for achieving the overhaul of Education System; that's all. But implementation of suggestions/recommendations lies with the politicians and our leaders. However, they do not have time to look into suggestions/recommendations; they are occupied with other priorities. Let us look back in time. Kothari Commission (Education Commission) Report (1964-66) which reviewed the state of education at all levels and gave recommendations to educate India. It is a very good report but was not implemented completely. Since then few more committees' reports were submitted as sought by the Govt. Recently, the Central Govt. has brought forth yet another new National Educational Policy 2020 (NEP-2020) whose effective implementation appears to be very difficult. The reason is simple. To produce excellent graduates we need motivated students with good attitude and aptitude for learning, for which to achieve qualified, competent and inspiring teachers are required. Along with these two factors what we need is the healthy ambience in the society which promotes the first two.

In countries like the US, the UK and others, studies on how to enhance the quality and competence of students have been conducted. It is demonstrated that we can develop students, whom we call 'second class' into 'first class' students. How can we achieve this kind of transformation in our country? Who has to change the "indifferent dull educational environment"? How it has to be done? Some will say, casually, we need to do this in the existing social context. How is it possible? Because, while appointing teachers we have to take care of reservation and then qualifications. We never bother whether qualified teachers are competent or not and, whether they can get along with colleagues and work harmoniously in groups or not. We also not bother about the salaries we pay. Most importantly, we never bother about searching for candidates who are better than the ones appointed.

Another strange situation exists in our system. We assign teachers all kinds of work not related to teaching. The work may concern census, elections, or corona related works. They do not have sufficient time and freedom to do well their work of teaching. So, it becomes difficult to expect excellence in their teaching. When the system does not care for a person, the person also will not care for the system. This is the story of Education in our country. It has become very difficult to understand as to how to go about improving the Educational System. If enlightened persons with good character, integrity and educated in a true sense come together and discuss issues and convey the same to willing leaders and enlightened politicians who can listen and act, then only it is possible to rejuvenate our Education System

This was the last talk delivered at Regional Science Center Dharwad in

Kannada by Late Prof. M. I. Savadatti, Former Vice-Chancellor of Mangalore University.
(https://www.youtube.com/watch?v=pBhtE TOrhBM).
It is translated into English by Prof. B. G. Mulimani, Former Vice Chancellor, Gulbarga University, Gulbarga and BLDE University, Vijayapura.

OBITUARY

Prof. I. M. Khazi
Department of Chemistry, Karnatak University Dharwad.
(*1967-2020*).

The sad demise of Prof. I. M. Khazi on 24th Aug 2020 has sent a shock wave to our family of chemists. This is a grievous loss for our community as he was a prominent, enthusiastic and leading personality in the field of the organic chemistry, having received much recognition in his academic, scientific and administrative career. Not only was he recipient of numerous awards for his contributions, he was also loved by his post graduate and doctoral students alike for his undivided concern and care. His untimely death has been a cause of much regret among his students, such an irreparable loss which can never be fulfilled. I would like to express my deepest sense of gratitude to his exceptional service in teaching and research over a period of more than two decades in the department of Chemistry, Karnatak University, Dharwad.

Prof. I. M. Khazi was born on 21st July, 1967 in a village named Rattihalli in Haveri District, having completed M.Sc in Organic Chemistry in 1990 from Karnatak University, Dharwad. With the sound knowledge of chemistry he qualified UGC-CSIR NET New Delhi (Chemical Sciences) in 1991, and he received his Ph.D. in organic chemistry from Karnatak University in 1995 under the guidance of Prof. C. S. Mahajanshetti.

In the year 1997 he was appointed as lecturer in Organic Chemistry, Karnatak University, Dharwad, due to his sheer hard work and dedication towards teaching and research, eventually in the year 2011 he was promoted to Professor. During his research career, he guided 21 students for their Doctoral degree, two students for their M. Phil and published more than 110 research papers in both national and international journals. His outstanding contribution in the field of chemistry lead to being recognized and honored with **Sir C V Raman Young Scientist** Award. In addition to academics has played tremendous rule in the many university administrative assignments such as Director PMEB KUD, Coordinator RUSA Programme, Coordinator UPE Programme, Coordinator CPEPA Programme to name a few.

I had the good fortune to work under him as doctoral student I, along with his other doctoral students salute him for his faith and concern in training and guiding us not only to face our careers, but also our lives as well.

Our Dept will forever remain grateful for his service to the various capacities as Lecturer, Senior Lecturer, Reader, Associate Professor and Professor. He will be missed and we pray that his soul has finally found a resting place.

Dr. Narahari Deshpande

OBITUARY

Prof. S. Basalingappa
Department of Zoology, Karnatak University Dharwad
(1936-2020)

Prof. S. Basalingappa was born in Sagar Gram, Shahapur Taluka, Gulbarga District on May 17, 1936. He graduated from Govt. College, Gulbarga in 1959 and moved to Dharwad to complete his MSc in Zoology at Karnatak University in 1961. He served as Lecturer and Head of Dept. of Biology at the B.V.B. College (1961-1965, on deputation from Bidar College) and also underwent the NCC Emergency Officers' training in Hyderabad in 1964.

Dr. Basalingappa did his PhD at Karnatak University under Dr C.J. George from whom he learnt various aspects of termite biology including ecological behavior, reproduction, population variations, aging of termite king and queen, nests and nesting behavior including social behavior, physiological and biological aspects. Dr. Basalingappa served as Lecturer, Reader, Professor of Zoology at Karnatak University and headed the Department of Zoology twice. He was Member of Academic Council (twice), Member of Senate (1992-94) and Registrar (Evaluation) during 1988-90. He was the first General Secretary for the Natural History Society for Zoology. He was able administrator, a popular teacher and a reputed scientist. He published more than 100 papers and delivered several talks at various institutions/universities.

Dr. Basalingappa remained active even after his retirement with the Bee-keeping Association by translating the scientific articles from English to Kannada, giving the local beekeepers a chance to read and follow the scientific progression. He kept himself busy delivering scientific talks, attending conferences and even workshops.

He always advised students to analyze the pros and the cons before taking up anything and he walked with them rather than directing them. He inculcated the life's values of simple living and high thinking adding the profound principle of honesty and integrity. His best advice was "live your life and do not regret".

Prof. Subhash Bhosale, Ponda, Goa
Prof. Raj Yadwad, Canada
Prof. Sanjeevreddy Modse, Bidar
Prof. Laxmi S. Inamdar, KUD

OBITUARY

PROFESSOR M.I. SAVADATTI
Founder Vice Chairman, Karnataka State Council for Higher Education, Bangalore
(8.01.1932 – 9.6.2021)

Professor Maharudra Irappa Savadatti, a great teacher, renowned scientist and educationist, born in 1932 in a farmer's family, was educated mainly at Dharwad. He had a brilliant academic record with B.Sc., M.Sc. and Ph.D. in Physics, followed by research in the area of combustion, free radicals and lasers. Professor Savadatti was a first generation learner with personal experience of rural life in village and actually participated in the work both on and off the farms.

Professor Savadatti worked in the UK with Chemistry Nobel Laureate Sir George Porter and in USA with Prof. H.P. Broida as a post-doctoral fellow. He had travelled widely and had developed an international feel and perspective. He worked on many national level committees, professional bodies, expert organizations, educational committees and had gained wide experience of men and matters. He had developed a national perspective with a deep commitment to quality and national good.

He worked in Karnatak University as Lecturer, Reader, Professor, Sr. Professor, Chairman of the Department of Physics, Dean Faculty of Science, etc., in an academic career spanning 33 years [1956-89]. He was solely responsible for initiating and establishing good laser facilities and development of the department of Physics at Karnatak University which led to recognition of Physics Dept as first Centre of Advanced Study in Karnataka state.

Professor Savadatti worked as member of the Syndicate for 9 years and was member of various bodies acquiring intimate knowledge of working of universities and working with people. He became President of Physics Section of India Science Congress during 1989-90.

As Vice-Chancellor of Mangalore [1989-95: two terms] Professor Savadatti developed infrastructure, introduced new and novel courses; and with no disruption of academic schedules, the University established its own place as a good University. He brought the University closer to society through establishment and involvement in District Committee for Science and Technology, Industry – University interactions, vitalizing NSS and participation in activities relevant to society.

Professor Savadatti, with deep interest in science education, worked as founding Vice-President and later on as President of Karnataka Rajya Vijnana Parishad, a

voluntary organization for spreading science and scientific temper, which secured the inaugural award instituted by the National Council of Science and Technology as the Best Organization.

Professor Savadatti established a record of working with diverse people, motivating people and managing complex issues - the skills he acquired over long years, the academic accomplishments and handling complex jobs, and situations that prevail at any top-level management. He had an objective grasp of complexities of the country as a whole.

Professor Savadatti was a member of the University Grants Commission [1996-99], New Delhi and Chairman/member of a few national and state level committees dealing with education, science and environment. As a member of UGC, he was instrumental in getting a UGC regional centre at Bangalore.

His contribution to higher education was recognized by Government of Karnataka in 1998 which awarded him with the "Rajyotsava Award". He was an active member of State level, national level committees and contributes significantly to the main stream of development and education. The Govt. of Karnataka nominated him a Vice-Chairman of Karnataka State Council for Higher Education [KSCHE] an apex level body to plan and monitor the activities and policies relating to higher education in the State.

For his outstanding contribution to the Higher Education and Science education, he was conferred D.Sc. (Hon) by the Karnatak University in Jan. 2010 and D.Sc. (*Honorary causa*) by the Rani Chennamma University, Belgaum (Feb. 2013). In 2018, Karnataka State Council for Higher Education (KSCST), GoK, Bangalore, awarded the prestigious Sir M. Visweswaraya Lifetime Achievement Award. Recently was bestowed with the Honorary Fellowship by the Karnatak Science & Technology Academy (KSTA) in March 2021.

Prof. B.G. Mulimani

Former Vice Chancellor, Gulbarga University, Gulbarga

and BLDE University, Vijayapura

KARNATAK UNIVERSITY JOURNAL OF SCIENCE
INSRTUCTIONS TO THE AUTHORS

General Information

Manuscript must be submitted as Microsoft Word document with text in Times New Roman font with size 12. The manuscript be structured as: Abstract, Introduction, Materials and Methods, Results and Discussions, Conclusions, Acknowledgment followed by References. The length of MS should not exceed 12 typed pages.

1. Title of research article should be centered and followed by authors, their affiliation, along with contact e-mail ID of the corresponding author.
2. Name of the corresponding author should be identified by an asterisk (*).
3. Abstract not exceeding 250 words be included on Title page followed by 4-5 key words. Each key word must be separated by a semicolon (;).
4. The references should be cited in text with a square bracket [21] and be limited to 30.
5. Subtitles used in the manuscript must be in bold, and follow the numbering order as: 1, 1.1, 1.2; 2, 2.1, 2,2; etc.
6. Text after the subtitle should follow directly without paragraph, whereas subsequent paragraphs must start with paragraphs.
7. Coloured figures will be included in print copy, if necessary.
8. Representation of figure, scheme and table should be in the body of the text as **Fig. 1, Scheme 1** and **Table1,** respectively. If the sentence starts with the indication of any Figure then it should be written as **Figure 1** (For example). The examples of figure, scheme and table captions are to be represented as:

Figure1. Fluorescence spectra of ternary quantum dots.
Scheme1. Synthesis of chromophores.
Table 1. Physical and thermal properties of NLO materials.

9. Style of references
   a. **Books**
      i. W. J. Koros, B. T.Chen, R. T. Chem, Handbook of Separation Process Technology, Wiley-Interscience: New York, USA, p67 (1987)
   b. **Book Chapter**
      i. M. Zhu, T. Y. Jhab, K. K. Sirkar, Optical plastics – a wonderful material, In: Basics of Non-linear Optics, T. Brouse, R. A. Huggins, eds. Elsevier: New York, USA, p54 (2001)
   c. **Journals**
      i. Photophysics and rotational diffusion dynamics of large prolate non-polar laser dyes Sanjeev R. Inamdar, J.R. Mannekutla, M.S. Sannaikar, M.N. Wari, B.G. Mulimani and M.I. Savadatti J. Mol. Liquids (Elsevier), 268C, 66-76 (2018)

ii.   P. M. Patil, Monisha Roy, A. Shashikant, S. Roy and E. Momoniat (2018): Triple diffusive mixed convection from an exponentially decreasing mainstream velocity, International Journal of Heat and Mass Transfer (Elsevier) 124, 298-306 (2018)

iii.   S. Sebastian, N. Sundaraganesan, Spectrochim. Acta (Elsevier), A75, 941-952 (2010).

d. Conference Proceedings

i.   K.P. Medium, A.S.R. Usha, C.K. Menon, Proc. 5th Annual Conference on Polymers, Istanbul, Turkey, Sept. 5-21, p. 47 (1997).

10. You may submit the manuscript as a single MS word file containing all the figures, tables, schemes, figure captions. Include a cover letter addressed to Chief Editor, KU J Science, Department of Physics, Karnatak University, Dharwad 580003 (e-mail: srinamdar@kud.ac.in; him_lax3@yahoo.com) that must contain the names and contact details of at least two potential reviewers.